

Bengt Holter

Adaptive Coded Modulation in Spatial and Multiuser Diversity Systems

Doctoral thesis
for the degree of doktor ingeniør

Trondheim, May 2005

Norwegian University of Science and Technology
Faculty of Information Technology, Mathematics
and Electrical Engineering
Department of Electronics and Telecommunications



NTNU

Norwegian University of Science and Technology

Doctoral thesis

for the degree of doktor ingeniør

Norwegian University of Science and Technology

Faculty of Information Technology, Mathematics and Electrical Engineering

Department of Electronics and Telecommunications

© Bengt Holter

ISBN 82-471-6966-5 (printed vers.)

ISBN 82-471-6965-7 (electronic vers.)

ISSN 1503-8181

Doctoral theses at NTNU, 2005:49

Printed by NTNU-trykk

Abstract

This thesis consists of five included papers plus an introduction. The majority of the papers are devoted to performance analysis of an adaptive coded modulation (ACM) scheme based on multidimensional trellis codes. Primarily, single-user systems exploiting spatial diversity are analysed, but results are also presented for a multiuser system exploiting multiuser diversity.

The performance of the ACM scheme is evaluated for slowly flat-fading channels. When spatial diversity is exploited at the receiver end only, the analysis is focused on two different combining techniques: *maximum ratio combining* (MRC) and *switched combining*. A multiple-input multiple-output (MIMO) diversity system is also considered, in which case the combined effect of both transmit and receive diversity is realized by using space-time block coding at the transmitter.

For wireless systems using spatial diversity, it is of interest to employ measures which can capture and quantify the performance improvement related to a reduced fading level. In this thesis, a measure called the amount of fading (AF) is used to characterize the behavior of the error rate curve at a high signal-to-noise ratio (SNR). In particular, closed-form expressions for the AF at the output of a MIMO diversity system are provided, and it is shown that for a constant correlation model, the average symbol error probability at high SNRs may be expressed in terms of the AF.

Finally, a set of switched multiuser access schemes are proposed based on switched diversity algorithms originally devised to select between antennas in a spatial diversity system. ACM is used on each selected link to ensure a high spectral efficiency of the system.

Preface

This dissertation is submitted in partial fulfillment of the requirements for the degree of *doktor ingeniør* at the Department of Electronics and Telecommunications, Norwegian University of Science and Technology (NTNU). My advisors have been Professor Geir E. Øien at the Department of Electronics and Telecommunications, NTNU, and Professor Kjell J. Hole at the Department of Informatics at the University of Bergen (UiB). The studies have been carried out in the period from January 2001 to February 2005. The work includes the equivalent of a year of full-time course studies.

As a doctoral student, I have had the opportunity to visit two research groups abroad. From May 2003 to March 2004, I was part of the Communication Theory Group headed by Professor Helmut Bölcskei at the Swiss Federal Institute of Technology (ETH) in Zürich, Switzerland. In February 2004, I visited the research group of Professor Mohamed-Slim Alouini at the University of Minnesota, Minneapolis, USA.

The work has been funded by a scholarship from the Research Council of Norway, via the project *Bandwidth-Efficient and Adaptive Transmission Schemes for Wireless Multimedia Communications* (BEATS), and SINTEF ICT.

Acknowledgements

I would like to thank my supervisors Professor Geir E. Øien and Professor Kjell J. Hole for their advice and valuable comments. Their enthusiasm and support inspired me to become a doctoral student. I am grateful to Professor Helmut Bölcskei, for letting me be a part of the Communication Theory Group at ETH in Zürich. I initiated most of my work during this stay. From the Communication Theory Group, I want to thank Ph.D. student Markus Gärtner for helping me with a lot of practical matters.

In the last four years, I have had the pleasure of meeting Professor Mohamed-Slim Alouini several times. I would like to thank him for many inspiring and fruitful discussions on topics of common interest. I want to

thank my colleagues at NTNU and SINTEF ICT. I have bothered several of you with some peculiar questions, and I have really appreciated your efforts on helping me with your insights. In particular, I want to thank Ola Jetlund and Duc Van Duong for contributing to new insights through inspiring discussions. I am grateful to my employer SINTEF ICT for financial support and my former research director Erik Olsen for letting me pursue a doctoral degree.

During my visit to the University of Minnesota in February 2004, I shared office with Henrik Holm. I would like to thank him and his wife Basobi for their hospitality and for letting me spend two nights at their house in Lakeville, a southern suburb of Minneapolis. It was freezing cold when I was in Minneapolis, so instead of sleeping in thin blankets at the hotel, it was really nice sleeping in a Norwegian style bed for two nights.

In my spare time, I am eager to play the trombone. In Zürich, I joined two orchestras: the wind band *Stadtmusik Zürich* and the *Nota-Bene Symphony Orchestra*. I want to thank Ralph Tonezzer, Markus Hahn, and Marco Lucarelli from the symphony orchestra. Upon my wish, we met twice to play trombone quartets, and we all enjoyed it very much. From *Stadtmusik Zürich*, I want to thank the entire trombone section: Hans-Peter Meier, Markus Strolz, Viola Kummer, Patrick Isker, and René Isker. They were all very helpful to me, translating the swiss-german comments from the conductor into either german or english.

I want to thank my family for all the support during the last four years. In particular, my mother Gerd, for her enthusiasm and positive attitude, and my identical twin brother Atle, for his knowledge in signal processing conveyed to me during our (almost) daily phone calls. Finally, I want to express my deepest and sincere thanks to my common-law spouse Ingrid for all her love, patience, and support.

Trondheim, February 2005
Bengt Holter

Contents

Contents	v
Figures	ix
Tables	xv
I Introduction	1
References	25
II Included papers	31
A Performance Analysis of a Rate-Adaptive Dual-Branch Switched Diversity System	33
1 Introduction	37
2 System and channel model	39
3 ASE and BER analysis	40
4 Maximizing the ASE	43
5 Comparison with MRC and SC	44
6 Impact of branch correlation	45
7 Impact of time delay	47
Uncorrelated branches	49
Correlated branches	50
8 Numerical results	51
9 Conclusion	53
References	59

B Impact of Spatial Correlation on Adaptive Coded Modulation Performance in Rayleigh Fading	63
1 Introduction	67
2 System and channel model	68
3 Statistics of the combined CSNR	70
4 Diversity order and coding gain	74
Exact PDF	75
Approximate PDF	76
5 Linear pilot-symbol assisted channel prediction	77
6 Correlation and ratio coefficient	78
Correlation coefficient	78
Ratio coefficient	80
7 ASE and BER analysis	80
8 Numerical results	84
9 Conclusion	86
References	97
C Limitations in Spectral Efficiency of a Rate-Adaptive MIMO System Utilizing Pilot-Aided Channel Prediction	101
1 Introduction	105
2 System model	105
3 Channel model	106
SIMO channel model	106
MIMO channel model	107
4 BER and ASE analysis	108
5 Numerical results	113
6 Conclusion	113
References	119
D On the Amount of Fading in MIMO Diversity Systems	121
1 Introduction	125
2 Statistics of the combined fading power	127
3 Amount of fading	128
4 AF_{con} and its relation to the average SER at high SNR	132
5 Numerical results	136
6 Conclusion	137
References	141

E	Multuser Switched Diversity Transmission	145
1	Introduction	149
2	System and channel model	150
3	ASE and BER analysis	151
4	Multuser access schemes	151
	Scan-and-wait transmission (SWT)	152
	Switch-and-examine transmission (SET)	153
	SET with post-selection (SETps)	154
	Selection combining transmission (SCT)	155
5	Average feedback load	156
	Trade-off between ASE performance and AFL	156
6	Average waiting time	157
7	Numerical results	157
8	Conclusion	158
	References	165
	 III Appendices	 167
1	The generalized Marcum Q -function	169
	References	171
2	Useful integration rules	173
	References	175
3	Detailed derivation of the expression in (B.35)	177
	References	181
4	ASE and average BER under idealized assumptions	183
	References	187
5	Comments on the results in [1]	189
	References	191
6	Proof of the Amount of Fading expression in (D.11)	193

7 An alternative expression for the determinant of a constant correlation matrix	195
References	197
8 Proofs of statistical results presented in Paper E	199
References	203
9 The optimal weights of an MRC receiver by means of an eigen-filter approach	205
References	211

Figures

1.1	The SNR range is split into $N + 1$ bins. When the instantaneous SNR falls in the lowest interval, an outage occurs; whereas in the upper N intervals, codes with rates $\{R_n\}_{n=1}^N$ are employed.	8
1.2	QAM constellation with 256 symbols. The symbol constellations with 4, 8, 16, 32, 64, and 128 signal points are nested within the 256-QAM constellation. The crosses constitute the symbol constellation with 8 signal points.	9
1.3	The boxes are BER estimates generated by software simulations, whereas the solid lines are estimates obtained from (1.3). The labels denote the number of symbols in the QAM signal constellations utilized by the four-dimensional trellis codes.	10
1.4	ACM system with pilot-symbol-assisted channel estimation (for coherent detection) and prediction (for transmitter adaptation).	13
A.1	The SNR range is split into $N + 1$ bins. When the instantaneous SNR falls in the lowest interval, an outage occurs; whereas in the upper N intervals, a code with rate R_n is employed.	54
A.2	The size of $R_q - \mathcal{A}_1$ for $m = 1$, governing the sign of the gradient in (A.12).	55
A.3	ASE as a function of $\bar{\gamma}$ when operating on i.i.d. Rayleigh fading channels. For SSC, $\gamma_T = \gamma_T^*$ for each value of $\bar{\gamma}$.	55
A.4	Switching threshold γ_T^* , maximizing the ASE over all fading bins, as a function $\bar{\gamma}$ and the Nakagami- m fading parameter.	56
A.5	Average BER as a function of $\bar{\gamma}$ and the Nakagami- m fading parameter. For SSC, $\gamma_T = \gamma_T^*$ for each value of $\bar{\gamma}$.	56
A.6	ASE as a function of $\bar{\gamma}$ and ρ_s when operating on identically distributed Rayleigh fading channels. In the single branch case, $\text{ASE} = \mathcal{A}_1$.	57
A.7	Average BER as a function of $\bar{\gamma}$ and ρ_s when operating on identically distributed Rayleigh fading channels. In the single branch case, $\overline{\text{BER}} = \mathcal{B}_1 / \mathcal{A}_1$.	57

A.8	Average BER as a function of normalized time delay $f_D\tau$ and the Nakagami- m fading parameter for $\rho_s = 0$, $\bar{\gamma} = 20$ dB and $\gamma_T = 17.6$ dB.	58
A.9	Average BER as a function of normalized time delay $f_D\tau$ for $\rho_s = \{0, 0.5\}$, $\bar{\gamma} = 20$ dB, and $\gamma_T = 17.6$ dB. In all cases where $m \in \{2, 4\}$, the angle of arrival of the LOS component is assumed to be in the direction of motion, i.e. $\theta_0 = 0$. In the single branch case, $\overline{\text{BER}} = \mathcal{B}_{1,\rho_t} / \mathcal{A}_1$	58
B.1	ACM system with pilot-symbol-assisted channel estimation (for coherent detection purposes) and prediction (for transmitter adaptation purposes).	87
B.2	The CSNR range is split into $N + 1$ bins. When the instantaneous CSNR falls in the lowest interval, an outage occurs; whereas in the upper N intervals, a code with rate R_n is employed.	87
B.3	Comparison of the exact and approximate PDFs for γ when $H = 2$ and the system is operating on identically distributed and spatially correlated Rayleigh fading channels ($\bar{\gamma} = 1$). . .	88
B.4	Comparison of the exact and approximate PDFs for γ when $H = 4$ and the system is operating on identically distributed and spatially correlated Rayleigh fading channels ($\bar{\gamma} = 1$). Top subfigure: constant correlation model. Bottom subfigure: exponential correlation model.	88
B.5	Diversity and coding gain realized at high CSNR for a system operating on identically distributed spatially correlated Rayleigh fading channels, using BPSK transmission only. The abbreviations con and exp in the legends of both subfigures are related to results obtained with a constant and exponential correlation model, respectively. Top subfigure: G_d in (B.21) obtained with the approximate PDF is depicted. It should be related to G_d in (B.17), obtained with the exact PDF, in which case $G_d = H$. Bottom subfigure: Expressions for G_c in (B.18) and (B.22) are depicted for $H = 4$	89
B.6	Average BER and ASE as a function $\bar{\gamma}_h$ when using the exact and approximate PDF ($H = 2$ and $\rho_{12} = \rho_{21} = \rho_s = 0.2$ in (4.2)). The assumptions are perfect channel knowledge and no time delay on the feedback channel.	90

B.7	Average BER and ASE as a function $\bar{\gamma}_h$ when using the exact and approximate PDF ($H = 2$ and $\rho_{12} = \rho_{21} = \rho_s = 0.7$ in (4.2)). The assumptions are perfect channel knowledge and no time delay on the feedback channel.	90
B.8	Average BER and ASE as a function $\bar{\gamma}_h$ when using the exact and approximate PDF with a constant correlation model ($H = 4$ and $\rho_{ij} = \rho_s = 0.7$ in (4.2)). The assumptions are perfect channel knowledge and no time delay on the feedback channel.	91
B.9	Average BER and ASE as a function $\bar{\gamma}_h$ when using the exact and approximate PDF with an exponential correlation model ($H = 4$ and $\rho_{ij} = \rho_s^{ i-j }$ in (4.2), with $\rho_s = 0.7$). The assumptions are perfect channel knowledge and no time delay on the feedback channel.	91
B.10	Average BER as a function $\bar{\gamma}_h$ and normalized time delay on the feedback channel when $H = 4$ and the system operating on uncorrelated Rayleigh fading channels. The pilot symbol spacing $L = 10$, and the prediction filter length is $K = 1000$	92
B.11	Average BER as a function $\bar{\gamma}_h$ and normalized time delay on the feedback channel when $H = 4$ and the system is operating on exponentially correlated Rayleigh fading channels ($\rho_s = 0.7$). The pilot symbol spacing $L = 10$, and the prediction filter length is $K = 1000$	92
B.12	Regions where the system performance is acceptable, plotted for $H = \{2, 4\}$, $L = 10$, $K = 1000$, and $\rho_s = \{0, 0.2, 0.7\}$. The curves indicate the largest delay that is allowed in order to achieve the BER requirements for a given average CSNR $\bar{\gamma}_h$. Thus, the performance is acceptable for each point specified by a CSNR/delay combination that is below and to the right of the curves.	93
B.13	Zero-delay ASE compared to the channel capacity (optimal rate adaptation with constant transmit power) [30, Sec. IV] for $H = 2$ and $\rho_s = \{0, 0.7\}$	94
B.14	Zero-delay ASE compared to the channel capacity (optimal rate adaptation with constant transmit power) [30, Sec. IV] for $H = 4$ and $\rho_s = \{0, 0.7\}$	94

B.15	ASE as a function of $\bar{\gamma}_h$ and normalized feedback time delay when $L = 10$, $H = 2$, and $\rho_s = 0.7$. The contour line divides the ASE into a relevant part where the BER constraints are fulfilled (to the left of the contour line) and an irrelevant part where the BER constraints are violated (to the right of the contour line). The prediction filter length is $K = 1000$	95
C.1	Transmitter	114
C.2	Receiver	114
C.3	Average BER as a function of feedback delay and of expected subchannel CSNR. $\kappa = 5$ antennas are utilized (1×4 system) and the pilot symbol spacing is $L = 7$. The prediction filter length is $K = 1000$	115
C.4	Average BER as a function of feedback delay and of expected subchannel CSNR. $\kappa = 4$ antennas are utilized (2×2 system with STBC G_2) and the pilot symbol spacing is $L = 7$ ($L_b = 8$). The prediction filter length is $K = 1000$	115
C.5	Average BER as a function of feedback delay and of expected subchannel CSNR. $\kappa = 6$ antennas are utilized (3×3 system with STBC H_3) and the pilot symbol spacing is $L = 7$ ($L_b = 11$). The prediction filter length is $K = 1000$	116
C.6	Average spectral efficiency as a function of expected subchannel CSNR [dB], plotted for various L and a normalized feedback time delay (symbol duration normalized with respect to maximum Doppler spread) of 0.25. For the 2×2 system, the STBC G_2 is employed. For the 3×3 system, the STBC H_3 is employed.	117
D.1	Numerical comparison of closed form expressions for the determinant of a constant correlation matrix \mathbf{R} . Left figure: $\det(\mathbf{R}) = (1 - x)^{L-1}(1 + x(L - 1))$. Right figure: $\det(\mathbf{R}) = \text{betacdf}(1 - x, L - 1, 2)$	138
D.2	AF_{con} (in dB) as a function of the power correlation coefficient $\rho = \rho_t = \rho_r$ for SIMO, MISO, and MIMO diversity systems ($n_T \times n_R$) operating on identically distributed Rayleigh fading channels: (a) ($1 \times n_R$); (b) ($2 \times n_R$); (c) ($3 \times n_R$); (d) ($4 \times n_R$).	138

D.3	<p>Top figure: Exact average SER (dashed lines) and approximate average SER at high SNR (solid lines) for a 3×3 MIMO diversity system operating on identically distributed Rayleigh fading channels (constant correlation models at each end of the MIMO link). A BPSK modulation scheme is utilized. Bottom figure: Relative (right) shift (in dB) of the SER benchmark curve presented in the top figure as a function of ρ_r when $\rho_t = 0$. Using the top x-axis as a reference, the AF realized by the 3×3 MIMO diversity system is compared (in percentage) to the AF of a single Rayleigh fading channel (100% reduction represents the non-fading AWGN channel).</p>	139
D.4	<p>Top figure: Exact average SER (dashed lines) and approximate average SER at high SNR (solid lines) for a 3×3 MIMO diversity system operating on identically distributed Rayleigh fading channels (constant correlation models at each end of the MIMO link). A BPSK modulation scheme is utilized. Bottom figure: Relative (right) shift (in dB) of the SER benchmark curve presented in the top figure as a function of ρ_r when $\rho_t = 0.5$. Using the top x-axis as reference, the AF realized by the 3×3 MIMO diversity system is compared (in percentage) to the AF of a single Rayleigh fading channel (100% reduction represents the non-fading AWGN channel).</p>	140
E.1	<p>ASE (unconstrained optimization) for the SCT, SETps, SET, and SWT access schemes when the multiuser system is assumed to be operating on i.i.d. Rayleigh fading channels with $\bar{\gamma} = [5, 15, 25]$ dB.</p>	160
E.2	<p>Optimal thresholds γ_T maximizing the ASE subject to no AFL constraints (unconstrained optimization). The multiuser system is assumed to be operating on i.i.d. Rayleigh fading channels with $\bar{\gamma} = 15$ dB.</p>	160
E.3	<p>AFL (unconstrained optimization) for the SCT, SETps, SET, and SWT access schemes. For reference purposes, the solid line visualizes the (linear) upper bound for the constraint $\text{AFL} \leq 0.3K$. The multiuser system is assumed to be operating on i.i.d. Rayleigh fading channels with $\bar{\gamma} = 15$ dB.</p>	161
E.4	<p>AFL for the SCT, SETps, SET, and SWT access schemes when $\text{AFL} \leq 0.3K$. When the constraint cannot be met, $\text{AFL} = 0$ for simplicity. The multiuser system is assumed to be operating on i.i.d. Rayleigh fading channels with $\bar{\gamma} = 15$ dB.</p>	161

E.5	ASE realized by the SETps access scheme when the AFL is upper bounded by $AFL \leq \alpha K$. When the constraint cannot be met, ASE = 0 for simplicity. The multiuser system is assumed to be operating on i.i.d. Rayleigh fading channels with $\bar{\gamma} = 15$ dB. .	162
E.6	ASE realized by the SET access scheme when the AFL is upper bounded by $AFL \leq \alpha K$. When the constraint cannot be met, ASE = 0 for simplicity. The multiuser system is assumed to be operating on i.i.d. Rayleigh fading channels with $\bar{\gamma} = 15$ dB. .	162
E.7	ASE realized by the SWT access scheme when the AFL is upper bounded by $AFL \leq \alpha K$. When the constraint cannot be met, ASE = 0 for simplicity. The multiuser system is assumed to be operating on i.i.d. Rayleigh fading channels with $\bar{\gamma} = 15$ dB. .	163
E.8	Average waiting time (AWT) for the SWT access scheme. When the constraint cannot be met, AWT = 0 for simplicity (when $AFL \leq 0.1K$, AWT = 0 for $K \leq 12$). The multiuser system is assumed to be operating on i.i.d. Rayleigh fading channels with $\bar{\gamma} = 15$ dB.	163
5.1	Comparison of the exact and approximate PDFs in [1, Fig. 1], including corrected results based on a complex representation of the covariance matrix in [1, Eq. (9)]. The curves are obtained for $\bar{\gamma} = 1$ and $m = 1$	190

Tables

A.1	PDF and CDF of the SNR per symbol γ for a single Nakagami- m fading channel	54
A.2	Parameters a_n and b_n with thresholds γ_n for $\text{BER}_0 = 10^{-4}$. . .	54
B.1	Expressions for ψ and θ for constant and exponential correlation models	87
C.1	Orthogonal designs for STBC	111

Abbreviations

ACM	Adaptive coded modulation
AF	Amount of fading
AFL	Average feedback load
ASE	Average spectral efficiency
AWGN	Additive white Gaussian noise
AWT	Average waiting time
BER	Bit-error-rate
BPSK	Binary phase-shift keying
BS	Base station
CDF	Cumulative distribution function
CF	Characteristic function
CSI	Channel state information
CSNR	Channel signal-to-noise ratio
dB	Decibel
DD	Decision-directed
LOS	Line-of-sight
MGF	Moment generating function
MIMO	Multiple-input multiple-output
MISO	Multiple-input single-output
M-PSK	M-ary phase-shift keying
MRC	Maximum ratio combining
NLOS	Non-line-of-sight
PDF	Probability density function
PMF	Probability mass function
QAM	Quadrature amplitude modulation
RV	Random variable
SC	Selection combining
SCT	Selection combining transmission
SEC	Switch-and-examine combining

SER	Symbol-error-rate
SET	Switch-and-examine transmission
SETps	Switch-and-examine transmission with post-selection
SIMO	Single-input multiple-output
SINR	Signal-to-interference plus noise ratio
SNR	Signal-to-noise ratio
SSC	Switch-and-stay combining
STBC	Space-time block coding
SWT	Scan-and-wait transmission
TDM	Time division multiplexed

Part I

Introduction

Introduction

In order to achieve high-speed transmission of data on a wireless channel, a reliable and spectrally efficient transmission scheme is needed. However, the hostility of the wireless channel makes this a challenging task, since signals tend to propagate along different paths due to reflection, scattering, and diffraction from obstructing objects. The received signal will then be a sum of randomly delayed signal components which will add either constructively or destructively, causing rapid fluctuations in the received signal level. This is called multipath fading, and through the years, it has been perceived as a phenomenon with detrimental effects on spectral efficiency. Based on this perception, wireless transmission schemes have traditionally been designed for the worst-case scenario by focusing on enabling the system to perform acceptably even in deep fading conditions. With such a design principle, spectral efficiency is sacrificed for link reliability.

A design principle focusing more on spectral efficiency is rate-adaptive transmission, where the basic concept is to exploit and track the time varying characteristics of the wireless channel to transmit with as high information rate as possible when the channel quality is good, and to lower the information rate (and trade it for link reliability) when the channel quality is reduced [1–5]. With such a transmission scheme, a feedback channel is required, on which the receiver reports channel state information (CSI) to the transmitter. Based on the reported CSI, the transmitter can make a decision on which rate to employ for the next transmission period. In particular, the transmitter may choose to select symbols from the biggest constellation meeting a predefined bit-error-rate (BER) requirement, to ensure that the spectral efficiency is maximized for an acceptable (target) BER. A promising method is to vary the constellation size and the channel coding scheme (error control) according to the channel conditions, in which case a rate-adaptive transmission scheme is called *adaptive coded modulation* (ACM) [6, 7].

Throughout this thesis, slowly flat-fading channels are assumed. The notion of a slow fading channel is related to the channel coherence time T_c ,

which is a measure of the time period where the fading process is correlated [8]. A fading process is characterized as slow if the symbol time period T_s is smaller than T_c , in which case a particular fading level will affect several successive symbols (block fading). In addition, if the fading process affects all the spectral components within a certain bandwidth in a similar manner, the fading is said to be frequency-flat. This is the case for narrowband systems, in which case the bandwidth B [Hz] of the transmitted signal is much smaller than the coherence bandwidth B_c [Hz] of the channel. The coherence bandwidth is a measure of the frequency range over which the fading process is correlated [8]. Since all the frequency components of a signal transmitted on a flat-fading channel are affected in the same way, it will not be distorted in frequency. That is, the flat-fading channel represents a multiplicative channel rather than a convolutional channel, and the complex baseband representation of the channel response may be written simply as a complex number $z = \alpha \cdot e^{-j\beta}$. All the frequencies within the signal bandwidth will then be subjected to the same attenuation α (also known as fading amplitude or fading envelope) and the same phase shift β . When evaluating the performance of digital communication techniques over slowly flat-fading channels, α may be viewed as a random variable (RV), where the probability density function (PDF) of α is dependent on the radio propagation environment [8].

The Rayleigh distribution is frequently used when there is no line-of-sight (LOS) between the transmitter and the receiver. In the presence of a LOS component, a Rice distribution or a Nakagami- m distribution may be applied. The two distributions are closely related, but due to the simplicity of the Nakagami- m distribution, it is often preferred, as it frequently leads to closed-form analytical expressions and insights which are difficult to obtain with the Rice distribution [9]. For a Nakagami- m fading model, the PDF of α is given by [10]

$$f_\alpha(\alpha) = \frac{2m^m \alpha^{2m-1}}{\Omega^m \Gamma(m)} e^{-\frac{m\alpha^2}{\Omega}}; \quad \alpha \geq 0, \quad (1.1)$$

where m is the Nakagami- m fading parameter which ranges from $1/2$ (half Gaussian model) to ∞ (additive white Gaussian noise (AWGN) channel), $\mathcal{E}\{\alpha^2\} = \Omega$, and $\Gamma(\cdot)$ is the gamma function [11, Eq. (8.310)].¹ A nice feature of the Nakagami- m distribution is that the Rayleigh distribution is included as a special case ($m = 1$). The Nakagami- m distribution often gives the best fit to land-mobile and indoor-mobile multipath propagation environments [8].

¹ $\mathcal{E}\{\cdot\}$ denotes the statistical average.

A wireless system may be classified in terms of the number of antennas used for transmission and reception. The most traditional configuration uses a single transmit antenna and a single receive antenna, in which case the system is defined as a single-input single-output (SISO) system. With multiple antennas at the receiver, the system is classified as a single-input multiple-output (SIMO) system. Similarly, with multiple transmit antennas and a single receive antenna, the system is a multiple-input single-output (MISO) system. Finally, if multiple antennas are employed at both sides of the link, the system is classified as a multiple-input multiple-output (MIMO) system. Traditionally, multiple antennas have been employed at the receiver end only, to combat the effects of multipath fading. This technique is known as *spatial diversity*, and it refers to the basic principle of picking up multiple copies of the same signal at different locations in space. A potential diversity gain is achieved and maximized if the antennas are sufficiently separated such that the fading characteristics are independent. With the advent of space-time codes, diversity gains may also be achieved in MISO and MIMO systems, irrespective of the transmitter having channel knowledge or not [12, 13].

Transmission schemes for MIMO systems may in general be divided into two categories: rate maximization schemes and diversity maximization schemes. MIMO systems within the two categories are known as *spatial multiplexing* systems and *MIMO diversity* systems, respectively [14]. A spatial multiplexing system utilizes the channel to provide increased spectral efficiency, by transmitting independent streams of data from each transmit antenna. In a rich scattering environment, each transmit antenna induces a different spatial signature at the receiver. The receiver exploits these signature differences to separate the individual data streams. An important information-theoretic result is that with spatial multiplexing, capacity scales linearly, rather than logarithmically, with increasing signal-to-noise ratio (SNR)² [15–17]. In addition, this increase in capacity comes at no extra bandwidth or power consumption.

A MIMO diversity system uses the channel to provide increased link reliability by jointly encoding the individual data streams to protect the data from errors caused by multipath fading. This is achieved by using a signal processing technique called space-time block coding (STBC) [12, 13]. Space-time block codes are designed to achieve the maximum diversity order for a given number of transmit and receive antennas, subject to the constraint

²In this thesis, SNR and CSNR (channel-signal-to-noise ratio) are interchangeably used as abbreviations for the signal-to-noise ratio. SNR is normally used, but CSNR is used in two of the included papers, for reference purposes.

of having a simple decoding algorithm. As such, they incur a loss in capacity because they convert the MIMO matrix channel into a scalar AWGN channel whose capacity is smaller than the true channel capacity [18].

Diversity schemes are usually classified according to the type of combining technique employed at the receiver. In the absence of interference, *maximum ratio combining* (MRC) [19] is the optimal combining scheme for any fading distribution, in the sense that it maximizes the received SNR. As such, it may be viewed as the stochastic counterpart of a matched filter [20]. In an MRC receiver, the output signal is the coherent sum of the signals from all the branches. In particular, the complex signal amplitudes on all the branches are co-phased and weighted according to their individual strength such that the SNR of the combined signal is maximized. In Appendix 9, the optimal complex weights (amplitude and phase) of an MRC receiver are derived by means of an eigenfilter approach, which was originally proposed in [21]. The optimality of the MRC receiver comes at the expense of complexity, since for coherent detection, complete knowledge of all channel parameters³, and separate receiver RF⁴/analog chains on all the branches are needed [8].

A less complex diversity scheme is *selection combining* (SC) [8, Sec. 9.7], where only a single branch and not the coherent sum is selected for further processing. In particular, an SC receiver monitors the instantaneous SNR on all the branches and selects the branch with the highest SNR. As a consequence, only a single receiver chain is needed for its implementation. However, since simultaneous and continuous monitoring of the channel state on all the branches is required, an SC receiver is often replaced by a *switched combining* receiver [8, Sec. 9.8]. In this case, the receiver is not always connected to the best branch, but is connected to a particular branch as long as the received SNR of that branch do not drop below a predefined threshold. If this happens, the receiver simply switches to another branch. With such an approach, the receiver at any time only needs to monitor the channel state of the currently selected branch. This contributes to reduce the complexity in comparison to the SC combiner, but it comes at the expense of a certain performance loss.

All the spatial diversity combining techniques mentioned above have in common that the diversity gain arises from independent signal paths received by multiple antennas. Another type of diversity is *multiuser diversity* [22, 23]. This type of diversity is naturally inherent in systems where

³For flat-fading channels, the amplitude and phase of the complex channel amplitudes on all the branches must be known.

⁴Radio frequency

several users are communicating with a base station (BS) on a shared frequency band. The diversity is attributed to the fact that for a given moment in time, different users usually have different channel conditions. In this situation, the total system throughput can be maximized by only letting the user having the best channel quality transmit at any given time [24, 25]. However, repeatedly scheduling the best user might not be a fair strategy to communicate on a shared frequency band, since the same favorable user might end up being selected every time. Hence, scheduling users in a multiuser system by exploiting multiuser diversity also involve fairness and latency issues. In addition, the BS needs feedback from the users to make a decision on which user to schedule for the next transmission period. If all the users are to report their channel status on a regular basis, it will contribute to drain the terminal batteries more rapidly and generate a lot of overhead traffic in the system. As a remedy, recent papers on scheduling and multiuser diversity are suggesting scheduling methods which reduce the amount of feedback information by letting the BS make a decision based on a predefined set of channel thresholds [26–29]. In general, this means that for a given moment in time, only a single user or a small group of users which can report channel conditions above a certain level are allowed to report it to the BS. The total number of users can be divided into smaller groups where users within a particular group exhibit almost similar channel conditions. When a certain group of users is addressed by the BS, users within that group are able to compete for the channel on equal terms.

Recently, it has been reported that additional use of spatial diversity in multiuser systems counteracts the performance gain obtained by multiuser transmission. In [30], it is argued that multiuser diversity with no spatial diversity outperforms schemes that employ both multiuser diversity and spatial diversity. However, in [31], it is commented that, if properly exploited, spatial diversity really do increase and not decrease the total diversity gain in a system that takes advantage of both spatial and multiuser diversity.

Adaptive coded modulation

A major part of this thesis is devoted to performance analysis of an ACM scheme based on multidimensional trellis codes originally designed for AWGN channels [7, 32]. Primarily, the analysis is focused on single-user systems exploiting spatial diversity, but results are also obtained for a multiuser system exploiting multiuser diversity. In the following, a brief summary of literature related to the ACM scheme in question is presented,

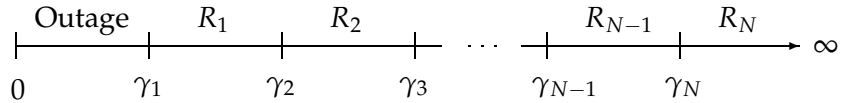


FIGURE 1.1: The SNR range is split into $N + 1$ bins. When the instantaneous SNR falls in the lowest interval, an outage occurs; whereas in the upper N intervals, codes with rates $\{R_n\}_{n=1}^N$ are employed.

along with relevant details of the ACM scheme.

In [7] and [32, Ch. 2], the ACM scheme based on multidimensional trellis codes is presented along with performance merits when applied on a SISO system operating on a Nakagami- m fading channel. Perfect channel knowledge at the receiver and perfect CSI at the transmitter are assumed (zero-error feedback channel with no time delay). A set of N 2 G -dimensional trellis codes are employed. Each code is based on quadrature amplitude modulation (QAM) signal constellations of varying size $M_n = 2^{k_n}$, where $n = \{1, 2, \dots, N\}$ and k_n is some positive integer. Rate adaptation is performed by splitting the SNR range into $N + 1$ fading regions (bins) as depicted in Figure 1.1. Each of the N codes is then assigned to operate within a particular fading region, except for the leftmost bin. The SNR thresholds in the set $\{\gamma_n\}_{n=1}^N$ are selected such that each code operates below a predefined target BER. When the instantaneous SNR γ falls within the fading region $\gamma_n \leq \gamma < \gamma_{n+1}$, the associated CSI, i.e. the fading region index n , is sent back to the transmitter. The transmitter then adapts its transmission rate and coding scheme by transmitting with a code realizing a spectral efficiency of R_n (measured in bits/s/Hz). The spectral efficiencies of the applied codes are organized such that $R_1 < R_2 < \dots < R_N$. This enables the system to transmit with high spectral efficiency when the instantaneous SNR is high, and to reduce the spectral efficiency as the SNR decreases. The target BER is not achieved when $\gamma < \gamma_1$, so no information is transmitted when γ falls into the leftmost interval $0 \leq \gamma < \gamma_1$ (outage). During this situation, the information must be buffered at the transmitter.

In general, for a 2 G -dimensional trellis code, where $G \in \{1, 2, \dots\}$, the spectral efficiency R_n of code n is obtained as follows. The encoder for code n accepts $p = G \log_2(M_n) - 1$ information bits at each time index $k = GT_s$. The encoder generates $p + 1 = G \log_2(M_n)$ coded bits which specify G transmittable QAM symbols from the n th constellation with M_n symbols. Since G (two-dimensional) QAM symbols generated at each time index k can be viewed as *one* 2 G -dimensional symbol, the generated code is

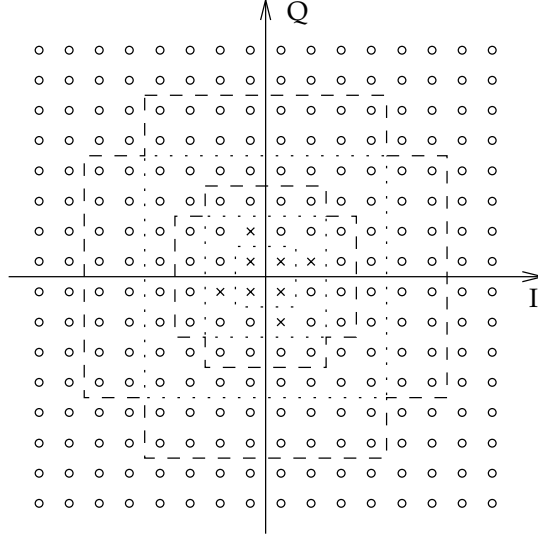


FIGURE 1.2: QAM constellation with 256 symbols. The symbol constellations with 4, 8, 16, 32, 64, and 128 signal points are nested within the 256-QAM constellation. The crosses constitute the symbol constellation with 8 signal points.

said to be a $2G$ -dimensional trellis code. As a result, p information bits are transmitted within GT_s uses of the channel. The information rate for code n may then be expressed as $R_n = (p/(GT_s))/B$. Assuming ideal Nyquist pulses (transmission with no intersymbol interference), we have $B = 1/T_s$, in which case the spectral efficiency of code n is equal to $R_n = k_n - 1/G$ [bits/s/Hz]. In this thesis, $N = 8$ four-dimensional trellis codes are used, i.e. $G = 2$. These codes are based on eight nested QAM signal constellations with $M_n = 2^{k_n} \in \{4, 8, 16, 32, 64, 128, 256, 512\}$ signal points for $k_n = n + 1$ and $n = 1, 2, \dots, 8$ (see Figure 1.2).⁵ Hence, the associated spectral efficiencies are $R_n = \{1.5, 2.5, \dots, 8.5\}$.

The *average* spectral efficiency (ASE) is obtained as the weighted sum of the spectral efficiencies $\{R_n\}_{n=1}^N$

$$\text{ASE} = \sum_{n=1}^N R_n \cdot P_n, \quad (1.2)$$

where the weight factor P_n is the probability that code n is used. Since this

⁵The QAM constellation with 512 symbols is omitted from Figure 1.2 due to space and visibility requirements.

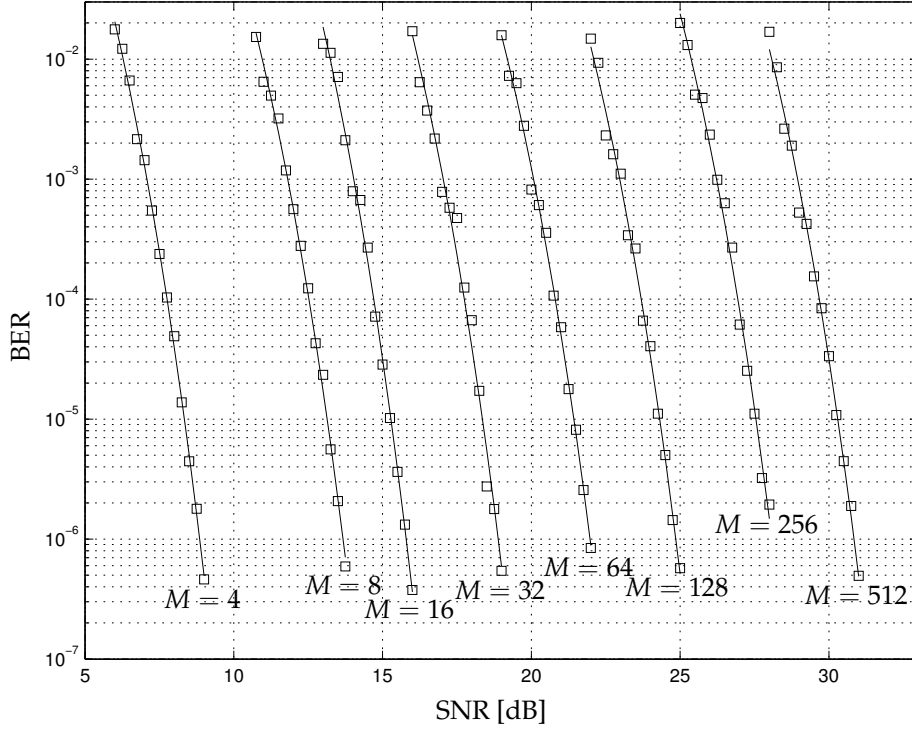


FIGURE 1.3: The boxes are BER estimates generated by software simulations, whereas the solid lines are estimates obtained from (1.3). The labels denote the number of symbols in the QAM signal constellations utilized by the four-dimensional trellis codes.

is equivalent to the probability that the instantaneous SNR falls within a particular fading bin n , the thresholds $\{\gamma_n\}_{n=1}^N$ must be known. In [7, Eq. (9)], it is argued that the BER when code n is applied on an AWGN channel, as a function of the SNR γ —denoted BER_n —may be approximated by the expression

$$\text{BER}_n \approx a_n \cdot e^{-\frac{b_n \gamma}{M_n}}, \quad (1.3)$$

where a_n and b_n are code-dependent constants found by least square curve fitting to simulated data on AWGN channels of varying SNRs. In Figure 1.3 [32, Fig. 2.2], the BER performance of the individual codes are depicted along with the results of the curve fitting technique.⁶ From the curve fitting technique and for a given target BER—denoted BER_0 —the thresholds

⁶According to [32], the BER results depicted in Figure 1.3 are obtained when the path length of the Viterbi decoder is 9.

$\{\gamma_n\}_{n=1}^N$ are obtained by assuming equality in (1.3), in which case

$$\begin{aligned}\gamma_n &= (M_n K_n) / b_n \quad n = 1, 2, \dots, N, \\ \gamma_{N+1} &= \infty\end{aligned}, \quad (1.4)$$

where $K_n = -\ln(\text{BER}_0 / a_n)$ [7, Eq. (5)].⁷

In [33, 34], the results in [7] and [32, Ch. 2] are extended to take both spatial diversity and feedback delay into account. Multiple antennas are introduced at the receiver, which effectively changes it from a SISO system to a SIMO system. MRC is used to combine the signals collected from H receiver antennas, and it is assumed that the MRC receiver operates on independent and identically distributed (i.i.d.) Rayleigh fading channels. A nonzero feedback delay τ is taken into account by assuming that the instantaneous SNR at time t has changed to γ_τ at time $t + \tau$. Since a change in the SNR reflects a change in the channel condition, there will be a mismatch between the reported CSI and the true state of the channel. This mismatch is modelled through the temporal correlation ρ between γ and γ_τ . In particular, the BER degradation due to a nonzero feedback delay is derived as a function of ρ .

In general, the average BER (averaged over all codes and SNRs) is obtained as the average number of bits in error, divided by the average number of bits transmitted [5]

$$\overline{\text{BER}} = \frac{\sum_{n=1}^N R_n \cdot \overline{\text{BER}}_n}{\sum_{n=1}^N R_n \cdot P_n}, \quad (1.5)$$

where $\overline{\text{BER}}_n$ is the average BER experienced when code n is applied. An expression for $\overline{\text{BER}}_n$ is derived by exploiting the approximation introduced in (1.3). However, a correction term for BER_n is introduced to account for the fact that (1.3) approaches a_n for low SNRs. Since a_n can be larger than one [7], the following expression is utilized in [33] and [34] to ensure that the exponential curve do not exceed 0.5:

$$\text{BER}_n = \begin{cases} a_n \cdot e^{-\frac{b_n \gamma}{M_n}} & \text{when } \gamma \geq \gamma_n^l \\ \frac{1}{2} & \text{when } \gamma < \gamma_n^l \end{cases} \quad (1.6)$$

The boundary $\gamma_n^l = \ln(2a_n)M_n/b_n$ is the smallest SNR such that the BER is no larger than 0.5 for either code.

⁷In [7], it is noted that it might not be obvious that $\gamma_n < \gamma_{n+1}$ for $n = 1, 2, \dots, N$ since a_n and b_n vary with n . However, the monotonicity is attributed to the fact that, for a given BER, the minimum required SNR for $n + 1$ is larger than the required SNR for code n when $M_{n+1} > M_n$. In practice, $0 < \text{BER}_0 < a_n$, in which case $K_n > 0$ and all the thresholds $\gamma_n > 0$.

At this point, it is noted that for two of the papers included in this thesis, the average BER performance is evaluated by utilizing the exponential BER approximation in (1.3) rather than the expression in (1.6), containing the correction term. However, according to [35], the average BER result is quite insensitive to overestimation for values above 10^{-1} . This is attributed to the fact that when the approximate BER curves for the individual codes are averaged, the values in the region above 10^{-1} are weighted by very low probabilities. Hence, it is then very unlikely that a code resulting in an instantaneous BER above 10^{-1} is selected. As a consequence, it is concluded that overestimation of the instantaneous BER at low SNRs has little or no influence on the average BER result.

In [32, Ch. 3] and [35], the results in [33, 34] are extended to include pilot-symbol assisted modulation (PSAM) [36], which is a technique where known symbols (pilot symbols) are multiplexed into the information data stream prior to transmission. Both the pilot symbols and the multiplexing scheme are known by the receiver and can be exploited for channel estimation and channel prediction. A baseband model of the rate-adaptive SIMO system is depicted in Figure 1.4, where channel estimation using PSAM is employed to achieve coherent detection of the data. In addition, PSAM is exploited for channel prediction to predict the future CSI as a remedy against the outdated CSI problem. Hence, instead of reporting a CSI based on the instantaneous SNR, a CSI based on a predicted SNR ahead in time is reported. Assuming that the prediction horizon equals the time delay on the feedback channel, the reported CSI will be more in accordance with the true state of the channel when it is used by the transmitter to select a code. Since the goal of the work in [32, Ch. 3] and [35] was to suggest bounds for the possible BER, ASE, and outage probability, a computationally intensive predictor, optimal in the *maximum a posteriori* (MAP) sense, is chosen. For details of MAP-optimal prediction with PSAM used in [32, 35], see [32, Sec. 3.5].

In Figure 1.4, the pilot symbols are extracted from the data symbols which are buffered before detection. Channel estimates at time instants other than pilot symbol instants are then obtained by using optimal non-causal Wiener interpolator filters provided on each antenna branch. Each of these filters operate on *maximum likelihood* (ML) estimates of the complex fading envelope at pilot symbol time instants. An estimate of this kind is the result of dividing a single observation of the noisy received signal by the known pilot symbol value [32, Eq. (3.8)]. In [37], it is noted that the interpolation coefficients can be kept constant over a whole pilot-period range L , but better channel estimates can be obtained if the interpolator coefficients are optimally updated for every received symbol. In this thesis,

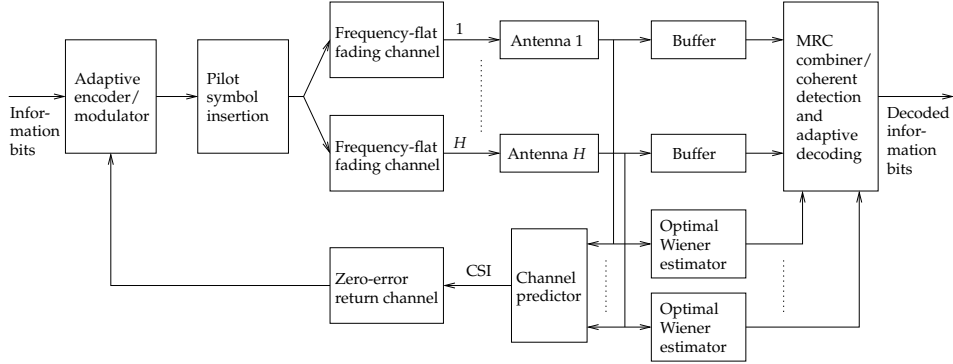


FIGURE 1.4: ACM system with pilot-symbol-assisted channel estimation (for coherent detection) and prediction (for transmitter adaptation).

as in [32], it assumed that the fading process is constant between two successive pilot symbols, in which case constant interpolation coefficients can be used.

Channel estimation by using periodic insertion of pilot symbols can be viewed as sampling of a band-limited process. For a maximum Doppler frequency of f_D [Hz], the sampling frequency, f_{samp} [Hz], of the fading process must be equal to $f_{samp} \geq 2f_D$ in order to conform to the Nyquist sampling theorem [38]. As the time interval between two pilot symbols is equal to the sampling period, it can be written as $T_{samp} = 1/f_{samp} = LT_s$ [s]. Invoking the Nyquist condition, the pilot symbol spacing L must then satisfy the condition $L \leq 1/(2W)$, where $W = f_D T_s$ is the normalized Doppler spread (denoted as fading bandwidth in [39]).⁸ According to [39, Eq. (21)], the estimation error of a single non-causal Wiener interpolator filter operating on a slowly varying Rayleigh fading channel is equal to

$$\sigma_e^2 = \frac{\Omega \cdot 2WLN_0}{P\Omega + 2WLN_0}, \quad (1.7)$$

where P [W] is the constant average transmit power, and N_0 is the variance of the complex AWGN. By once again applying the Nyquist condition and focusing on channel estimation on branch h , $2WL \leq 1$, which gives $\sigma_e^2 \leq \Omega/\bar{\gamma}_h$ [32, Eq. (3.7)], where $\bar{\gamma}_h = \frac{\Omega P}{N_0}$ is the average SNR received on branch h . Hence, it is noted that unless the average SNR is very low, it can be assumed that the estimation error in the receiver is negligible compared to the prediction error, i.e. signal detection can be assumed to be perfect.

⁸With the assumption of slow fading channels, $W \ll 0.5$.

Contributions of the included papers

This thesis consists of five papers, which are numbered with the capital letters A, B, C, D, and E. In the following, a summary of the included papers is presented.

Paper A

Bengt Holter and Geir E. Øien, "Performance analysis of a rate-adaptive dual-branch switched diversity system," *submitted to IEEE Transactions on Wireless Communications*.

In Paper A, the rate-adaptive SISO system in [7] is extended to a 1×2 SIMO system by using a dual-branch switched diversity combiner at the receiver. Similar extensions are reported in the literature, but they have so far only been focused on the MRC receiver [33, 34]. However, since MRC represents the diversity scheme with the highest complexity, other and less complex diversity schemes are often preferred in practice. A switched diversity combiner requires just a single receiver chain for its implementation, and only the channel state of the currently selected branch needs to be monitored. As such, it represents an attractive choice for a low complexity receiver.

The performance is evaluated for a system operating on identically distributed Nakagami- m fading channels with perfect channel knowledge at the receiver and instantaneous/time-delayed feedback of CSI. Both uncorrelated and correlated antenna branches are considered. The optimal switching threshold that maximizes the ASE is identified for the case of uncorrelated antenna branches.

It is concluded that in order to maximize the ASE for a given average SNR on the channels, the switching threshold must be identical to one of the predefined thresholds of the ACM scheme. In this case, the performance in terms of ASE and average BER is close to the performance obtained with both MRC and SC, but at a significantly lower complexity. The system benefits from second order diversity only as long as the switching threshold is in the vicinity of the average SNR on the channels. Hence, the performance approaches that of a single branch receiver if the switching threshold is either too low or too high compared to the average SNR. Similarly, the ASE approaches that of a single branch receiver when spatial correlation is introduced. The same effect is also visible for the average BER, but mainly at high SNR values. The impact of time-delayed feedback is presented for two isotropic scattering models: with and without a LOS

component. In general, a normalized time delay of 10^{-2} is tolerated without a noticeable degradation in the average BER. A slight increase in tolerance is achieved by increasing the Nakagami- m fading parameter. In all cases, the time delay tolerance is smallest when there is a LOS component present, and the angle of arrival is in the same direction as the direction of motion. This causes the fastest decorrelation of the channel.

To our knowledge, a performance analysis of a switched diversity system utilizing an ACM scheme has not yet been reported in the literature. Paper A may be viewed as an attempt to fill this gap.

Paper B

Bengt Holter and Geir E. Øien, "Impact of spatial correlation on adaptive coded modulation performance in Rayleigh fading," *submitted to IEEE Transactions on Vehicular Technology*.

In Paper B, a performance analysis of an ACM scheme operating on a SIMO system with identically distributed and spatially correlated Rayleigh fading channels is presented. PSAM is employed for channel estimation and channel prediction, and MRC is used to combine signals from H receiver antennas. Rate adaptation is performed by providing the transmitter with CSI as *predicted* by the receiver. Numerical examples are provided for the case of Jakes fading spectrum and MAP-optimal predictor coefficients. As such, Paper B represents an extension of [32, Ch. 3] and [35] by taking spatial correlation into account.

In [32, Ch. 3] and [35], an important part of the analysis is based on the knowledge of the joint distribution of the true and predicted SNR, since the temporal correlation between these two entities is a vital parameter affecting the error performance. In particular, for uncorrelated Rayleigh fading channels, both the true and the predicted SNR are individually gamma distributed. As a result, the joint distribution is a bivariate gamma distribution. However, for spatially correlated channels, neither the true nor the predicted SNR will be gamma distributed. In fact, their true densities do not belong to any standard distribution, so the joint distribution needed to quantify the correlation is not known.

In Paper B, this is alleviated by approximating the true and the predicted SNR to be gamma distributed RVs with first and second order moments identical to those of the exact distribution. It is demonstrated that by using this approach, the same type of analysis as in [32, Ch. 3] and [35] may be pursued with good accuracy for both low and medium SNR values. The SNR range must however be upper limited, since the gamma distribu-

tion does not contribute to realize the true slope (diversity order) or coding gain of the error rate curve at high SNR. The valid SNR range is determined by comparing results for the error rate curves obtained with the true (non-gamma) PDF and the approximate (gamma) PDF under idealized assumptions (perfect channel knowledge, perfect CSI, and zero delay on the feedback channel). It is argued that the imposed SNR upper limit does not represent a major limitation of the work, since at high SNR, only the largest available signal constellation will be used. In this case, the system resembles a fixed rate system, for which the effects of channel correlation is well known and well documented in the literature (see for instance [8, Sec. 9.6]).

Spatial/temporal separability is assumed, i.e. the normalized cross correlation between complex fading envelopes on different branches is represented as a product of the individual spatial and temporal correlations. Under this assumption, the temporal correlation coefficient between the true and predicted SNR is shown to be identical to the one obtained for uncorrelated channels in [32, Ch. 3] and [35]. According to [40], spatial/temporal separability of the cross correlation function is adequate for gauging average system behavior.

For a given set of SNR thresholds/fading bins, it is concluded that spatial correlation has a significant impact on the BER performance, by reducing "the acceptable BER" region, where the system operates reliably with respect to average SNR and permitted time delay on the feedback channel. However, when the system operates below the target BER (acceptable region), the performance degradation in terms of ASE caused by spatial correlation is not large.

Paper C

Bengt Holter, Geir E. Øien, Kjell J. Hole, and Henrik Holm, "Limitations in spectral efficiency of a rate-adaptive MIMO system utilizing pilot-aided channel prediction," in *Proc. Vehicular Technology Conference*, Jeju, Korea, April 2003.

In Paper C, the rate-adaptive SIMO system in [32, Ch. 3] and [35] is extended to a MIMO system. In particular, a MIMO *diversity* system is considered, in which case orthogonal STBC is used at the transmitter to maximize the diversity order [14]. For such a MIMO system, performance merits can be obtained by following the same analysis approach as in [32, Ch. 3] and [35]. PSAM is used for channel estimation and channel prediction, but since multiple transmit antennas are introduced, the channel estimation task is different from a SIMO system. Identical pilot symbols can not be transmit-

ted simultaneously from all the transmit antennas, since the received signal on each branch will then be a combination of channel responses.

Hence, in order to estimate all the channels, the pilot symbol can only be transmitted by a single antenna at a time [12, Sec. VB].⁹ As a result, sampling of the channel with PSAM is performed by letting the pilot symbol alternate between the transmit antennas.

An obvious disadvantage of this channel estimation technique is that more time is spent on transmitting pilot-symbols, which contributes to reduce the ASE compared to a SIMO system with the same set of available codes, the same SNR thresholds, and the same pilot symbol period. Another factor contributing to reduce the ASE is that the code rate of an orthogonal STBC based on a complex signal constellation is less than one when more than two transmit antennas are employed [13].

Based on these facts, it is concluded that the ASE of the considered MIMO diversity system is upper bounded, for a given pilot period L , by the ASE of the SIMO system in [32, Ch. 3] and [35]. Apart from that, it is observed that the acceptable BER region is very similar for SIMO and MIMO systems having the same diversity order.

Unfortunately, the original published version of Paper C contains some misprints and some minor errors in the numerical results. These have been corrected in Paper C. For the sake of clarity, a list of the corrected misprints and some comments to Paper C are provided:

- All the performance results in Paper C are *numerical* results. Hence, the word *simulation*, which is used several times in the original paper [41], is misleading and have been replaced by the word *numerical* in Paper C.
- In [41], the pilot symbol spacing on a single branch L_b is written as $L_b = (1/R_s)m \cdot n_T + n_T$. This is not wrong, but it is applicable only to the orthogonal designs G_2 , G_4 , and H_3 . In Paper C, it has been replaced by the more general expression $L_b = (1/R_s)m \cdot K + n_T$
- The numerical results depicted in Fig. 4 and 5 in [41] are obtained by using the pilot symbol spacing L on the input of the space-time encoder. However, prior to transmission, the distance between pilot-symbols is increased to L_b on each branch. Hence, instead of $L = 7$, the results should have been derived with $L_b = 8$ and $L_b = 11$, respectively. In Paper C, these results have been corrected. Since the changes from L to L_b in these cases are very small, the new results are not far from the original ones in [41].

⁹In [12, Sec. VB], it is argued that simultaneous transmission of pilot-symbols may be used in a MISO system if orthogonal pilot symbols are employed.

-
- In [41, Fig. 6], the relative differences in ASE between a 1×4 , 2×2 , and a 3×3 system are depicted for various pilot symbol spacings L at the input of the space-time encoder. For the 2×2 system, the STBC G_2 is employed, while for the 3×3 system, the STBC H_3 is employed. This information has been added to the figure caption of Figure C.6 in Paper C. The ASE is almost independent of the feedback delay when the normalized delay is in the region $0 - 0.25$, but due to space limitations, this is not reflected in [41]. As a result, the ASE obtained for a normalized time delay of 0.25 (depicted in Figure C.6), is almost identical to the result obtained with zero time delay. However, it is emphasized here that the ASE results depicted in Figure C.6 are meaningful only for the CSNR/delay combinations where the target BER constraint is fulfilled in the Figures C.3, C.4, and C.5.
 - In the third paragraph of Section 3 (SIMO channel model), there is a misprint. The overall expected CSNR has been corrected from γ to $\bar{\gamma}$ in Paper C.
 - In the numerical results, the spectral efficiencies $\{R_n\}_{n=1}^N$ are derived for $G = 2$ (as employed in [7, 32]). The use of $G = 2$ is not explicitly mentioned in [41], but included in Paper C.
 - In [41, Eq. (5)], a subindex n is missing. In Paper C, it has been corrected to $\text{BER}_n \approx a_n \cdot e^{-\frac{b_n \gamma}{M_n}}$.
 - In [41, Eq. (6)], there are two misprints. In Paper C, the following corrections have been made. Firstly, the sign \cong is changed into an equality. Secondly, the condition $\gamma \leq \gamma_n^l$ is changed to $\gamma < \gamma_n^l$.
 - For consistency, the notation of the normalized complementary incomplete gamma function has been changed from $Q(x, y)$ to $\bar{\Gamma}(x, y)$ to avoid confusion with the generalized first order Marcum-Q function.
 - Finally, it is noted that since the pilot symbols are transmitted on one branch at a time, it is assumed that each such symbol is transmitted with the total available power.

Paper D

Bengt Holter and Geir E. Øien, "On the amount of fading in MIMO diversity systems," *accepted for publication in IEEE Transactions on Wireless Communications*.

For wireless systems using spatial diversity combining techniques to reduce the impact of fading, it is of interest to employ measures which can capture and quantify the performance improvement related to a reduced fading level. The average error rate is typically used, in which case a potential improvement is quantified through a slope change and/or a horizontal shift of the error rate curve relative to a benchmark curve at high SNR. However, the exact error rate may in some cases be difficult to evaluate analytically, since it requires statistical averaging of the conditional error rate with a particular fading distribution. A more simple yet effective way of quantifying the severity of fading can be obtained by using a measure directly related to the moments of the fading distribution itself. One such measure is the *amount of fading* (AF) [42], defined as the variance of the squared fading amplitude divided by the squared mean. As such, the AF is related to the kurtosis, which is a measure of the peakedness of a distribution. The higher the kurtosis, the lower the concentration of the density function around its mean. It takes its minimum value for deterministic variables. In particular, the AF is equal to the kurtosis minus 1 [43].

In [42], the AF was introduced to quantify the severity of fading experienced at the output of a SISO system when different channel fading models were applied. In particular, for the Nakagami- m fading model, $AF = 1/m$ for $m \geq 1/2$. Hence, as the Nakagami- m fading parameter increases, the AF decreases. In the limit, as $m \rightarrow \infty$, the Nakagami- m fading channel converges to a nonfading AWGN channel with $AF = 0$. In [8, Ch. 2], expressions for the AF in a SISO system are presented for a wide variety of fading distributions.

In contrast to a SISO system, the AF is in Paper D employed to quantify the degree of fading experienced at the output of a MIMO diversity system. A closed-form expression is presented when the system operates on identically distributed spatially correlated Nakagami- m fading channels. With the assumption of independent correlation properties at the transmitter and the receiver, the AF is presented for identically distributed Rayleigh fading channels and different types of correlation models. By capitalizing on recent results in [44], it is shown that for a constant correlation model, the average symbol error probability at the output of a MIMO diversity system at high SNR may be expressed in terms of the AF.

Paper E

Bengt Holter, Mohamed-Slim Alouini, Geir E. Øien and Hong-Chuan Yang, "Multiuser switched diversity transmission," in *Proc. Vehicular Technology Conference*, Los Angeles, USA, September 2004.

In a multiuser system, multiuser diversity may be exploited to maximize the average system throughput by always serving the user with the best channel. A traditional way of performing this task in a time-division multiplexed system is to let the BS probe all the users and select the user which reports the best channel quality at any given time-slot. This method yields the best ASE for a given target BER, but it comes at the expense of a high and deterministic *feedback load* (number of users the BS has to probe before one user is given access to the channel).

The key observation utilized in Paper E is that algorithms originally devised to select between antennas in a spatial diversity system may also be applied as multiuser access schemes. The reasoning behind this argument is that a system exploiting multiuser diversity may be looked upon as a traditional spatial diversity system, in which the antennas of the spatial diversity combiner (acting as a BS) have been replaced by users, each having a single antenna. As a result, a multiuser access scheme based on always serving the user with the strongest channel is equivalent to SC. The feedback load of SC is deterministic and equal to the total number of users connected to the BS. In an attempt to simplify the selection procedure and reduce the feedback load, a set of *switched* multiuser access schemes are proposed. The new access schemes are all based on *switched* diversity algorithms originally devised to select between antennas in a spatial diversity system, and the basic principle is to look for an *acceptable* user rather looking for the ultimate best user. A user qualifies as an acceptable user and is selected by the BS when the reported channel quality is above a predefined switching threshold.

The ACM scheme in [7] is utilized on each selected link to ensure a high ASE of the system. For simplicity, i.i.d. Rayleigh fading channels across the different users are assumed, and the individual users and the BS are all equipped with just a single antenna. Perfect channel knowledge is assumed at both the BS and the users.

Numerical results quantifying the trade-off between ASE and *average* feedback load (AFL) are presented, using the access scheme based on SC as a benchmark. It is concluded that the proposed access schemes can contribute to reduce the AFL significantly without experiencing a big performance loss. In addition, it is argued that the switched access schemes are quite attractive also from a fairness perspective.

For Paper E, the following comments are in order:

- one may argue that with a fixed guard time, the benefit of using a switched access scheme is lost, since the BS or the selected terminal anyway has to wait until the guard period is finished before transmission of data can commence. As a result, since the entire guard time period is used, all the users could have been asked for their channel status. However, with the proposed switched access schemes, all the terminals may operate in a sleep mode or power saving mode as long as they do not transmit data or respond to a call from the BS. This leads to significant power savings compared to the benchmark scheme where each terminal must power up and report their channel status in every time slot. In addition, less traffic is generated in the system, since on average, just a small percentage of the users need to report their channel status for each time slot. Both these gains come at the expense of a small reduction in ASE.

Main contributions of the thesis

As a summary, this section states the main contributions of the thesis.

- A performance analysis of an ACM scheme in a SIMO system using a dual-branch switched diversity combiner at the receiver is presented. To our knowledge, this has not yet been reported in the literature.
- A performance analysis of an ACM scheme in a SIMO system with an MRC receiver operating on identically distributed but *spatially correlated* Rayleigh fading channels is presented.
- A performance analysis of an ACM scheme in a MIMO diversity system is presented. The reduction in ASE incurred by using ACM and PSAM in such a system has been quantified.
- The degree of fading mitigating at the output of a MIMO diversity system has been quantified by using a measure called *amount of fading*. In particular, a closed-form expression for the amount of fading is derived for a MIMO diversity system operating on identically distributed and spatially correlated Nakagami- m fading channels. For independent correlation properties at the transmitter and receiver, amount of fading expressions are derived for different antenna correlation models.
- By capitalizing on results in [44], it is shown that for a constant correlation model, the average symbol error probability at the output of a MIMO diversity system at high SNR may be expressed in terms of the amount of fading.

-
- Spatial diversity algorithms originally devised to select between antennas have been utilized as multiuser access schemes in a multiuser system. The proposed access schemes can contribute to reduce the average feedback load significantly compared to systems relying on feedback from all the users, without experiencing a big performance loss.
 - An eigenfilter approach to obtain the optimal weights of an MRC receiver is presented.

Suggestions for further research

In Paper B and C, PSAM is utilized for channel estimation and channel prediction. However, the pilot symbol spacing L is fixed, and the pilot symbols are transmitted with the same power as the data symbols. A natural extension is to include adaptive PSAM, where both L and the power ratio between pilots and data symbols are adaptively optimized to maximize the ASE subject to the constraint $\text{BER} \leq \text{BER}_0$. In addition, imperfect CSI at both the receiver and transmitter should be taken into account. Current research within this area is reported in [45–48].

In Paper C, the focus is on reliable transmission by exploiting multiple antennas at both the transmitter and the receiver to maximize the overall diversity order. A natural extension is to investigate the performance of ACM in a spatial multiplexing system. In addition, only narrowband flat-fading channels have been considered. Orthogonal frequency division multiplexing (OFDM) could be introduced to extend the methods of ACM to wideband transmission. In particular, the combination of OFDM and MIMO is an interesting topic for further research. OFDM can transform a frequency-selective MIMO channel into a set of parallel frequency-flat MIMO channels, as long as the length of the channel impulse response is smaller than or equal to the cyclic prefix (CP) length. As such, narrowband spatial multiplexing receivers can be applied on a tone-by-tone basis [49]. STBC can also be combined with OFDM transmission, achieving spatial diversity gains over frequency-selective fading channels. Then, STBC is applied on adjacent blocks of data symbols (OFDM symbols) rather than on individual data symbols.

Finally, an interesting topic for further research within the context of adaptive MIMO systems is to apply reconfigurable antenna arrays. Recall that in multiple-antenna channels, the channel capacity grows linearly with the number of spatial degrees of freedom. However, as noted in [50], packing more antennas in a given area will just make the fading correlated, so

increasing the number of antennas within a confined space cannot increase the capacity indefinitely. With the advent of RF MEMS¹⁰ [51], a class of new components which display superior high-frequency performance relative to conventional semiconductor devices can be used to implement reconfigurable antenna arrays [52]. A reconfigurable antenna array can adapt its geometrical size by changing the antenna element spacing using MEMS switches [53]. As such, the number of spatial degrees of freedom can be adapted to the current needs. For instance, beamforming requires closely spaced antennas to avoid grating lobes, while spatial diversity techniques for diversity maximization will perform well if the antennas are sufficiently separated to ensure low correlation. Hence, a reconfigurable antenna array represents additional degrees of freedom in an adaptive MIMO system.

¹⁰Micro-Electro-Mechanical Systems

References

- [1] J. F. Hayes, "Adaptive feedback communications," *IEEE Transactions on Communication Technology*, vol. COM-16, pp. 29–34, February 1968.
- [2] J. K. Cavers, "Variable-rate transmission for Rayleigh fading channels," *IEEE Transactions on Communications*, vol. COM-20, no. 1, pp. 15–22, February 1972.
- [3] W. T. Webb and R. Steele, "Variable-rate QAM for mobile radio," *IEEE Transactions on Communications*, vol. 43, no. 7, pp. 2223–2230, July 1995.
- [4] A. J. Goldsmith and S. -G. Chua, "Variable-rate variable-power M-QAM for fading channels," *IEEE Transactions on Communications*, vol. 45, no. 10, pp. 1218–1230, October 1997.
- [5] M. -S. Alouini and A. J. Goldsmith, "Adaptive modulation over Nakagami fading channels," *Wireless Personal Communications*, vol. 13, pp. 119–143, May 2000.
- [6] A. J. Goldsmith and S. -G. Chua, "Adaptive coded modulation for flat fading channels," *IEEE Transactions on Communications*, vol. 46, no. 5, pp. 595–602, May 1998.
- [7] K. J. Hole, H. Holm, and G. E. Øien, "Adaptive multidimensional coded modulation on flat fading channels," *IEEE Journal on Selected Areas in Communications*, vol. 18, no. 7, pp. 1153–1158, July 2000.
- [8] M. K. Simon and M. -S. Alouini, *Digital Communications over Fading Channels: A Unified Approach to Performance Analysis*. New York: Wiley, 2000.
- [9] G. L. Stüber, *Principles of Mobile Communications*. Second edition, Kluwer Academic Publishers, 2001.

- [10] M. Nakagami, "The m -distribution, a general formula of intensity distribution of rapid fading," *Statistical Methods in Radio Wave Propagation*, pp. 3–36, June 1960.
- [11] I. S. Gradshteyn and I. M. Ryzhik, *Table of Integrals, Series, and Products*. 5th ed., San Diego, CA: Academic Press, 1994.
- [12] S. M. Alamouti, "A simple transmit diversity technique for wireless communications," *IEEE Journal on Selected Areas in Communications*, vol. 16, no. 8, pp. 1451–1458, October 1998.
- [13] V. Tarokh, H. Jafarkhani, and A. R. Calderbank, "Space-time block codes from orthogonal designs," *IEEE Transactions on Information Theory*, vol. 45, no. 5, pp. 1456–1467, July 1999.
- [14] R. W. Heath, "Space-time signaling in multi-antenna systems," Ph.D. dissertation, Stanford University, November 2001.
- [15] G. J. Foschini and M. J. Gans, "On limits of wireless communications in a fading environment when using multiple antennas," *Wireless Personal Communications*, vol. 6, pp. 311–335, March 1998.
- [16] B. Holter, "On the capacity of the MIMO channel - a tutorial introduction." in *Proc. IEEE Norwegian Symposium on Signal Processing*, pp. 167–172, October 2001.
- [17] D. Gesbert, M. Shafi, D. S. Shiu, P. J. Smith, and A. Naguib, "From theory to practice: an overview of MIMO space-time coded wireless systems," *IEEE Journal on Selected Areas in Communications*, vol. 21, no. 3, pp. 281–302, April 2003.
- [18] S. Sandhu and A. Paulraj, "Space-time block codes: a capacity perspective," *IEEE Communications Letters*, vol. 4, no. 12, pp. 384–386, December 2000.
- [19] D. G. Brennan, "Linear diversity combining techniques," in *Proc. IRE*, vol. 47, pp. 1075–1102, 1959.
- [20] S. Haykin, *Adaptive Filter Theory*. Prentice-Hall, Inc., 2002.
- [21] B. Holter and G. E. Øien, "The optimal weights of a maximum ratio combiner using an eigenfilter approach," in *Proc. 5th IEEE Nordic Signal Processing Symposium*, October 2002.

-
- [22] R. Knopp and P. A. Humblet, "Information capacity and power control in single cell multiuser communications," in *Proc. IEEE International Conference on Communications*, vol. 1, pp. 331–335, June 1995.
- [23] P. Viswanath, D. N. C. Tse, and R. Laroia, "Opportunistic beamforming using dumb antennas," *IEEE Transactions on Information Theory*, vol. 48, no. 6, pp. 1277–1294, June 2002.
- [24] D. N. C. Tse and S. V. Hanly, "Multiaccess fading channels - part I: Polymatroid structure, optimal resource allocation and throughput capacities," *IEEE Transactions on Information Theory*, vol. 44, no. 7, pp. 2796–2815, November 1998.
- [25] L. Li and A. J. Goldsmith, "Capacity and optimal resource allocation for fading broadcast channels - part I: Ergodic capacity," *IEEE Transactions on Information Theory*, vol. 47, no. 3, pp. 1083–1102, March 2001.
- [26] D. Gesbert and M. -S. Alouini, "How much feedback is multi-user diversity really worth ?" in *Proc. IEEE International Conference on Communications*, pp. 234–238, June 2004.
- [27] L. Yang, M. -S. Alouini, and D. Gesbert, "Further results on selective multi-user diversity," in *Proc. Seventh ACM/IEEE International Symposium on Modeling, Analysis and Simulation of Wireless and Mobile Systems*, October 2004.
- [28] H. Koubaa, V. Hassel, and G. E. Øien, "Multiuser diversity gain enhancement by guard time reduction," *Temporary Document TD(05)-038, 12th Management Committee Meeting, COST Action 273 Towards Mobile Multimedia Broadband Networks*, January 2005.
- [29] V. Hassel, M. -S. Alouini, D. Gesbert, and G. E. Øien, "Minimizing feedback load for nested scheduling algorithms," *accepted for publication in Proc. IEEE Vehicular Technology Conference*, May 2005.
- [30] R. Gozali, R. M. Buehrer, and B. D. Woerner, "The impact of multiuser diversity on space-time block coding," *IEEE Communications Letters*, vol. 7, no. 5, pp. 213–215, May 2003.
- [31] E. G. Larsson, "On the combination of spatial diversity and multiuser diversity," *IEEE Communications Letters*, vol. 8, no. 8, pp. 517–519, August 2004.

- [32] H. Holm, "Adaptive coded modulation and channel estimation tools for flat fading channels," Ph.D. dissertation, The Norwegian University of Science and Technology, April 2002 (available at: <http://www.tele.ntnu.no/projects/beats/theses.htm>).
- [33] K. J. Hole, H. Holm, and G. E. Øien, "Analysis of adaptive coded modulation with antenna diversity and feedback delay," in *Proc. IST Mobile Communications Summit*, pp. 865–870, September 2001.
- [34] —, "Performance analysis of adaptive coded modulation with antenna diversity and feedback delay," *Teletronikk*, vol. 98, no. 1, pp. 106–113, 2002.
- [35] G. E. Øien, H. Holm, and K. J. Hole, "Impact of channel prediction on adaptive coded modulation performance in Rayleigh fading," *IEEE Transactions on Vehicular Technology*, vol. 53, no. 3, pp. 758–769, May 2004.
- [36] J. K. Cavers, "An analysis of pilot symbol assisted modulation for Rayleigh fading channels," *IEEE Transactions on Vehicular Technology*, vol. 40, no. 4, pp. 686–693, November 1991.
- [37] J. M. Torrance and L. Hanzo, "Comparative study of pilot symbol assisted modulation schemes," in *Proc. IEE Sixth International Conference on Radio Receivers and Associated Systems*, no. 415, pp. 36–41, September 1995.
- [38] S. Haykin, *Communication Systems*. John Wiley & Sons, Inc., 1994.
- [39] G. E. Øien and K. J. Hole, "Maximum average spectral efficiency of slowly varying Rayleigh fading channels with pilot-symbol-assisted channel estimation," in *Proc. European Personal Mobile Communications Conference*, February 2001.
- [40] P. J. Smith and M. Shafi, "The impact of complexity in MIMO channel models," in *Proc. IEEE International Conference on Communications*, vol. 5, pp. 2924–2928, June 2004.
- [41] B. Holter, G. E. Øien, K. J. Hole, and H. Holm, "Limitations in spectral efficiency of a rate-adaptive MIMO system utilizing pilot-aided channel prediction," in *Proc. Vehicular Technology Conference*, vol. 1, pp. 282–286, April 2003.

-
- [42] U. Charash, "Reception through Nakagami fading multipath channels with random delays," *IEEE Transactions on Communications*, vol. COM-27, no. 4, pp. 657–670, April 1979.
- [43] S. Verdú, "Spectral efficiency in the wideband regime," *IEEE Transactions on Information Theory*, vol. 48, no. 6, pp. 1319–1343, June 2002.
- [44] Z. Wang and G. B. Giannakis, "A simple and general parameterization quantifying performance in fading channels," *IEEE Transactions on Communications*, vol. 51, no. 8, pp. 1389–1398, August 2003.
- [45] D. V. Duong and G. E. Øien, "Adaptive trellis-coded modulation with imperfect channel state information at the receiver and transmitter," in *Proc. Nordic Radio Symposium*, August 2004.
- [46] D. V. Duong, G. E. Øien, and K. J. Hole, "Adaptive coded modulation with receive antenna diversity and imperfect channel knowledge at receiver and transmitter," *Temporary Document TD(05)-009, 12th Management Committee Meeting, COST Action 273 Towards Mobile Multimedia Broadband Networks*, January 2005.
- [47] D. V. Duong, B. Holter, and G. E. Øien, "Optimal pilot spacing and power in rate-adaptive MIMO diversity systems with imperfect transmitter CSI," *submitted to the VI IEEE Workshop on Signal Processing Advances in Wireless Communications*, 2005.
- [48] X. Cai and G. B. Giannakis, "Adaptive PSAM accounting for channel estimation and prediction errors," *IEEE Transactions on Wireless Communications*, vol. 4, no. 1, pp. 246–256, January 2005.
- [49] H. Bölcskei, D. Gesbert, and A. J. Paulraj, "On the capacity of OFDM-based spatial multiplexing systems," *IEEE Transactions on Communications*, vol. 50, no. 2, pp. 225–234, February 2002.
- [50] A. S. Y. Poon, R. W. Brodersen, and D. N. C. Tse, "Degrees of freedom in multiple-antenna channels: A signal space approach," *IEEE Transactions on Information Theory*, vol. 51, no. 2, pp. 523–536, February 2005.
- [51] M. Sadiku, "MEMS," *IEEE Potentials*, vol. 21, no. 1, pp. 4–5, February 2002.
- [52] B. A. Centiner, H. Jafarkhani, J. -Y. Qian, H. J. Yoo, A. Grau, and F. D. Flaviis, "Multifunctional reconfigurable MEMS integrated anten-

nas for adaptive MIMO systems," *IEEE Communications Magazine*, vol. 42, no. 12, pp. 62–70, December 2004.

- [53] E. R. Brown, "RF-MEMS switches for reconfigurable integrated circuits," *IEEE Transactions on Microwave Theory*, vol. 46, no. 11, pp. 1868–1880, November 1998.

Part II

Included papers

Paper A

**Performance Analysis of a
Rate-Adaptive Dual-Branch
Switched Diversity System**

Bengt Holter and Geir E. Øien

Submitted to
IEEE Transactions on Wireless Communications

Abstract

In this paper, a performance analysis of a dual-branch switched diversity system operating on identically distributed Nakagami- m fading channels is presented. An adaptive coded modulation (ACM) scheme is employed to increase the spectral efficiency of the system. The ACM scheme consists of a set of multidimensional trellis codes originally designed for additive white Gaussian noise channels, where the codes are based on quadrature amplitude modulation (QAM) signal constellations of varying size. The performance is evaluated by assuming perfect channel knowledge at the receiver and instantaneous-/time-delayed feedback of channel state information, conveyed from the receiver to the transmitter on a zero-error feedback channel. Both uncorrelated and correlated antenna branches are considered. The optimal switching threshold in terms of maximizing the average spectral efficiency is identified in the case of uncorrelated antenna branches.

1 Introduction

Adaptive coded modulation (ACM) is an efficient transmission scheme to simultaneously achieve both high spectral efficiency and a low bit-error rate (BER) in a wireless communication system. The basic principle is to utilize channel state information (CSI) conveyed from the receiver to the transmitter to adapt to changing channel conditions by transmitting with high information rates under favorable channel conditions, and reducing the information rate in response to channel degradation. In [1, 2], a method for assessing performance merits of an ACM system is employed to evaluate the average spectral efficiency (ASE) of a rate-adaptive coding scheme utilizing a set of multidimensional trellis codes originally designed for additive white Gaussian noise (AWGN) channels. The analysis is based on a single-input multiple-output (SIMO) channel model with statistically independent and identically distributed (i.i.d.) Rayleigh fading channels. Perfect coherent detection is assumed and maximum ratio combining (MRC) is employed to maximize the received signal-to-noise ratio (SNR). The MRC receiver is frequently used in the literature for analysis purposes as a benchmark receiver, since it represents the optimal (in a maximum SNR sense) diversity scheme in the absence of interference.¹ However, it also represents the diversity scheme with the highest complexity, since it requires continuous monitoring of all channel fading parameters and a separate receiver chain for all the branches. As a result, less complex diversity schemes are typically used in practice. Our motivation for the present paper is to investigate the performance loss incurred by using a simpler combining technique than MRC.

A less complex diversity scheme than MRC is selection combining (SC). An SC combiner continuously monitors the channel state on all the diversity branches, but instead of using the information provided by all the branches, only the best branch is selected for further processing. Hence, it requires just a single receiver chain for its implementation. However, since all the branches must be monitored in order to be able to pick the best branch at any time, the SC combiner is often approximated by an even simpler *switched diversity* combiner. In this case, the receiver is not always connected to the best branch, but is connected to a particular branch as long as the received SNR of that branch do not drop below a predetermined threshold. When the SNR drops below the threshold, the receiver simply switches to another branch. As a result, the receiver at any time only needs to mon-

¹When interference is present, the optimal combining scheme is denoted an optimum combiner, maximizing the instantaneous received signal-to-interference plus noise ratio (SINR) [3], [4, Ch. 10].

itor the channel state of the currently selected branch. This contributes to reduce the complexity in comparison to the SC combiner, but it comes at the expense of a certain performance loss.²

Several strategies regarding how to select a new branch when the SNR drops below the selected threshold have been reported in the literature. For simplicity, the receiver may simply switch to the next branch and stick with it regardless of its actual fading condition. This switching technique is commonly denoted *switch-and-stay combining* (SSC) [5]. The receiver may also choose to examine the potential switch-to branch before switching takes place, to ensure a certain degree of branch quality. This switching technique is commonly denoted *switch-and-examine combining* (SEC) [6]. In [6], it was shown that SEC performance improves with additional branches in general, whereas the performance of multibranch SSC for equicorrelated and identically distributed channels is the same as for the dual-branch case. In particular, for the dual-branch case, SSC and SEC represent identical switching strategies.

In [7], a discrete-time model using a SSC strategy was introduced to develop a performance analysis of a dual-branch switched diversity system, using noncoherent frequency shift keying operating on independent Rayleigh channels. The analysis in [7] was later extended to include a Nakagami- m fading model [8]. In [9], a slightly different switching strategy than [7] was presented for both uncorrelated and correlated branches, leading to closed-form solutions for the optimal switching thresholds in a minimum probability of error sense. Building on the framework developed in [7, 9] and [10], an extensive performance analysis of a dual-branch switched diversity system was presented in [5], deriving new generic and exact analytical results for the performance of SSC when used in conjunction with several M-ary signal constellations. Recently, the analysis in [5] was extended to a multibranch switched diversity system, covering both SSC and SEC switching strategies [6]. Additional work, specifically related to the performance of dual-branch switched diversity receivers can be found in [11–16].

All the referenced papers on switched diversity limit their studies to systems using only a single fixed signal constellation. Indeed, to our knowledge, a performance analysis of a switched diversity system utilizing an ACM scheme has not yet been reported in the literature. However, this is of practical interest, since the introduction of some diversity in the system

²To avoid switching during data transmission, switched diversity schemes are typically implemented in a discrete-time fashion. Channel estimation and switching to an alternative diversity branch are done periodically during a guard period between two consecutive time slots.

will lower the probability of the deep fades for which channel prediction, necessary for the use of ACM, becomes too unreliable. In an attempt to fill this gap, and building on the framework presented in [1, 2], a performance analysis of an ACM scheme is therefore presented in this paper, with a dual-branch switched diversity combiner being used at the receiver.

The remainder of this paper is organized as follows. Section 2 presents the system and channel model. In Section 3, the ASE and BER analysis is presented, assuming uncorrelated antenna branches. Note that the analysis principles in Section 3 in general are applicable to any fading distribution, but the versatile Nakagami- m fading model is used as an example [17]. In Section 4, the optimal switching threshold in terms of maximizing the ASE is derived. ASE and average BER expressions for dual-branch MRC and SC receivers are presented in Section 5, since these are used as benchmark receivers in this paper. In Section 6, the effect of branch correlation is taken into account. Note that in contrast to Section 3, the results presented in Section 6 are only valid for the Nakagami- m fading model. In Section 7, the impact of time-delayed feedback is investigated, and results for the average BER are presented for both uncorrelated and correlated antenna branches. Numerical results are presented in Section 8, and the main results of the paper are summarized in Section 9.

2 System and channel model

A single user dual-branch SIMO system operating on two i.i.d. Nakagami- m fading channels is considered. The transmission rate on the wireless link is adaptively adjusted by utilizing a rate-adaptive coding scheme, using a set of N multidimensional trellis codes originally designed for AWGN channels. The codes are based on quadrature amplitude modulation (QAM) signal constellations with different number of symbols $M_n = 2^{k_n}$, where k_n is some positive integer. Rate adaptation is performed by splitting the received SNR range into $N + 1$ fading regions (bins) as depicted in Figure A.1.

The set $\{\gamma_n\}_{n=1}^N$ contains the lower thresholds of the N fading regions, selected such that a target BER—denoted BER_0 —is achieved for each available code in the rate-adaptive scheme. Let γ_{SSC} denote the SNR per symbol at the output of the SSC combiner, and let γ_T denote the predetermined switching threshold. When γ_{SSC} falls within fading region n ($\gamma_n \leq \gamma_{\text{SSC}} < \gamma_{n+1}$), the associated CSI, i.e. the fading region index n , is sent back to the transmitter through a dedicated feedback channel.³ Based on the reported

³Note that for $n = N$, $\gamma_{N+1} = \infty$.

CSI, the transmitter then adapts its transmission rate according to the quality of the channel, by transmitting with a signal constellation realizing a spectral efficiency of R_n . If $0 \leq \gamma_{ssc} < \gamma_1$, no information is transmitted (outage). In the subsequent analysis, as in [18], the following two idealized assumptions are employed: (1) the receiver has perfect channel knowledge, and (2) the feedback channel is zero-error. Initially, no time delay will be assumed on the feedback channel, but this constraint is relaxed later on in the paper.

For i.i.d. channels, the probability density function (PDF) of the output SNR of a dual-branch SSC combiner may in general be written as [5]

$$p_{\gamma_{ssc}}(\gamma) = \begin{cases} P_{\gamma}(\gamma_T) \cdot p_{\gamma}(\gamma) & \gamma < \gamma_T \\ (1 + P_{\gamma}(\gamma_T)) \cdot p_{\gamma}(\gamma) & \gamma \geq \gamma_T \end{cases} \quad (\text{A.1})$$

where $p_{\gamma}(\gamma)$ and $P_{\gamma}(\gamma)$ are the PDF and the cumulative distribution function (CDF) of the output SNR per symbol γ for a single branch receiver, respectively. In Table A.1, expressions for the PDF and CDF are presented for the Nakagami- m fading model, where $\bar{\gamma}$ represents the average SNR on a single channel, $\beta = \bar{\gamma}/m$, $\Gamma(\cdot)$ is the gamma function [19, Sec. 8.31], and $\Gamma(\cdot, \cdot)$ is the complementary incomplete gamma function [19, Sec. 8.35].

3 ASE and BER analysis

The ASE of the system⁴ is obtained as a weighted sum of the spectral efficiencies of each individual code, where the weight factor P_n for code n is equal to the probability that this code is used, i.e. the probability that the SNR falls into fading bin n :

$$\text{ASE} = \sum_{n=1}^N R_n \cdot P_n = \sum_{n=1}^N R_n \cdot \int_{\gamma_n}^{\gamma_{n+1}} p_{\gamma_{ssc}}(\gamma) d\gamma. \quad (\text{A.2})$$

The average BER (averaged over all codes and all SNRs) is given as the average number of bits in error, divided by the average number of bits transmitted [2]:

$$\overline{\text{BER}} = \frac{\sum_{n=1}^N R_n \cdot \overline{\text{BER}}_n}{\sum_{n=1}^N R_n \cdot P_n}, \quad (\text{A.3})$$

where $\overline{\text{BER}}_n$ is the average BER experienced when code n is applied. An expression for $\overline{\text{BER}}_n$ is obtained by utilizing the exponential approximation

⁴Measured in bits/s/Hz [1, 2].

$\text{BER}_n = a_n \cdot e^{-b_n \gamma / M_n}$ for the BER-SNR relationship for varying γ [1]:

$$\overline{\text{BER}}_n = \int_{\gamma_n}^{\gamma_{n+1}} a_n \cdot e^{-\frac{b_n \gamma}{M_n}} p_{\gamma_{\text{SSC}}}(\gamma) d\gamma, \quad (\text{A.4})$$

where a_n and b_n are code-dependent constants, found by least-square fitting to simulated data on AWGN channels. Note that the expression for BER_n is invertible, so the lower threshold of each fading region in Figure A.1 required to achieve BER_0 can be identified as $\gamma_n = (M_n/b_n) \ln(a_n/\text{BER}_0)$. Values for a_n , b_n , M_n , and γ_n are summarized in Table A.2 for the target $\text{BER}_0 = 10^{-4}$ and $N = 8$ (the number of codes used in the numerical examples in Section 8).

Inserting (A.1) into (A.2) and restricting γ_T to be larger than γ_1 , P_n may in general be divided into three parts.⁵

$$P_n = \begin{cases} P_n^{\text{left}} & = \mathcal{I}(n) \cdot P_\gamma(\gamma_T) & \gamma_{n+1} < \gamma_T \\ P_n^{\text{in}} & = \mathcal{I}_{\gamma_T}(n) + P_n^{\text{left}} & \gamma_n < \gamma_T \leq \gamma_{n+1} \\ P_n^{\text{right}} & = \mathcal{I}(n) + P_n^{\text{left}} & \gamma_T \leq \gamma_n \end{cases}, \quad (\text{A.5})$$

where $\mathcal{I}(n) = \int_{\gamma_n}^{\gamma_{n+1}} p_\gamma(\gamma) d\gamma$ and $\mathcal{I}_{\gamma_T}(n) = \int_{\gamma_T}^{\gamma_{n+1}} p_\gamma(\gamma) d\gamma$.

The superscripts in (A.5) are introduced to distinguish between the different expressions for P_n , depending on the placement of γ_T on the SNR axis in Figure A.1. For the fading bins located to the left of γ_T , $P_n = P_n^{\text{left}}$. For the fading bin containing γ_T , $P_n = P_n^{\text{in}}$. For the fading bins located to the right of γ_T , $P_n = P_n^{\text{right}}$. The results in (A.5) are applicable to any fading distribution, but when applying the one-branch PDF and CDF of a Nakagami- m fading channel summarized in Table A.1, the following results for P_n^{left} , $\mathcal{I}(n)$, and $\mathcal{I}_{\gamma_T}(n)$ are obtained:

$$\begin{aligned} P_n^{\text{left}} &= \mathcal{I}(n) \cdot (1 - \bar{\Gamma}(m, \gamma_T/\beta)), \\ \mathcal{I}(n) &= \bar{\Gamma}(m, \gamma_n/\beta) - \bar{\Gamma}(m, \gamma_{n+1}/\beta), \\ \mathcal{I}_{\gamma_T}(n) &= \bar{\Gamma}(m, \gamma_T/\beta) - \bar{\Gamma}(m, \gamma_{n+1}/\beta), \end{aligned}$$

where $\bar{\Gamma}(x, y) = \Gamma(x, y)/\Gamma(x)$ is the normalized complementary incomplete gamma function.

Inserting (A.1) into (A.4), $\overline{\text{BER}}_n$ too will have three different solutions based on the placement of γ_T . Using the same notation rules as introduced

⁵For simplicity, γ_T is restricted not to reside within the interval range $0 \leq \gamma < \gamma_1$ (outage region).

for P_n , the solution can be written as

$$\overline{\text{BER}}_n = \begin{cases} \overline{\text{BER}}_n^{\text{left}} & = \mathcal{J}(n) \cdot P_\gamma(\gamma_T) & \gamma_{n+1} < \gamma_T \\ \overline{\text{BER}}_n^{\text{in}} & = \mathcal{J}_{\gamma_T}(n) + \overline{\text{BER}}_n^{\text{left}} & \gamma_n < \gamma_T \leq \gamma_{n+1} \\ \overline{\text{BER}}_n^{\text{right}} & = \mathcal{J}(n) + \overline{\text{BER}}_n^{\text{left}} & \gamma_T \leq \gamma_n \end{cases}, \quad (\text{A.6})$$

where $\mathcal{J}(n) = \int_{\gamma_n}^{\gamma_{n+1}} a_n e^{-\frac{b_n \gamma}{M_n}} p_\gamma(\gamma) d\gamma$ and $\mathcal{J}_{\gamma_T}(n) = \int_{\gamma_T}^{\gamma_{n+1}} a_n e^{-\frac{b_n \gamma}{M_n}} p_\gamma(\gamma) d\gamma$. For a Nakagami- m fading model, the following results are easily derived:

$$\begin{aligned} \overline{\text{BER}}_n^{\text{left}} &= \mathcal{J}(n) \cdot (1 - \bar{\Gamma}(m, \gamma_T / \beta)), \\ \mathcal{J}(n) &= C_n \cdot (\bar{\Gamma}(m, \mu_n \gamma_n) - \bar{\Gamma}(m, \mu_n \gamma_{n+1})), \\ \mathcal{J}_{\gamma_T}(n) &= C_n \cdot (\bar{\Gamma}(m, \mu_n \gamma_T) - \bar{\Gamma}(m, \mu_n \gamma_{n+1})), \end{aligned}$$

where $C_n = \frac{a_n}{(\beta \mu_n)^m}$ and $\mu_n = (b_n \beta + M_n) / (M_n \beta)$.

In the following, the index $q \in [1, 2, \dots, N]$ will be used to denote the fading bin in which γ_T is placed. For $\gamma_q \leq \gamma_T < \gamma_{q+1}$, the numerator and denominator of (A.3) can be written as

$$\sum_{n=1}^N R_n \cdot \overline{\text{BER}}_n = \begin{cases} R_1 \cdot \overline{\text{BER}}_1^{\text{in}} + \sum_{n=2}^N R_n \cdot \overline{\text{BER}}_n^{\text{right}} & q = 1 \\ \sum_{n=1}^{q-1} R_n \cdot \overline{\text{BER}}_n^{\text{left}} + R_q \cdot \overline{\text{BER}}_q^{\text{in}} \\ + \sum_{n=q+1}^N R_n \cdot \overline{\text{BER}}_n^{\text{right}} & q \in [2, N-1] \\ \sum_{n=1}^{N-1} R_n \cdot \overline{\text{BER}}_n^{\text{left}} + R_N \cdot \overline{\text{BER}}_N^{\text{in}} & q = N \end{cases} \quad (\text{A.7})$$

$$\sum_{n=1}^N R_n \cdot P_n = \begin{cases} R_1 \cdot P_1^{\text{in}} + \sum_{n=2}^N R_n \cdot P_n^{\text{right}} & q = 1 \\ \sum_{n=1}^{q-1} R_n \cdot P_n^{\text{left}} + R_q \cdot P_q^{\text{in}} \\ + \sum_{n=q+1}^N R_n \cdot P_n^{\text{right}} & q \in [2, N-1] \\ \sum_{n=1}^{N-1} R_n \cdot P_n^{\text{left}} + R_N \cdot P_N^{\text{in}} & q = N \end{cases} \quad (\text{A.8})$$

Introducing the notation $\mathcal{A}_1 \triangleq \sum_{n=1}^N R_n \mathcal{I}(n)$, $\mathcal{A}_{q+1} \triangleq \sum_{n=q+1}^N R_n \mathcal{I}(n)$, $\mathcal{B}_1 \triangleq \sum_{n=1}^N R_n \mathcal{J}(n)$, and $\mathcal{B}_{q+1} \triangleq \sum_{n=q+1}^N R_n \mathcal{J}(n)$, the average BER can in general

be expressed as

$$\overline{\text{BER}} = \frac{P_\gamma(\gamma_T)\mathcal{B}_1 + R_q\mathcal{J}_{\gamma_T}(q) + \mathcal{B}_{q+1}}{P_\gamma(\gamma_T)\mathcal{A}_1 + R_q\mathcal{I}_{\gamma_T}(q) + \mathcal{A}_{q+1}}, \quad (\text{A.9})$$

where $\mathcal{A}_{q+1} = \mathcal{B}_{q+1} = 0$ for $q = N$. Written explicitly in terms of γ_T , when assuming the system to be operating on i.i.d. Nakagami- m fading channels, the ASE and average BER is equal to

$$\text{ASE} = (R_q - \mathcal{A}_1)\bar{\Gamma}(m, \gamma_T/\beta) + \mathcal{T}_q, \quad (\text{A.10})$$

and

$$\overline{\text{BER}} = \frac{R_q\mathcal{C}_q\bar{\Gamma}(m, \mu_q\gamma_T) - \mathcal{B}_1\bar{\Gamma}(m, \gamma_T/\beta) + \mathcal{S}_q}{(R_q - \mathcal{A}_1)\bar{\Gamma}(m, \gamma_T/\beta) + \mathcal{T}_q}, \quad (\text{A.11})$$

respectively, where $\mathcal{S}_q = \mathcal{B}_1 + \mathcal{B}_{q+1} - R_q\mathcal{C}_q\bar{\Gamma}(m, \mu_q\gamma_{q+1})$ and $\mathcal{T}_q = \mathcal{A}_1 + \mathcal{A}_{q+1} - R_q\bar{\Gamma}(m, \gamma_{q+1}/\beta)$. Note that the ASE and the average BER essentially are functions of q , γ_T , $\bar{\gamma}$, and m .

4 Maximizing the ASE

In this section, the switching threshold γ_T that maximizes the ASE within a single fading bin q is determined, by assuming that $\bar{\gamma}$ and m are fixed. Then, based on this result, the optimal fading bin q^* and the associated optimal threshold γ_T^* , maximizing the ASE over all fading bins, is determined. Since the ASE is a key performance measure only when the system is operating at acceptable BER levels, the optimization of (A.10) can formally be defined as an optimization problem with a side constraint: *maximize* ASE *subject to* $\text{BER} \leq \text{BER}_0$.

However, since $\text{BER} \leq \text{BER}_0$ is used as a design criteria to obtain the thresholds $\{\gamma_n\}_{n=1}^N$, both the instantaneous and the average BER are guaranteed to be lower than or equal to BER_0 as long as perfect channel knowledge is assumed [18]. Hence, the side constraint is already introduced, and the ASE in (A.10) may be optimized as if it represented an unconstrained optimization problem. The partial derivative of (A.10) with respect to γ_T is equal to

$$\frac{\partial \text{ASE}}{\partial \gamma_T} = -(R_q - \mathcal{A}_1) \cdot \mathcal{G}_{\gamma_T}(m, \beta), \quad (\text{A.12})$$

where $\mathcal{G}_{\gamma_T}(m, \beta) = \frac{\gamma_T^{m-1} e^{-\gamma_T/\beta}}{\beta^m \Gamma(m)}$. Since $\mathcal{G}_{\gamma_T}(m, \beta) > 0$ for $1/2 \leq m \leq 4$, $\bar{\gamma} \geq 0$ dB, and $0 < \gamma_T < \infty$, the derivative has the following properties when $\gamma_q \leq \gamma_T < \gamma_{q+1}$: (1) monotonically decreasing if $R_q - \mathcal{A}_1 > 0$, which

implies $\gamma_T = \gamma_q$ (2) monotonically increasing if $R_q - \mathcal{A}_1 < 0$, which implies $\gamma_T = \gamma_{q+1}$. Hence, γ_T maximizing the ASE within bin q is one of the two fading bin endpoints. In Figure A.2, $R_q - \mathcal{A}_1$ is depicted as function of $\bar{\gamma}$, $m = 1$, and $q = [1, 2, \dots, 7]$. It is observed that $R_q - \mathcal{A}_1$ is positive at low average SNR and negative at high average SNR. Hence, $\gamma_T = \gamma_q$ for low average SNR, and $\gamma_T = \gamma_{q+1}$ for high average SNR. The switching point between these two solutions, denoted $\bar{\gamma}^*$, can be determined from the equality condition $R_q = \mathcal{A}_1$.⁶ Using Newton's method, $\bar{\gamma}^*$ can be determined by means of the recursion

$$\bar{\gamma}^*(i+1) = \bar{\gamma}^*(i) + \frac{R_q - \mathcal{A}_1}{\sum_{n=1}^N R_n \left(\frac{\gamma_n}{\bar{\gamma}^*(i)} \mathcal{G}_{\gamma_n}(m, \beta_i) - \frac{\gamma_{n+1}}{\bar{\gamma}^*(i)} \mathcal{G}_{\gamma_{n+1}}(m, \beta_i) \right)}, \quad (\text{A.13})$$

where $i = 0, 1, \dots$, $\beta_i = \bar{\gamma}^*(i)/m$, and $\mathcal{I}(n) = \bar{\Gamma}(m, \gamma_n/\beta_i) - \bar{\Gamma}(m, \gamma_{n+1}/\beta_i)$ is used to obtain \mathcal{A}_1 . The initial value $\bar{\gamma}^*(0)$ can be selected as γ_1 . Knowing that the set of thresholds maximizing the ASE within bin q is limited to either γ_q or γ_{q+1} , the optimal threshold γ_T^* , maximizing the ASE among all fading bins, is derived as follows:

$$\gamma_T^* = \gamma_{q^*} \quad \text{where} \quad q^* = \arg \max_{\gamma_T = \{\gamma_q\}_{q=1}^N} \text{ASE}. \quad (\text{A.14})$$

In Figure A.4, γ_T^* is depicted as a function of $\bar{\gamma}$ for $m = \{1, 2, 4\}$.

5 Comparison with MRC and SC

This section contains analytical expressions for the ASE and average BER for the benchmark diversity receivers used in this paper, namely the dual-branch MRC receiver and the dual-branch SC receiver. Spatially uncorrelated channels are assumed. The PDF of the output SNR of an SC receiver operating on two i.i.d. fading channels may in general be written as $p_{\gamma_{sc}}(\gamma) = 2p_\gamma(\gamma)P_\gamma(\gamma)$ [4, Eq. (6.28)]. Inserting $p_{\gamma_{sc}}(\gamma)$ into (A.2), and with the aid of Table A.1, the ASE for SC operating on Nakagami- m fading channels is equal to

$$\text{ASE} = \sum_{n=1}^N R_n \cdot \left([1 - \bar{\Gamma}(m, \gamma_{n+1}/\beta)]^2 - [1 - \bar{\Gamma}(m, \gamma_n/\beta)]^2 \right). \quad (\text{A.15})$$

⁶When $\bar{\gamma} = \bar{\gamma}^*$, (A.12) is equal to zero, and any value for γ_T within the range $\gamma_q \leq \gamma_T < \gamma_{q+1}$ will in fact maximize the ASE.

For integer m values, a closed-form expression for the average BER with SC can then be derived with the aid of (2.5) in Appendix 2:

$$\overline{\text{BER}} = \frac{\sum_{n=1}^N R_n \cdot 2 \left[\mathcal{J}(n) - \frac{a_n}{(\beta v_n)^m \Gamma(m)} \sum_{k=0}^{m-1} \frac{\Gamma(\alpha, v_n \gamma_n) - \Gamma(\alpha, v_n \gamma_{n+1})}{k! (\beta v_n)^k} \right]}{\sum_{n=1}^N R_n \cdot \left([1 - \bar{\Gamma}(m, \gamma_{n+1}/\beta)]^2 - [1 - \bar{\Gamma}(m, \gamma_n/\beta)]^2 \right)}, \quad (\text{A.16})$$

where $\alpha = m + k$ and $v_n = \frac{2}{\beta} + \frac{b_n}{M_n}$. For i.i.d. Rayleigh fading channels (i.e. $m = 1$), the average BER can also be expressed compactly as

$$\overline{\text{BER}} = \frac{\sum_{n=1}^N R_n \cdot 2a_n \cdot [B(x_{n+1}; 2, y_n) - B(x_n; 2, y_n)]}{\sum_{n=1}^N R_n \cdot (x_{n+1}^2 - x_n^2)}, \quad (\text{A.17})$$

where $x_n = 1 - e^{-\gamma_n/\bar{\gamma}}$, $y_n = 1 + b_n \bar{\gamma}/M_n$, and $B(\cdot; \cdot, \cdot)$ denotes the incomplete beta function [20].

For an MRC receiver operating on two i.i.d. Nakagami- m fading channels, the PDF of the output SNR is given by $p_{\gamma_{\text{mrc}}}(\gamma) = \mathcal{G}_\gamma(2m, \beta)$. Inserting $p_{\gamma_{\text{mrc}}}(\gamma)$ into (A.2) and (A.4), the following ASE and average BER expressions are obtained for the MRC case:

$$\text{ASE} = \sum_{n=1}^N R_n \cdot (\bar{\Gamma}(2m, \gamma_n/\beta) - \bar{\Gamma}(2m, \gamma_{n+1}/\beta)), \quad (\text{A.18})$$

$$\overline{\text{BER}} = \frac{\sum_{n=1}^N R_n \cdot \left(\frac{a_n}{(\beta \mu_n)^{2m}} (\bar{\Gamma}(2m, \mu_n \gamma_n) - \bar{\Gamma}(2m, \mu_n \gamma_{n+1})) \right)}{\sum_{n=1}^N R_n \cdot (\bar{\Gamma}(2m, \gamma_n/\beta) - \bar{\Gamma}(2m, \gamma_{n+1}/\beta))}. \quad (\text{A.19})$$

6 Impact of branch correlation

In this section, the impact of branch correlation is considered. Spatial correlation between the antenna branches may arise e.g. from insufficient antenna spacing in small-size terminals. For identically distributed but spatially correlated Nakagami- m fading channels, the PDF of the output SNR may be written as [9]

$$p_{\gamma_{\text{ssc}}}(\gamma) = \begin{cases} \mathcal{G}_\gamma(m, \beta) \cdot (1 - Q_m(\alpha_s \sqrt{\gamma}, \beta_s)) & \gamma \leq \gamma_T \\ \mathcal{G}_\gamma(m, \beta) \cdot (2 - Q_m(\alpha_s \sqrt{\gamma}, \beta_s)) & \gamma > \gamma_T \end{cases}, \quad (\text{A.20})$$

where $\mathcal{G}_\gamma(m, \beta) = p_\gamma(\gamma)$ in Table A.1, $Q_m(\cdot, \cdot)$ is the generalized Marcum-Q function (see Appendix 1), $\alpha_s = \sqrt{\frac{2\rho_s}{(1-\rho_s)\beta}}$, $\beta_s = \sqrt{\frac{2\gamma_T}{(1-\rho_s)\beta}}$, and ρ_s denotes the normalized spatial power correlation coefficient. Using the same type

of analysis as presented for uncorrelated branches in Section 3, the equivalent representation of P_n in (A.5), but valid for correlated branches, is

$$P_{n,\rho_s} = \begin{cases} P_{n,\rho_s}^{\text{left}} &= \mathcal{I}(n) - \mathcal{I}_{\rho_s}(n) & \gamma_{n+1} < \gamma_T \\ P_{n,\rho_s}^{\text{in}} &= \mathcal{I}_{\gamma_T}(n) + P_{n,\rho_s}^{\text{left}} & \gamma_n < \gamma_T \leq \gamma_{n+1} \\ P_{n,\rho_s}^{\text{right}} &= \mathcal{I}(n) + P_{n,\rho_s}^{\text{left}} & \gamma_T \leq \gamma_n \end{cases}, \quad (\text{A.21})$$

where $\mathcal{I}_{\rho_s}(n) = \int_{\gamma_n}^{\gamma_{n+1}} \mathcal{G}_\gamma(m, \beta) Q_m(\alpha_s \sqrt{\gamma}, \beta_s) d\gamma$. We can solve $\mathcal{I}_{\rho_s}(n)$ in terms of an infinite sum with the aid of (2.4) in Appendix 2:

$$\begin{aligned} \mathcal{I}_{\rho_s}(n) &= \frac{(1 - \rho_s)^m}{\Gamma(m)} \sum_{i=0}^{\infty} \frac{\rho_s^i}{i!} \Gamma(m + i, \beta_s^2/2) \\ &\times (\bar{\Gamma}(m + i, \mu_s \gamma_n) - \bar{\Gamma}(m + i, \mu_s \gamma_{n+1})), \end{aligned} \quad (\text{A.22})$$

where $\mu_s = \frac{1}{(1 - \rho_s)\beta}$. For a Rayleigh fading model, $\mathcal{I}_{\rho_s}(n)$ can be solved in closed form with the aid of (2.2) in Appendix 2:

$$\begin{aligned} \mathcal{I}_{\rho_s}(n) &= e^{-\gamma_n/\bar{\gamma}} Q_1(\alpha_s \sqrt{\gamma_n}, \beta_s) - e^{-\gamma_{n+1}/\bar{\gamma}} Q_1(\alpha_s \sqrt{\gamma_{n+1}}, \beta_s) \\ &+ e^{-\gamma_T/\bar{\gamma}} \left[Q_1\left(\sqrt{2\mu_s \gamma_{n+1}}, \frac{\alpha_s \beta_s}{\sqrt{2\mu_s}}\right) \right. \\ &\left. - Q_1\left(\sqrt{2\mu_s \gamma_n}, \frac{\alpha_s \beta_s}{\sqrt{2\mu_s}}\right) \right], \end{aligned} \quad (\text{A.23})$$

assuming $m = 1$ in μ_s , α_s , and β_s .

Defining the integral $\mathcal{J}_{\rho_s}(n) = \int_{\gamma_n}^{\gamma_{n+1}} a_n e^{-\frac{b_n \gamma}{M_n}} \mathcal{G}_\gamma(m, \beta) Q_m(\alpha_s \sqrt{\gamma}, \beta_s) d\gamma$, the equivalent representation of $\overline{\text{BER}}_n$ in (A.6), valid for correlated branches, is now equal to

$$\overline{\text{BER}}_{n,\rho_s} = \begin{cases} \overline{\text{BER}}_{n,\rho_s}^{\text{left}} &= \mathcal{J}(n) - \mathcal{J}_{\rho_s}(n) & \gamma_{n+1} < \gamma_T \\ \overline{\text{BER}}_{n,\rho_s}^{\text{in}} &= \mathcal{J}_{\gamma_T}(n) + \overline{\text{BER}}_{n,\rho_s}^{\text{left}} & \gamma_n < \gamma_T \leq \gamma_{n+1} \\ \overline{\text{BER}}_{n,\rho_s}^{\text{right}} &= \mathcal{J}(n) + \overline{\text{BER}}_{n,\rho_s}^{\text{left}} & \gamma_T \leq \gamma_n \end{cases}. \quad (\text{A.24})$$

Once again applying (2.4) in Appendix 2, $\mathcal{J}_{\rho_s}(n)$ can be written as

$$\begin{aligned} \mathcal{J}_{\rho_s}(n) &= \frac{a_n}{(\omega_n \beta)^m \Gamma(m)} \sum_{i=0}^{\infty} \frac{\alpha_s^{2i}}{2^i i!} \frac{\Gamma(m + i, \beta_s^2/2)}{\omega_n^i} \\ &\times [\bar{\Gamma}(m + i, \omega_n \gamma_n) - \bar{\Gamma}(m + i, \omega_n \gamma_{n+1})], \end{aligned} \quad (\text{A.25})$$

where $\omega_n = \mu_n + \alpha_s^2/2$. For a Rayleigh fading model, $\mathcal{J}_{\rho_s}(n)$ can also be expressed in closed form by applying (2.2) in Appendix 2:

$$\begin{aligned} \mathcal{J}_{\rho_s}(n) &= \frac{a_n}{\bar{\gamma}\mu_n} \left[e^{-\mu_n\gamma_n} Q_1(\alpha_s\sqrt{\gamma_n}, \beta_s) - e^{-\mu_n\gamma_{n+1}} Q_1(\alpha_s\sqrt{\gamma_{n+1}}, \beta_s) \right. \\ &\quad + e^{-\frac{\mu_n\beta_s^2}{2\gamma_n}} \left(Q_1\left(\sqrt{2\omega_n\gamma_{n+1}}, \frac{\alpha_s\beta_s}{\sqrt{2\omega_n}}\right) \right. \\ &\quad \left. \left. - Q_1\left(\sqrt{2\omega_n\gamma_n}, \frac{\alpha_s\beta_s}{\sqrt{2\omega_n}}\right) \right) \right], \end{aligned} \quad (\text{A.26})$$

assuming $m = 1$ in μ_n , α_s , and β_s . Defining $\mathcal{A}_{1,\rho_s} \triangleq \sum_{n=1}^N R_n(\mathcal{I}(n) - \mathcal{I}_{\rho_s}(n))$ and $\mathcal{B}_{1,\rho_s} \triangleq \sum_{n=1}^N R_n(\mathcal{J}(n) - \mathcal{J}_{\rho_s}(n))$, the overall BER may finally be expressed as⁷

$$\overline{\text{BER}} = \frac{\mathcal{B}_{1,\rho_s} + R_q \mathcal{J}_{\gamma_T}(q) + \mathcal{B}_{q+1}}{\mathcal{A}_{1,\rho_s} + R_q \mathcal{I}_{\gamma_T}(q) + \mathcal{A}_{q+1}}, \quad (\text{A.27})$$

7 Impact of time delay

So far, it has been assumed that the CSI has been conveyed to the transmitter on an zero-error feedback channel with no time delay (instantaneous feedback). In practice however, there will always be a non-zero time delay. Due to channel fluctuations, the CSI provided to the transmitter may therefore be regarded as imperfect by the time it is used to select an appropriate code. In this section, we adopt the approach in [18] to study how a non-zero time delay on the feedback channel will affect the performance of the proposed rate-adaptive system when operating on two identically distributed Nakagami- m fading channels. Denoting the instantaneous output SNR per symbol at times t and $t + \tau$ by γ_{ssc} and $\gamma_{ssc,\tau}$ respectively, the temporal correlation ρ_t between γ_{ssc} and $\gamma_{ssc,\tau}$ can be related solely to the time delay τ , and viewed as a measure of how fast the channel is changing while the CSI is conveyed back to the transmitter on the feedback channel.

Note that the ASE of the system will not be affected by the time delay, since it is assumed that the CSI, i.e. the fading region index n , is identified at the receiver. The selected code n will then be used regardless of whether the channel has changed state or not during the time delay τ . The average BER however will be affected, since the time delay may lead to a mismatch between the selected code and the actual state of the channel. If the BER

⁷(A.27) reduces to (A.9) for $\rho_s = 0$, since $\mathcal{I}_{\rho_s}(n)|_{\rho_s=0} = \bar{\Gamma}(m, \gamma_T/\beta) \cdot \mathcal{I}(n)$. Then $P_{n,\rho_s}^{\text{left}} = P_n^{\text{left}}$, which gives $\mathcal{A}_{1,\rho_s} = P_\gamma(\gamma_T)\mathcal{A}_1$. Likewise, $\mathcal{J}_{\rho_s}(n)|_{\rho_s=0} = \bar{\Gamma}(m, \gamma_T/\beta) \cdot \mathcal{J}(n)$. Then $\overline{\text{BER}}_{n,\rho_s}^{\text{left}} = \overline{\text{BER}}_n^{\text{left}}$, and $\mathcal{B}_{1,\rho_s} = P_\gamma(\gamma_T)\mathcal{B}_1$.

goes higher than BER_0 , the ASE is no longer a meaningful performance measure.

Denoting the time delayed version of $\overline{\text{BER}}_n$ as $\overline{\text{BER}}_{n,\rho_t}$, we can write [18]

$$\begin{aligned} \overline{\text{BER}}_{n,\rho_t} &= \int_{\gamma_n}^{\gamma_{n+1}} \int_0^\infty a_n \cdot e^{-\frac{b_n \gamma_{\text{SSC},\tau}}{M_n}} \\ &\times p_{\gamma_{\text{SSC},\tau}|\gamma_{\text{SSC}}}(\gamma_{\text{SSC},\tau}|\gamma_{\text{SSC}}) d\gamma_{\text{SSC},\tau} p_{\gamma_{\text{SSC}}}(\gamma) d\gamma, \end{aligned} \quad (\text{A.28})$$

where $p_{\gamma_{\text{SSC},\tau}|\gamma_{\text{SSC}}}(\gamma_{\text{SSC},\tau}|\gamma_{\text{SSC}})$ is the PDF of $\gamma_{\text{SSC},\tau}$ conditioned on γ_{SSC} . However, at a fixed moment in time, the instantaneous output SNR of the SSC combiner is identical to the instantaneous SNR of a single branch receiver, i.e. $\gamma_{\text{SSC}} = \gamma$. Hence, $\gamma_{\text{SSC},\tau} = \gamma_\tau$, and (A.28) may be rewritten as

$$\overline{\text{BER}}_{n,\rho_t} = \int_{\gamma_n}^{\gamma_{n+1}} \int_0^\infty a_n \cdot e^{-\frac{b_n \gamma_\tau}{M_n}} p_{\gamma_\tau|\gamma}(\gamma_\tau|\gamma) d\gamma_\tau p_{\gamma_{\text{SSC}}}(\gamma) d\gamma. \quad (\text{A.29})$$

Naturally, γ and γ_τ will be correlated. Assuming that the system operates on slowly-varying channels, in the sense that the average SNR $\bar{\gamma}$ remains constant over the time delay τ (i.e., $\mathcal{E}\{\gamma\} = \mathcal{E}\{\gamma_\tau\} = \bar{\gamma}$),⁸ and that the system operates on identically distributed Nakagami- m fading channels, the joint PDF of γ and γ_τ can be described by a bivariate gamma distribution [5]

$$\begin{aligned} p_{\gamma,\gamma_\tau}(\gamma,\gamma_\tau) &= \frac{\gamma^{(m-1)/2} \gamma_\tau^{(m-1)/2}}{\beta^{m+1} (1-\rho_t) \Gamma(m) \rho_t^{(m-1)/2}} e^{-\frac{\gamma+\gamma_\tau}{(1-\rho_t)\beta}} \\ &\times I_{m-1} \left(\frac{2\sqrt{\rho_t \gamma \gamma_\tau}}{(1-\rho_t)\beta} \right), \end{aligned} \quad (\text{A.30})$$

where $I_{m-1}(\cdot)$ is the modified Bessel function of the first kind and order $m-1$ [19], and ρ_t is the normalized temporal correlation coefficient between γ and γ_τ . In a Rayleigh fading environment, isotropic scattering of the multipath components is assumed [21], and ρ_t can be expressed in terms of the time delay τ , the mobile speed v [m/s], and the wavelength λ_c [m] of the carrier frequency as $\rho_t = J_0^2(2\pi f_D \tau)$ [21, Eq. (2.68)], where $J_0(\cdot)$ is the zero-order Bessel function of the first kind [19], and $f_D = v/\lambda_c$ is the maximum Doppler frequency.

For a Nakagami- m fading model with $m > 1$, a line-of-sight (LOS) component is present in the received signal. Considering an isotropic scattering environment with a LOS component, ρ_t can be expressed as $\rho_t = \frac{1}{1+2K} (J_0^2(2\pi f_D \tau) + 2K J_0(2\pi f_D \tau) \cos(2\pi f_D \tau \cos \theta_0))$ [21, Eq. (2.71)], where

⁸ $\mathcal{E}\{\cdot\}$ denotes the statistical average.

$K = \frac{\sqrt{m^2 - m}}{m - \sqrt{m^2 - m}}$, and θ_0 is the angle between the LOS component and the direction of motion [21, Fig. 2.5].⁹ In the following, expressions for $\overline{\text{BER}}_{n,\rho_t}$ are derived for spatially uncorrelated and correlated branches, respectively.

Uncorrelated branches

Using Bayes' rule $p_{\gamma_\tau|\gamma}(\gamma_\tau|\gamma) = p_{\gamma,\gamma_\tau}(\gamma, \gamma_\tau)/p_\gamma(\gamma)$ and inserting (A.1) in (A.29), $\overline{\text{BER}}_{n,\rho_t}$ may be expressed as

$$\overline{\text{BER}}_{n,\rho_t} = \begin{cases} P_\gamma(\gamma_T) \int_{\gamma_n}^{\gamma_{n+1}} \mathcal{F}(\gamma) d\gamma & \gamma < \gamma_T \\ (1 + P_\gamma(\gamma_T)) \int_{\gamma_n}^{\gamma_{n+1}} \mathcal{F}(\gamma) d\gamma & \gamma \geq \gamma_T \end{cases}, \quad (\text{A.31})$$

where $\mathcal{F}(\gamma) = \int_0^\infty a_n e^{-\frac{b_n \gamma_\tau}{M_n}} p_{\gamma,\gamma_\tau}(\gamma, \gamma_\tau) d\gamma_\tau = \frac{a_n \mathcal{D}_n^m}{\beta^m \Gamma(m)} \gamma^{m-1} e^{-g_n \gamma}$, where $\mathcal{D}_n = \frac{M_n}{b_n \beta (1 - \rho_t) + M_n}$, and $g_n = \frac{1 - \mathcal{D}_n \rho_t}{(1 - \rho_t) \beta}$. Inserting $\mathcal{F}(\gamma)$ in (A.31), $\overline{\text{BER}}_{n,\rho_t}$ can be divided into three parts as follows:

$$\overline{\text{BER}}_{n,\rho_t} = \begin{cases} \overline{\text{BER}}_{n,\rho_t}^{\text{left}} & = \mathcal{J}_{\rho_t}(n) \cdot P_\gamma(\gamma_T) & \gamma_{n+1} < \gamma_T \\ \overline{\text{BER}}_{n,\rho_t}^{\text{in}} & = \mathcal{J}_{\gamma_T, \rho_t}(n) + \overline{\text{BER}}_{n,\rho_t}^{\text{left}} & \gamma_n < \gamma_T \leq \gamma_{n+1} \\ \overline{\text{BER}}_{n,\rho_t}^{\text{right}} & = \mathcal{J}_{\rho_t}(n) + \overline{\text{BER}}_{n,\rho_t}^{\text{left}} & \gamma_T < \gamma_n \end{cases}, \quad (\text{A.32})$$

where $\mathcal{J}_{\rho_t}(n) = \int_{\gamma_n}^{\gamma_{n+1}} \mathcal{F}(\gamma) d\gamma$, and $\mathcal{J}_{\gamma_T, \rho_t}(n) = \int_{\gamma_T}^{\gamma_{n+1}} \mathcal{F}(\gamma) d\gamma$. For a Nakagami- m fading model, we have

$$\begin{aligned} \overline{\text{BER}}_{n,\rho_t}^{\text{left}} &= \mathcal{J}_{\rho_t}(n) \cdot (1 - \bar{\Gamma}(m, \gamma_T / \beta)), \\ \mathcal{J}_{\rho_t}(n) &= \frac{a_n \mathcal{D}_n^m}{(\beta g_n)^m} (\bar{\Gamma}(m, g_n \gamma_n) - \bar{\Gamma}(m, g_n \gamma_{n+1})), \\ \mathcal{J}_{\gamma_T, \rho_t}(n) &= \frac{a_n \mathcal{D}_n^m}{(\beta g_n)^m} (\bar{\Gamma}(m, g_n \gamma_T) - \bar{\Gamma}(m, g_n \gamma_{n+1})). \end{aligned}$$

Using the same approach as in (A.7), and introducing the notation $\mathcal{B}_{1,\rho_t} \triangleq \sum_{n=1}^N R_n \mathcal{J}_{\rho_t}(n)$, and $\mathcal{B}_{q+1,\rho_t} \triangleq \sum_{n=q+1}^N R_n \mathcal{J}_{\rho_t}(n)$, the overall BER can finally be expressed as¹⁰

$$\overline{\text{BER}}_{\rho_t} = \frac{P_\gamma(\gamma_T) \mathcal{B}_{1,\rho_t} + R_q \mathcal{J}_{\gamma_T, \rho_t}(q) + \mathcal{B}_{q+1,\rho_t}}{P_\gamma(\gamma_T) \mathcal{A}_1 + R_q \mathcal{I}_{\gamma_T}(q) + \mathcal{A}_{q+1}}. \quad (\text{A.33})$$

⁹In [18], $\rho_t = J_0^2(2\pi f_D \tau)$ is applied for all $m \in \{1, 2, 4\}$. As a result, the maximum time delay before the target BER is exceeded is not a function of θ_0 [18, Fig. 14/15]. But as shown in the present paper, there are actually some visible performance differences when looking at the two extremes $\theta_0 \in \{0, \pi/2\}$.

¹⁰(A.33) reduces to (A.9) for $\rho_t = 1$, since $\mathcal{D}_n = 1$ and $\lim_{\rho_t \rightarrow 1} g_n = \mu_n$. Then $\overline{\text{BER}}_{n,\rho_t}^{\text{left}} = \overline{\text{BER}}_n^{\text{left}}$, $\mathcal{J}_{\rho_t}(n) = \mathcal{J}(n)$, and $\mathcal{J}_{\gamma_T, \rho_t}(n) = \mathcal{J}_{\gamma_T}(n)$.

Correlated branches

Recall that in the case of correlated branches, our study is limited to the case of identically distributed Nakagami- m fading channels, i.e. $p_\gamma(\gamma) = \mathcal{G}_\gamma(m, \beta)$. For spatially correlated channels, the time delayed version of $\overline{\text{BER}}_n$ is denoted $\overline{\text{BER}}_{n, \rho_t, \rho_s}$. By applying Bayes' rule and inserting (A.20) in (A.29), $\overline{\text{BER}}_{n, \rho_t, \rho_s}$ may be expressed as

$$\overline{\text{BER}}_{n, \rho_t, \rho_s} = \begin{cases} \int_{\gamma_n}^{\gamma_{n+1}} \mathcal{F}(\gamma)(1 - Q_m(\alpha_s \sqrt{\gamma}, \beta_s)) d\gamma & \gamma \leq \gamma_T \\ \int_{\gamma_n}^{\gamma_{n+1}} \mathcal{F}(\gamma)(2 - Q_m(\alpha_s \sqrt{\gamma}, \beta_s)) d\gamma & \gamma > \gamma_T \end{cases}. \quad (\text{A.34})$$

Defining $\mathcal{J}_{\rho_t, \rho_s}(n) = \int_{\gamma_n}^{\gamma_{n+1}} \mathcal{F}(\gamma) Q_m(\alpha_s \sqrt{\gamma}, \beta_s) d\gamma$, $\overline{\text{BER}}_{n, \rho_t, \rho_s}$ may be divided into three parts as follows:

$$\overline{\text{BER}}_{n, \rho_t, \rho_s} = \begin{cases} \overline{\text{BER}}_{n, \rho_t, \rho_s}^{\text{left}} & = \mathcal{J}_{\rho_t}(n) - \mathcal{J}_{\rho_t, \rho_s}(n) & \gamma_{n+1} < \gamma_T \\ \overline{\text{BER}}_{n, \rho_t, \rho_s}^{\text{in}} & = \mathcal{J}_{\gamma_T, \rho_t}(n) + \overline{\text{BER}}_{n, \rho_t, \rho_s}^{\text{left}} & \gamma_n < \gamma_T \leq \gamma_{n+1} \\ \overline{\text{BER}}_{n, \rho_t, \rho_s}^{\text{right}} & = \mathcal{J}_{\rho_t}(n) + \overline{\text{BER}}_{n, \rho_t, \rho_s}^{\text{left}} & \gamma_T < \gamma_n \end{cases}, \quad (\text{A.35})$$

where $\delta_n = g_n + \alpha_s^2/2$. When m is a positive integer,

$$\begin{aligned} \mathcal{J}_{\rho_t, \rho_s}(n) &= \frac{a_n \mathcal{D}_n^m}{(\beta \delta_n)^m \Gamma(m)} \left[\sum_{i=0}^{\infty} \left(1 - \frac{g_n}{\delta_n}\right)^i \right. \\ &\quad \times \bar{\Gamma}(m+i, \beta_s^2/2) (\bar{\Gamma}(m+i, \delta_n \gamma_n) - \bar{\Gamma}(m+i, \delta_n \gamma_{n+1})) \\ &\quad \left. \times \prod_{k=1}^{m-1} (i+k) \right]. \end{aligned} \quad (\text{A.36})$$

For a Rayleigh fading model, $\mathcal{J}_{\rho_t, \rho_s}(n)$ can be written in closed form as

$$\begin{aligned} \mathcal{J}_{\rho_t, \rho_s}(n) &= \frac{a_n \mathcal{D}_n}{\gamma g_n} \left[e^{-g_n \gamma_n} Q_1(\alpha_s \sqrt{\gamma_n}, \beta_s) - e^{-g_n \gamma_{n+1}} Q_1(\alpha_s \sqrt{\gamma_{n+1}}, \beta_s) \right. \\ &\quad + e^{-\frac{g_n \beta_s^2}{2\delta_n}} \left(Q_1\left(\sqrt{2\delta_n \gamma_{n+1}}, \frac{\alpha_s \beta_s}{\sqrt{2\delta_n}}\right) \right. \\ &\quad \left. \left. - Q_1\left(\sqrt{2\delta_n \gamma_n}, \frac{\alpha_s \beta_s}{\sqrt{2\delta_n}}\right) \right) \right], \end{aligned} \quad (\text{A.37})$$

assuming $m = 1$ in g_n , \mathcal{D}_n , α_s , and β_s . Defining $\mathcal{B}_{1,\rho_t,\rho_s} \triangleq \sum_{n=1}^N R_n(\mathcal{J}_{\rho_t}(n) - \mathcal{J}_{\rho_t,\rho_s}(n))$, the overall BER is obtained as¹¹

$$\overline{\text{BER}}_{\rho_t,\rho_s} = \frac{\mathcal{B}_{1,\rho_t,\rho_s} + R_q \mathcal{J}_{\gamma_T,\rho_t}(q) + \mathcal{B}_{q+1,\rho_t}}{\mathcal{A}_{1,\rho_s} + R_q \mathcal{I}_{\gamma_T}(q) + \mathcal{A}_{q+1}} \quad (\text{A.38})$$

Note that ρ_s is assumed to be constant throughout the time delay τ . Hence, spatial and temporal correlation are assumed to be separable so that overall correlation can be represented as a product of the spatial and temporal correlation coefficients [13]. According to [22], this approach is adequate for gauging average system behavior.

8 Numerical results

In this section, some numerical examples of the results derived in this paper are presented for $N = 8$, $\{M_n\}_{n=1}^N = \{4, 8, 16, 32, 64, 128, 256, 512\}$, and $\{R_n\}_{n=1}^N = \{1.5, 2.5, \dots, 8.5\}$.¹² In Figure A.3, the maximum ASE is depicted for different types of diversity combiners when operating on i.i.d. Rayleigh fading channels. For the SSC combiner, the ASE is maximized by employing the optimal switching threshold γ_T^* for each value of $\bar{\gamma}$. As a result, the performance of SSC is close to the performance of both MRC and SC. In Figure A.4, γ_T^* used to generate the SSC curve in Figure A.3 is depicted as a function of $\bar{\gamma}$ and the Nakagami- m fading parameter. It is a stepwise function where the discrete values of γ_T^* are identical to the predefined thresholds $\{\gamma_n\}_{n=1}^N$ of the rate-adaptive scheme. As the Nakagami- m parameter is increased, the stepwise function is shifted to the left, reflecting that an increase in γ_T^* occurs at an earlier stage when the channels become more stable.

In Figure A.5, the average BER is depicted when operating on i.i.d. Nakagami- m fading channels with $m \in \{1, 2\}$. For SSC, results are depicted when γ_T^* is used as switching threshold. The target $\overline{\text{BER}}_0 = 10^{-4}$ is achieved, and the performance is almost identical to MRC and SC at low and medium $\bar{\gamma}$. Note that the diversity advantage of SSC is lost at high $\bar{\gamma}$. The reason is that γ_T^* is not increased beyond γ_N , the highest threshold of the rate-adaptive scheme. Since the instantaneous SNR easily exceeds γ_N

¹¹(A.38) reduces to (A.33) for $\rho_s = 0$, since $Q_m(0, \beta_s) = \bar{\Gamma}(m, \gamma_T/\beta)$ [4, Eq. (4.44)]. Then $\mathcal{J}_{\rho_t,\rho_s}(n) = \bar{\Gamma}(m, \gamma_T/\beta) \mathcal{J}_{\rho_t}(n)$, $\overline{\text{BER}}_{n,\rho_t,\rho_s}^{\text{left}} = \overline{\text{BER}}_{n,\rho_t}^{\text{left}}$, and $\mathcal{B}_{1,\rho_t,\rho_s} = P_\gamma(\gamma_T) \mathcal{B}_{1,\rho_t}$. In addition, $\mathcal{A}_{1,\rho_s} = P_\gamma(\gamma_T) \mathcal{A}_1$.

¹²In this paper, the spectral efficiencies $\{R_n\}_{n=1}^N$ are derived from [2, Eq. (2.2)], using a four-dimensional trellis code ($G = 2$).

when $\bar{\gamma}$ is large, the switching rate between the branches will tend to decrease. When the switching rate is reduced, the SSC receiver approaches a single branch receiver. This effect is reflected in Figure A.5 for SSC at high average SNR, since the average BER curves have slopes equal to one and two for $m = 1$ and $m = 2$, respectively. The slopes are then identical to the average BER slopes of a single branch receiver for $m = 1$ and $m = 2$, respectively.

In Figure A.6 and Figure A.7, the impact of fading correlation is depicted when operating in identically distributed Rayleigh fading channels. The switching threshold γ_T is now chosen to be fixed at $\gamma_T = 17.6$ dB, to illustrate how the performance is affected by not adapting γ_T to $\bar{\gamma}$ on the channels. According to Figure A.4, $\gamma_T = 17.6$ dB maximizes the ASE for spatially uncorrelated channels in the vicinity of $\bar{\gamma} = 20$ dB. Indeed, in Figure A.6, it is observed that the ASE for spatially uncorrelated channels and $\gamma_T = 17.6$ dB is identical to the maximum ASE in this particular SNR region. In addition, it is observed that for $\rho_s = 0.9$, the ASE is reduced, and it approaches the ASE obtained with just a single branch receiver.

From Figure A.7, it is concluded that spatial correlation has not a big impact on the average BER performance. When $\gamma_T = 17.6$ dB, the average BER is almost identical to the result obtained by using $\gamma_T = \gamma_T^*$, except at high $\bar{\gamma}$. At high $\bar{\gamma}$, a relatively low and fixed value of γ_T will not be well adapted to the actual channel quality, and the switching process between the branches will then diminish rather than continue. Since $\gamma_T^* > 17.6$ dB at high $\bar{\gamma}$, it contributes to reduce the average BER level compared to the case of $\gamma_T = 17.6$ dB due to a higher switching rate.

In Figure A.8 and Figure A.9, the impact of time delay on the feedback channel is depicted for spatially uncorrelated and correlated channels, respectively. The average BER performance is presented as a function of the normalized time delay $f_D\tau$ for $\bar{\gamma} = 20$ dB and $\gamma_T = 17.6$ dB. The system is assumed to be operating on identically distributed Nakagami- m fading channels. For $m \in \{2, 4\}$, results are presented for two isotropic scattering models: with and without a LOS component. From Figure A.8, it is observed that a normalized time delay $f_D\tau = 10^{-2}$ can be tolerated without a noticeable degradation in the average BER. The acceptable performance range before the target $\text{BER}_0 = 10^{-4}$ is exceeded is slightly higher for $m > 1$, and it increases with the Nakagami- m parameter. With $f_D\tau = 10^{-2}$ and a 2 GHz carrier frequency, a time delay up to 1.5 ms can be tolerated for pedestrians with a speed of 1 m/s (3.6 km/hr), and a time delay up to 0.05 ms can be tolerated for mobile vehicles with a speed of 30 m/s (108 km/hr).

When comparing the results obtained with the two different scattering

models, worst case performance is obtained with the isotropic model with a LOS component at $\theta_0 = 0$, i.e. the angle of arrival of the LOS component is in the same direction as the direction of motion. This situation causes the fastest decorrelation of the channel. For the model with no LOS component applied in [18], the result is mid-between the two extremes $\theta_0 \in \{0, \pi/2\}$ of the LOS model.

In Figure A.9, it is observed that spatial correlation causes only a minor reduction in the acceptable performance range. In addition, the performance approaches that of a single branch receiver as ρ_s is increased, and impact of spatial correlation as diminishing returns for higher values of the Nakagami- m fading parameter.

9 Conclusion

A performance analysis of a rate-adaptive dual-branch switched diversity system operating on identically distributed Nakagami- m fading channels has been presented. When using the optimal switching threshold, the performance is close to the performance of both MRC and SC in terms of ASE and average BER, at a significantly lower complexity. It has also been shown that in order to maximize the ASE for a given average SNR on the channels, the switching threshold γ_T of the switched diversity receiver must be identical to one of the predefined thresholds of the rate-adaptive scheme.

TABLE A.1: PDF and CDF of the SNR per symbol γ for a single Nakagami- m fading channel

Model	Parameter	PDF ($p_\gamma(\gamma)$)	CDF ($P_\gamma(\gamma)$)
Nakagami- m	$m \geq \frac{1}{2}$	$\frac{\gamma^{m-1} e^{-\gamma/\beta}}{\beta^m \Gamma(m)}$	$1 - \frac{\Gamma(m, \gamma/\beta)}{\Gamma(m)}$

TABLE A.2: Parameters a_n and b_n with thresholds γ_n for $\text{BER}_0 = 10^{-4}$.

n	M_n	a_n	b_n	γ_n [dB]
1	4	188.7471	9.8118	7.7
2	8	288.8051	6.8792	12.4
3	16	161.6898	7.8862	14.6
4	32	142.6920	7.8264	17.6
5	64	126.2118	7.4931	20.8
6	128	121.5189	7.7013	23.7
7	256	79.8360	7.1450	26.9
8	512	34.6128	6.9190	29.7

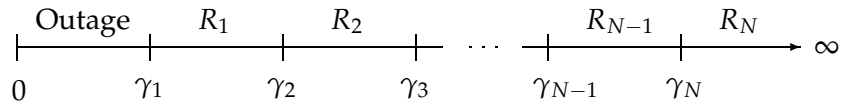


FIGURE A.1: The SNR range is split into $N + 1$ bins. When the instantaneous SNR falls in the lowest interval, an outage occurs; whereas in the upper N intervals, a code with rate R_n is employed.

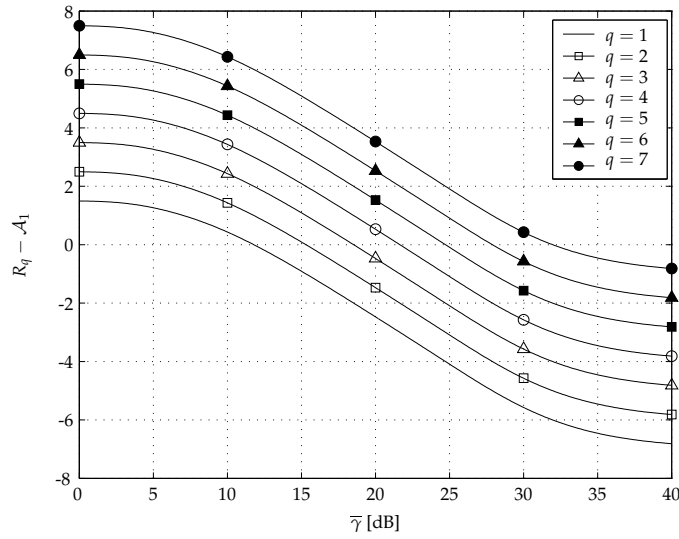


FIGURE A.2: The size of $R_q - \mathcal{A}_1$ for $m = 1$, governing the sign of the gradient in (A.12).

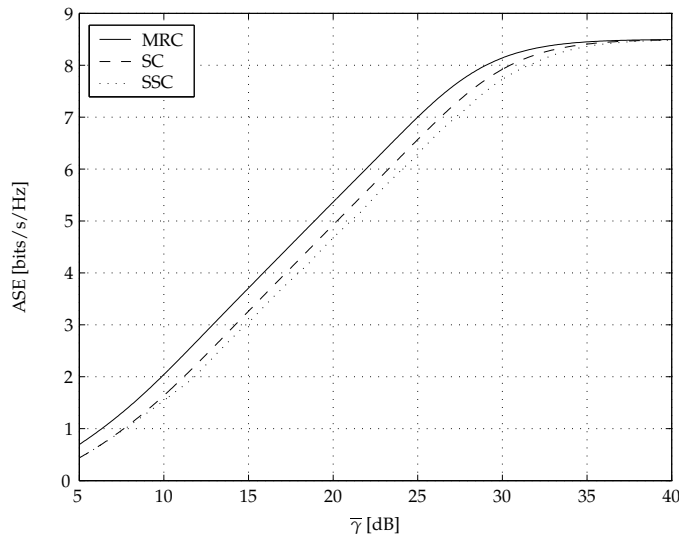


FIGURE A.3: ASE as a function of $\bar{\gamma}$ when operating on i.i.d. Rayleigh fading channels. For SSC, $\gamma_T = \gamma_T^*$ for each value of $\bar{\gamma}$.

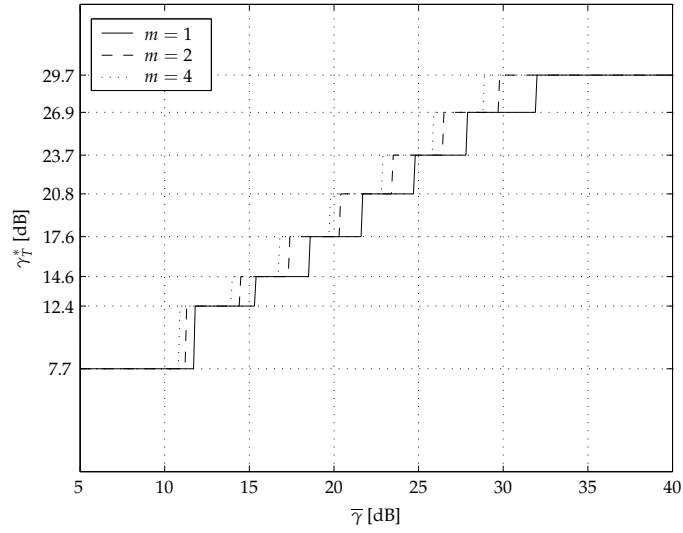


FIGURE A.4: Switching threshold γ_T^* , maximizing the ASE over all fading bins, as a function $\bar{\gamma}$ and the Nakagami- m fading parameter.

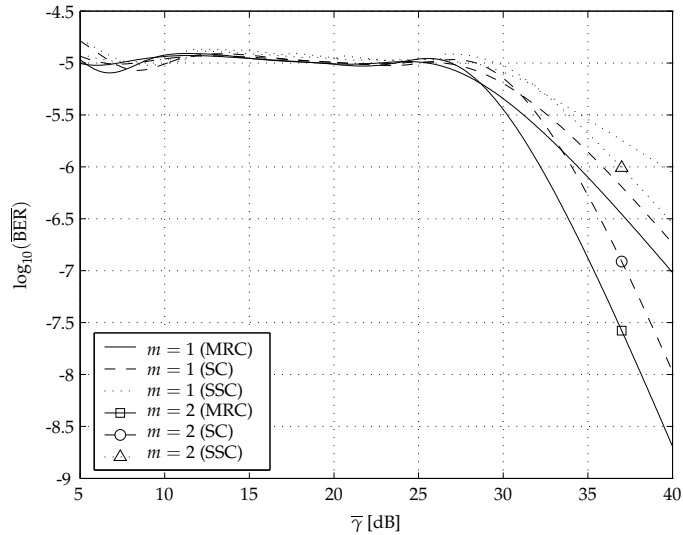


FIGURE A.5: Average BER as a function of $\bar{\gamma}$ and the Nakagami- m fading parameter. For SSC, $\gamma_T = \gamma_T^*$ for each value of $\bar{\gamma}$.

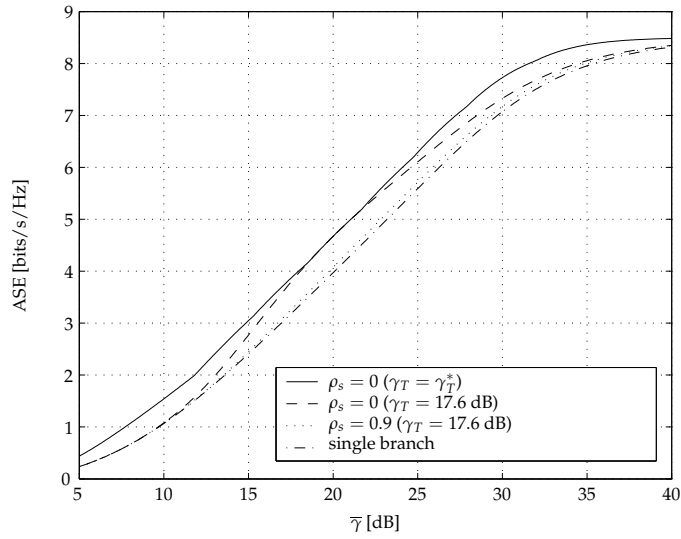


FIGURE A.6: ASE as a function of $\bar{\gamma}$ and ρ_s when operating on identically distributed Rayleigh fading channels. In the single branch case, $\text{ASE} = \mathcal{A}_1$.

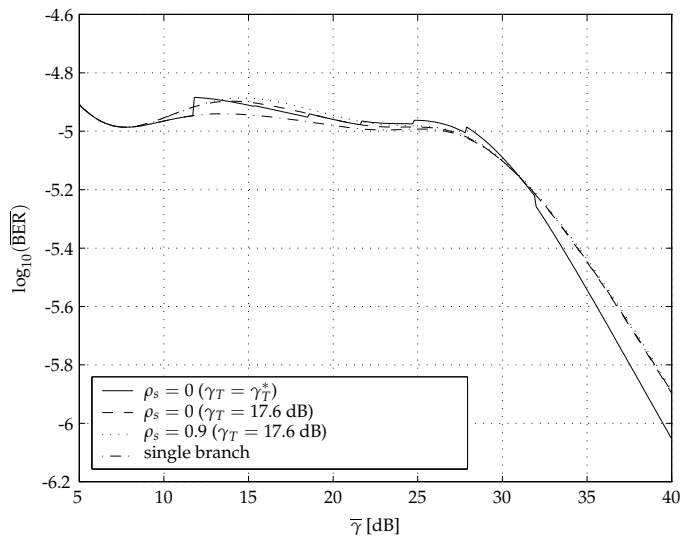


FIGURE A.7: Average BER as a function of $\bar{\gamma}$ and ρ_s when operating on identically distributed Rayleigh fading channels. In the single branch case, $\overline{\text{BER}} = \mathcal{B}_1 / \mathcal{A}_1$.

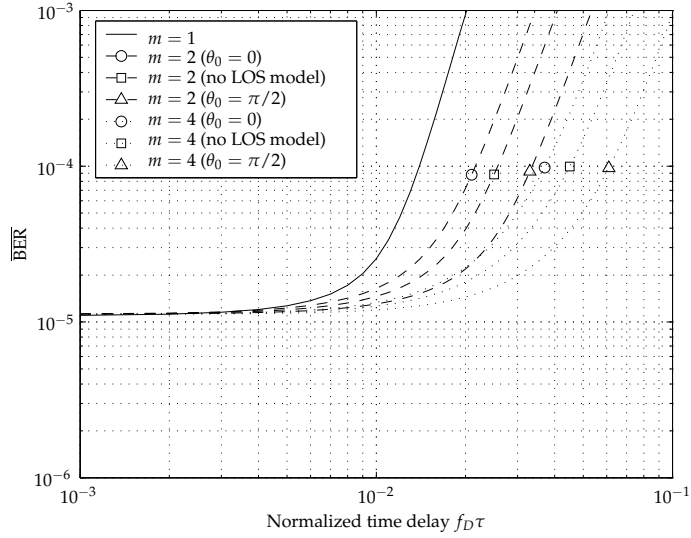


FIGURE A.8: Average BER as a function of normalized time delay $f_D\tau$ and the Nakagami- m fading parameter for $\rho_s = 0$, $\bar{\gamma} = 20$ dB and $\gamma_T = 17.6$ dB.

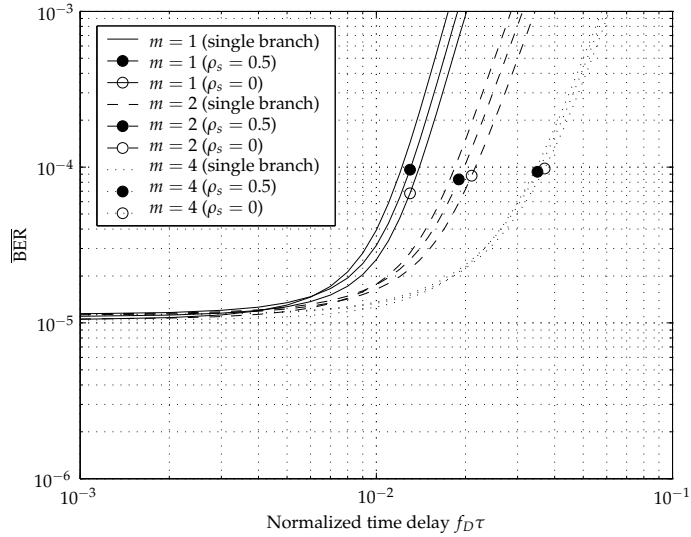


FIGURE A.9: Average BER as a function of normalized time delay $f_D\tau$ for $\rho_s = \{0, 0.5\}$, $\bar{\gamma} = 20$ dB, and $\gamma_T = 17.6$ dB. In all cases where $m \in \{2, 4\}$, the angle of arrival of the LOS component is assumed to be in the direction of motion, i.e. $\theta_0 = 0$. In the single branch case, $\bar{\text{BER}} = \mathcal{B}_{1, \rho_t} / \mathcal{A}_1$.

References

- [1] K. J. Hole, H. Holm, and G. E. Øien, "Adaptive multidimensional coded modulation on flat fading channels," *IEEE Journal on Selected Areas in Communications*, vol. 18, no. 7, pp. 1153–1158, July 2000.
- [2] H. Holm, "Adaptive coded modulation and channel estimation tools for flat fading channels," Ph.D. dissertation, The Norwegian University of Science and Technology, April 2002 (available at: <http://www.tele.ntnu.no/projects/beats/theses.htm>).
- [3] J. H. Winters, "Optimum combining in digital mobile radio with cochannel interference," *IEEE Transactions on Vehicular Technology*, vol. VT-33, no. 3, pp. 144–155, August 1984.
- [4] M. K. Simon and M. -S. Alouini, *Digital Communications over Fading Channels: A Unified Approach to Performance Analysis*. New York: Wiley, 2000.
- [5] Y. -C. Ko, M. -S. Alouini, and M. K. Simon, "Analysis and optimization of switched diversity systems," *IEEE Transactions on Vehicular Technology*, vol. 49, no. 5, pp. 1813–1831, September 2000.
- [6] H. -C. Yang and M. -S. Alouini, "Performance analysis of multibranch switched diversity systems," *IEEE Transactions on Communications*, vol. 51, no. 5, pp. 782–794, May 2003.
- [7] M. Blanco and K. Zdunek, "Performance and optimization of switched diversity systems for detection of signals with Rayleigh fading," *IEEE Transactions on Communications*, vol. COM-27, no. 12, pp. 1887–1895, December 1979.
- [8] M. Blanco, "Diversity receiver performance in Nakagami fading," in *Proc. IEEE Southeastern Conference*, pp. 529–532, April 1983.

- [9] A. A. Abu-Dayya and N. C. Beaulieu, "Analysis of switched diversity systems on generalized-fading channels," *IEEE Transactions on Communications*, vol. 42, no. 11, pp. 2959–2966, November 1994.
- [10] —, "Switched diversity on microcellular Ricean channels," *IEEE Transactions on Vehicular Technology*, vol. 43, no. 4, pp. 970–976, November 1994.
- [11] C. Tellambura, A. Annamalai, and V. K. Bhargava, "Unified analysis of switched diversity systems in independent and correlated fading channels," *IEEE Transactions on Communications*, vol. 49, no. 11, pp. 1955–1965, November 2001.
- [12] L. Yang and M. -S. Alouini, "Average level crossing rate and average outage duration of switched diversity systems," in *Proc. IEEE Global Telecommunications Conference*, vol. 2, pp. 1420–1424, November 2002.
- [13] G. Femenias, "Reference-based dual switch and stay diversity systems over correlated Nakagami fading channels," *IEEE Transactions on Vehicular Technology*, vol. 52, no. 4, pp. 902–918, July 2003.
- [14] N. C. Sagias, D. A. Zogas, G. K. Karagiannidis, and G. S. Tombras, "Performance analysis of switched diversity receivers in Weibull fading," *IEE Electronics Letters*, vol. 39, no. 20, pp. 1472–1473, October 2003.
- [15] —, "Error-rate analysis of switched diversity receivers in Weibull fading," *IEE Electronics Letters*, vol. 40, no. 11, pp. 681–682, May 2004.
- [16] H. -C. Yang and M. -S. Alouini, "Markov chains and performance comparison of switched diversity systems," *IEEE Transactions on Communications*, vol. 52, no. 7, pp. 1113–1125, July 2004.
- [17] M. Nakagami, "The m -distribution, a general formula of intensity distribution of rapid fading," *Statistical Methods in Radio Wave Propagation*, pp. 3–36, June 1960.
- [18] M. S. Alouini and A. J. Goldsmith, "Adaptive modulation over Nakagami fading channels," *Wireless Personal Communications*, vol. 13, pp. 119–143, May 2000.
- [19] I. S. Gradshteyn and I. M. Ryzhik, *Table of Integrals, Series, and Products*. 5th ed., San Diego, CA: Academic Press, 1994.

-
- [20] <http://mathworld.wolfram.com>.
- [21] G. L. Stüber, *Principles of Mobile Communications*. Second edition, Kluwer Academic Publishers, 2001.
- [22] P. J. Smith and M. Shafi, "The impact of complexity in MIMO channel models," in *Proc. IEEE International Conference on Communications*, vol. 5, pp. 2924–2928, June 2004.

Paper B

**Impact of Spatial Correlation
on Adaptive Coded
Modulation Performance in
Rayleigh Fading**

Bengt Holter and Geir E. Øien

Submitted to
IEEE Transactions on Vehicular Technology

Abstract

In this paper, a performance analysis of an adaptive coded modulation (ACM) scheme operating on identically distributed and spatially correlated Rayleigh fading channels is presented. The ACM scheme consists of a set of multidimensional trellis codes originally designed for additive white Gaussian noise channels, with codes being based on quadrature amplitude modulation signal constellations of varying size. Rate adaptation is made possible by providing the transmitter with channel state information, by feeding back the channel signal-to-noise ratio as predicted by the receiver. Approximate closed-form expressions for the average bit-error rate and the average spectral efficiency are derived, and numerical examples are given for the case of Jakes correlation profile and maximum *a posteriori*-optimal predictor coefficients.

1 Introduction

There is currently a rapid growth of services becoming available from portable and wireless devices. As these services become more and more complex, new and spectrally efficient transmission schemes supporting higher information rates will be needed in future wireless systems. This is a challenging task, since radio signals transmitted on wireless links often propagate in very hostile environments. Adaptive coded modulation (ACM) is a promising tool for increasing the spectral efficiency of time-varying mobile channels while maintaining a predictable bit-error-rate (BER) [1–5]. The concept of ACM is to transmit with high information rates under favorable channel conditions and to reduce the information rate in response to channel degradation. An important restriction is that the transmitter needs to have accurate channel-state information (CSI), which in practice must be estimated by the receiver and conveyed to the transmitter on a dedicated feedback channel.

Naturally, there is time delay associated with transmission of data on the feedback channel. Due to channel fluctuations during this time delay, the reported CSI may deviate from the true state of the channel by the time it is used by the transmitter. To alleviate this problem, a CSI predicted ahead in time may be reported, rather than reporting the instantaneous CSI. In [6], the effects of this method are investigated by describing how estimation error and feedback delay affect some key performance measures of an ACM system when using a linear fading-envelope predictor. An important part of this analysis is based on the knowledge of the joint distribution of the true and predicted *channel signal-to-noise ratio* (CSNR), since the correlation between these two entities is an important parameter affecting the error performance. The system is assumed to be operating on spatially independent and identically distributed Rayleigh fading channels, and in that case, the joint distribution is a bivariate gamma distribution, because both the true and predicted CSNR are individually gamma distributed and mutually correlated. A single-input multiple-output (SIMO) flat-fading channel is considered, and maximum ratio combining (MRC) is used at the receiver to maximize the received CSNR.

In this paper, the results in [6] are extended to include identically distributed but spatially *correlated* Rayleigh fading channels. Then, in contrast to [6], neither the true nor the predicted CSNR (as defined in [6]) will be gamma distributed. However, as presented here, the same type of analysis as in [6] may be pursued with good accuracy if the densities of both the true and the predicted CSNR are approximated by gamma distributions. To this end, an approximate probability density function (PDF) of the com-

bined CSNR in MRC systems operating on correlated Nakagami- m fading channels [7] is utilized [8]. Results for a Rayleigh fading model is obtained for $m = 1$.

The rest of the present paper is organized as follows. The system and channel model are presented in Section 2. In Section 3, the statistics of the combined CSNR at the output of an MRC receiver are discussed. For clarity reasons, the case of uncorrelated channels is revisited briefly before spatial correlation is introduced. In Section 4, it is demonstrated that the approximate PDF introduced in Section 3 does not realize the true diversity order or coding gain at high CSNR. However, this does not represent a major limitation of our work, since at high CSNR, only the highest available information rate will be employed. Hence, at high CSNR, the ACM system will behave like a system using only a single fixed information rate, and in that case, the effects of spatial channel correlation are well known. Section 5 briefly discusses linear pilot-symbol assisted channel prediction. In Section 6, it is shown that when the spatial/temporal correlation coefficient is written as a product in terms of the spatial and temporal parts, the correlation coefficient between the true and predicted CSNR is unchanged from the case of uncorrelated channels. In Section 7, approximate closed-form expressions for the ASE and average BER are derived, followed by numerical results in Section 8. Finally, the main contributions of the paper are summarized in Section 9.

2 System and channel model

The rate-adaptive system depicted in Figure B.1 is considered. Denoting the transmitted complex baseband signal (after pilot-symbol insertion) at time index k by $x(k)$, the received signal at time index k at each of the H receive antennas can be expressed as $\mathbf{y}(k) = \mathbf{z}(k)x(k) + \mathbf{n}(k)$, where $\mathbf{z}(k) = [z_1(k), z_2(k), \dots, z_H(k)]^T$ is the channel vector, and $\mathbf{n}(k) = [n_1(k), n_2(k), \dots, n_H(k)]^T$ is the additive white Gaussian noise (AWGN) vector.¹ The received signal on branch h can be written as $y_h(k) = z_h(k) \cdot x(k) + n_h(k)$, where the random variable (RV) $z_h(k)$ is the *complex fading amplitude*, and $n_h(k)$ is complex-valued with statistically independent real and imaginary parts. $x(k)$ represents the information signal, except at the pilot symbol instants $k = pL$ ($p \in \mathbb{Z}, L \in \mathbb{Z}^+$), where L represents the minimum number of time instances between two pilot symbols. Its value will be a tradeoff between a sufficiently high sampling rate of the channel (small L) and a high spectral efficiency (large L). It is assumed that all pilot symbols have the same ab-

¹The superscript T denotes a transpose operation.

solute value $|x(pL)| = a_p$, and that data and pilot symbols are transmitted with the same power.²

The transmission rate is adapted by using a set of N multidimensional trellis codes originally designed for AWGN channels [3]. The codes are based on quadrature amplitude modulation (QAM) signal constellations with different number of symbols $M_n = 2^{k_n}$, where k_n is some positive integer, and $n = 1, 2, \dots, N$. Rate adaptation is performed by splitting the received CSNR range into $N + 1$ fading regions (bins) as depicted in Figure B.2. The lower thresholds of each bin, $\{\gamma_n\}_{n=1}^N$, are selected such that a target BER—denoted BER_0 —is always achieved for each available code in the rate-adaptive scheme. When the CSNR $\gamma(k) \triangleq \gamma$ falls within fading region n ($\gamma_n \leq \gamma < \gamma_{n+1}$), the associated CSI, i.e. the fading region index n , is sent back to the transmitter. The transmitter then adapts its transmission rate and coding scheme according to the quality of the channel, by transmitting with a code realizing a spectral efficiency of R_n . If $0 \leq \gamma < \gamma_1$, no information is transmitted (outage), and the information must be buffered at the transmitter end.

It is assumed that the CSI is conveyed on a zero-error feedback channel. However, with a non-zero time delay τ , the CSI may have become outdated by the time it is used. A consequence of a CSI mismatch is that the transmitter may select either a too low or a too high information rate, leading to changes in the average BER and ASE compared to the case of perfect CSI. In [4–6], this problem is alleviated by letting the receiver report a CSI predicted ahead in time, rather than reporting the instantaneous CSI. It will then be more in accordance with the true state of the channel by the time it is used by the transmitter. As in [6], the time delay τ is assumed to be an integer number of pilot symbol intervals $\tau = kLT_s$, where $k \in \mathbb{Z}^+$ is the number of pilot symbol intervals, and T_s [s] is the duration of a single channel symbol. The CSNR is predicted every time a new pilot symbol arrives at the receiver, and a computationally intensive predictor, optimal in the *maximum a posteriori* (MAP) sense, is used.

Channel estimation and prediction is performed independently for each channel, and each channel is assumed to be slowly varying so that the fading remains relatively constant over many channel symbols. CSI estimation is accomplished by using an optimal noncausal Wiener interpolator filter, which will smooth the noise, improve CSI reliability beyond what can be

²This represents a suboptimal approach, since power can be adapted and allocated differently to pilot and data symbols in such a way that the ASE is maximized while keeping the BER below a predefined level [9]. However, power adaptation is outside the scope of the present paper, since our aim is to isolate the effect of spatial correlation and compare with results in [6].

achieved by a predictor, and allow for true coherent detection to be used. Hence, perfect coherent detection in the receiver is assumed.

The system is assumed to be operating on wide-sense stationary (WSS)³ and identically distributed Rayleigh fading channels, i.e. the fading amplitude $|z_h(k)| \triangleq \alpha_h$ is a Rayleigh distributed RV. The PDF of α_h is then equal to $f_{\alpha_h}(\alpha_h) = \frac{2\alpha_h}{\Omega} \cdot e^{-\alpha_h^2/\Omega}$ [4, Eq. (3.4)], where $\Omega = \mathcal{E}\{\alpha_h^2\}$ represents the average fading power of the channel.⁴ When α_h is Rayleigh distributed, the channel gain α_h^2 may be equivalently characterized by several standard PDFs; the exponential distribution with mean Ω [11, Eq. (5.9.10)], the chi-squared distribution with 2 degrees of freedom [11, Eq. (7.2.1)], or the gamma distribution with shape factor 1 and scale factor Ω .⁵ In this paper, α_h^2 is viewed as a gamma distributed RV, because this facilitates the direct use of previously reported results on the sum of correlated gamma variates. This is needed in order to identify the density of the combined channel gain $\alpha^2 = \sum_{h=1}^H \alpha_h^2$ and the associated CSNR at the output of the MRC receiver.

When α_h^2 is a gamma distributed RV with mean Ω , it follows by transformation of random variables that the CSNR per branch $\gamma_h(k) \triangleq \gamma_h = \frac{\alpha_h^2 \cdot P}{N_0 B}$ is also a gamma distributed RV with mean $\bar{\gamma}_h = \frac{\Omega P}{N_0 B}$ (average CSNR on branch h). Here, P [W] is the constant average transmit power, N_0 [W/Hz] is the one-sided power spectral density of the complex AWGN on each channel, and B [Hz] is the one-sided information bandwidth. Due to our assumption of identically distributed channels, both Ω and $\bar{\gamma}_h$ will be independent of h . However, the latter will be indexed by h anyway, to indicate that this is the average CSNR per branch and not the average combined CSNR.

3 Statistics of the combined CSNR

In this section, we look at the statistics of the combined CSNR, i.e. the CSNR at the output of the MRC receiver. Since the gamma distribution is used extensively in this section, a definition is included here for the sake of completeness.

³A stochastic process is called wide-sense stationary when the mean value of the process is independent of time (a constant) and the autocorrelation function measured at two different time indices is only dependent on the time difference [10].

⁴ $\mathcal{E}\{\cdot\}$ denotes the statistical average.

⁵See the definition of the gamma distribution in Section 3.

Definition 1 (The gamma distribution)

X follows a gamma distribution with shape factor $\psi > 0$ and scale factor $\theta > 0$ when the PDF of X is given by

$$f_X(x) = \frac{x^{\psi-1}e^{-x/\theta}}{\theta^\psi\Gamma(\psi)}U(x), \quad (\text{B.1})$$

where $\Gamma(\cdot)$ is the gamma function and $U(\cdot)$ is the unit step function. The short hand notation $X \sim \mathcal{G}(\psi, \theta)$ is used to denote that X follows a gamma distribution with shape factor ψ and scale factor θ . With this definition of the gamma distribution, the mean $\bar{x} = \mathcal{E}\{X\} = \psi\theta$ and the variance $\sigma_X^2 = \mathcal{E}\{X^2\} - \bar{x}^2 = \psi\theta^2$. \square

For an MRC receiver with H branches, the combined CSNR γ may in general be expressed as [12]

$$\gamma = \sum_{h=1}^H \gamma_h. \quad (\text{B.2})$$

From the previous section, we recall that for identically distributed Rayleigh fading channels, all the CSNRs in the set $\{\gamma_h\}_{h=1}^H$ are gamma distributed RVs with shape factor 1 and scale factor $\bar{\gamma}_h$. A key assumption in [6] is that the channels are uncorrelated. In that case, $\gamma \sim \mathcal{G}(H, \bar{\gamma}_h)$. However, the CSI reported back to the transmitter is not based on the true instantaneous CSNR γ , but on a predicted CSNR $\hat{\gamma}(k+j) \triangleq \hat{\gamma}$ (predicted j symbols ahead in time to account for the overall time delay $\tau = kLT_s = j \cdot T_s$). When channel prediction is performed independently on each branch, a reasonable prediction of the combined channel gain at the output of the MRC receiver is given by $\hat{\alpha}^2(k+j) \triangleq \hat{\alpha}^2 = \sum_{h=1}^H \hat{\alpha}_h^2(k+j)$ [6, Eq. (6)], where $\hat{\alpha}_h^2(k+j) \triangleq \hat{\alpha}_h^2$ is the predicted channel gain on branch h . According to [4, 13], all the predicted channel gains in the set $\{\hat{\alpha}_h^2\}_{h=1}^H$ may be viewed as gamma distributed RVs with shape factor 1 and scale factor $\hat{\Omega}$, where $\hat{\Omega} = r\Omega$, and r is a constant which depends on the predictor coefficients. Based on the predicted channel gains on each branch, the associated predicted CSNR at the output of the MRC combiner may be expressed as

$$\hat{\gamma} = \sum_{h=1}^H \hat{\gamma}_h, \quad (\text{B.3})$$

where $\hat{\gamma}_h = \frac{\hat{\alpha}_h^2 P}{N_0 B}$. For uncorrelated channels, (B.3) represents a sum of uncorrelated gamma variates, and since $\hat{\alpha}_h^2 \sim \mathcal{G}(1, r\Omega)$, $\hat{\gamma}$ is distributed according to $\hat{\gamma} \sim \mathcal{G}(H, r\bar{\gamma}_h)$. Hence, in the case of uncorrelated channels, the joint distribution of γ and $\hat{\gamma}$ is a bivariate gamma distribution [6, Definition

1], because γ and $\hat{\gamma}$ both are individually gamma distributed and mutually correlated.

In practice however, spatial correlation between the branches may arise, e.g. from insufficient antenna spacing in small size terminals. Then it may be deduced from (B.2) and (B.3) that both γ and $\hat{\gamma}$ represent sums of correlated gamma variates. Focusing on the true CSNR, the PDF of γ in the dual branch case may then be written as a type I McKay distribution [14, Eq. (20)]. For $H \geq 2$, a closed-form expression for the PDF of γ is given in [15, Eq. (12)], which is valid when there is constant correlation between all the branches.⁶ For arbitrarily correlated gamma variates and $H \geq 2$, an infinite sum representation for the PDF of γ is presented in [17, Eq. (5)].

Unfortunately, none of the densities mentioned above belong to any standard distribution, so the joint distribution needed to quantify the correlation between γ and $\hat{\gamma}$ is not known. However, according to [8], the PDF of a sum of correlated gamma variates may be approximated by a gamma distribution with the first two moments identical to those of the exact distribution.⁷ For identically distributed Rayleigh fading channels, the exact mean and variance of γ may be written as [18]

$$\bar{\gamma} = \left(\frac{P}{N_0 B} \right) \cdot \sum_{h=1}^H \lambda_h, \quad (\text{B.4})$$

and

$$\sigma_\gamma^2 = \left(\frac{P}{N_0 B} \right)^2 \cdot \sum_{h=1}^H \lambda_h^2, \quad (\text{B.5})$$

respectively. Here, $\{\lambda_h\}_{h=1}^H$ is the set of eigenvalues from the complex channel correlation matrix \mathbf{R}_z , defined as

$$\mathbf{R}_z = \mathcal{E}\{\mathbf{z}(k)\mathbf{z}(k)^H\} = \Omega \cdot \begin{bmatrix} 1 & r_{12} & \cdots & r_{1H} \\ r_{21} & 1 & \cdots & r_{2H} \\ \vdots & \vdots & \ddots & \vdots \\ r_{H1} & r_{H2} & \cdots & 1 \end{bmatrix}, \quad (\text{B.6})$$

where $r_{ji} = r_{ij}^* = \mathcal{E}\{z_i(k)z_j^*(k)\}$ ($i, j = 1, 2, \dots, H$).⁸

⁶The PDF in [15, Eq. (12)] is based on the work by Gurland [16].

⁷See Appendix 5 for some comments on the results in [8].

⁸The normalized (complex) correlation coefficient $r_{ji} = r_{ij}^* = \frac{\text{Cov}(z_i(k), z_j^*(k))}{\sqrt{\text{Var}(z_i(k))\text{Var}(z_j^*(k))}}$. Since

the complex fading amplitudes in the set $\{z_h(k)\}_{h=1}^H$ are complex Gaussians with zero mean, $r_{ij}^* = \mathcal{E}\{z_i(k)z_j^*(k)\}/\Omega$. The superscript H denotes Hermitian transpose (conjugate transpose).

To have identical first and second order moments with the exact distribution, the mean and variance of the gamma distribution in (B.1) must be equal to $\bar{x} = \bar{\gamma}$ and $\sigma_X^2 = \sigma_\gamma^2$, respectively. The shape and scale factors needed to generate these moments may then be written as [18]

$$\psi = \frac{(\psi\theta)^2}{\psi\theta^2} = \frac{\bar{x}^2}{\sigma_X^2} = \frac{\bar{\gamma}^2}{\sigma_\gamma^2} = \frac{1}{\text{AF}}, \quad (\text{B.7})$$

and

$$\theta = \frac{\bar{x}}{\psi} = \frac{\bar{\gamma}}{\psi} = \bar{\gamma} \cdot \text{AF}, \quad (\text{B.8})$$

where AF is an abbreviation for *amount of fading*. This is a measure originally introduced by Charash [19] in order to quantify the severity of fading experienced for a particular channel model, and it is defined as the ratio between the variance and the squared mean of the CSNR. Based on the results in [18], expressions for ψ and θ are presented in Table B.1 for an MRC system operating identically distributed and spatially correlated Nakagami- m fading channels.⁹ Expressions are presented for both a constant correlation model and an exponential correlation model, where ρ_s is the normalized spatial power correlation coefficient between two adjacent antennas, i.e.

$$\rho_s = \frac{\text{Cov}(\gamma_{h+1}, \gamma_h)}{\sqrt{\text{Var}(\gamma_{h+1})\text{Var}(\gamma_h)}} = \frac{\text{Cov}(\alpha_{h+1}^2, \alpha_h^2)}{\sqrt{\text{Var}(\alpha_{h+1}^2)\text{Var}(\alpha_h^2)}}, \quad (\text{B.9})$$

for $h = 1, 2, \dots, H - 1$. Note that for both correlation models, the scale factor θ can be expressed in terms of the shape factor ψ as $\theta = \frac{H\bar{\gamma}_h}{\psi}$.

In Figure B.3, a comparison of the exact PDF of γ in [14, Eq. (20)] and the approximation $\gamma \sim \mathcal{G}(\psi, \theta)$ for a dual branch MRC system operating on identically distributed Rayleigh fading channels is depicted for $\rho_s = \{0.2, 0.7\}$. It reveals a good agreement especially at high CSNRs, but deviations in the lower tail. In Figure B.4, a similar comparison is depicted for both a constant correlation model and an exponential correlation model

⁹For exponential correlation and $\rho_s < 1$, the denominator of the shape factor ψ in Table B.1 is derived from [18, Eq. (18)], in which case $\theta = \frac{\bar{\gamma}_h}{m} \left(1 + 2 \sum_{h=1}^{H-1} \left(1 - \frac{h}{H}\right) \rho_s^h\right) = \frac{\bar{\gamma}_h}{m} \left(1 + \frac{2\rho_s}{1-\rho_s} \left(1 - \frac{1-\rho_s^H}{H(1-\rho_s)}\right)\right)$. This result is identical to an original result by Kotz and Adams [20, Eq. (1.3)], and to r/M in [15, Eq. (14d)]. However, it is noted that even though the result in [15, Eq. (14d)] is based on the paper by Kotz and Adams, it is written in terms of the correlation coefficient of the underlying Gaussian processes which produce the fading on the channels, whereas in this paper (and in [20, Eq. (1.3)]), it is written in terms of the power correlation coefficient.

with $H = 4$. The deviations in the lower tail are in this case somewhat larger than in the dual branch case, especially for $\rho_s = 0.7$.

For simplicity, the shape factor in (B.1) will from now on be denoted m_d , in order to use the same notation as in [8], i.e. $\psi = 1/AF = m_d$. In addition, γ and $\hat{\gamma}$ are from now on approximated as gamma distributed with parameters $\gamma \sim \mathcal{G}(m_d, \theta)$ and $\hat{\gamma} \sim \mathcal{G}(m_d, \hat{\theta})$, where $\hat{\theta} = r\theta$. By using these approximations, the same type of analysis as in [6] may be pursued, since the bivariate gamma distribution may now be applied as the joint distribution between γ and $\hat{\gamma}$. According to the short hand notation of the bivariate gamma distribution in [6, Definition 1], γ and $\hat{\gamma}$ are now assumed to be jointly distributed according to

$$\gamma, \hat{\gamma} \sim \mathcal{G} \left(m_d, \frac{H\bar{\gamma}_h}{m_d}, \frac{rH\bar{\gamma}_h}{m_d}, \rho \right), \quad (\text{B.10})$$

where ρ is the normalized correlation coefficient between γ and $\hat{\gamma}$, i.e.,

$$\rho = \frac{\text{Cov}(\hat{\gamma}, \gamma)}{\sqrt{\text{Var}(\hat{\gamma})\text{Var}(\gamma)}}. \quad (\text{B.11})$$

In the numerical examples, it is demonstrated that in terms of ASE and average BER, the approximation in (B.10) is valid with very good accuracy for $H = 2$ when $0 \leq \bar{\gamma}_h \leq 40$ dB, and for $H = 4$ when $0 \leq \bar{\gamma}_h \leq 30$ dB. The reason that the valid range of $\bar{\gamma}_h$ must be upper limited is that the approximate PDF does not realize the true slope (diversity order) or coding gain of the error rate curve at high CSNR. In the next section, this fact is demonstrated by invoking some recent results by Wang and Giannakis [21].

4 Diversity order and coding gain

In [21], the average symbol error rate (SER)—denoted P_E —of an uncoded (or coded) system at high CSNR is approximated by the expression

$$P_E \approx (G_c \cdot \bar{\gamma})^{-G_d}, \quad (\text{B.12})$$

where G_c represents the coding gain, and G_d represents the diversity order. The diversity order determines the slope of the average SER curve versus $\bar{\gamma}$ at high CSNR in a log-log scale, whereas the coding gain (in dB) determines the shift of the curve in CSNR relative to a benchmark curve given by $(\bar{\gamma})^{-G_d}$.

Exact PDF

Using the exact PDF $f_\gamma(\gamma)$ for γ when operating on identically distributed and arbitrarily correlated Nakagami- m fading channels [17, Eq. (5)] (reproduced in Appendix 4), the *moment generating function* (MGF) associated with $f_\gamma(\gamma)$, defined by

$$\mathcal{M}_\gamma(s) = \int_0^\infty e^{s\gamma} f_\gamma(\gamma) d\gamma, \quad (\text{B.13})$$

can be expressed as [17]

$$\mathcal{M}_\gamma(s) = \prod_{h=1}^H \left(1 - \frac{s\bar{\gamma}_h}{m} \lambda_h \right)^{-m}, \quad (\text{B.14})$$

where m is the Nakagami- m fading parameter, s is the variable of the transform domain, $\{\lambda_h\}_{h=1}^H$ denote the eigenvalues of a $H \times H$ power correlation matrix \mathbf{C} defined by

$$\mathbf{C} = \begin{bmatrix} 1 & \sqrt{\rho_{12}} & \cdots & \sqrt{\rho_{1H}} \\ \sqrt{\rho_{21}} & 1 & \cdots & \sqrt{\rho_{2H}} \\ \vdots & \vdots & \ddots & \vdots \\ \sqrt{\rho_{H1}} & \sqrt{\rho_{H2}} & \cdots & 1 \end{bmatrix}, \quad (\text{B.15})$$

and ρ_{ij} is the normalized spatial power correlation coefficient between branch i and j . Applying Proposition 3 in [21] to the MGF in (B.14), the approximate SER at high CSNR may be written as¹⁰

$$P_E \approx \frac{2^{Hm-1} b \Gamma(Hm + \frac{1}{2})}{\sqrt{\pi} \Gamma(Hm + 1)} \cdot \left(\frac{1}{k} \right)^{Hm}, \quad (\text{B.16})$$

where $b = [\det(\mathbf{C})]^{-m} \left(\frac{m}{\bar{\gamma}_h} \right)^{Hm}$, and k is a fixed code-dependent positive constant [21]. From (B.12), the system may then be characterized by

$$G_d = Hm, \quad (\text{B.17})$$

and

$$G_c = k \left(\frac{2^{Hm-1} p \Gamma(Hm + \frac{1}{2})}{\sqrt{\pi} \Gamma(Hm + 1)} \right)^{-1/Hm}, \quad (\text{B.18})$$

where $p = [\det(\mathbf{C})]^{-m} \cdot m^{Hm}$.

¹⁰This result differs from the result presented in [21, Eq. (10)], since the MGF of the received CSNR has been utilized and not the MGF of the fading power as used in [21]. Hence, the average CSNR $\bar{\gamma}$ is in this paper included in the factor b , whereas in [21], it is not.

Approximate PDF

When the true PDF $f_\gamma(\gamma)$ is approximated by a gamma distribution $\gamma \sim \mathcal{G}(m_d, \theta)$, the MGF becomes

$$\mathcal{M}_\gamma(s) = \frac{1}{(1 - s\theta)^{m_d}}. \quad (\text{B.19})$$

Applying Proposition 3 from [21] to this MGF, the approximate expression for the average SER at high CSNR is then equal to

$$P_E \approx \frac{2^{m_d-1} b \Gamma(m_d + \frac{1}{2})}{\sqrt{\pi} \Gamma(m_d + 1)} \cdot \left(\frac{1}{k}\right)^{m_d}, \quad (\text{B.20})$$

where $b = \theta^{-m_d}$. At high CSNR, the system is characterized by

$$G_d = m_d, \quad (\text{B.21})$$

and

$$G_c = k \left(\frac{2^{m_d-1} p \Gamma(m_d + \frac{1}{2})}{\sqrt{\pi} \Gamma(m_d + 1)} \right)^{-1/m_d}, \quad (\text{B.22})$$

where $p = (H/m_d)^{-m_d}$.

In Figure B.5, G_d (top subfigure) and G_c (bottom subfigure) are depicted as functions of ρ_s for BPSK¹¹ transmission on Rayleigh fading channels ($m = 1$ and $k = 2$ [21]). Since G_d for the exact PDF is fixed and equal to H , only the diversity order for the approximate PDF is depicted in the top subfigure. It is observed that when the approximate PDF is used, the error rate curve at high CSNR quickly deviates from the true slope H as spatial correlation increases. As explained in [21], this difference comes as a result of the deviations in the lower tail between the exact and approximate PDFs in Figures B.3 and B.4. In the bottom subfigure, it is observed that G_c also decreases as a function of ρ_s , which is reflected in a right horizontal shift of the error rate curve as spatial correlation increases. For high correlation values ($\rho_s > 0.7$), G_c based on the exact PDF decreases more rapidly, whereas G_c based on the approximate PDF saturates at 0 dB, resulting in a large deviation from the true value.

In [22, Fig. 1], deviations in both diversity order and coding gain are easily visible. The results are obtained for a system transmitting with only a single, fixed signal constellation, and the approximate BER curve is obtained by approximating the PDF by a sum of exponentially correlated

¹¹Binary phase-shift keying.

gamma variates with a gamma distribution (a method proposed by Kotz and Adams [20]). It is observed that the approximate average BER curve is many orders of magnitude higher than the exact average BER curve obtained with a constant correlation model. As noted in [22], this is not an intuitive result, since for the same value of ρ_s , a better performance is expected for an exponential correlation model than for a constant correlation model. It is argued that the large deviations are due to inappropriate use of the approximate PDF, and according to [22], the range of parameter values which yields an acceptable approximation is $H \geq 5$, $m \sim 2$, and $\rho_s \leq 0.2 \sim 0.3$. However, despite these results, it is shown later in the present paper that the approximate PDF in our case may be used for low and medium CSNR even for $H \in \{2, 4\}$, $m = 1$, and $0 \leq \rho_s < 1$. One possible explanation of this is that in the present paper, higher rate codes are selected for transmission as the CSNR increases. This causes the error rate curve to have a slower descent as a function of increasing CSNR compared to a similar system using fixed rate transmission. As a consequence, it is observed in the present paper that the error rate curves obtained with the approximate PDF are in accordance with the error rate curves obtained with the true PDF over a wider range of parameters. In particular, deviations between the error rate curves are in this paper only visible when the highest available code is employed.

5 Linear pilot-symbol assisted channel prediction

Linear prediction of the fading process is used.¹² Allowing for complex predictor filter coefficients, a prediction of the complex fading amplitude $z_h(i+j)$ ($i = pL$, $p \in \mathbb{Z}$) can be written on the form [6, Eq. (4)]

$$\hat{z}_h(i+j) = \sum_{k=0}^{K-1} f_{j,h}^*(k) \cdot \tilde{z}_h(i-kL) = \mathbf{f}_{j,h}^H \tilde{\mathbf{z}}_{h,i}, \quad (\text{B.23})$$

where $\mathbf{f}_{j,h}^H = [f_{j,h}^*(0), \dots, f_{j,h}^*(K-1)]$ is the predictor filter coefficient vector for branch h and delay j , K is the predictor order, and

$$\tilde{\mathbf{z}}_{h,i} = [\tilde{z}_h(i), \tilde{z}_h(i-L), \dots, \tilde{z}_h(i-(K-1)L)]^T \quad (\text{B.24})$$

is a vector of K memoryless maximum likelihood estimates of the complex fading amplitude in the last K pilot-symbol instants [6, Eq. (3)]. Due to the WSS assumption, the time index i will from now on be omitted when referring to $\tilde{\mathbf{z}}_{h,i}$ and other vectors where it is applicable.

¹²See [6, Sec. III] for a more thorough explanation of why a linear predictor is used.

The MAP-optimal prediction filter coefficients for the complex fading amplitude on a Rayleigh fading channel can be expressed as [4, Eq. (3.57)]¹³

$$\mathbf{f}_{j,\text{MAP}}^T = \mathbf{r}_j^T \left(\mathbf{R} + \frac{1}{\bar{\gamma}_h} \mathbf{I} \right)^{-1}, \quad (\text{B.25})$$

where $\mathbf{r}_j = \mathcal{E}\{\mathbf{z}_h \mathbf{z}_h^*(i+j)\}/\Omega$ is a normalized correlation vector. It contains the correlation between the fading at the pilot symbol instants $\mathbf{z}_h = [z_h(i), z_h(i-L), \dots, z_h(i-(K-1)L)]^T$, and the fading to be predicted at time instant $i+j$, i.e. $z_h(i+j)$. The matrix $\mathbf{R} = \mathcal{E}\{\mathbf{z}_h \mathbf{z}_h^H\}/\Omega$ is the autocorrelation matrix of the fading process on a single branch at the pilot-symbol instants. For the Jakes spectrum [23, Sec. 2.1] utilized in [6], the autocorrelation of the fading is real and given by $\mathcal{E}\{z_h(i+j)z_h^*(i-kL)\} = \Omega \cdot J_0(2\pi f_D(j+kL)T_s)$, where $J_0(\cdot)$ is the zeroth-order Bessel function of the first kind, $f_D = (v/c)f_c$ is the maximum Doppler frequency [Hz], v is the terminal speed [m/s], f_c is the carrier frequency [Hz], and c is the speed of light [m/s]. The k th entry of \mathbf{r}_j , denoted $\mathbf{r}_j(k)$, is equal to [4, Eq. (3.68)]

$$\mathbf{r}_j(k) = J_0(2\pi f_D(j+kL)T_s). \quad (\text{B.26})$$

Likewise, a single entry at the k th row and l th column of \mathbf{R} , denoted $\mathbf{R}(k,l)$, is equal to [4, Eq. (3.69)]

$$\mathbf{R}(k,l) = J_0(2\pi f_D|k-l|LT_s). \quad (\text{B.27})$$

Since $\hat{z}_h(i+j) = \mathbf{f}_j^H \hat{\mathbf{z}}_h$, the predicted channel gain on branch h may in general be written as $\hat{\alpha}_h^2 = |\hat{z}_h(k+j)|^2 = |\mathbf{f}_j^H \hat{\mathbf{z}}_h|^2$.

6 Correlation and ratio coefficient

Correlation coefficient

The correlation between the true and predicted CSNR in (B.11) is an important parameter affecting the BER performance of the ACM system. Since $\gamma = \frac{\alpha^2 P}{N_0 B}$ and $\hat{\gamma} = \frac{\hat{\alpha}^2 P}{N_0 B}$, ρ may also be defined as

$$\rho = \frac{\text{Cov}(\hat{\alpha}^2, \alpha^2)}{\sqrt{\text{Var}(\hat{\alpha}^2)\text{Var}(\alpha^2)}}. \quad (\text{B.28})$$

¹³Since the MAP-optimal filter coefficients only depend on the delay j when the channels are identically distributed, the channel subscript h is disregarded.

Recall that for spatially correlated channels, the approximations $\gamma \sim \mathcal{G}(m_d, \theta)$ and $\hat{\gamma} \sim \mathcal{G}(m_d, \hat{\theta})$ were introduced in Section 3. Using transformation of random variables, it can then be shown that $\alpha^2 \sim \mathcal{G}(m_d, H\Omega/m_d)$, and $\hat{\alpha}^2 \sim \mathcal{G}(m_d, rH\Omega/m_d)$. It follows that ρ may be expressed as

$$\rho = \frac{\mathcal{E}\{\hat{\alpha}^2 \alpha^2\} - (H\Omega)^2 r}{(H\Omega)^2 r} \cdot m_d \quad (\text{B.29})$$

For uncorrelated Rayleigh fading channels, $m_d = H$, and (B.29) reduces to [6, Eq. (8)]. Focusing on the correlation between α^2 and $\hat{\alpha}^2$, it may be written as

$$\mathcal{E}\{\hat{\alpha}^2 \alpha^2\} = \mathcal{E}\left\{\sum_{h=1}^H \hat{\alpha}_h^2 \sum_{h=1}^H \alpha_h^2\right\} = \sum_{h=1}^H \sum_{i=1}^H \mathcal{E}\{\hat{\alpha}_h^2 \alpha_i^2\}. \quad (\text{B.30})$$

For a constant correlation model, this simplifies to

$$\begin{aligned} \mathcal{E}\{\hat{\alpha}^2 \alpha^2\} &= \sum_{h=1}^H \mathcal{E}\{\hat{\alpha}_h^2 \alpha_h^2\} + \sum_{h=1}^H \sum_{i \neq h}^H \mathcal{E}\{\hat{\alpha}_h^2 \alpha_i^2\} \\ &= H\mathcal{E}\{\hat{\alpha}_h^2 \alpha_h^2\} + H(H-1)\mathcal{E}\{\hat{\alpha}_h^2 \alpha_i^2\}. \end{aligned} \quad (\text{B.31})$$

In contrast to [6, Eq. (8)], the expression for ρ now contains a term which involve the covariance between the predicted channel gain in branch h and the true channel gain in branch i , where $i \neq h$. Hence, the expression $\mathcal{E}\{\hat{\alpha}_h^2 \alpha_i^2\}$ involves correlation in both space and time. In the following, it is assumed that the normalized correlation coefficient in both space and time $\rho_{z,st}$ can be written as [24]

$$\rho_{z,st} = \rho_{z,s} \cdot \rho_{z,t}, \quad (\text{B.32})$$

where¹⁴

$$\rho_{z,t} = \frac{\text{Cov}(z_h(k+\tau), z_h^*(k))}{\sqrt{\text{Var}(z_h(k+\tau))\text{Var}(z_h^*(k))}}, \quad (\text{B.33})$$

and

$$\rho_{z,s} = \frac{\text{Cov}(z_{h+1}(k), z_h^*(k))}{\sqrt{\text{Var}(z_{h+1}(k))\text{Var}(z_h^*(k))}}. \quad (\text{B.34})$$

According to [24], this approach is adequate for gauging *average* system behavior. Assuming a Jakes fading spectrum, the following result is obtained (presented in detail in Appendix 3):

$$\mathcal{E}\{\hat{\alpha}_h^2 \alpha_i^2\} = \Omega^2 r + \rho_s \Omega^2 |\mathbf{f}_j^H \mathbf{r}_j|^2, \quad (\text{B.35})$$

¹⁴The subindex t is used to denote temporal correlation, whereas the subindex s is used to denote spatial correlation.

where $\rho_s = |\rho_{z,s}|^2$ is the normalized spatial power correlation coefficient as defined in (B.9).¹⁵ Inserting (B.35) in (B.31) and using $\mathcal{E}\{\hat{\alpha}_h^2 \alpha_h^2\} = \Omega^2 r + \Omega^2 |\mathbf{f}_j^H \mathbf{r}_j|^2$ [6, Eq. (40)], ρ is equal to

$$\rho = \frac{|\mathbf{f}_j^H \mathbf{r}_j|^2}{r}, \quad (\text{B.36})$$

which is identical to the result for spatially uncorrelated channels ($\rho_s = 0$) [4, Eq. (3.21)]. This result also holds for the exponential correlation model, in which case

$$\begin{aligned} \mathcal{E}\{\hat{\alpha}^2 \alpha^2\} &= \sum_{h=1}^H \mathcal{E}\{\hat{\alpha}_h^2 \alpha_h^2\} + \sum_{h=1}^H \sum_{i \neq h} \mathcal{E}\{\hat{\alpha}_h^2 \alpha_i^2\} \\ &= H \mathcal{E}\{\hat{\alpha}_h^2 \alpha_h^2\} + 2H \sum_{h=1}^{H-1} \left(1 - \frac{h}{H}\right) \mathcal{E}\{\hat{\alpha}_{h+1}^2 \alpha_1^2\}, \end{aligned} \quad (\text{B.37})$$

and

$$\mathcal{E}\{\hat{\alpha}_{h+1}^2 \alpha_1^2\} = \Omega^2 r + \rho_s^h \Omega^2 |\mathbf{f}_j^H \mathbf{r}_j|^2 \quad (\text{B.38})$$

for $h = 1, 2, \dots, H-1$. It is tempting to conjecture that the same result will hold for any correlation model, but this is not proven here.

Ratio coefficient

Assuming that $a_p = \sqrt{P}$, where P is the average transmit power, r is equal to [6, Appendix]

$$r = \frac{\hat{\Omega}}{\Omega} = \mathbf{f}_j^H \mathbf{R} \mathbf{f}_j + \frac{\|\mathbf{f}_j\|^2}{\bar{\gamma}_h}. \quad (\text{B.39})$$

Since ρ is unchanged from the case of uncorrelated channels, the following identity is true when MAP-optimal predictor coefficients are used [4, Eq. (3.66)], [6, Eq. (28)]:

$$r = |\mathbf{f}_{j,\text{MAP}}^H \mathbf{r}_j| = \rho. \quad (\text{B.40})$$

7 ASE and BER analysis

The ASE¹⁶ of the system is obtained as a weighted sum of the spectral efficiencies of each individual code, where the weight factor P_n for code n is

¹⁵See [25, Appendix A] on how the power correlation coefficient in general is related to the correlation coefficient of the underlying Gaussian processes that produce the fading on the channels.

¹⁶Measured in bits/s/Hz [3, 4].

equal to the probability that this code is used:

$$\text{ASE} = \sum_{n=1}^N R_n \cdot P_n = \sum_{n=1}^N R_n \cdot \int_{\gamma_n}^{\gamma_{n+1}} f_{\hat{\gamma}}(\hat{\gamma}) d\hat{\gamma}. \quad (\text{B.41})$$

From Section 3, it is assumed that $\hat{\gamma} \sim \mathcal{G}(m_d, r\theta)$; hence

$$f_{\hat{\gamma}}(\hat{\gamma}) = \frac{\hat{\gamma}^{m_d-1} e^{-\hat{\gamma}/(r\theta)}}{(r\theta)^{m_d} \Gamma(m_d)}.$$

Then,

$$P_n = \bar{\Gamma} \left(m_d, \frac{m_d \gamma_n}{rH\bar{\gamma}_h} \right) - \bar{\Gamma} \left(m_d, \frac{m_d \gamma_{n+1}}{rH\bar{\gamma}_h} \right), \quad (\text{B.42})$$

where $\bar{\Gamma}(\cdot, \cdot) = \Gamma(\cdot, \cdot) / \Gamma(\cdot)$ is the normalized complementary incomplete gamma function. For uncorrelated Rayleigh fading channels, $m_d = H$, and (B.42) reduces to [6, Eq. (11)].¹⁷ When $2G$ -dimensional ($G \in \mathbb{Z}^+$) trellis codes are used, the information rate of code n , R_n , can be expressed as [3, 4]

$$R_n = \left(\log_2(M_n) - \frac{1}{G} \right) \cdot \frac{L-1}{L}. \quad (\text{B.43})$$

Since every L th channel symbol is a pilot symbol, the information rate is reduced by the fraction $(L-1)/L$. As noted in [6], the ASE is a meaningful measure only as long as the target BER constraint is fulfilled. If the BER becomes greater than BER_0 , the system does not provide the desired transmission reliability and the received data might be meaningless to the end user.

The average BER (averaged over all codes and all CSNRs) is given as the average number of bits in error, divided by the average number of bits transmitted [4]:

$$\overline{\text{BER}} = \frac{\sum_{n=1}^N R_n \cdot \overline{\text{BER}}_n}{\sum_{n=1}^N R_n \cdot P_n}. \quad (\text{B.44})$$

The average BER for code n , $\overline{\text{BER}}_n$, may be written as [2]

$$\overline{\text{BER}}_n = \int_{\gamma_n}^{\gamma_{n+1}} \int_0^{\infty} \text{BER}_n(\gamma|\hat{\gamma}) f_{\gamma, \hat{\gamma}}(\gamma, \hat{\gamma}) d\gamma d\hat{\gamma}, \quad n = 1, 2, \dots, N \quad (\text{B.45})$$

¹⁷The incomplete gamma function used in [6] is defined in [26, Eq. (11.3)], whereas the normalized complementary incomplete gamma function used in this paper is based on the definition in [27, Sec. 8.35]. These are identical functions, but to avoid confusion with the first order Marcum-Q function, commonly denoted as $Q(\cdot, \cdot)$ in the literature, the notation $\bar{\Gamma}(\cdot, \cdot)$ is used in this paper.

where $\text{BER}_n(\gamma, \hat{\gamma})$ is the BER experienced when code n is applied. The choice of n is based on the belief that the CSNR is $\hat{\gamma}$, while it actually is γ . Hence, n , and all functions of n should be viewed as dependent on $\hat{\gamma}$. Furthermore, $f_{\gamma, \hat{\gamma}}(\gamma, \hat{\gamma})$ is the joint distribution of γ and $\hat{\gamma}$. Recall that in our case, both γ and $\hat{\gamma}$ are approximated to be gamma distributed RVs, and as such, the joint distribution $f_{\gamma, \hat{\gamma}}(\gamma, \hat{\gamma})$ is the bivariate gamma distribution in (B.10).

When code n is operating on an AWGN channel with CSNR γ , the BER-CSNR relationship for varying γ may be approximated by the expression [3]

$$\text{BER}_n \approx a_n \cdot e^{-\frac{b_n \gamma}{M_n}}, \quad (\text{B.46})$$

where a_n and b_n are code-dependent constants found by least-square fitting to simulated BER-CSNR data on AWGN channels.¹⁸ This approximation is accurate for any CSNR resulting in $\text{BER} < 10^{-1}$ [3]. However, it approaches a_n for low CSNRs, and since a_n can be larger than one [3], the following approximate BER expression for code n is utilized [4], [6, Eq. (14)]:

$$\text{BER}_n(\gamma|\hat{\gamma}) = \begin{cases} a_n \cdot e^{-\frac{b_n \gamma}{M_n}} & \text{when } \gamma \geq \gamma_n^l \\ \frac{1}{2} & \text{when } \gamma < \gamma_n^l \end{cases} \quad (\text{B.47})$$

The boundary $\gamma_n^l = \ln(2a_n)M_n/b_n$ is the smallest CSNR such that the BER is no larger than 0.5 for either code. It is obtained by assuming equality in (B.46) and solving for γ when $\text{BER} = 0.5$. The CSNR thresholds in the set $\{\gamma_n\}_{n=1}^N$, required to achieve a given target BER_0 , are obtained in a similar fashion. This means that the thresholds are designed for a system with perfect CSI. A more robust system is achieved if the thresholds are adjusted to account for imperfect CSI, but this comes at the expense of a reduced ASE [28]. However, by introducing *adaptive* pilot-symbol assisted modulation (PSAM), increased robustness can be achieved with less reduction in ASE [9, 29]. Such an approach is not pursued in this paper, since our aim is to isolate the impact of spatial correlation and compare with results obtained in [6]. Values for a_n , b_n , M_n , and γ_n are summarized in [6, Tab. I] for the target $\text{BER}_0 = 10^{-4}$ and $N = 8$ (the number of codes used in the numerical examples in Section 8).

The integral for $\overline{\text{BER}}_n$ may now be solved as

$$\begin{aligned} \overline{\text{BER}}_n &= \int_{\gamma_n}^{\gamma_{n+1}} \mathcal{J}1(n, \hat{\gamma}) - (\mathcal{J}21(n, \hat{\gamma}) - \mathcal{J}22(n, \hat{\gamma})) d\hat{\gamma} \\ &= \mathcal{I}1(n) - (\mathcal{I}21(n) - \mathcal{I}22(n)), \end{aligned} \quad (\text{B.48})$$

¹⁸In [6, Fig. 3], the accuracy of this BER approximation is depicted for example codes $n = 1, 2, 3$.

where

$$\mathcal{J}1(n, \hat{\gamma}) = \int_0^{\infty} a_n \cdot e^{-\frac{b_n \gamma}{M_n}} f_{\gamma, \hat{\gamma}}(\gamma, \hat{\gamma}) d\gamma \quad (\text{B.49})$$

$$\mathcal{J}21(n, \hat{\gamma}) = \int_0^{\gamma_n^l} a_n \cdot e^{-\frac{b_n \gamma}{M_n}} f_{\gamma, \hat{\gamma}}(\gamma, \hat{\gamma}) d\gamma \quad (\text{B.50})$$

$$\mathcal{J}22(n, \hat{\gamma}) = \frac{1}{2} \int_0^{\gamma_n^l} f_{\gamma, \hat{\gamma}}(\gamma, \hat{\gamma}) d\gamma. \quad (\text{B.51})$$

$\mathcal{I}1(n)$, $\mathcal{I}21(n)$, and $\mathcal{I}22(n)$ are the integrals of $\mathcal{J}1(n, \hat{\gamma})$, $\mathcal{J}21(n, \hat{\gamma})$, and $\mathcal{J}22(n, \hat{\gamma})$, respectively. Proceeding in the same manner as in [4, Appendix C], the following results are obtained:

$$\begin{aligned} \mathcal{I}1(n) &= a_n \left(\frac{m_d}{\frac{b_n H \bar{\gamma}_h}{M_n} + m_d} \right)^{m_d} \left[\bar{\Gamma} \left(m_d, \frac{\gamma_n}{H r \bar{\gamma}_h} \cdot \frac{m_d \left(\frac{b_n H \bar{\gamma}_h}{M_n} + m_d \right)}{\frac{b_n H \bar{\gamma}_h}{M_n} (1 - \rho) + m_d} \right) \right. \\ &\quad \left. - \bar{\Gamma} \left(m_d, \frac{\gamma_{n+1}}{H r \bar{\gamma}_h} \cdot \frac{m_d \left(\frac{b_n H \bar{\gamma}_h}{M_n} + m_d \right)}{\frac{b_n H \bar{\gamma}_h}{M_n} (1 - \rho) + m_d} \right) \right], \end{aligned} \quad (\text{B.52})$$

$$\begin{aligned} \mathcal{I}21(n) &= a_n \sum_{k=0}^{\infty} \frac{\Gamma(k + m_d)}{\Gamma(k + 1) \Gamma(m_d)} \left(\frac{\rho}{1 - \rho} \right)^k \left(\frac{m_d}{\frac{b_n H \bar{\gamma}_h}{M_n} + \frac{m_d}{1 - \rho}} \right)^{k + m_d} \\ &\quad \times \left[1 - \bar{\Gamma} \left(k + m_d, \gamma_n^l \left(\frac{b_n}{M_n} + \frac{m_d}{H(1 - \rho) \bar{\gamma}_h} \right) \right) \right] \\ &\quad \times \left[\bar{\Gamma} \left(k + m_d, \frac{m_d \gamma_n}{H r \bar{\gamma}_h (1 - \rho)} \right) \right. \\ &\quad \left. - \bar{\Gamma} \left(k + m_d, \frac{m_d \gamma_{n+1}}{H r \bar{\gamma}_h (1 - \rho)} \right) \right], \end{aligned} \quad (\text{B.53})$$

and

$$\begin{aligned} \mathcal{I}22(n) &= \frac{1}{2} \sum_{k=0}^{\infty} \frac{\Gamma(k + m_d)}{\Gamma(k + 1) \Gamma(m_d)} \rho^k (1 - \rho)^{m_d} \\ &\quad \times \left[1 - \bar{\Gamma} \left(k + m_d, \frac{\gamma_n^l m_d}{H \bar{\gamma}_h (1 - \rho)} \right) \right] \\ &\quad \times \left[\bar{\Gamma} \left(k + m_d, \frac{\gamma_n m_d}{H r \bar{\gamma}_h (1 - \rho)} \right) \right. \\ &\quad \left. - \bar{\Gamma} \left(m_d + k, \frac{\gamma_{n+1} m_d}{H r \bar{\gamma}_h (1 - \rho)} \right) \right]. \end{aligned} \quad (\text{B.54})$$

For uncorrelated Rayleigh fading channels ($m_d = H$), all expressions reduces to the results in [6].

8 Numerical results

For comparison reasons, a system with similar parameters to the one in [6] is investigated. Hence, $N = 8$ 4-dimensional trellis codes are used ($G = 2$ in (B.43)), giving a maximal ASE of $R_8 = 8.5 \cdot (L - 1)/L$. The target BER is equal to $\text{BER}_0 = 10^{-4}$, and the a_n and b_n parameters in (B.47), valid for each individual code, are summarized in [6, Tab. 1] together with the CSNR thresholds $\{\gamma_n\}_{n=1}^N$. Other parameters not directly tied to the codes, albeit dependent on the implementation, are the carrier frequency $f_c = 2$ GHz, bandwidth $B = 400$ kHz, and a terminal velocity of $v = 30$ m/s. The prediction filter length is $K = 1000$. Note that since the correlation coefficient ρ between the true and predicted CSNR derived in this paper is unchanged from the one in [6], all the results for ρ depicted in [6, Sec. VB] are equally valid for the results presented in this paper.

To verify that the exact PDF of the combined CSNR on correlated channels may be approximated by a gamma distribution, a series of results comparing the performance obtained with the exact and approximate PDF under idealized assumptions are depicted in Figures B.6 - B.9. It is assumed that the approximate PDF can be used instead of the exact PDF in the range where the performance obtained with the approximate PDF is identical to or close to the performance obtained with the exact PDF. Here, idealized assumptions are understood as perfect channel knowledge and zero delay on the feedback channel, i.e. $\hat{\gamma} = \gamma$ and $\rho = 1$. Under these conditions, analytical expressions for the ASE and the average BER based on the exact/approximate PDFs are derived in Appendix 4.

From Figure B.6 and B.7, a comparison using idealized assumptions is depicted for $H = 2$, pilot spacing $L = 10$, and $\rho_s \in \{0.2, 0.7\}$. In general, a good match is observed within the CSNR range $0 \leq \bar{\gamma}_h \leq 40$ dB, but there is a small and increasing mismatch for the average BER when $\bar{\gamma}_h > 35$ dB, particularly for $\rho_s = 0.7$. This is due to the wrong diversity order and coding gain realized by the approximate PDF at high CSNR, as explained in Section 4. Similar results for the case of $H = 4$ and $\rho_s = 0.7$ are depicted in Figure B.8 and B.9. In Figure B.8, a constant correlation model is considered, whereas in Figure B.9, an exponential correlation model is used. It is observed that for $H = 4$, the mismatch for the average BER at high CSNR is much more pronounced. Hence, the valid CSNR range for which the approximate PDF can be used to measure the average BER performance is limited to $0 \leq \bar{\gamma}_h \leq 30$ dB. For the ASE, the range can be extended to $\bar{\gamma}_h = 40$ dB.

In Figure B.10 and B.11, the expressions in Section 7 are employed to obtain results for the average BER as a function of $\bar{\gamma}_h$ and normalized feed-

back time delay¹⁹ for $H = 4$ and $L = 10$. In Figure B.10, the result for uncorrelated channels is depicted, whereas in Figure B.11, the result for exponentially correlated channels with $\rho_s = 0.7$ is depicted. Note that for a given target BER_0 , the operation of the system is perceived as acceptable whenever the $\text{BER} < \text{BER}_0$. The shape of the BER surface is, therefore, not significant, except for the contour at $\text{BER}_0 = 10^{-4}$. In Figure B.12, the contour lines at $\text{BER}_0 = 10^{-4}$ have been plotted for $H \in \{2, 4\}$, $L = 10$, and $\rho_s \in \{0, 0.2, 0.7\}$. The curves indicate the largest time delay that is allowed in order to achieve the target $\text{BER}_0 = 10^{-4}$ for each given value of $\bar{\gamma}_h$. In general, it is observed that spatial correlation reduces the acceptable time delay on the feedback channel. In particular, for $\bar{\gamma}_h = 10$ dB, $H = 2$, and $L = 10$, an acceptable feedback delay of $350 \mu\text{s}$ was obtained in [6]. For $\rho_s = 0.7$, the acceptable delay is reduced to $103 \mu\text{s}$, i.e. approximately one third of the acceptable delay obtained with uncorrelated antennas.

As long as the system is operating at acceptable BER levels, the ASE is the key performance measure. In Figure B.13 ($H = 2$) and B.14 ($H = 4$), the zero-delay ASE realized on uncorrelated channels [6, Fig. 11] is compared to the corresponding ASE on correlated channels, for $\rho_s = 0.7$ and pilot spacing $L = 10$. As reference, results for the channel capacity on identically distributed and spatially correlated Rayleigh fading channels using optimal rate adaptation and constant transmit power are included [30, Sec. IV]. It is observed that the performance degradation for the capacity and the ASE due to spatial correlation are on the same small order.

For uncorrelated channels, it was observed in [6, Fig. 10] that the ASE is almost independent of the feedback time delay. Since the temporal correlation coefficient ρ between the true and predicted CSNR is unchanged from [6], similar results are observed in this paper for correlated channels. As such, the ASE depicted in the Figures B.6 - B.9 (obtained at zero time delay) are also valid when time delay is introduced. However, these curves are only valid and meaningful as long as the time delay is within the acceptable region, i.e. when the BER requirement is fulfilled. In Figure B.15, this is illustrated by presenting the ASE in a three-dimensional graph as function of $\bar{\gamma}_h$ and normalized feedback time delay when $L = 10$, $H = 2$, and $\rho_s = 0.7$. The contour line, which is identical to the one in Figure B.12 with legend $\rho_s = 0.7$ ($H = 2$), divides the ASE into a relevant part where the BER constraints are fulfilled (to the left of the contour line) and an irrele-

¹⁹The time delay τ is assumed to be an integer number of pilot symbol intervals $\tau = kLT_s = jT_s$, where $j = kL$. The normalized time delay τ_{norm} is then equal to $\tau_{norm} = \tau/T_D = j \cdot f_D T_s$, where $T_D = 1/f_D$, f_D is the maximum Doppler frequency, and T_s is the duration of a single channel symbol. For $f_c = 2$ GHz, $v = 30$ m/s and $B = 400$ kHz, the normalized Doppler spread is $f_D T_s = 5 \cdot 10^{-4}$.

vant part where the BER constraints are violated (to the right of the contour line). Compared to a similar result in [6, Fig. 10], the relevant part has been reduced due to spatial correlation between the antennas.

9 Conclusion

The impact of spatial correlation on ACM performance on identically distributed and spatially correlated Rayleigh fading channels has been investigated. It is observed that spatial correlation has a significant impact on the BER performance, by reducing the acceptable BER region where the system operates reliably with respect to average CSNR and permitted time delay on the feedback channel. However, when the system operates below the target BER_0 (acceptable region), the performance degradation in terms of ASE caused by spatial correlation is not large.

The results derived in this paper are based on the two following assumptions: (i) the exact PDF of the combined CSNR at the output of an MRC receiver may be approximated by a gamma distribution, having identical first and second order moments to those of the exact PDF. As a result, the BER results are in error at high CSNR, since the gamma distribution do not realize the true diversity order and coding gain at high CSNR. This however, does not represent a major limitation of our work, since at high CSNR, only the highest information rate is employed. Hence, at high CSNR, the ACM system will behave like a system using only a single fixed information rate, and in that case, the effects of spatial channel correlation is well known. From the numerical results, a valid CSNR range for the approximation is determined based on comparing performance results obtained with the exact and approximate PDF under idealized assumptions. (ii) spatial/temporal separability is assumed, such that the normalized cross correlation between complex fading envelopes on different branches is given by a product of the individual spatial and temporal correlations. As a result, the temporal correlation between the true and predicted CSNR is unchanged from the case of uncorrelated channels. Using more elaborate cross correlation functions [31, 32] may lead to different results.

TABLE B.1: Expressions for ψ and θ for constant and exponential correlation models

Correlation model	ψ	θ
Constant	$\frac{Hm}{1+\rho_s(H-1)}$	$\frac{\bar{\gamma}_h}{m} (1 + \rho_s(H-1))$
Exponential	$\frac{Hm}{1 + \frac{2\rho_s}{1-\rho_s} \left(1 - \frac{1-\rho_s^H}{H(1-\rho_s)}\right)}$	$\frac{\bar{\gamma}_h}{m} \left(1 + \frac{2\rho_s}{1-\rho_s} \left(1 - \frac{1-\rho_s^H}{H(1-\rho_s)}\right)\right)$

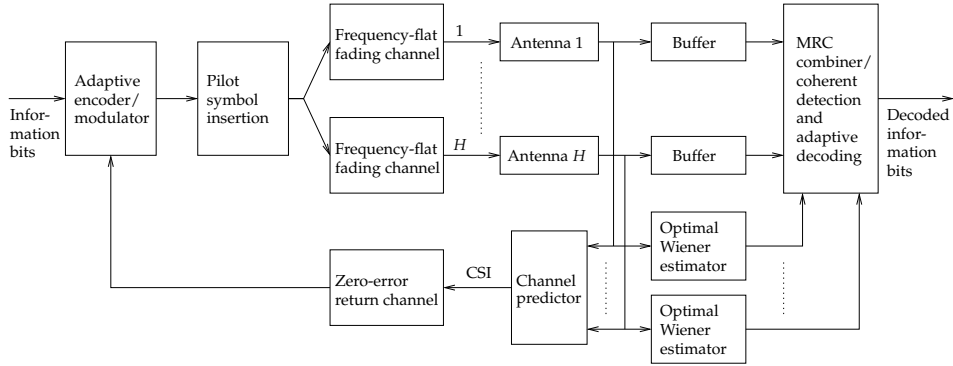
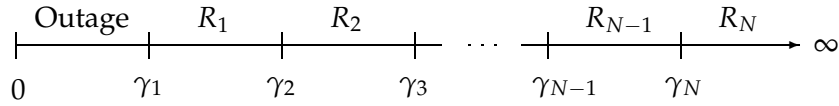


FIGURE B.1: ACM system with pilot-symbol-assisted channel estimation (for coherent detection purposes) and prediction (for transmitter adaptation purposes).


 FIGURE B.2: The CSNR range is split into $N + 1$ bins. When the instantaneous CSNR falls in the lowest interval, an outage occurs; whereas in the upper N intervals, a code with rate R_n is employed.

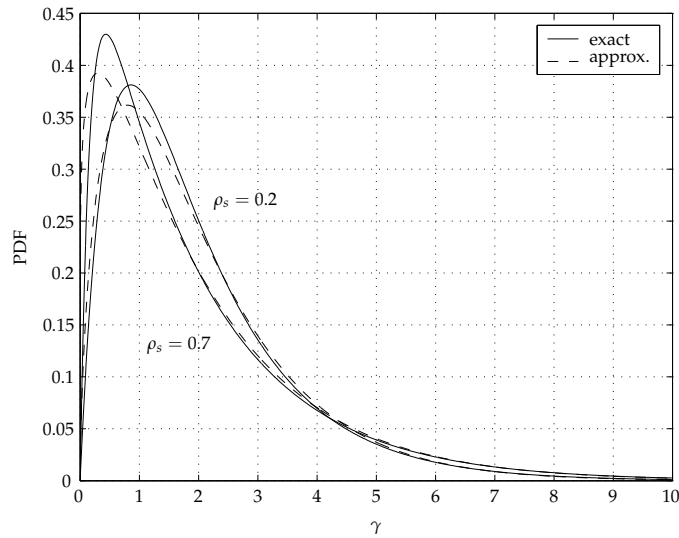


FIGURE B.3: Comparison of the exact and approximate PDFs for γ when $H = 2$ and the system is operating on identically distributed and spatially correlated Rayleigh fading channels ($\bar{\gamma} = 1$).

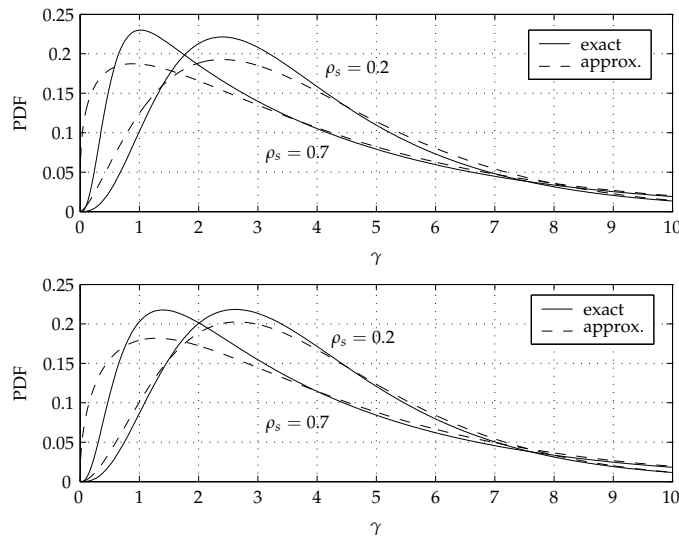


FIGURE B.4: Comparison of the exact and approximate PDFs for γ when $H = 4$ and the system is operating on identically distributed and spatially correlated Rayleigh fading channels ($\bar{\gamma} = 1$). **Top subfigure:** constant correlation model. **Bottom subfigure:** exponential correlation model.

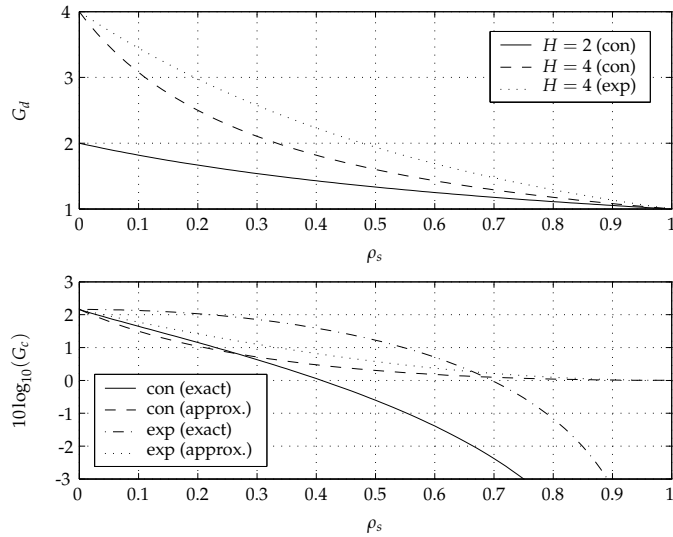


FIGURE B.5: Diversity and coding gain realized at high CSNR for a system operating on identically distributed spatially correlated Rayleigh fading channels, using BPSK transmission only. The abbreviations con and exp in the legends of both subfigures are related to results obtained with a constant and exponential correlation model, respectively. **Top subfigure:** G_d in (B.21) obtained with the approximate PDF is depicted. It should be related to G_d in (B.17), obtained with the exact PDF, in which case $G_d = H$. **Bottom subfigure:** Expressions for G_c in (B.18) and (B.22) are depicted for $H = 4$.

B. IMPACT OF SPATIAL CORRELATION ON ADAPTIVE CODED MODULATION PERFORMANCE IN RAYLEIGH FADING

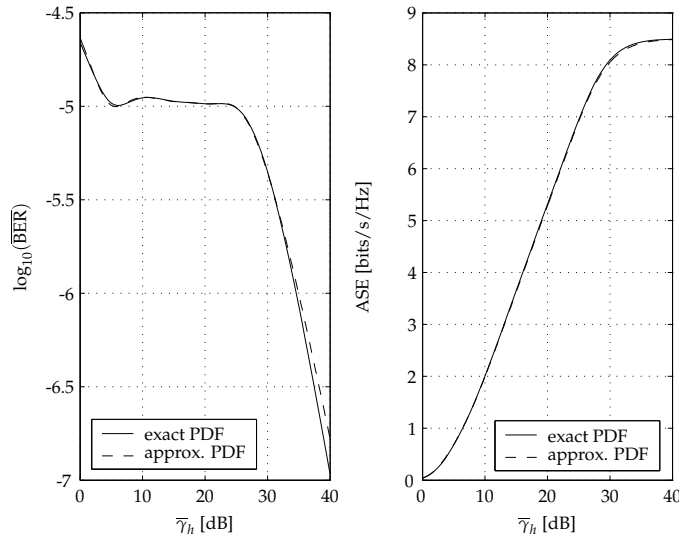


FIGURE B.6: Average BER and ASE as a function $\bar{\gamma}_h$ when using the exact and approximate PDF ($H = 2$ and $\rho_{12} = \rho_{21} = \rho_s = 0.2$ in (4.2)). The assumptions are perfect channel knowledge and no time delay on the feedback channel.

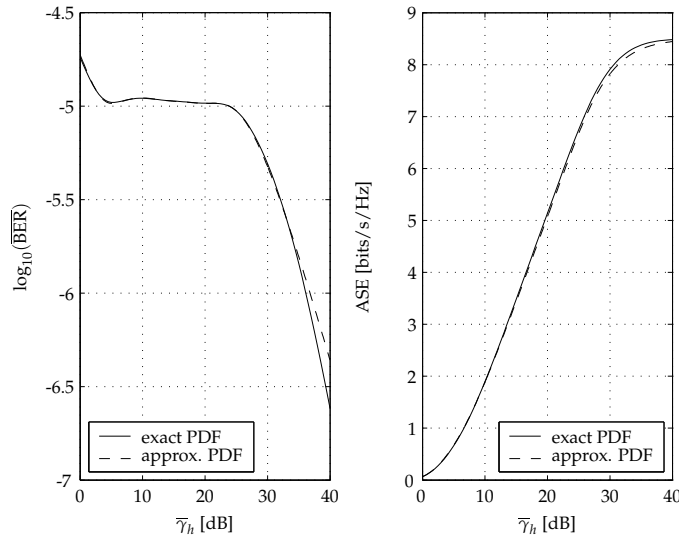


FIGURE B.7: Average BER and ASE as a function $\bar{\gamma}_h$ when using the exact and approximate PDF ($H = 2$ and $\rho_{12} = \rho_{21} = \rho_s = 0.7$ in (4.2)). The assumptions are perfect channel knowledge and no time delay on the feedback channel.

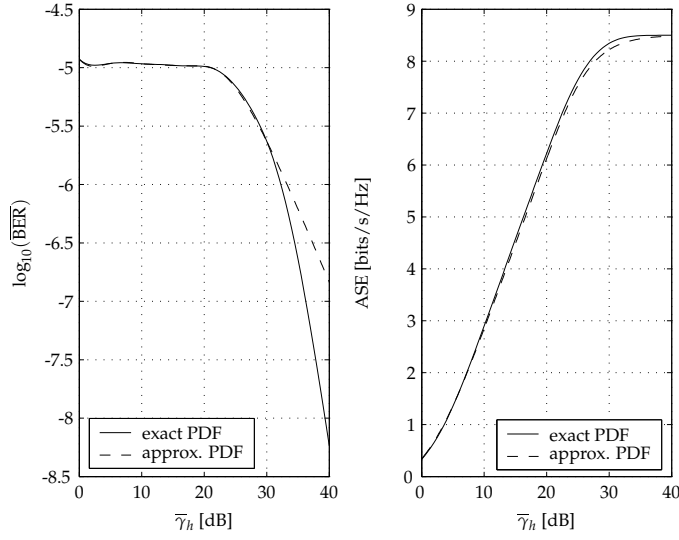


FIGURE B.8: Average BER and ASE as a function $\bar{\gamma}_h$ when using the exact and approximate PDF with a constant correlation model ($H = 4$ and $\rho_{ij} = \rho_s = 0.7$ in (4.2)). The assumptions are perfect channel knowledge and no time delay on the feedback channel.

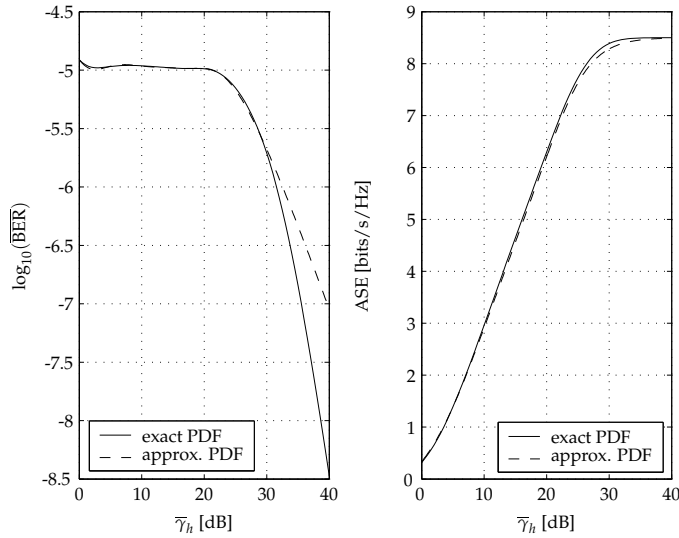


FIGURE B.9: Average BER and ASE as a function $\bar{\gamma}_h$ when using the exact and approximate PDF with an exponential correlation model ($H = 4$ and $\rho_{ij} = \rho_s^{|i-j|}$ in (4.2), with $\rho_s = 0.7$). The assumptions are perfect channel knowledge and no time delay on the feedback channel.

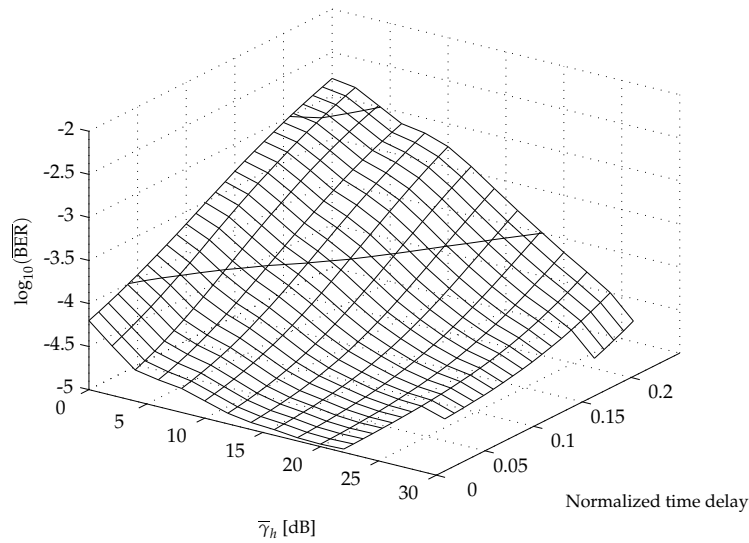


FIGURE B.10: Average BER as a function $\bar{\gamma}_h$ and normalized time delay on the feedback channel when $H = 4$ and the system operating on uncorrelated Rayleigh fading channels. The pilot symbol spacing $L = 10$, and the prediction filter length is $K = 1000$.

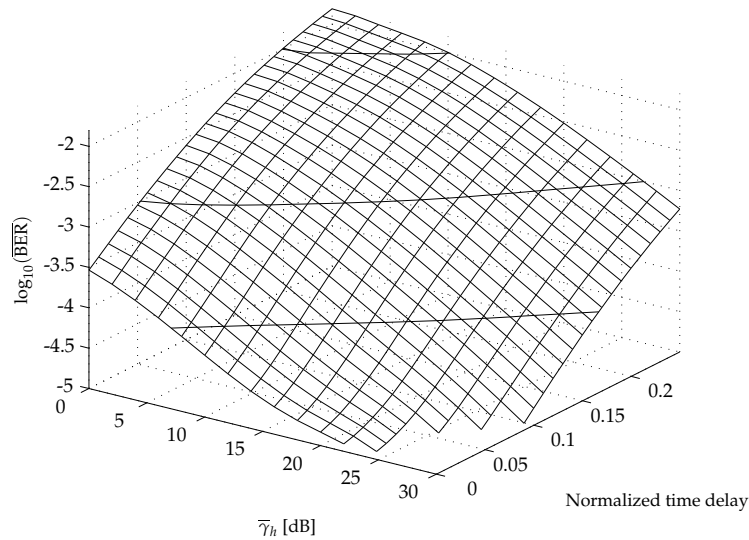


FIGURE B.11: Average BER as a function $\bar{\gamma}_h$ and normalized time delay on the feedback channel when $H = 4$ and the system is operating on exponentially correlated Rayleigh fading channels ($\rho_s = 0.7$). The pilot symbol spacing $L = 10$, and the prediction filter length is $K = 1000$.

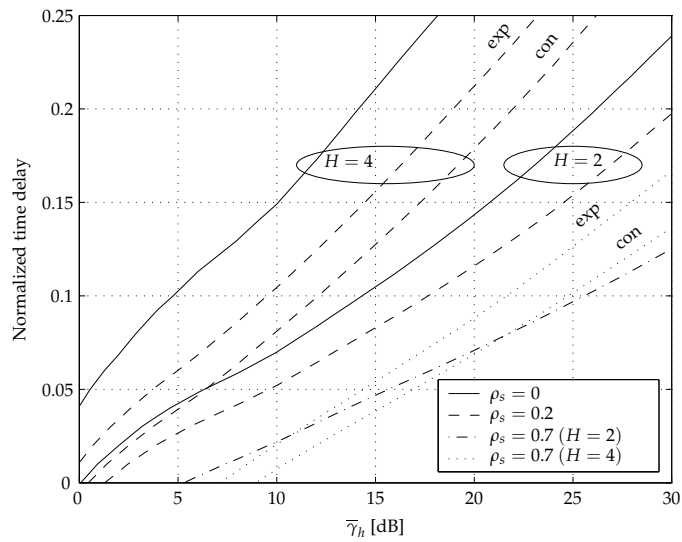


FIGURE B.12: Regions where the system performance is acceptable, plotted for $H = \{2, 4\}$, $L = 10$, $K = 1000$, and $\rho_s = \{0, 0.2, 0.7\}$. The curves indicate the largest delay that is allowed in order to achieve the BER requirements for a given average CSNR $\bar{\gamma}_h$. Thus, the performance is acceptable for each point specified by a CSNR/delay combination that is below and to the right of the curves.

B. IMPACT OF SPATIAL CORRELATION ON ADAPTIVE CODED MODULATION PERFORMANCE IN RAYLEIGH FADING

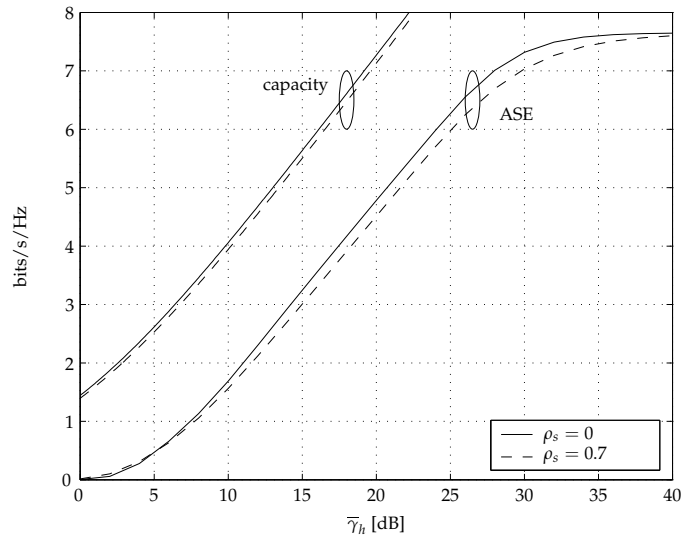


FIGURE B.13: Zero-delay ASE compared to the channel capacity (optimal rate adaptation with constant transmit power) [30, Sec. IV] for $H = 2$ and $\rho_s = \{0, 0.7\}$.

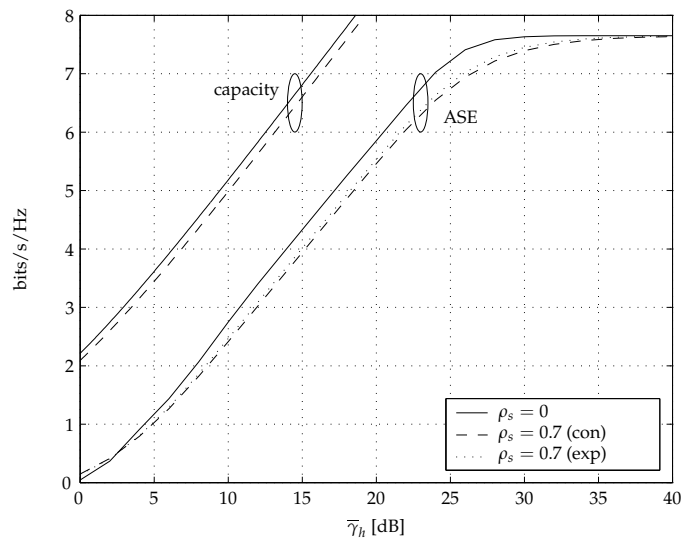


FIGURE B.14: Zero-delay ASE compared to the channel capacity (optimal rate adaptation with constant transmit power) [30, Sec. IV] for $H = 4$ and $\rho_s = \{0, 0.7\}$.

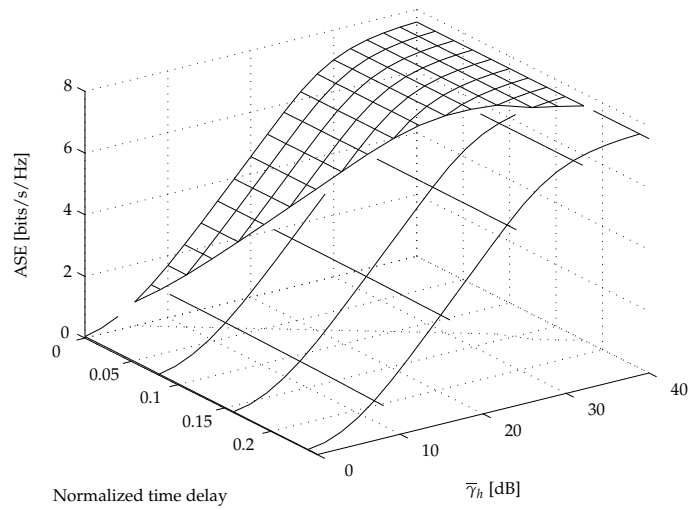


FIGURE B.15: ASE as a function of $\bar{\gamma}_h$ and normalized feedback time delay when $L = 10$, $H = 2$, and $\rho_s = 0.7$. The contour line divides the ASE into a relevant part where the BER constraints are fulfilled (to the left of the contour line) and an irrelevant part where the BER constraints are violated (to the right of the contour line). The prediction filter length is $K = 1000$.

References

- [1] A. J. Goldsmith and S. -G. Chua, "Variable-rate variable-power M-QAM for fading channels," *IEEE Transactions on Communications*, vol. 45, no. 10, pp. 1218–1230, October 1997.
- [2] M. S. Alouini and A. J. Goldsmith, "Adaptive modulation over Nakagami fading channels," *Wireless Personal Communications*, vol. 13, pp. 119–143, May 2000.
- [3] K. J. Hole, H. Holm, and G. E. Øien, "Adaptive multidimensional coded modulation on flat fading channels," *IEEE Journal on Selected Areas in Communications*, vol. 18, no. 7, pp. 1153–1158, July 2000.
- [4] H. Holm, "Adaptive coded modulation and channel estimation tools for flat fading channels," Ph.D. dissertation, The Norwegian University of Science and Technology, April 2002 (available at: <http://www.tele.ntnu.no/projects/beats/theses.htm>).
- [5] S. Falahati, A. Svensson, M. Sternad, and M. Hong, "Adaptive trellis-coded modulation over predicted flat fading channels," in *Proc. IEEE Vehicular Technology Conference*, vol. 3, pp. 1532–1536, October 2003.
- [6] G. E. Øien, H. Holm, and K. J. Hole, "Impact of channel prediction on adaptive coded modulation performance in Rayleigh fading," *IEEE Transactions on Vehicular Technology*, vol. 53, no. 3, pp. 758–769, May 2004.
- [7] M. Nakagami, "The m -distribution, a general formula of intensity distribution of rapid fading," *Statistical Methods in Radio Wave Propagation*, pp. 3–36, June 1960.
- [8] C. Mun, C. -H. Kang, and H. -K. Park, "Approximation of SNR statistics for MRC diversity systems in arbitrarily correlated Nakagami

- fading channels," *IEE Electronics Letters*, vol. 35, no. 4, pp. 266–267, February 1999.
- [9] D. V. Duong and G. E. Øien, "Adaptive trellis-coded modulation with imperfect channel state information at the receiver and transmitter," in *Proc. Nordic Radio Symposium*, August 2004.
- [10] J. G. Proakis, *Digital Communications*. Mc-Graw-Hill, Inc., 1995.
- [11] M. H. DeGroot and M. J. Schervish, *Probability and Statistics*. Addison-Wesley, 2002.
- [12] D. G. Brennan, "Linear diversity combining techniques," in *Proc. IRE*, vol. 47, pp. 1075–1102, 1959.
- [13] X. Tang, M. S. Alouini, and A. Goldsmith, "Effect of channel estimation error on M-QAM BER performance in Rayleigh fading," *IEEE Transactions on Communications*, vol. 47, no. 12, pp. 1856–1864, December 1999.
- [14] H. Holm and M. -S. Alouini, "Sum and difference of two squared correlated Nakagami variates in connection with the McKay distribution," *IEEE Transactions on Communications*, vol. 52, no. 8, pp. 1367–1376, August 2004.
- [15] V. A. Aalo, "Performance of maximal-ratio diversity systems in a correlated Nakagami-fading environment," *IEEE Transactions on Communications*, vol. 43, no. 8, pp. 2360–2369, August 1995.
- [16] J. Gurland, "Distribution of the maximum of the arithmetic mean of correlated random variables," *The Annals of Mathematical Statistics*, vol. 26, no. 2, pp. 294–300, June 1955.
- [17] M. -S. Alouini, A. Abdi, and M. Kaveh, "Sum of gamma variates and performance of wireless communication systems over Nakagami-fading channels," *IEEE Transactions on Vehicular Technology*, vol. 50, no. 6, pp. 1471–1479, November 2001.
- [18] B. Holter and G. E. Øien, "On the amount of fading for MIMO diversity systems," *accepted for publication in IEEE Transactions on Wireless Communications*.
- [19] U. Charash, "Reception through Nakagami fading multipath channels with random delays," *IEEE Transactions on Communications*, vol. COM-27, no. 4, pp. 657–670, April 1979.

-
- [20] S. Kotz and J. W. Adams, "Distribution of sum of identically distributed exponentially correlated gamma-variables," *The Annals of Mathematical Statistics*, vol. 35, no. 1, pp. 277–283, March 1964.
- [21] Z. Wang and G. B. Giannakis, "A simple and general parameterization quantifying performance in fading channels," *IEEE Transactions on Communications*, vol. 51, no. 8, pp. 1389–1398, August 2003.
- [22] P. Lombardo, G. Fedele, and M. M. Rao, "MRC performance for binary signals in Nakagami fading with general branch correlation," *IEEE Transactions on Communications*, vol. 47, no. 1, pp. 44–52, January 1999.
- [23] G. L. Stüber, *Principles of Mobile Communications*. Second edition, Kluwer Academic Publishers, 2001.
- [24] P. J. Smith and M. Shafi, "The impact of complexity in MIMO channel models," in *Proc. IEEE International Conference on Communications*, vol. 5, pp. 2924–2928, June 2004.
- [25] M. O. Hasna, M. -S. Alouini, and M. K. Simon, "Effect of fading correlation on the outage probability of cellular mobile radio systems," in *Proc. IEEE Vehicular Technology Conference*, vol. 3, pp. 1794–1798, October 2001.
- [26] N. M. Temme, *Special Functions: An Introduction to Classical Functions of Mathematical Physics*. New York: Wiley, 1996.
- [27] I. S. Gradshteyn and I. M. Ryzhik, *Table of Integrals, Series, and Products*. 5th ed., San Diego, CA: Academic Press, 1994.
- [28] G. E. Øien, H. Holm, and K. J. Hole, "Adaptive coded modulation with imperfect channel state information: System design and performance analysis aspects," *invited paper in Proc. IEEE International Symposium on Advances in Wireless Communications*, September 2002.
- [29] X. Cai and G. B. Giannakis, "Adaptive PSAM accounting for channel estimation and prediction errors," *IEEE Transactions on Wireless Communications*, vol. 4, no. 1, pp. 246–256, January 2005.
- [30] R. K. Mallik, M. Z. Win, J. W. Shao, M. -S. Alouini, and A. J. Goldsmith, "Channel capacity of adaptive transmission with maximal ratio combining in correlated Rayleigh fading," *IEEE Transactions on Wireless Communications*, vol. 3, no. 4, pp. 1124–1133, July 2004.

- [31] W. C. Y. Lee, "Level crossing rates of an equal-gain predetection diversity combiner," *IEEE Transactions on Communication Technology*, vol. COM-18, no. 4, pp. 417–426, August 1970.
- [32] A. Abdi and M. Kaveh, "A versatile spatio-temporal correlation function for mobile fading channels with non-isotropic scattering," in *Proc. 10th IEEE Workshop on Statistical Signal and Array Processing*, pp. 58–62, August 2000.

Paper C

Limitations in Spectral Efficiency of a Rate-Adaptive MIMO System Utilizing Pilot-Aided Channel Prediction

Bengt Holter, Geir E. Øien, Kjell J. Hole, and Henrik Holm

Published in
Proceedings IEEE Vehicular Technology Conference
Jeju, Korea, April 2003.

Abstract

A performance analysis of an adaptive coded modulation (ACM) system operating on a multiple-input multiple-output (MIMO) channel with uncorrelated Rayleigh fading subchannels is presented. Rate adaptation is based on periodically transmitted channel state information (CSI) back to the transmitter, providing information about the channel signal-to-noise ratio (CSNR) *as predicted by the receiver*. Transmit diversity is utilized by employing space-time block coding (STBC) at the transmitter.

1 Introduction

Adaptive coded modulation (ACM) is a promising data transmission scheme for simultaneously achieving high spectral efficiency and a low bit error rate (BER) on wireless and mobile channels [1]. In [2], a method for assessing performance merits of an ACM system has been employed to evaluate the average spectral efficiency (ASE) of a rate-adaptive coding scheme utilizing any set of multi-dimensional trellis codes originally designed for additive white Gaussian noise (AWGN) channels. The analysis is based on a single-input multiple-output (SIMO) flat-fading channel with statistically independent and identically distributed (i.i.d.) Rayleigh fading subchannels. Perfect coherent detection is assumed and maximum ratio combining (MRC) is employed to maximize the overall received *channel signal-to-noise ratio* (CSNR).

Motivated by the fact that many base stations already are equipped with multiple antennas, the results in [2] are extended to encompass a multiple-input multiple-output (MIMO) flat-fading channel. In a MIMO system, the benefit of transmitting from multiple antennas may be utilized to improve either the diversity order or the information rate of the system. These two transmission strategies are commonly denoted as MIMO diversity and spatial multiplexing, respectively [3]. In this study, a MIMO diversity system is analysed, since it represents a natural extension of the approach in [2]. Transmit diversity is realized by utilizing space-time block coding (STBC) at the transmitter [4, 5].

The rest of this paper is organized as follows. In Section 2, the system model is presented. The MIMO channel model is presented in Section 3, and in Section 4, formulas to determine the average BER and ASE of a rate-adaptive MIMO diversity system is presented. Simulation results are presented in Section 5 and conclusions are given in Section 6.

2 System model

The rate-adaptive MIMO diversity system considered is depicted in Figure C.1 (transmitter) and Figure C.2 (receiver). The number of transmit and receive antennas is denoted by n_T and n_R , respectively. The adaptive coded modulator/demodulator contains N transmitter-receiver pairs, indexed by $n \in \{1, 2, \dots, N\}$. Transmitter n has a spectral efficiency of R_n information bits/s/Hz, such that $R_1 < R_2 < \dots < R_N$, and is designed to provide $\text{BER} \leq \text{BER}_0$ (target BER) on an AWGN channel with $\text{CSNR} \geq \gamma_n$.

The codes are based on quadrature amplitude modulation (QAM) signal constellations with different number of symbols $M_n = 2^{k_n}$, where k_n is some positive integer. Rate adaptation is performed by splitting the CSNR range into $N + 1$ fading regions (bins) and letting the transmitter respond according to the overall (total) CSNR *as predicted by the receiver*. When the predicted CSNR falls within the fading region $[\gamma_n, \gamma_{n+1})$, the associated channel state information (CSI), i.e. the fading region index n , is sent back to the transmitter. The transmitter then adapts its transmission rate according to the predicted quality of the channel by transmitting with a signal constellation realizing a spectral efficiency of R_n . If the predicted CSNR falls into the interval $[0, \gamma_1)$, no information is transmitted (outage).

The CSI is assumed conveyed to the transmitter through a zero-error feedback channel, but by the time the CSI is received by the transmitter, it may deviate from the *true* channel state due to a non-zero return channel time-delay τ . As a result, the transmitter may transmit at either a too low or too high information rate, affecting the average BER, ASE, and outage probability of the system. The time-delay τ consists of a sum of the processing time used for CSNR prediction, transmission protocol delays, physical feedback transmission time, and time used for transmitter reconfiguration [2]. Other factors contributing to the system performance are the temporal fading correlation, the average channel quality, the number of codes/signal constellations, and how the CSNR is predicted.

For comparison reasons, all numerical results presented in Section 5 are based on the same assumptions as in [2] regarding the temporal fading correlation (Jakes spectrum) and the number of codes/signal constellations. A channel predictor optimal in the *maximum a posteriori* sense is utilized, and the CSI estimation is assumed done by an optimal non-causal Wiener interpolator filter, allowing true coherent detection to be assumed.

3 Channel model

In this section, the MIMO channel model is presented. In order to relate the results obtained in this study with the results presented in [2], the SIMO channel model and some important CSNR statistic results obtained in [2] are reviewed in the first subsection.

SIMO channel model

A flat-fading SIMO system with n_R receive antennas and MRC at the receiver is considered. The complex baseband representation of the received signal at each of the receiving antennas can be expressed as $\mathbf{x} = \mathbf{h}s + \mathbf{n}$,

where $\mathbf{x} \in \mathbb{C}^{n_R}$ denotes the vector of received signals per channel use, s denotes the transmit symbol, $\mathbf{h} \in \mathbb{C}^{n_R}$ denotes the SIMO channel vector, and $\mathbf{n} \in \mathbb{C}^{n_R}$ denotes the AWGN vector, where each entry of the vector is a zero-mean, complex Gaussian random variable with equal variance σ_n^2 .

The MRC output is a linear combination of the branch signals, and the overall received CSNR per symbol may be expressed as [6]

$$\gamma = \frac{P_T \|\mathbf{h}\|_2^2}{\sigma_n^2}, \quad (\text{C.1})$$

where P_T denotes the constant average transmit power and $\|\cdot\|_2^2$ denotes the squared Euclidean norm. From (C.1), the statistics of γ is governed by the statistics of $\|\mathbf{h}\|_2^2$. The envelopes of the entries in the channel vector \mathbf{h} are modelled as i.i.d. Rayleigh random variables. From this assumption, it can be shown that the overall CSNR γ will follow a Gamma distribution $\mathcal{G}(\alpha, \beta)$ with shape parameter $\alpha = n_R$ and scale factor $\beta = \bar{\gamma}_l$, where $\bar{\gamma}_l$ denotes the average CSNR received on any channel l . Note that due to the i.i.d assumption of the channels, the average CSNR on all channels will be equal. However, the average CSNR per channel $\bar{\gamma}_l$ will still be indexed by l in order to indicate that this is not the overall expected CSNR γ . Also due to the independence assumption of the subchannels, the *predicted* overall CSNR $\hat{\gamma}$ may be expressed as a Gamma distributed random variable $\hat{\gamma} \sim \mathcal{G}(n_R, r\bar{\gamma}_l)$, where the parameter r is the ratio between the expectation of the predicted and the true CSNR.

MIMO channel model

In a flat-fading MIMO diversity system, the complex baseband representation of the input/output relations can be expressed as $\mathbf{x} = \mathbf{H}\mathbf{s} + \mathbf{n}$, where $\mathbf{x} \in \mathbb{C}^{n_R}$ denotes the vector of received signals per channel use, $\mathbf{s} \in \mathbb{C}^{n_T}$ denotes the vector of transmit symbols, $\mathbf{H} \in \mathbb{C}^{n_R \times n_T}$ denotes the MIMO channel matrix, and $\mathbf{n} \in \mathbb{C}^{n_R}$ denotes the AWGN vector, where each entry of the vector is a zero-mean, complex Gaussian random variable with equal variance σ_n^2 . The complex entry h_{ij} of the channel matrix \mathbf{H} denotes a flat-fading channel between transmit antenna j and receive antenna i . It will be assumed that all envelopes in \mathbf{H} are i.i.d. Rayleigh random variables.

Using STBC at the transmitter, the total received CSNR per symbol may be written as [7]

$$\gamma = \frac{P_T \|\mathbf{H}\|_F^2}{\sigma_n^2 n_T}, \quad (\text{C.2})$$

where $\|\cdot\|_F^2$ denotes the squared Frobenius norm. From (C.2), the statistics of γ is governed by the statistics of $\|\mathbf{H}\|_F^2$. Using transformation of random

variables it can be shown that γ is a Gamma distributed random variable $\gamma \sim \mathcal{G}(\kappa, \frac{\bar{\gamma}_l}{n_T})$, where $\kappa = n_T \cdot n_R$. As for the SIMO system, the predicted CSNR may also be expressed as a Gamma distributed random variable $\hat{\gamma} \sim \mathcal{G}(\kappa, \frac{r\bar{\gamma}_l}{n_T})$.

It can be seen that the CSNR analysis of the SIMO system and the MIMO diversity system analysed in this subsection is very similar. Thus, by inserting the new CSNR statistics obtained in this section, the results in [2] may be extended to a MIMO diversity system using the same analysis approach.

4 BER and ASE analysis

The BER (averaged over all codes and all CSNRs) is given as the average number of bits in error, divided by the average number of bits transmitted [2]

$$\overline{\text{BER}} = \frac{\sum_{n=1}^N R_n \cdot \overline{\text{BER}}_n}{\sum_{n=1}^N R_n P_n}, \quad (\text{C.3})$$

where R_n is the information rate of code n , P_n is the probability that code n will be used, and $\overline{\text{BER}}_n$ is the average BER experienced when code n is applied. This may be written as [8]

$$\overline{\text{BER}}_n = \int_{\gamma_n}^{\gamma_{n+1}} \int_0^{\infty} \text{BER}_n(\gamma, \hat{\gamma}) f_{\gamma, \hat{\gamma}}(\gamma, \hat{\gamma}) d\gamma d\hat{\gamma}, \quad (\text{C.4})$$

where $\text{BER}_n(\gamma, \hat{\gamma})$ is the BER experienced when code n is applied, and $f_{\gamma, \hat{\gamma}}(\gamma, \hat{\gamma})$ is the joint distribution of the predicted and true CSNR. Since both the true and the predicted CSNR can be modelled as Gamma distributed random variables, $f_{\gamma, \hat{\gamma}}(\gamma, \hat{\gamma})$ is a bivariate Gamma distribution.

When code n is operating on an AWGN channel with CSNR γ , the BER-CSNR relationship for varying γ may be approximated by the expression [1]

$$\text{BER}_n \approx a_n \cdot e^{-\frac{b_n \gamma}{M_n}}, \quad (\text{C.5})$$

where a_n and b_n are code-dependent constants found by least-square curve fitting to simulated BER-CSNR data on AWGN channels. This approximation is accurate for any CSNR resulting in $\text{BER} < 10^{-1}$ [9]. However, the approximation approaches a_n for low CSNRs, and since a_n can be larger than one [1], the following approximate BER expression for code n is utilized [2]

$$\text{BER}_n(\gamma, \hat{\gamma}) = \begin{cases} a_n \cdot e^{-\frac{b_n \gamma}{M_n}} & \text{when } \gamma \geq \gamma_n^l \\ \frac{1}{2} & \text{when } \gamma < \gamma_n^l \end{cases} \quad (\text{C.6})$$

The boundary $\gamma_n^l = \ln(2a_n)M_n/b_n$ is the smallest CSNR such that the BER is no larger than 0.5 for either code in the set. The boundary is obtained by assuming equality in (C.5), setting $\text{BER} = 0.5$, and solving for γ . Note that the function in (C.5) is invertible, so the smallest CSNR required to achieve a given target BER, denoted BER_0 , can be found. Inserting (C.6) into (C.4), the average BER when trellis code n is employed may be expressed as a sum of three separate integrals [2],

$$\begin{aligned}\overline{\text{BER}}_n &= \int_{\gamma_n}^{\gamma_{n+1}} \mathcal{J}1(n, \hat{\gamma}) - (\mathcal{J}21(n, \hat{\gamma}) - \mathcal{J}22(n, \hat{\gamma}))d\hat{\gamma} \\ &= \mathcal{I}1(n) - (\mathcal{I}21(n) - \mathcal{I}22(n)),\end{aligned}\quad (\text{C.7})$$

where

$$\mathcal{J}1(n, \hat{\gamma}) = \int_0^{\infty} a_n \cdot e^{-\frac{b_n \gamma}{M_n}} f_{\gamma, \hat{\gamma}}(\gamma, \hat{\gamma}) d\gamma \quad (\text{C.8})$$

$$\mathcal{J}21(n, \hat{\gamma}) = \int_0^{\gamma_n^l} a_n \cdot e^{-\frac{b_n \gamma}{M_n}} f_{\gamma, \hat{\gamma}}(\gamma, \hat{\gamma}) d\gamma \quad (\text{C.9})$$

$$\mathcal{J}22(n, \hat{\gamma}) = \frac{1}{2} \int_0^{\gamma_n^l} f_{\gamma, \hat{\gamma}}(\gamma, \hat{\gamma}) d\gamma. \quad (\text{C.10})$$

Using the CSNR statistics for a MIMO diversity system presented in Section 3, the bivariate Gamma distribution may be written as

$$\begin{aligned}f_{\gamma, \hat{\gamma}}(\gamma, \hat{\gamma}) &= \frac{(\gamma \hat{\gamma})^{(\kappa-1)/2}}{\Gamma(\kappa) \left[r \left(\frac{\bar{\gamma}_l}{n_T} \right)^2 \right]^{(\kappa+1)/2} (1-\rho) \cdot \rho^{(\kappa-1)/2}} \\ &\times e^{-\frac{\gamma}{\frac{\bar{\gamma}_l}{n_T}(1-\rho)}} \cdot e^{-\frac{\hat{\gamma}}{\frac{\bar{\gamma}_l}{n_T}(1-\rho)}} \\ &\times I_{\kappa-1} \left(\frac{2\sqrt{\rho}}{1-\rho} \sqrt{\frac{\gamma \hat{\gamma}}{r \left(\frac{\bar{\gamma}_l}{n_T} \right)^2}} \right),\end{aligned}\quad (\text{C.11})$$

where ρ is the normalized power correlation coefficient between the true and predicted CSNR, $\Gamma(\cdot)$ is the gamma function, and $I_{\kappa-1}(\cdot)$ is the modified Bessel function of the first kind and order $\kappa - 1$. The following closed-

form expressions for $\mathcal{I}1(n)$, $\mathcal{I}21(n)$, and $\mathcal{I}22(n)$ in (C.7) are obtained:

$$\begin{aligned} \mathcal{I}1(n) &= a_n \left(\frac{n_T}{\frac{b_n \bar{\gamma}_l}{M_n} + n_T} \right)^\kappa \\ &\times \left[\bar{\Gamma} \left(\kappa, \frac{\gamma_n}{\bar{\gamma}_l r} \cdot \frac{n_T \left(\frac{b_n \bar{\gamma}_l}{M_n} + n_T \right)}{(1-\rho) \frac{b_n \bar{\gamma}_l}{M_n} + n_T} \right) \right. \\ &\left. - \bar{\Gamma} \left(\kappa, \frac{\gamma_{n+1}}{\bar{\gamma}_l r} \cdot \frac{n_T \left(\frac{b_n \bar{\gamma}_l}{M_n} + n_T \right)}{(1-\rho) \frac{b_n \bar{\gamma}_l}{M_n} + n_T} \right) \right], \end{aligned} \quad (\text{C.12})$$

$$\begin{aligned} \mathcal{I}21(n) &= a_n \sum_{k=0}^{\infty} \frac{\Gamma(k+\kappa)}{\Gamma(k+1)\Gamma(\kappa)} \left(\frac{\rho}{1-\rho} \right)^k \\ &\times \left(\frac{n_T}{\frac{b_n \bar{\gamma}_l}{M_n} + \frac{n_T}{(1-\rho)}} \right)^{k+\kappa} \\ &\times \left[1 - \bar{\Gamma} \left(k + \kappa, \gamma_n^l \left(\frac{b_n}{M_n} + \frac{n_T}{(1-\rho)\bar{\gamma}_l} \right) \right) \right] \\ &\times \left[\bar{\Gamma} \left(k + \kappa, \frac{n_T \gamma_n}{(1-\rho)\bar{\gamma}_l r} \right) \right. \\ &\left. - \bar{\Gamma} \left(k + \kappa, \frac{n_T \gamma_{n+1}}{(1-\rho)\bar{\gamma}_l r} \right) \right], \end{aligned} \quad (\text{C.13})$$

and

$$\begin{aligned} \mathcal{I}22(n) &= \frac{1}{2} \sum_{k=0}^{\infty} \frac{\Gamma(k+\kappa)}{\Gamma(k+1)\Gamma(\kappa)} \rho^k (1-\rho)^\kappa \\ &\times \left[1 - \bar{\Gamma} \left(k + \kappa, \frac{n_T \gamma_n^l}{(1-\rho)\bar{\gamma}_l} \right) \right] \\ &\times \left[\bar{\Gamma} \left(k + \kappa, \frac{n_T \gamma_n}{(1-\rho)\bar{\gamma}_l r} \right) \right. \\ &\left. - \bar{\Gamma} \left(k + \kappa, \frac{n_T \gamma_{n+1}}{(1-\rho)\bar{\gamma}_l r} \right) \right], \end{aligned} \quad (\text{C.14})$$

where $\bar{\Gamma}(x, y) = \Gamma(x, y)/\Gamma(x)$ is the normalized complementary incomplete gamma function. With $n_T = 1$ ($\kappa = n_R$), all closed-form expressions are reduced to the SIMO expressions in [2]. For a 2G-dimensional (2G-D) trellis

code utilized in [2], where $G \in \{1, 2, \dots\}$, the information rate R_n is obtained as follows. The encoder for code n accepts $p = G \cdot \log_2(M_n) - 1$ information bits at each time index $G \cdot T_s$, where T_s denotes the time between transmission of two consecutive QAM modulation symbols. The encoder generates $p + 1 = G \cdot \log_2(M_n)$ coded bits which specify G QAM modulation symbols from the n th QAM constellation with $M_n = 2^{k_n}$ symbols. Thus, p information bits are transmitted within $G \cdot T_s$ uses of the channel. The information rate for code n , in information bits per channel use, is then $R_n = \frac{p/(GT_s)}{B}$, where B is the signaling bandwidth. Assuming ideal Nyquist pulses, $B = 1/T_s$, the spectral efficiency of code n is $R_n = k_n - 1/G$ measured in bits/s/Hz.

Using pilot-aided channel prediction, every L th channel symbol is a pilot symbol and thus does not convey information. The information rate of code n can then be expressed as $R_n = (k_n - 1/G) \cdot \frac{L-1}{L}$. When pilot-aided channel prediction is utilized in a MIMO diversity system with n_T transmit antennas, n_T times as many pilot symbols are needed as in the SIMO case [4]. It is assumed that when a pilot symbol enters the space-time encoder, it is cyclically shifted and transmitted only once from each transmit antenna within n_T time periods. The data symbols that follows are encoded according to the rules of the chosen STBC.

In this study, the space-time encoder maps K input QAM symbols into n_T orthogonal sequences of length T , where $T = (K/R_s)T_s$, and R_s is the code rate of the employed STBC. Table C.1 summarizes the characteristics of some orthogonal STBC originally derived in [5] for 2, 3, and 4 transmit antennas [10]. Since the different orthogonal designs accept different

TABLE C.1: Orthogonal designs for STBC

<i>Orthogonal design</i>	n_T	R_s	K	T
G_2	2	1	2	2
G_3	3	1/2	4	8
G_4	4	1/2	4	8
H_3	3	3/4	3	4
H_4	4	3/4	3	4

number of input symbols, the following rules of pilot symbol spacing are

assumed:

$$L = \begin{cases} m \cdot n_T + 1 & \text{for } G_2, G_4, H_3 \\ m \cdot 4 + 1 & \text{for } G_3 \\ m \cdot 3 + 1 & \text{for } H_4 \end{cases}, \quad (\text{C.15})$$

where $m \in \mathbb{Z}^+, m \neq 0$. Employing either of the space time codes presented in Table C.1, the pilot symbol spacing on a single antenna branch L_b can be written as $L_b = (1/R_s)m \cdot K + n_T$. The new pilot spacing L_b can be expressed in terms of the original pilot spacing L as $L_b = (L - 1)/R_s + n_T$.

Using the assumptions on pilot spacing in (C.15), the spectral efficiency of code n in a MIMO diversity system, denoted R_n^{STBC} , can be expressed as

$$\begin{aligned} R_n^{\text{STBC}} &= (k_n - 1/G) \cdot \frac{(L_b - n_T)R_s}{L_b} \\ &= (k_n - 1/G) \cdot \frac{(L - 1) \cdot R_s}{L - 1 + n_T R_s}. \end{aligned} \quad (\text{C.16})$$

The ASE is a weighted sum of the information rates R_n^{STBC} for the individual codes [2]

$$\text{ASE} = \sum_{n=1}^N R_n^{\text{STBC}} \cdot P_n, \quad (\text{C.17})$$

where the probability P_n is simply the probability that the predicted CSNR falls into the interval $[\gamma_n, \gamma_{n+1})$, i.e. $P_n = \int_{\gamma_n}^{\gamma_{n+1}} f_{\hat{\gamma}}(\hat{\gamma}) d\hat{\gamma}$. The predicted overall CSNR $\hat{\gamma}$ is—as is the actual overall CSNR—a Gamma distributed random variable. The probability P_n can be identified as

$$P_n = \bar{\Gamma} \left(\kappa, \frac{\gamma_n n_T}{r \bar{\gamma}_l} \right) - \bar{\Gamma} \left(\kappa, \frac{\gamma_{n+1} n_T}{r \bar{\gamma}_l} \right). \quad (\text{C.18})$$

The ASE for a MIMO diversity system utilizing pilot-aided channel prediction can then be written as

$$\begin{aligned} \text{ASE} &= \sum_{n=1}^N (\log_2(M_n) - 1/G) \cdot \left(\frac{(L - 1) \cdot R_s}{L - 1 + n_T R_s} \right) \\ &\times \left[\bar{\Gamma} \left(\kappa, \frac{\gamma_n n_T}{r \bar{\gamma}_l} \right) - \bar{\Gamma} \left(\kappa, \frac{\gamma_{n+1} n_T}{r \bar{\gamma}_l} \right) \right]. \end{aligned} \quad (\text{C.19})$$

Due to an increased number of pilot symbols and the fact that for $n_T > 2$, the code-rate $R_s < 1$ for complex signal constellations [5], the ASE of the MIMO diversity system is upper bounded for a given L by the ASE of the SIMO system in [2]. In the next section, all the closed-form formulas derived in this section are utilized to obtain numerical results on BER and ASE performance of a rate-adaptive MIMO diversity system.

5 Numerical results

For all the results presented in this section, the channel is assumed to be quasi-static, i.e. the fading amplitudes of the channel matrix \mathbf{H} are assumed to be constant between two successive pilot symbols. A rate-adaptive codec with eight 4-dimensional trellis codes is utilized ($G = 2$), and for a target $\text{BER}_0 = 10^{-4}$, the parameters a_n and b_n along with the threshold values γ_n^l are the same as presented in Table 3.1 in [2]. Parameters not directly tied to the codes, albeit dependent on the implementation are the carrier frequency $f_c = 2$ GHz, a bandwidth of $B = 400$ kHz, and a terminal velocity of $v = 30$ m/s. In Figure C.3, C.4, and C.5, the average BER as a function of feedback delay and of expected subchannel CSNR for a 1×4 , 2×2 , and a 3×3 system is presented. The contour lines identify the target $\text{BER}_0 = 10^{-4}$, and the operation of the system is acceptable whenever $\text{BER} \leq \text{BER}_0$. It can be seen that due to the increased stability (diversity order) of the 3×3 system, the BER performance is acceptable within a greater range of CSNRs and delays than the 1×4 and the 2×2 system. The acceptable range for the 1×4 and the 2×2 system is very similar due to the same diversity order. The price paid for the 2×2 and the 3×3 system is the reduction in ASE. In Figure C.6, the relative differences in ASE between a 1×4 , 2×2 , and 3×3 system are depicted.

6 Conclusion

The performance results of a rate-adaptive SIMO system in [2] have been extended to encompass a MIMO diversity system, utilizing STBC at the transmitter. Even though the benefit of having multiple antennas can be utilized to increase the overall diversity order and thus the robustness of BER performance of the system, the increased number of pilot symbols needed to perform channel estimation and prediction reduces the attainable average spectral efficiency of the system. Clearly, in order to take full advantage of the combined capacity potential of MIMO subchannels and ACM, another prediction technique is needed. Decision-directed (DD) estimation or a DD/pilot-aided hybrid may be a candidate.

C. LIMITATIONS IN SPECTRAL EFFICIENCY OF A RATE-ADAPTIVE MIMO SYSTEM UTILIZING PILOT-AIDED CHANNEL PREDICTION

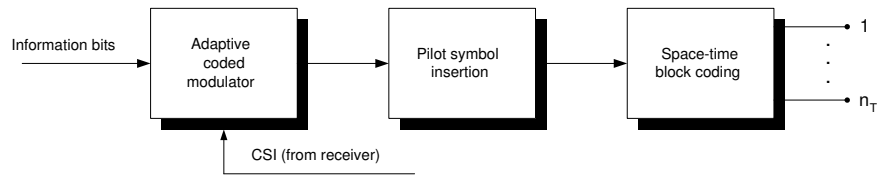


FIGURE C.1: Transmitter

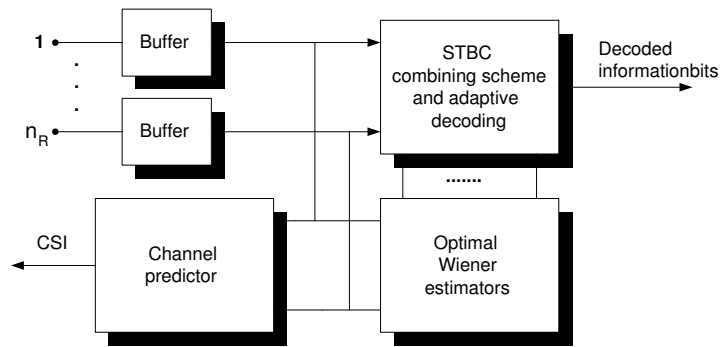


FIGURE C.2: Receiver

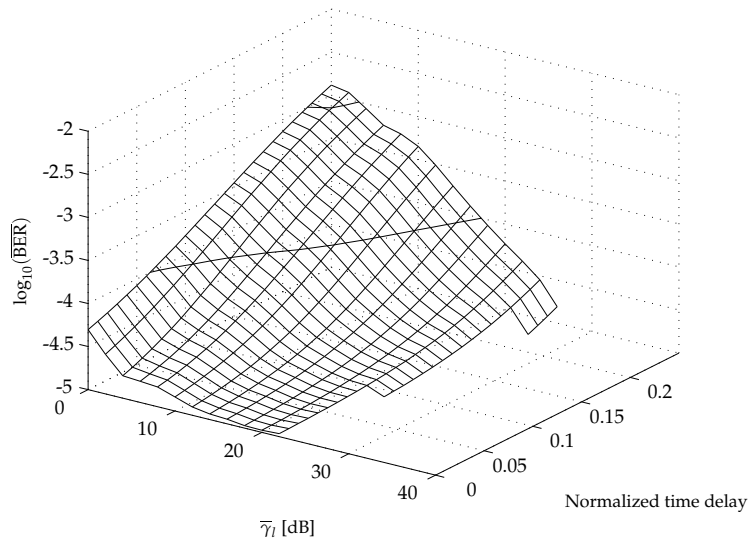


FIGURE C.3: Average BER as a function of feedback delay and of expected subchannel CSNR. $\kappa = 5$ antennas are utilized (1×4 system) and the pilot symbol spacing is $L = 7$. The prediction filter length is $K = 1000$.

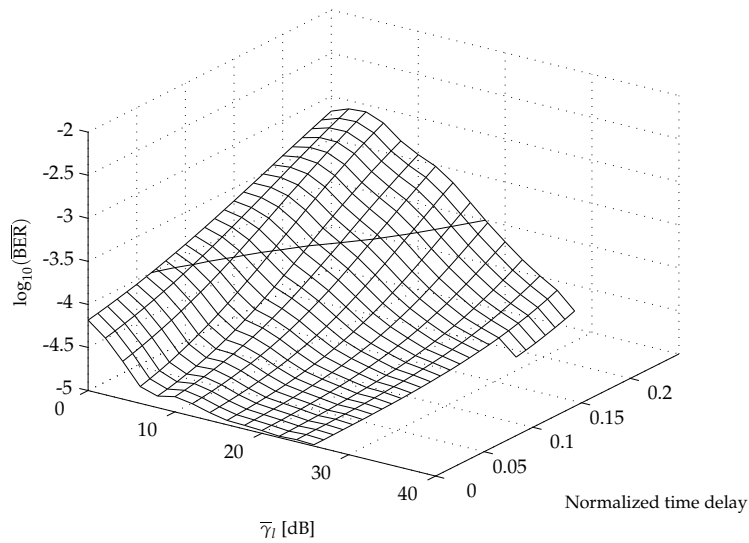


FIGURE C.4: Average BER as a function of feedback delay and of expected subchannel CSNR. $\kappa = 4$ antennas are utilized (2×2 system with STBC G_2) and the pilot symbol spacing is $L = 7$ ($L_b = 8$). The prediction filter length is $K = 1000$.

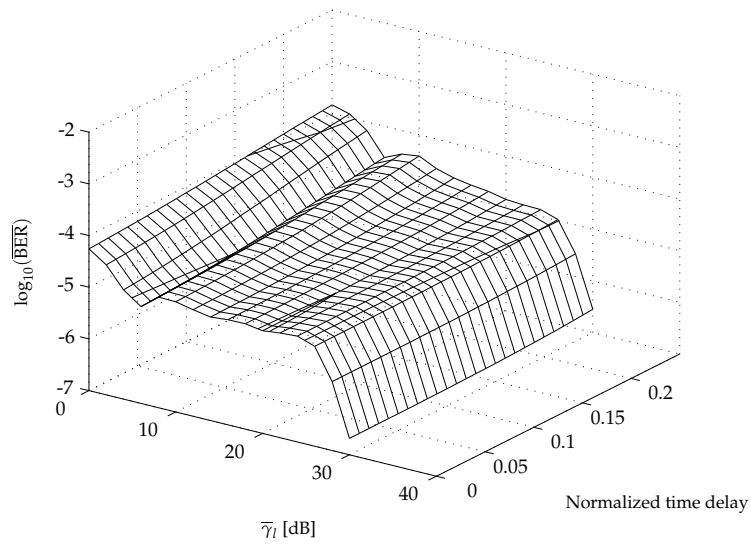


FIGURE C.5: Average BER as a function of feedback delay and of expected subchannel CSNR. $\kappa = 6$ antennas are utilized (3×3 system with STBC H_3) and the pilot symbol spacing is $L = 7$ ($L_b = 11$). The prediction filter length is $K = 1000$.

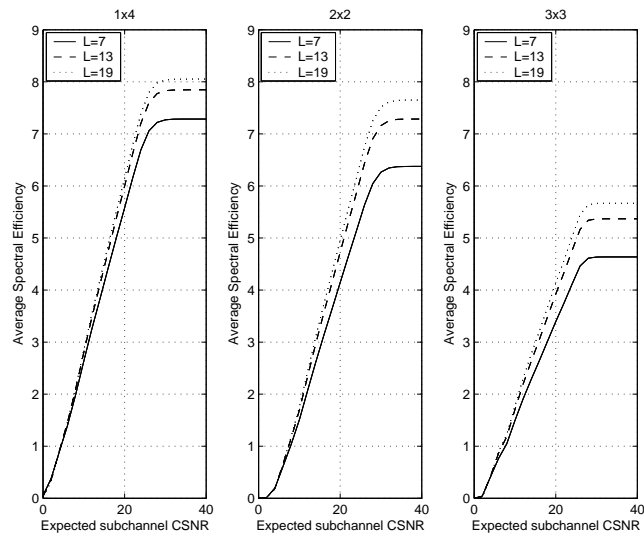


FIGURE C.6: Average spectral efficiency as a function of expected subchannel CSNR [dB], plotted for various L and a normalized feedback time delay (symbol duration normalized with respect to maximum Doppler spread) of 0.25. For the 2×2 system, the STBC G_2 is employed. For the 3×3 system, the STBC H_3 is employed.

References

- [1] K. J. Hole, H. Holm, and G. E. Øien, "Adaptive multidimensional coded modulation on flat fading channels," *IEEE Journal on Selected Areas in Communications*, vol. 18, no. 7, pp. 1153–1158, July 2000.
- [2] H. Holm, "Adaptive coded modulation and channel estimation tools for flat fading channels," Ph.D. dissertation, The Norwegian University of Science and Technology, April 2002 (available at: <http://www.tele.ntnu.no/projects/beats/theses.htm>).
- [3] R. W. Heath, "Space-time signaling in multi-antenna systems," Ph.D. dissertation, Stanford University, November 2001.
- [4] S. M. Alamouti, "A simple transmit diversity technique for wireless communications," *IEEE Journal on Selected Areas in Communications*, vol. 16, no. 8, pp. 1451–1458, October 1998.
- [5] V. Tarokh, H. Jafarkhani, and A. R. Calderbank, "Space-time block codes from orthogonal designs," *IEEE Transactions on Information Theory*, vol. 45, no. 5, pp. 1456–1467, July 1999.
- [6] B. Holter and G. E. Øien, "The optimal weights of a maximum ratio combiner using an eigenfilter approach," in *Proc. 5th IEEE Nordic Signal Processing Symposium*, October 2002.
- [7] S. Sandhu and A. Paulraj, "Space-time block codes: a capacity perspective," *IEEE Communications Letters*, vol. 4, no. 12, pp. 384–386, December 2000.
- [8] M. -S. Alouini and A. Goldsmith, "Adaptive modulation over Nakagami fading channels," *Wireless Personal Communications*, vol. 13, pp. 119–143, May 2000.
- [9] K. J. Hole, H. Holm, and G. E. Øien, "Performance analysis of adaptive coded modulation with antenna diversity and feedback delay," *Teletronikk*, vol. 98, no. 1, pp. 106–113, 2002.

- [10] R. Gozali and B. D. Woerner, "On the robustness of space-time block codes to spatial correlation," in *Proc. IEEE Vehicular Technology Conference*, vol. 2, pp. 832–836, May 2002.

Paper D

On the Amount of Fading in MIMO Diversity Systems

Bengt Holter and Geir E. Øien

Accepted for publication in
IEEE Transactions on Wireless Communications

Abstract

In this paper, a closed-form expression is presented for the amount of fading (AF) experienced at the output of a space-time block coded multiple-input multiple-output (MIMO) diversity system operating on identically distributed spatially correlated Nakagami- m fading channels. For the separable correlation model (Kronecker model), the AF is presented for identically distributed Rayleigh fading channels and different types of antenna correlation models. For a MIMO diversity system based on the Kronecker model, it is shown, by capitalizing on recent results in [1], that the average symbol-error-rate at high signal-to-noise ratio may be directly expressed in terms of the AF when a constant correlation model is assumed.

1 Introduction

Several performance measures may be employed to characterize the behavior of wireless communication systems operating on fading channels. For systems utilizing spatial diversity techniques, it is of interest to employ measures which can capture and quantify the improvement on system performance caused by reducing the fading-induced fluctuations of the received signal. Commonly encountered measures in this respect are the average symbol-error-rate (SER) or the average bit-error-rate (BER). The diversity order of a spatial diversity system is usually determined by the slope of the average SER curve at high signal-to-noise ratios (SNRs), whereas different levels of correlation between the diversity branches are visible as shifted versions of the SER curve relative to a benchmark SER curve. However, as noted in [2], the average error rate may in some cases be difficult to evaluate analytically, since it requires statistical averaging of the conditional error rate over the statistics of the fading. A more simple yet effective way of quantifying the severity of fading (and the effect of correlation) can be obtained by using a measure directly related to the moments of the fading distribution itself.

In [3] Charash introduced the notion of *amount of fading* (AF) to quantify the severity of fading experienced for a particular channel model. In terms of the probability density function (PDF) of the instantaneous fading amplitude $\alpha = |h|$ of a single complex fading channel h , the AF is defined by [3, Eq. (2)], [4, Eq. (2.5)]

$$\text{AF} = \frac{\text{Var}\{\alpha^2\}}{(\mathcal{E}\{\alpha^2\})^2}, \quad (\text{D.1})$$

with $\mathcal{E}\{\cdot\}$ and $\text{Var}\{\cdot\}$ denoting the statistical average and variance, respectively.¹ For a single Nakagami- m fading channel [6], $\text{AF} = 1/m$. Hence, for large values of m (line-of-sight), the fading channel will approach a non-fading additive white Gaussian noise (AWGN) channel. For a single Rayleigh fading channel ($m = 1$), $\text{AF} = 1$.

Although the AF originally was defined and applied to quantify the severity of fading experienced at the output of a single fading channel, it is in this paper employed to quantify the degree of fading experienced at the output of a multiple-input multiple-output (MIMO) system. The benefit of

¹As noted in [5], the AF as defined by Charash is equal to the kurtosis minus 1. The kurtosis is equal to the degree of peakedness of a distribution and it is defined as a normalized form of the fourth central moment, i.e. for a random variable X , the kurtosis $\kappa = \mathcal{E}\{X^4\}/\mathcal{E}^2\{X^2\}$.

transmitting from multiple antennas in a wireless system may either be utilized to improve the diversity order (high reliability solution) or improve the capacity (high rate solution). These two transmission strategies are commonly denoted *MIMO diversity* and *spatial multiplexing*, respectively [7]. In this study, a MIMO diversity system is considered, where transmit diversity is realized by utilizing space-time block coding (STBC)² at the transmitter [8, 9].

There are some examples in the literature of how the AF can be applied as a performance measure in communication systems employing spatial diversity. In [2], closed-form expressions for the AF are obtained for three dual-branch diversity combining techniques in the presence of log-normal fading, namely, maximum ratio combining (MRC) [4, Sec. 9.2], selection combining (SC) [4, Sec. 9.7], and switch-and-stay combining (SSC) [4, Sec. 9.8]. In [10], the square root of the AF was applied to the combiner output to assess the effectiveness of a hybrid selection/MRC diversity combining scheme in the presence of Rayleigh fading.³

In this paper, the AF is presented for a MIMO diversity system operating on identically distributed spatially correlated Nakagami- m fading channels. The necessary moments are derived by utilizing a recent and compact representation of the characteristic function (CF) of the (instantaneous) combined fading power at the output of a MIMO diversity system [11]. Subsequently, it is assumed that the correlation properties at the transmitter is independent of the correlation properties at the receiver. Under this assumption, the channel correlation matrix can be written as a Kronecker product [12, Ch. 9] of a transmit correlation matrix and a receive correlation matrix [13, 14]. In the literature, this model is frequently denoted the Kronecker model. The Kronecker model has been validated for non-line-of-sight (NLOS) scenarios [15, 16], but the accuracy of the model has recently been questioned, at least for antennas with high spatial resolution (large antenna arrays) [17–19]. Since all the measurement campaigns referenced in this paper (both supporting and questioning the Kronecker model) have been conducted in NLOS scenarios (typically modelled with Rayleigh fading channels), the AF expressions based on the Kronecker model are in this paper limited to systems operating on Rayleigh fading channels.

The remainder of this paper is organized as follows. Section 2 presents

²Space-time block codes are designed to achieve the maximum diversity order for a given number of transmit and receive antennas subject to the constraint of having a simple decoding algorithm.

³The square root of the AF is equal to a statistical measure known as *coefficient of variation*.

statistical information of the combined fading power in a MIMO diversity system. In Section 3, this information is used to obtain a compact closed-form expression for the AF. The general result (valid for identically distributed Nakagami- m fading channels) is then simplified by introducing the Kronecker model and by incorporating different types of antenna correlation models. In Section 4, it is shown that by capitalizing on recent results in [1], the average SER at high SNR may be expressed in terms of the AF when a constant correlation model is assumed at both ends of the MIMO link. Numerical results are presented in Section 5, and the main results of the paper are summarized in Section 6.

2 Statistics of the combined fading power

To obtain an expression for the AF, the statistics of either the combined SNR or combined fading power must be known. For a flat-fading MIMO diversity system with n_T transmit antennas and n_R receive antennas, the combined SNR (per symbol) may be written as [20]

$$\gamma_c = \frac{P_T \|\mathbf{H}\|_F^2}{\sigma^2 n_T} = \frac{P_T}{\sigma^2 n_T} \sum_{i=1}^{n_R} \sum_{j=1}^{n_T} \alpha_{ij}^2, \quad (\text{D.2})$$

where $\|\mathbf{H}\|_F^2$ represents the combined fading power (squared Frobenius norm of the channel matrix \mathbf{H} [12]), and $\alpha_{ij}^2 = |h_{ij}|^2$ represents the fading power of a single narrowband channel between the j th transmitter and the i th receiver. From (D.2), it can be seen that the statistics of γ_c is governed by the statistics of $\|\mathbf{H}\|_F^2$. For simplicity, just a single subscript n will be used to distinguish between the entries of the channel matrix,⁴ and the squared Frobenius norm may then be expressed as $\|\mathbf{H}\|_F^2 = \sum_{n=1}^N \alpha_n^2$, where $N = n_T \cdot n_R$ denotes the maximum number of channels in the MIMO channel. Viewing all the fading amplitudes in the set $\{\alpha_n\}_{n=1}^N$ as identically distributed Nakagami- m random variables (RVs) [6], the PDF of a single fading amplitude α_n is equal to [6]

$$p(\alpha_n) = \frac{2m^m \alpha_n^{2m-1}}{\Omega^m \Gamma(m)} \cdot e^{-\frac{m\alpha_n^2}{\Omega}}, \quad (\text{D.3})$$

where $\Gamma(\cdot)$ denotes the *gamma function*⁵, $\Omega = \mathcal{E}\{\alpha_n^2\}$ denotes the average fading power, and m is the Nakagami fading parameter.

⁴ $n = n(i, j) = n_T \cdot (i - 1) + j$ for $i \in [1, 2, \dots, n_R]$ and $j \in [1, 2, \dots, n_T]$.

⁵ $\Gamma(z) = \int_0^\infty t^{z-1} e^{-t} dt$, $\Re(z) > 0$ [21].

When the instantaneous fading amplitude α_n is distributed according to (D.3), the instantaneous fading power α_n^2 will follow a gamma distribution⁶ with shape parameter m and scale parameter $\frac{\Omega}{m}$. In short, $\alpha_n^2 \sim \mathcal{G}(m, \frac{\Omega}{m})$. Hence, $\|\mathbf{H}\|_F^2$ represents a sum of N identically distributed possibly correlated gamma variates.

3 Amount of fading

The CF of $\|\mathbf{H}\|_F^2 \triangleq \alpha_c^2$, representing a sum of N identically distributed correlated gamma variates, may be written compactly as [11]

$$\Phi_{\alpha_c^2}(w) = |\mathbf{I}_{N \times N} - w\mathbf{R}_H|^{-m} = |\mathbf{I}_{N \times N} - w\Lambda|^{-m} = \prod_{n=1}^N (1 - w\lambda_n)^{-m}, \quad (\text{D.4})$$

where w is the variable of the transform domain, $|\cdot|$ denotes the determinant operator, $\mathbf{I}_{N \times N}$ is the identity matrix of size $N \times N$, and Λ is the diagonal eigenvalue matrix of the (complex) channel correlation matrix $\mathbf{R}_H = \mathcal{E}\{\text{vec}(\mathbf{H})\text{vec}(\mathbf{H})^H\}$, containing the set of eigenvalues $\{\lambda_n\}_{n=1}^N$.⁷ Since \mathbf{R}_H is a Hermitian matrix, the existence of Λ is guaranteed by the spectral theorem [12, Theorem 6.2].⁸ The moments of an RV can be determined from its CF according to [22, Eq. (2-1-74)]:

$$\mathcal{E}\{\alpha_c^{2q}\} = \frac{1}{j^q} \cdot \left. \frac{d^q \Phi_{\alpha_c^2}(w)}{dw^q} \right|_{w=0}. \quad (\text{D.5})$$

⁶ $Y = \alpha_n^2$ follows a gamma distribution with shape parameter $a > 0$ and scale parameter $b > 0$ when the PDF of Y is given by $p_Y(y) = \frac{y^{a-1} e^{-y/b}}{b^a \Gamma(a)}$. The short hand notation $Y \sim \mathcal{G}(a, b)$ is used to denote that Y follows a gamma distribution with shape parameter a and scale parameter b .

⁷The superscript $(\cdot)^H$ denotes the Hermitian transpose operator, and the $\text{vec}(\cdot)$ operator stacks the individual columns of the argument matrix on top of each other, i.e. represents the matrix as a single column vector [12, Sec. 9.3].

⁸In addition, this means that the algebraic multiplicity of eigenvalues in \mathbf{R}_H (the number of eigenvalues) is equal to the geometric multiplicity of eigenvalues (the size of the nullspace spanned by the eigenvectors). Thus, if \mathbf{R}_H is a $N \times N$ Hermitian matrix of rank $r < N$ (rank-deficient), exactly $N - r$ of the eigenvalues of \mathbf{R}_H are equal to zero. This means that the effective number of terms contributing to the product in (D.4) (i.e. product terms different from 1) in general is equal to r . For full rank matrices, $r = N$. In this paper, it is assumed that \mathbf{R}_H is full rank.

Using logarithmic derivation [23], the first and second order derivatives of (D.4) may be expressed as

$$\Phi'_{\alpha_c^2}(w) = \left[\sum_{n=1}^N \frac{m\lambda_n}{1-w\lambda_n} \right] \cdot \Phi_{\alpha_c^2}(w), \quad (\text{D.6})$$

$$\Phi''_{\alpha_c^2}(w) = \left[\sum_{n=1}^N \frac{m\lambda_n^2}{(1-w\lambda_n)^2} + \left(\sum_{n=1}^N \frac{m\lambda_n}{1-w\lambda_n} \right)^2 \right] \cdot \Phi_{\alpha_c^2}(w). \quad (\text{D.7})$$

Using (D.5), the mean and variance of α_c^2 may be identified as

$$\mathcal{E}\{\alpha_c^2\} = m \cdot \sum_{n=1}^N \lambda_n, \quad (\text{D.8})$$

$$\text{Var}\{\alpha_c^2\} = m \cdot \sum_{n=1}^N \lambda_n^2. \quad (\text{D.9})$$

According to (D.1), the AF may now be expressed as $\text{AF} = \frac{\sum_{n=1}^N \lambda_n^2}{m \cdot (\sum_{n=1}^N \lambda_n)^2}$. For normalized average power on all channels, i.e. $\mathcal{E}\{\alpha_n^2\} = \Omega = 1$ for all $n \in [1, 2, \dots, N]$, the channel correlation matrix \mathbf{R}_H will contain just 1s on the main diagonal. Since the sum of eigenvalues equals the sum of diagonal entries in a matrix [24, Ch. 5], the AF for identically distributed Nakagami- m fading channels may be written as

$$\text{AF} = \frac{\text{tr}(\Lambda^2)}{m \cdot N^2}, \quad (\text{D.10})$$

where $\text{tr}(\cdot)$ is the matrix trace operator [12].

In the following, it is assumed that the correlation between the antennas at the transmitter is independent of the correlation between the antennas at the receiver. This separability assumption (Kronecker model) has been validated by some authors [15, 16], and has become quite popular due to its analytical tractability. However, note that some authors recently have questioned its accuracy [17–19].

All the measurement campaigns on the Kronecker model referenced in this paper (both supporting and questioning the Kronecker model) have been conducted in NLOS scenarios. As a result, we have chosen to limit the analysis based on the Kronecker model to identically distributed Rayleigh fading channels. According to Appendix 6, the AF may then be written

$$\text{AF} = \frac{\sum_{j=1}^{n_T} \|\mathbf{t}_j\|^2 \sum_{i=1}^{n_R} \|\mathbf{r}_i\|^2}{N^2}, \quad (\text{D.11})$$

where $\|\cdot\|^2$ denotes the squared Euclidean vector norm, and the vectors \mathbf{t}_j and \mathbf{r}_i denote rows j and i of the transmit and receive correlation matrices, respectively. Next, it is shown that the result in (D.11) may be simplified even further when specific types of antenna correlation models are taken into account. For simplicity, results are presented for identical correlation models at the transmitter and the receiver. Results for other scenarios (i.e. non-identical correlation models at the transmitter and the receiver) may also easily be obtained, although not presented in this paper.

Constant correlation

For a constant correlation model, applicable for an array of three antennas placed on an equilateral triangle or for closely spaced antennas other than linear arrays [25], the correlation matrix \mathbf{R}_Y of size $n_Y \times n_Y$ at the transmitter/receiver may be written

$$\mathbf{R}_Y = \begin{bmatrix} 1 & y & \cdots & y \\ y^* & 1 & \cdots & y \\ \vdots & \vdots & \ddots & \vdots \\ y^* & y^* & \cdots & 1 \end{bmatrix}, \quad (\text{D.12})$$

where the subscript $Y \in \{T, R\}$ is used to distinguish between the transmit correlation matrix \mathbf{R}_T and the receive correlation matrix \mathbf{R}_R , $y \in \{t, r\}$ denotes the complex transmit/receive correlation coefficient, and y^* denotes the complex conjugate of y . For constant correlation matrices at each end of the MIMO link, the AF (denoted AF_{con}) is expressible as

$$\text{AF}_{con} = \frac{[1 + |t|^2(n_T - 1)]}{n_T} \cdot \frac{[1 + |r|^2(n_R - 1)]}{n_R}. \quad (\text{D.13})$$

An alternative expression to (D.13) is obtained by noting that the fading amplitude (envelope) correlation coefficient ρ^{env} and the fading power correlation coefficient ρ^{pow} may be assumed equal for all practical purposes [6, 26]. The correlation between fading envelopes can also be approximated by the squared amplitude of the complex correlations in \mathbf{R}_H , referred to as power correlation coefficients [26], [27, Eq. (35)]. Hence, $\rho_{ij}^{env} \approx |\mathbf{R}_H(i, j)|^2 = \rho_{ij}^{pow}$, where $\mathbf{R}_H(i, j)$ represents a single entry of the matrix at the i th row and j th column. As a result, (D.13) may also be written

$$\text{AF}_{con} = \text{AF}_{Tx} \cdot \text{AF}_{Rx} = \frac{[1 + \rho_t(n_T - 1)]}{n_T} \cdot \frac{[1 + \rho_r(n_R - 1)]}{n_R}, \quad (\text{D.14})$$

where $\rho_t = |t|^2$ and $\rho_r = |r|^2$ represent the transmit and receive power correlation coefficients, respectively.

Circular correlation

A circular correlation model may apply to antennas lying on a circle, or four antennas placed on a square [25]. The correlation matrix \mathbf{R}_Y can then be written as

$$\mathbf{R}_Y = \begin{bmatrix} 1 & y_2 & y_3 & \cdots & y_{n_Y} \\ y_{n_Y}^* & 1 & y_2 & \cdots & y_{n_Y-1} \\ y_{n_Y-1}^* & y_{n_Y}^* & 1 & \cdots & y_{n_Y-2} \\ \vdots & \vdots & \vdots & \ddots & \vdots \\ y_2^* & y_3^* & y_4^* & \cdots & 1 \end{bmatrix}, \quad (\text{D.15})$$

where $y_1 = 1$. Since every correlation matrix is Hermitian, it implies that $y_2 = y_{n_Y}^*, y_3 = y_{n_Y-1}^*, \dots$. The AF with circular correlation at each end of the MIMO link (denoted AF_{cir}) can be expressed as

$$\text{AF}_{cir} = \frac{\sum_{j=1}^{n_T} |t_j|^2}{n_T} \cdot \frac{\sum_{i=1}^{n_R} |r_i|^2}{n_R}. \quad (\text{D.16})$$

Exponential correlation

An exponential correlation model may apply to an equispaced linear array of antenna elements [4]. The correlation matrix \mathbf{R}_Y can be written

$$\mathbf{R}_Y = \begin{bmatrix} 1 & y & \cdots & y^{n_Y-1} \\ y^* & 1 & \cdots & y^{n_Y-2} \\ \vdots & \vdots & \ddots & \vdots \\ (y^*)^{n_Y-1} & (y^*)^{n_Y-2} & \cdots & 1 \end{bmatrix}. \quad (\text{D.17})$$

For exponential correlation on each side of the MIMO link, the AF (denoted AF_{exp}) can be expressed as

$$\text{AF}_{exp} = \frac{[1 + 2 \sum_{j=1}^{n_T-1} (1 - \frac{j}{n_T}) |t|^{2j}] [1 + 2 \sum_{i=1}^{n_R-1} (1 - \frac{i}{n_R}) |r|^{2i}]}{n_T n_R}. \quad (\text{D.18})$$

In [4], numerical results of the average SER and outage probability in a MRC system show that the constant correlation model suffers only a minor performance degradation compared to the exponential correlation, but the performance difference is more noticeable for a large number of diversity paths and high correlation between the paths. As a result, the constant correlation model may be employed as a worst case correlation scenario, since the impact of correlation on system performance for other correlation models typically will be less severe. Hence, among the correlation profiles used in this paper, the impact of fading correlation is most severe (highest AF) for the constant correlation model.

4 AF_{con} and its relation to the average SER at high SNR

In this section, it is shown that for a constant correlation matrix at either side of a MIMO diversity system operating on identically distributed spatially correlated Rayleigh fading channels, the average SER at high SNR may be expressed in terms of AF_{con} . To this end, we will be invoking some recent results by Wang and Giannakis [1].

Approximate SER

In [1], the average SER P_E of an uncoded (or coded) system at high SNR is approximated by the expression

$$P_E \approx (G_c \cdot \bar{\gamma})^{-G_d}, \quad (\text{D.19})$$

where G_c represents a *coding gain*, and G_d represents the *diversity order*. The diversity order determines the slope of the average SER curve versus the received average SNR $\bar{\gamma}$ at high SNR in a log-log scale, whereas the coding gain (in dB) determines the shift of the curve in SNR relative to a benchmark SER curve given by $(\bar{\gamma}^{-G_d})$.

Capitalizing on results in [25], the *moment generating function* (MGF) $\mathcal{M}_{\gamma_c}(s)$ of the combined SNR γ_c of a MIMO diversity system with identically distributed channels may be expressed as

$$\mathcal{M}_{\gamma_c}(s) = \prod_{n=1}^N \left(1 - \frac{s\bar{\gamma}}{n_T} \lambda_n \right)^{-1}, \quad (\text{D.20})$$

where s is the variable of the transform domain, $\{\lambda_n\}_{n=1}^N$ denote the eigenvalues of a $N \times N$ power correlation matrix \mathbf{C} defined by

$$\mathbf{C} = \begin{bmatrix} 1 & \sqrt{\rho_{12}} & \cdots & \sqrt{\rho_{1N}} \\ \sqrt{\rho_{21}} & 1 & \cdots & \sqrt{\rho_{2N}} \\ \vdots & \vdots & \ddots & \vdots \\ \sqrt{\rho_{N1}} & \sqrt{\rho_{N2}} & \cdots & 1 \end{bmatrix}, \quad (\text{D.21})$$

and ρ_{ij} denotes the power correlation coefficient between the instantaneous SNR received on channels i and j , respectively.⁹ When decoupled correla-

⁹The parameter ρ_{ij} represents a power correlation coefficient since $\rho_{ij} = \text{Cov}(\gamma_i, \gamma_j) / \sqrt{\text{Var}(\gamma_i)\text{Var}(\gamma_j)} = \text{Cov}(\alpha_i^2, \alpha_j^2) / \sqrt{\text{Var}(\alpha_i^2)\text{Var}(\alpha_j^2)}$, where α_i^2 denotes the instantaneous fading power received on channel i , α_j^2 denotes the instantaneous fading power received on channel j , and the expressions $\text{Cov}(\cdot, \cdot)$ and $\text{Var}(\cdot)$ denote covariance and variance of its arguments, respectively.

tion properties are assumed, the power correlation matrix \mathbf{C} may be written as a Kronecker product $\mathbf{C} = \mathbf{C}_{Tx} \otimes \mathbf{C}_{Rx}$ of the transmit and receive power correlation matrices, respectively.

Applying Proposition 3 from [1] to the MGF in (D.20), the approximate (yet accurate) expression for the average SER P_E at high SNR may be written as¹⁰

$$P_E \approx \frac{2^{N-1} b \Gamma(N + \frac{1}{2})}{\sqrt{\pi} \Gamma(N + 1)} \cdot \left(\frac{1}{k}\right)^N, \quad (\text{D.22})$$

where $b = [\det(\mathbf{C}_{Tx} \otimes \mathbf{C}_{Rx})]^{-1} \left(\frac{n_T}{\bar{\gamma}}\right)^N$, and k is a fixed code-dependent positive constant [1]. Using (D.19), the MIMO diversity system may then be characterized by the following diversity order and coding gain at high SNR:

$$G_d = N \quad (\text{D.23})$$

$$G_c = k \left(\frac{2^{N-1} p \Gamma(N + \frac{1}{2})}{\sqrt{\pi} \Gamma(N + 1)} \right)^{-1/N}, \quad (\text{D.24})$$

where $p = [\det(\mathbf{C}_{Tx})^{n_R} \cdot \det(\mathbf{C}_{Rx})^{n_T}]^{-1} \cdot n_T^N$. Here, the following matrix identity has been utilized [12, Eq. (9.8)]:

$$\det(\mathbf{C}_{Tx} \otimes \mathbf{C}_{Rx}) = \det(\mathbf{C}_{Tx})^{n_R} \cdot \det(\mathbf{C}_{Rx})^{n_T}. \quad (\text{D.25})$$

For uncorrelated channels, the determinant of the Kronecker product in (D.25) is equal to 1, and thus, as pointed out in [1], correlation increases P_E by a factor $[\det(\mathbf{C}_{Tx})^{n_R} \cdot \det(\mathbf{C}_{Rx})^{n_T}]^{-1} \geq 1$. A general increase in the number of transmit antennas will also increase P_E for power limited systems as long as the channel matrix is assumed unknown at the transmitter, since the available power at the transmitter must be divided between the transmit antennas. As a consequence, a penalty in error performance will be incurred [8]. If the channel matrix is known prior to transmission, beamforming could be utilized, and no error performance penalty would be incurred.

If the correlation level is increased, a corresponding increase in the AF will be experienced at the diversity combiner output. Our goal now is to express P_E in (D.22) in terms of the AF to directly relate this performance measure to the effect of correlation on diversity system performance. In

¹⁰This result differs from the result presented in [1, Eq. (10)], since the MGF of the combined SNR has been utilized and not the MGF of the fading power as used in [1]. Hence, the average SNR $\bar{\gamma}$ is in this paper included in the factor b , whereas in [1], it is not.

the following, an alternative expression for the determinant of a constant correlation matrix is utilized to express (D.22) in terms of AF_{con} .

When both \mathbf{C}_{R_x} and \mathbf{C}_{T_x} are constant correlation matrices, their determinants may be written in closed form as [28]

$$\det(\mathbf{C}_{R_x}) = (1 - \sqrt{\rho_r})^{n_R-1}(1 + \sqrt{\rho_r}(n_R - 1)), \quad (\text{D.26})$$

$$\det(\mathbf{C}_{T_x}) = (1 - \sqrt{\rho_t})^{n_T-1}(1 + \sqrt{\rho_t}(n_T - 1)), \quad (\text{D.27})$$

where both ρ_r and ρ_t are real numbers taking on values between zero and one. Since normalized average power has been assumed on all channels, we have observed (see Figure D.1) that the cumulative distribution function (CDF) of a beta distributed RV [29] can be used as an alternative closed-form expression for the determinants in (D.26) and (D.27). Hence, we may view $\sqrt{\rho_r}$ and $\sqrt{\rho_t}$ as beta distributed RVs (see Appendix 7), which implies:

$$\begin{aligned} \det(\mathbf{C}_{R_x}) &= I\left(1 - \sqrt{\frac{n_R \cdot AF_{R_x} - 1}{n_R - 1}}; n_R - 1, 2\right) \\ &\triangleq \text{betacdf}(AF_{R_x}), \end{aligned} \quad (\text{D.28})$$

$$\begin{aligned} \det(\mathbf{C}_{T_x}) &= I\left(1 - \sqrt{\frac{n_T \cdot AF_{T_x} - 1}{n_T - 1}}; n_T - 1, 2\right) \\ &\triangleq \text{betacdf}(AF_{T_x}), \end{aligned} \quad (\text{D.29})$$

where $I(\cdot; \cdot, \cdot)$ denotes the regularized beta function [30]. Upon inserting (D.28) and (D.29) into (D.22), the average SER may now be expressed as

$$P_E \approx \frac{2^{N-1}\Gamma(N + \frac{1}{2})}{\sqrt{\pi}\Gamma(N + 1)} \cdot \left(\frac{n_T}{k\bar{\gamma}}\right)^N \cdot [\text{betacdf}(AF_{T_x})]^{-n_R} \cdot [\text{betacdf}(AF_{R_x})]^{-n_T}, \quad (\text{D.30})$$

valid for $n_T \geq 2$ and $n_R \geq 2$.

Exact SER

To evaluate the result in (D.30), it is compared to an exact SER expression. As an example, a binary phase-shift keying (BPSK) modulation scheme will be utilized. Using a general M -ary phase-shift keying (M -PSK) modulation scheme as a starting point, an expression for a BPSK modulation scheme is later obtained by letting $M = 2$. According to [4, Eq. (5.67)], the average SER performance of a M -PSK modulation scheme over a fading channel is expressible as

$$P_E = \frac{1}{\pi} \int_0^{(M-1)\pi/M} \mathcal{M}_\gamma\left(-\frac{\mathcal{G}_{psk}}{\sin^2\theta}\right) d\theta, \quad (\text{D.31})$$

where M is equal to the number of symbols in the signal constellation, $g_{psk} = \sin^2(\pi/M)$, and $\mathcal{M}_\gamma(\cdot)$ denotes the MGF of the received SNR. For a MIMO diversity system, the MGF of the combined SNR is given by (D.20), but due to the multiplicative property of eigenvalues in a Kronecker product, the expression in (D.20) may also be written as

$$\mathcal{M}_{\gamma_c}(s) = \prod_{i=1}^{n_R} \prod_{j=1}^{n_T} \left(1 - \frac{s\bar{\gamma}}{n_T} \lambda_i \lambda_j \right)^{-1}, \quad (\text{D.32})$$

where the sets $\{\lambda_j\}_{j=1}^{n_T}$ and $\{\lambda_i\}_{i=1}^{n_R}$ denote the eigenvalues of the transmit and receive power correlation matrices \mathbf{C}_{T_x} and \mathbf{C}_{R_x} , respectively.¹¹ Upon inserting (D.32) into (D.31), replacing the variable s in (D.32) with the factor $-g_{psk}/\sin^2\theta$ and assuming that both \mathbf{C}_{T_x} and \mathbf{C}_{R_x} are constant correlation matrices, the eigenvalues of the two matrices can be expressed in closed form [28]. After some manipulations (D.31) reduces to

$$\begin{aligned} P_E &= \frac{1}{\pi} \int_0^u [1 + g\lambda_{t,1}\lambda_{r,1}]^{-(n_R-1)(n_T-1)} \\ &\times [1 + g\lambda_{r,1}\lambda_{t,2}]^{-(n_R-1)} \\ &\times [1 + g\lambda_{t,1}\lambda_{r,2}]^{-(n_T-1)} \\ &\times [1 + g\lambda_{t,2}\lambda_{r,2}]^{-1} d\theta, \end{aligned} \quad (\text{D.33})$$

where $u = \frac{(M-1)\pi}{M}$, $\lambda_{t,1} = 1 - \sqrt{\rho_t}$, $\lambda_{r,1} = 1 - \sqrt{\rho_r}$, $\lambda_{t,2} = 1 + \sqrt{\rho_t}(n_T - 1)$, $\lambda_{r,2} = 1 + \sqrt{\rho_r}(n_R - 1)$, and $g = \frac{\bar{\gamma}g_{psk}}{n_T \sin^2\theta}$. By letting $M = 2$ (BPSK), the exact SER expression in (D.33) can be compared to the approximate SER expression in (D.30) with $k = 2$ [1].

In [1], the coding gain G_c was defined as the (left) shift of the average SER curve relative to the benchmark curve ($\bar{\gamma}^{-G_d}$). To quantify the impact of increased AF in G_c for a fixed modulation scheme, the benchmark curve utilized in this paper is given by the approximate average SER curve at high SNR realized with uncorrelated channels. For correlated channels, the average SER curve is then visible as a (right) shifted version of the benchmark curve, and the relative shift represents the loss in coding gain due to correlation between the diversity branches (increased AF).¹² The relative loss in coding gain ΔG_c (in dB) may be expressed as

$$\Delta G_c = 10 \cdot \left(\frac{n_R \cdot \log[\det(\mathbf{C}_{T_x})] + n_T \cdot \log[\det(\mathbf{C}_{R_x})]}{N} \right), \quad (\text{D.34})$$

¹¹For $n_T = 1$, the MGF in (D.32) reduces the MGF in [4, Eq. (9.173)], valid for a single-input multiple-output (SIMO) system.

¹²Note that with the current benchmark definition, the placement of the benchmark will differ depending on the size of the MIMO diversity system (total number of antennas).

or equivalently,

$$\Delta G_c = 10 \cdot \left(\frac{n_R \cdot \log[\text{betacdf}(\text{AF}_{Tx})] + n_T \cdot \log[\text{betacdf}(\text{AF}_{Rx})]}{N} \right), \quad (\text{D.35})$$

valid when $n_T \geq 2$ and $n_R \geq 2$.

5 Numerical results

In this section, some numerical examples of the results derived in this paper are presented. Since the impact of correlation is most noticeable for the constant correlation model, the results are limited to MIMO systems operating on identically distributed Rayleigh fading channels with constant correlation models at each end of the MIMO link. Related results for other correlation models will typically be less severe.

In Figure D.2, AF_{con} in (D.14) is depicted as a function of the power correlation coefficient $\rho = \rho_t = \rho_r$ for both single-input multiple-output (SIMO), multiple-input single-output (MISO), and MIMO diversity systems. By comparing the various subfigures, it can be seen that AF_{con} is progressively reduced when the number of antennas is increased either at the transmitter or the receiver. As expected, the reduction is largest for uncorrelated antennas. In Figure D.3 and Figure D.4, the approximate average SER in (D.30) is compared to the exact result in (D.33) for a 3×3 MIMO diversity system and a BPSK modulation scheme. In Figure D.3 (top subfigure), it can be seen that approximate average SER curve for correlated channels at high SNR can be obtained as a (right) shifted version of the approximate average SER curve for uncorrelated channels (benchmark). This is visualized for $\rho_r = 0.8$. In the bottom subfigure, ΔG_c is depicted as a function of both ρ_r (lower x -axis) and AF_{con} (upper x -axis). Using the lower x -axis as reference, $\rho_r = 0.8$ amounts to a right shift of -5 dB from the benchmark curve, which is in agreement with the observed difference of the curves in the top subfigure. According to the upper x -axis, the AF is reduced by 71% compared to a single Rayleigh fading channel when $\rho_r = 0.8$ (and $\rho_t = 0$). For uncorrelated channels ($\rho_t = \rho_r = 0$), a 3×3 MIMO diversity system reduces the AF by 89% compared to a single Rayleigh fading channel, which is equivalent to ninth order diversity.

In Figure D.4 (top subfigure), the same set of curves as depicted in Figure D.3 (top subfigure) are presented, but this time when $\rho_t = 0.5$. Once again, excellent agreement between the exact and approximate curves at high SNR is observed. From Figure D.4 (bottom subfigure), it can be seen that ΔG_c has increased from -5 dB to -7.3 dB when $\rho_r = 0.8$, due to $\rho_t = 0.5$

at the transmitter. This corresponds to 42% reduction in the AF compared to a single Rayleigh fading channel.

6 Conclusion

A closed-form expression for the AF in a MIMO diversity system operating on identically distributed spatially correlated Nakagami- m fading channels has been presented. For the Kronecker model, the AF has been presented for identically distributed Rayleigh fading channels and different correlation models. Capitalizing on recent results in [1], it has been shown that the approximate average SER at high SNR of a MIMO diversity system based on the Kronecker model can be expressed as a function of the AF when a constant correlation model is assumed.

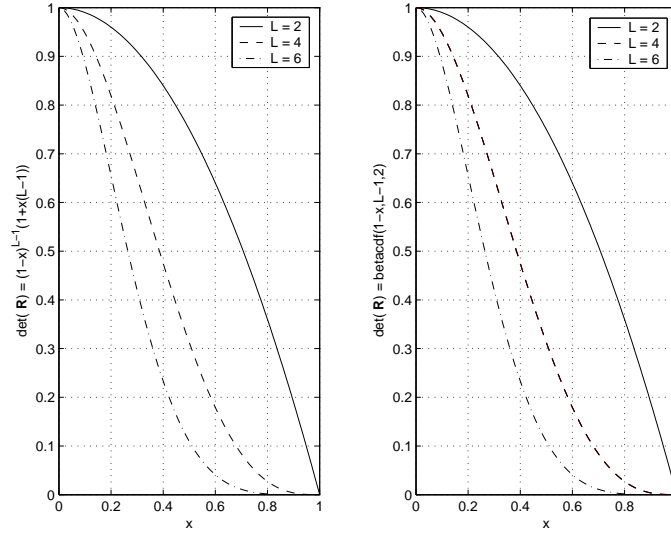


FIGURE D.1: Numerical comparison of closed form expressions for the determinant of a constant correlation matrix \mathbf{R} . **Left figure:** $\det(\mathbf{R}) = (1-x)^{L-1}(1+x(L-1))$. **Right figure:** $\det(\mathbf{R}) = \text{betacdf}(1-x, L-1, 2)$.

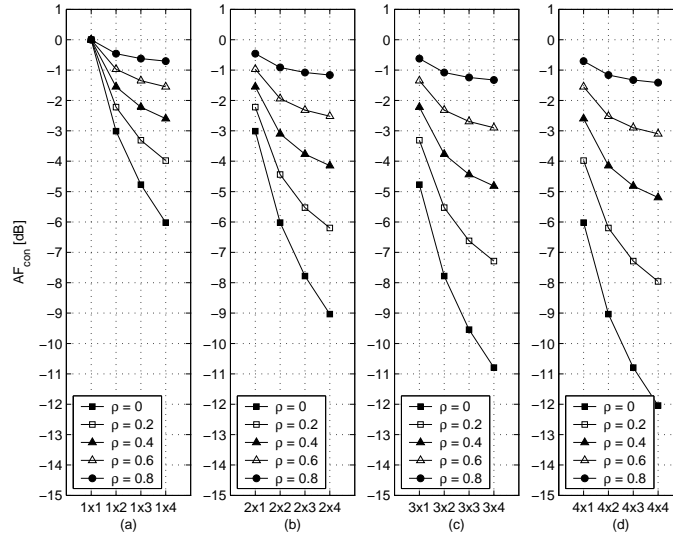


FIGURE D.2: AF_{con} (in dB) as a function of the power correlation coefficient $\rho = \rho_t = \rho_r$ for SIMO, MISO, and MIMO diversity systems ($n_T \times n_R$) operating on identically distributed Rayleigh fading channels: (a) ($1 \times n_R$); (b) ($2 \times n_R$); (c) ($3 \times n_R$); (d) ($4 \times n_R$).

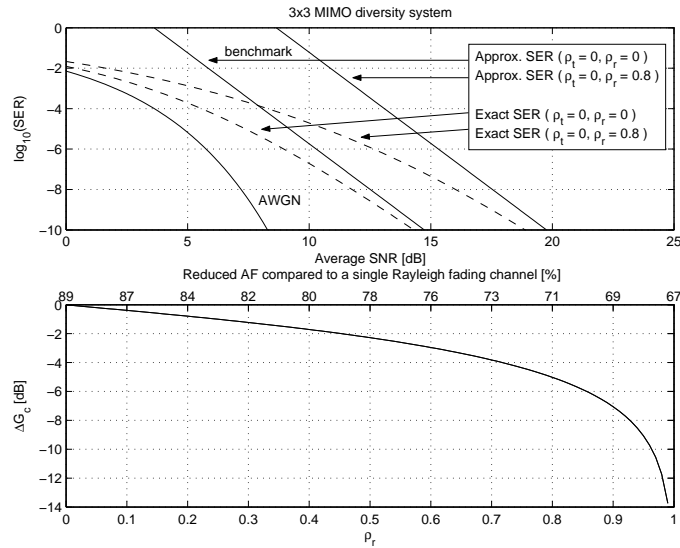


FIGURE D.3: **Top figure:** Exact average SER (dashed lines) and approximate average SER at high SNR (solid lines) for a 3×3 MIMO diversity system operating on identically distributed Rayleigh fading channels (constant correlation models at each end of the MIMO link). A BPSK modulation scheme is utilized. **Bottom figure:** Relative (right) shift (in dB) of the SER benchmark curve presented in the top figure as a function of ρ_r when $\rho_t = 0$. Using the top x -axis as a reference, the AF realized by the 3×3 MIMO diversity system is compared (in percentage) to the AF of a single Rayleigh fading channel (100% reduction represents the non-fading AWGN channel).

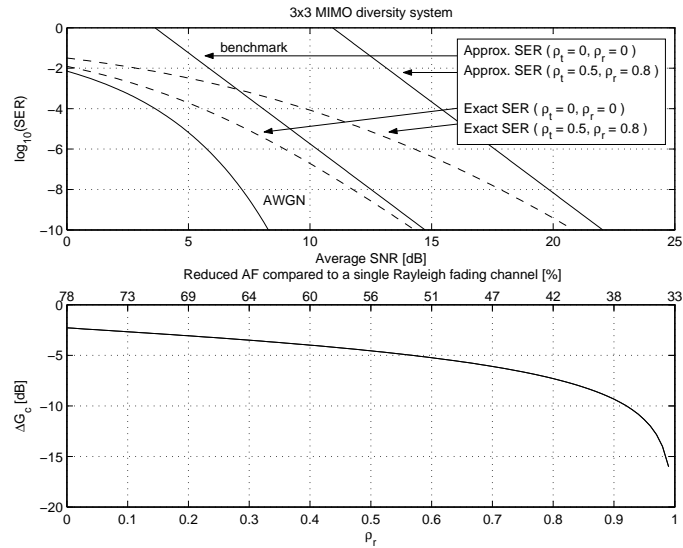


FIGURE D.4: **Top figure:** Exact average SER (dashed lines) and approximate average SER at high SNR (solid lines) for a 3×3 MIMO diversity system operating on identically distributed Rayleigh fading channels (constant correlation models at each end of the MIMO link). A BPSK modulation scheme is utilized. **Bottom figure:** Relative (right) shift (in dB) of the SER benchmark curve presented in the top figure as a function of ρ_r when $\rho_t = 0.5$. Using the top x -axis as reference, the AF realized by the 3×3 MIMO diversity system is compared (in percentage) to the AF of a single Rayleigh fading channel (100% reduction represents the non-fading AWGN channel).

References

- [1] Z. Wang and G. B. Giannakis, "A simple and general parameterization quantifying performance in fading channels," *IEEE Transactions on Communications*, vol. 51, no. 8, pp. 1389–1398, August 2003.
- [2] M. -S. Alouini and M. K. Simon, "Dual diversity over log-normal fading channels," *IEEE Transactions on Communications*, vol. 50, no. 12, pp. 1946–1959, December 2002.
- [3] U. Charash, "Reception through Nakagami fading multipath channels with random delays," *IEEE Transactions on Communications*, vol. 27, no. 4, pp. 657–670, April 1979.
- [4] M. K. Simon and M. -S. Alouini, *Digital Communication over Fading Channels: A Unified Approach to Performance Analysis*. John Wiley & Sons, Inc., 2000.
- [5] S. Verdú, "Spectral efficiency in the wideband regime," *IEEE Transactions on Information Theory*, vol. 48, no. 6, pp. 1319–1343, June 2002.
- [6] M. Nakagami, "The m -distribution, a general formula of intensity distribution of rapid fading," *Statistical Methods in Radio Wave Propagation*, pp. 3–36, June 1960.
- [7] R. W. Heath, "Space-time signaling in multi-antenna systems," Ph.D. dissertation, Stanford University, November 2001.
- [8] S. M. Alamouti, "A simple transmit diversity technique for wireless communications," *IEEE Journal on Selected Areas in Communications*, vol. 16, no. 8, pp. 1451–1458, October 1998.
- [9] V. Tarokh, H. Jafarkhani, and A. R. Calderbank, "Space-time block codes from orthogonal designs," *IEEE Transactions on Information Theory*, vol. 45, no. 5, pp. 1456–1467, July 1999.

- [10] M. Z. Win and J. H. Winters, "Analysis of hybrid selection/maximal-ratio combining in Rayleigh fading," *IEEE Transactions on Communications*, vol. 47, no. 12, pp. 1773–1776, December 1999.
- [11] M. Wennström, "On MIMO systems and adaptive arrays for wireless communication," Ph.D. dissertation, Uppsala University, September 2002 (available at: <http://www.signal.uu.se/Publications/abstracts/a022.html>).
- [12] T. K. Moon and W. C. Stirling, *Mathematical methods and algorithms for signal processing*. Prentice Hall, Inc., 1999.
- [13] J. P. Kermoal, L. Schumacher, K. I. Pedersen, P. E. Mogensen, and F. Frederiksen, "A stochastic MIMO radio channel model with experimental validation," *IEEE Journal on Selected Areas in Communications*, vol. 20, no. 6, pp. 1211–1226, August 2002.
- [14] A. Giorgetti, M. Chiani, M. Shafi, and P. J. Smith, "Level crossing rates and MIMO capacity fades: Impacts of spatial/temporal channel correlation," in *Proc. IEEE International Conference on Communications*, pp. 3046–3050, May 2003.
- [15] K. Yu, B. Ottersten, D. McNamara, P. Karlsson, and M. Beach, "Second order statistics of NLOS indoor MIMO channels based on 5.2 GHz measurements," in *Proc. IEEE GLOBECOM*, pp. 156–160, November 2001.
- [16] D. Chizhik, J. Ling, P. W. Wolniansky, R. A. Valenzuela, N. Costa, and K. Huber, "Multiple-input multiple-output measurements and modeling in Manhattan," *IEEE Journal on Selected Areas in Communications*, vol. 21, no. 3, pp. 321–331, April 2003.
- [17] H. Özcelik, M. Herdin, W. Weichselberger, J. Wallace, and E. Bonek, "Deficiencies of Kronecker MIMO radio channel model," *IEE Electronics Letters*, vol. 39, no. 16, pp. 1209–1210, August 2003.
- [18] J. Wallace, H. Özcelik, M. Herdin, E. Bonek, and M. Jensen, "Power and complex envelope correlation for modeling measured indoor MIMO channels: A beamforming evaluation," in *Proc. IEEE Vehicular Technology Conference*, pp. 363–367, October 2003.
- [19] T. S. Pollock, "Correlation modelling in MIMO systems: When can we Kronecker?" in *Proc. Australian Communications Theory Workshop*, pp. 149–153, February 2004.

-
- [20] S. Sandhu and A. J. Paulraj, "Space-time block codes: a capacity perspective," *IEEE Communications Letters*, vol. 4, no. 12, pp. 384–386, December 2000.
- [21] N. M. Temme, *Special Functions: An Introduction to the Classical Functions of Mathematical Physics*. John Wiley & Sons, Inc., 1996.
- [22] J. G. Proakis, *Digital Communications*. Mc-Graw-Hill, 1995.
- [23] C. H. Edwards Jr. and D. E. Penney, *Calculus with Analytic Geometry*. Prentice Hall, Inc., 1994.
- [24] G. Strang, *Linear algebra and its applications*. Harcourt Brace Jovanovich, Inc., 1988.
- [25] M. -S. Alouini, A. Abdi and M. Kaveh, "Sum of gamma variates and performance of wireless communication systems over Nakagami fading channels," *IEEE Transactions on Vehicular Technology*, vol. 50, no. 6, pp. 1471–1480, November 2001.
- [26] J. N. Pierce and S. Stein, "Multiple diversity with nonindependent fading," in *Proc. IRE*, vol. 48, pp. 89–104, January 1960.
- [27] J. Luo and J. R. Zeidler, "A statistical simulation model for correlated Nakagami fading channels," in *Proc. International Conference on Communication Technology*, vol. 2, pp. 1680–1684, August 2000.
- [28] S. J. Press, *Applied Multivariate Analysis: Using Bayesian and frequentist methods of inference*. Holt, Rinehart, Winston, 2nd edition, 1972.
- [29] M. H. DeGroot and M. J. Schervish, *Probability and Statistics*. Addison-Wesley, 2002.
- [30] <http://mathworld.wolfram.com>.

Paper E

Multiuser Switched Diversity Transmission

Bengt Holter, Mohamed-Slim Alouini, Geir E. Øien and Hong-Chuan Yang

Published in
Proceedings IEEE Vehicular Technology Conference
Los Angeles, USA, September 2004.

Abstract

In this paper, a set of multiuser access schemes are proposed based on switched diversity algorithms originally devised to select between antennas in a spatial diversity system. Instead of relying on feedback from all the users in a multiuser communication system to identify the best user on a time-slot basis (having the best channel quality among all the users), the proposed multiuser access schemes are performed in a sequential manner, looking not for the best user but for an acceptable user. A user qualifies as an acceptable user and is selected by the base station when the reported channel quality is above a pre-defined switching threshold. The proposed schemes result in a lower average spectral efficiency (ASE) than using the optimal selective diversity scheme, but a gain is obtained by reducing the feedback load. Numerical results that quantify the trade-off between ASE and average feedback load (AFL) are presented, showing that the AFL can be reduced significantly compared to the optimal selective diversity scheme without experiencing a big performance loss. In addition, it is argued that the proposed multiuser access schemes can be quite attractive also from a fairness perspective.

1 Introduction

In a traditional spatial diversity system, the diversity gain arises from independent signal paths received by multiple antennas. In a multiuser communication system, multiuser diversity (independent fading channels across different users) can be exploited to maximize the average throughput by always serving the user with the strongest channel [1, 2]. A traditional way of performing this task in a time division multiplexed (TDM) system is to let the base station (BS) probe all the users and select the user which reports the best channel quality at any given time-slot. The selected user is given access to the channel to either upload or download information, and the average spectral efficiency (ASE) of the system can be maximized by transmitting with the highest possible rate supported by the selected channel.

The key observation utilized in this paper is that algorithms originally devised to select between antennas in a spatial diversity combiner also may be applied as multiuser access schemes, since multiuser diversity may be looked upon as spatial diversity, in which the antennas of the spatial diversity combiner (acting as a BS) have been replaced by users (each having a single antenna). Hence, a multiuser access scheme based on always serving the user with the strongest channel is equivalent to the selection combining (SC) scheme in a spatial diversity system [3, Sec. 9.7]. It yields the best ASE for a certain target bit-error-rate (BER), but it comes at the expense of a high feedback load. Indeed, defining feedback load N_e as the number of estimated paths/users per time-slot before channel access [4], the feedback load of the multiuser access scheme based on the SC algorithm will be deterministic and equal to K (the number of users connected to the BS). In an attempt to simplify the selection procedure and reduce the feedback load, a set of *switched* multiuser access schemes are proposed. These access schemes are based on switched diversity algorithms originally devised to select between antennas in a spatial diversity system, and the basic principle is to look for an *acceptable* user instead of the best user, i.e. a user with a channel quality above a predefined switching threshold.

In short, a switched multiuser access scheme works as follows: the BS starts probing the users in a sequential fashion, requesting the signal-to-noise ratio (SNR) of the first user and then comparing it to the switching threshold. If the SNR is below the threshold, the BS moves on to the second user. This user SNR probing/checking process continues until (i) either one user is above the threshold (this user is selected for the subsequent transmission time) (ii) all K users have been examined and all have failed to exceed the switching threshold, in which either the last examined user

is selected (for simplicity), the best user among all the probed users is selected, or one waits a period longer than the channel coherence time and starts a new sequential search.

Using a sequential search to identify an acceptable user can contribute to increase fairness in a multiuser system, since the sequence in which to probe the users can be made different from one time-slot to the next. When independent and identically distributed (i.i.d.) channels are assumed, the users will be competing for the channel on equal terms. In this case, on average, all K users will have accessed the channel after K time-slots.

2 System and channel model

A TDM system is considered, where only one user has channel access per time-slot (for uplink or downlink). A single time-slot is divided into a guard time and an information transmission time. During the guard time, the BS selects the user who will have access to the channel in the subsequent transmission time. The guard time is assumed fixed and equal to the amount of time necessary to probe all the users. The time duration of a single time-slot is assumed roughly equal to the channel coherence time, and the data burst is assumed to experience the same fading conditions as the preceding guard period (block fading). For simplicity, i.i.d. Rayleigh fading channels across the different users are assumed, and the individual users and the BS are all equipped with just a single antenna. Finally, perfect channel state information is assumed available at both the BS and the users.

A rate-adaptive coding scheme using a set of N multidimensional trellis codes originally designed for additive white Gaussian noise (AWGN) channels is assumed utilized on each selected link to ensure a high ASE of the system [5]. In this paper, $N = 8$ different codes based on quadrature amplitude modulation (QAM) signal constellations of growing size $\{M_n\}_{n=1}^N = \{4, 8, 16, 32, 64, 128, 256, 512\}$ are utilized. Rate adaptation is performed by splitting the SNR range into $N + 1$ fading regions (bins), and the separate fading regions are defined by the SNR thresholds $0 < \gamma_1 < \gamma_2 < \dots < \gamma_N < \gamma_{N+1} = \infty$. Code n with spectral efficiency R_n [bits/s/Hz] is used for transmission if the SNR γ of the selected channel/user is reported to be within the fading region $\gamma_n \leq \gamma < \gamma_{n+1}$. The lower limit γ_n of each fading region is equal to the lowest SNR which guarantees that a predefined target BER ($\text{BER}_0 = 10^{-4}$) is achieved by code n .

3 ASE and BER analysis

The ASE of the system is obtained as a sum of the spectral efficiencies $\{R_n\}_{n=1}^N = \{1.5, 2.5, \dots, 8.5\}$ for the individual codes, weighted by the probability P_n that code n is used:¹

$$\text{ASE} = \sum_{n=1}^N R_n \cdot P_n, \quad (\text{E.1})$$

where

$$P_n = \int_{\gamma_n}^{\gamma_{n+1}} p_{\gamma_{\text{BS}}}(\gamma) d\gamma, \quad (\text{E.2})$$

The function $p_{\gamma_{\text{BS}}}(\gamma)$ denotes the probability density function (PDF) of the output SNR at the BS. The shape of this PDF will depend on the mode of operation of the selected multiuser access scheme.

The BER, when averaged over all codes and SNRs, is given as the average number of bits in error divided by the average number of bits transmitted [5, 6]:

$$\overline{\text{BER}} = \frac{\sum_{n=1}^N R_n \cdot \overline{\text{BER}}_n}{\sum_{n=1}^N R_n \cdot P_n}, \quad (\text{E.3})$$

where $\overline{\text{BER}}_n$ is the average BER experienced when code n is applied. An expression for $\overline{\text{BER}}_n$ is obtained by utilizing the exponential approximation $\text{BER}_n = a_n \cdot e^{-b_n \gamma / M_n}$ for the BER-SNR relationship for varying γ [5], thus

$$\overline{\text{BER}}_n = \int_{\gamma_n}^{\gamma_{n+1}} a_n \cdot e^{-\frac{b_n \gamma}{M_n}} p_{\gamma_{\text{BS}}}(\gamma) d\gamma, \quad (\text{E.4})$$

where a_n and b_n are code-dependent constants found by least-square fitting to simulated data on AWGN channels. The expression for BER_n is invertible, so the smallest SNR required to achieve BER_0 can be identified as $\gamma_n = (M_n / b_n) \ln(a_n / \text{BER}_0)$.

4 Multiuser access schemes

In the following subsections, ASE and average BER expressions for a set of multiuser access schemes are presented. The schemes are listed in terms of increasing complexity. For later reference, the PDF and CDF² of the output

¹In practice, the ASE of all the access schemes presented in this paper should be reduced by a factor $\frac{T_i}{T_g + T_i}$, where T_g is the guard time interval, and T_i is the information transmission time interval. The factor is omitted, since we emphasize on the relative differences in ASE.

²Cumulative distribution function.

SNR of a single-input single-output Rayleigh fading channel is equal to and denoted as $p_\gamma(\gamma) = \frac{1}{\bar{\gamma}}e^{-\gamma/\bar{\gamma}}$ and $P_\gamma(\gamma) = 1 - e^{-\gamma/\bar{\gamma}}$, respectively. The symbol $\bar{\gamma}$ denotes the average SNR, equal on all channels.

Scan-and-wait transmission (SWT)

The SWT multiuser access scheme is based on a multibranch scan-and-wait combining scheme [4] and it works as follows: during the guard time interval, a sequential search is initiated by the BS, requesting the SNR of each user and comparing it to a switching threshold γ_T . The SNR probing/checking process continues until either one user is above γ_T (this user is selected for the subsequent transmission time) or all K users have been examined and all have failed to exceed γ_T . In the latter case, the BS simply waits a period longer than the channel coherence time (deliberate outage) before it starts a new sequential search. This procedure can be repeated indefinitely until a user with an acceptable SNR is found. With this approach, the output SNR can be described by the following PDF [4, Eq. (6)]:

$$p_{\gamma_{\text{SWT}}}(\gamma) = \begin{cases} \frac{p_\gamma(\gamma)}{1-P_\gamma(\gamma_T)} & \gamma \geq \gamma_T \\ 0 & \text{otherwise} \end{cases}. \quad (\text{E.5})$$

Even though the PDF in (E.5) is correct, it represents the PDF the output SNR when the waiting procedure already is included, since the probability of not exceeding γ_T is zero. In order to better relate the results of the SWT scheme to the other access schemes presented in this paper, the PDF reflecting the output SNR *per time-slot* is needed. Such a PDF can be obtained by assuming that the last examined user is selected (for simplicity) if all K users have failed to exceed γ_T . However, the selected user is not allowed to transmit anything in the subsequent transmission time. The operation of selecting a user at the end will only ensure that the probability of not exceeding γ_T will be different from zero. Since no users are allowed to transmit information if all have failed to exceed γ_T , the correct ASE and BER expressions are obtained by letting $\{R_n\}_{n=1}^N = 0$ (no transmission) when $\gamma < \gamma_T$. Under these conditions, the following PDF may be utilized [7]:

$$p_{\gamma_{\text{SWT}}}^T(\gamma) = \begin{cases} \sum_{k=0}^{K-1} [P_\gamma(\gamma_T)]^k p_\gamma(\gamma) & \gamma \geq \gamma_T \\ [P_\gamma(\gamma_T)]^{K-1} p_\gamma(\gamma) & \gamma < \gamma_T \end{cases}. \quad (\text{E.6})$$

Replacing $p_{\gamma_{\text{BS}}}(\gamma)$ with $p_{\gamma_{\text{SWT}}}^T(\gamma)$ in (E.2) and letting $p = P_\gamma(\gamma_T)$ for notational simplicity, the following ASE is obtained:

$$\text{ASE}_{\text{SWT}} = \sum_{k=0}^{K-1} p^k \left[R_q \cdot e^{-\gamma_T/\bar{\gamma}} + \sum_{n=q+1}^N \alpha_n \cdot e^{-\gamma_n/\bar{\gamma}} \right], \quad (\text{E.7})$$

where $\alpha_n = (R_n - R_{n-1})$. Note that ASE_{SWT} is a function of the index $q \in [1, 2, \dots, N]$, which denotes the fading region in which γ_T is placed. For fixed K and $\bar{\gamma}$, ASE_{SWT} will have N separate solutions corresponding to γ_T residing within each of the N separate fading regions.³ Defining γ_T (for fixed K and $\bar{\gamma}$) as the switching threshold that maximizes the ASE, it is obtained as

$$\gamma_T = \arg \max_{\gamma_1 \leq \gamma \leq \gamma_N} (\text{ASE}_{\text{SWT}}). \quad (\text{E.8})$$

Defining the set $\mathcal{X}_n = \{\gamma \in \mathbb{R} : \gamma_n \leq \gamma < \gamma_{n+1}\}$ and using the indicator function

$$\mathcal{I}_{\mathcal{X}_n}(\gamma_T) = \begin{cases} 1 & \text{if } \gamma_T \in \mathcal{X}_n \\ 0 & \text{if } \gamma_T \notin \mathcal{X}_n \end{cases}, \quad (\text{E.9})$$

the optimal switching threshold is residing within the fading region

$$q = \arg \max_{n \in [1, 2, \dots, N]} (\mathcal{I}_{\mathcal{X}_n}(\gamma_T)). \quad (\text{E.10})$$

Replacing $p_{\gamma_{\text{BS}}}(\gamma)$ with $p_{\gamma_{\text{SWT}}}^T(\gamma)$ in (E.4), the average BER may be written as in (E.11).

$$\begin{aligned} \overline{\text{BER}}_{\text{SWT}} &= \frac{\left[\frac{R_q a_q}{\mu_q \bar{\gamma}} \cdot e^{-\mu_q \gamma_T} + \sum_{n=q+1}^N \frac{R_n a_n}{\mu_n \bar{\gamma}} \cdot e^{-\mu_n \gamma_n} - \sum_{n=q}^{N-1} \frac{R_n a_n}{\mu_n \bar{\gamma}} \cdot e^{-\mu_n \gamma_{n+1}} \right]}{\text{ASE}_{\text{SWT}}} \\ &\times \sum_{k=0}^{K-1} p^k, \end{aligned} \quad (\text{E.11})$$

where $\mu_n = \frac{b_n \bar{\gamma} + M_n}{M_n \bar{\gamma}}$. No effort of minimizing $\overline{\text{BER}}_{\text{SWT}}$ (or any other BER expressions in this paper) as a function of γ_T has been done, since the BER performance already is perceived as acceptable when the predefined target BER_0 is met.

Switch-and-examine transmission (SET)

The SET scheme is based on a multibranch switch-and-examine combining scheme [7]. It is equal to the SWT scheme except for the following: the last probed user is allowed to transmit information if all K users have failed to exceed γ_T and the reported SNR is above γ_1 (the lowest SNR needed to meet the target BER_0). Thus, in practice, the switching threshold for the

³ γ_T may not reside inside the interval range $0 \leq \gamma_T < \gamma_1$, since this may result in an outage situation even though a user is above the threshold.

SET scheme is relaxed to $\gamma_T = \gamma_1$ for the last probed user in order to reduce the outage probability. This leads to an improvement in the ASE of the SET scheme compared to the SWT scheme. For the SET scheme, the PDF of the output SNR is equal to [7, Eq. (35)]

$$p_{\gamma_{\text{SET}}}(\gamma) = \begin{cases} \sum_{k=0}^{K-1} [P_\gamma(\gamma_T)]^k p_\gamma(\gamma) & \gamma \geq \gamma_T \\ [P_\gamma(\gamma_T)]^{K-1} p_\gamma(\gamma) & \gamma < \gamma_T \end{cases}, \quad (\text{E.12})$$

which is equal to $p_{\gamma_{\text{SWT}}}^T(\gamma)$. Replacing $p_{\gamma_{\text{BS}}}(\gamma)$ with $p_{\gamma_{\text{SET}}}(\gamma)$ in (E.2), the ASE may be written as

$$\text{ASE}_{\text{SET}} = p^{K-1} S_1^A + (R_q v_q + S_{q+1}^A) \sum_{k=0}^{K-2} p^k, \quad (\text{E.13})$$

where $S_1^A = \sum_{n=1}^N R_n \delta_n$, $S_{q+1}^A = \sum_{n=q+1}^N R_n \delta_n$, $\delta_n = (e^{-\gamma_n/\bar{\gamma}} - e^{-\gamma_{n+1}/\bar{\gamma}})$, and $v_q = (e^{-\gamma_T/\bar{\gamma}} - e^{-\gamma_{q+1}/\bar{\gamma}})$. By replacing $p_{\gamma_{\text{BS}}}(\gamma)$ with $p_{\gamma_{\text{SET}}}(\gamma)$ in (E.4), the following solution for the average BER is obtained:

$$\overline{\text{BER}}_{\text{SET}} = \frac{p^{K-1} S_1^B + (R_q Y_q + S_{q+1}^B) \sum_{k=0}^{K-2} p^k}{\text{ASE}_{\text{SET}}}, \quad (\text{E.14})$$

where $S_1^B = \sum_{n=1}^N R_n \Delta_n$, $S_{q+1}^B = \sum_{n=q+1}^N R_n \Delta_n$, $\Delta_n = \frac{a_n}{\mu_n \bar{\gamma}} (e^{-\mu_n \gamma_n} - e^{-\mu_n \gamma_{n+1}})$, and $Y_q = \frac{a_q}{\mu_q \bar{\gamma}} (e^{-\mu_q \gamma_T} - e^{-\mu_q \gamma_{q+1}})$.

SET with post-selection (SETps)

This is the same selection procedure as SET, except that if no acceptable link has been found, the best one of all the probed users exceeding γ_1 is selected at the end instead of just picking the last one for simplicity [8]. For this scheme, the PDF of the output SNR is given by [8]

$$p_{\gamma_{\text{SETps}}}(\gamma) = \begin{cases} \sum_{k=0}^{K-1} [P_\gamma(\gamma_T)]^k p_\gamma(\gamma) & \gamma \geq \gamma_T \\ K [P_\gamma(\gamma)]^{K-1} p_\gamma(\gamma) & \gamma < \gamma_T \end{cases}. \quad (\text{E.15})$$

Upon replacing $p_{\gamma_{\text{BS}}}(\gamma)$ with $p_{\gamma_{\text{SETps}}}(\gamma)$ in (E.2), the following ASE is obtained:

$$\begin{aligned} \text{ASE}_{\text{SETps}} &= p^K R_q - R_1 [P_\gamma(\gamma_1)]^K - \sum_{n=2}^q [P_\gamma(\gamma_n)]^K \alpha_n \\ &+ (R_q v_q + S_{q+1}^A) \sum_{k=0}^{K-1} p^k. \end{aligned} \quad (\text{E.16})$$

Replacing $p_{\gamma_{\text{BS}}}(\gamma)$ with $p_{\gamma_{\text{SETps}}}(\gamma)$ in (E.4) and using binomial expansion of $P_{\gamma}(\gamma)$, the average BER may be written as

$$\overline{\text{BER}}_{\text{SETps}} = \frac{\frac{K}{\bar{\gamma}} \cdot \Sigma + \left(R_q Y_q + S_{q+1}^B\right) \sum_{k=0}^{K-1} p^k}{\text{ASE}_{\text{SETps}}}, \quad (\text{E.17})$$

where

$$\Sigma = \left(\sum_{n=1}^{q-1} R_n a_n \Lambda(w_n, \gamma_n, \gamma_{n+1}) + R_q a_q \Lambda(w_q, \gamma_q, \gamma_T) \right).$$

In the definition of Σ , the following notation has been introduced:

$$\Lambda(a, b, c) = \sum_{k=0}^{K-1} \binom{K-1}{k} \frac{(-1)^k}{a} (e^{-ab} - e^{-ac}),$$

$$\text{and } w_n = \frac{b_n \bar{\gamma} + (k+1) M_n}{M_n \bar{\gamma}}.$$

Selection combining transmission (SCT)

The SCT scheme is the benchmark scheme with which all the proposed switched based access schemes are compared. Within each guard time interval, all K users are probed and the BS selects the user which reports the highest SNR. With this mode of operation, the PDF of the output SNR is equal to [9, Eq. (5.85)]

$$p_{\gamma_{\text{SCT}}}(\gamma) = K [P_{\gamma}(\gamma)]^{K-1} p_{\gamma}(\gamma). \quad (\text{E.18})$$

Replacing $p_{\gamma_{\text{BS}}}(\gamma)$ with $p_{\gamma_{\text{SCT}}}(\gamma)$ in (E.2), the ASE may be expressed as

$$\text{ASE}_{\text{SCT}} = \sum_{n=1}^N R_n \cdot \left([P_{\gamma}(\gamma_{n+1})]^K - [P_{\gamma}(\gamma_n)]^K \right). \quad (\text{E.19})$$

Likewise, replacing $p_{\gamma_{\text{BS}}}(\gamma)$ with $p_{\gamma_{\text{SCT}}}(\gamma)$ in (E.4), the average BER for the SCT transmission scheme can be written as

$$\overline{\text{BER}}_{\text{SCT}} = \frac{K \sum_{n=1}^N R_n a_n \Omega_n}{\text{ASE}_{\text{SCT}}}, \quad (\text{E.20})$$

where $\Omega_n = B_{P_{\gamma}(\gamma_{n+1})}(K, \beta_n) - B_{P_{\gamma}(\gamma_n)}(K, \beta_n)$, $\beta_n = 1 + \frac{b_n \bar{\gamma}}{M_n}$, and $B_z(x, y)$ denotes the incomplete beta function.⁴

⁴ $B_z(x, y) = \int_0^z u^{x-1} (1-u)^{y-1} du.$

5 Average feedback load

The SCT scheme yields the best ASE of the multiuser access schemes presented in Section 4, but it comes at the expense of a high and deterministic feedback load. For the proposed switched multiuser access schemes on the other hand, the feedback load N_e will no longer be deterministic, but can be modelled as a discrete random variable (RV) described by the probability mass function (PMF):

$$P[N_e = k] = \begin{cases} p^{k-1} \cdot (1 - p) & k = 1, \dots, K - 1 \\ p^{K-1} & k = K \\ 0 & \text{otherwise} \end{cases}. \quad (\text{E.21})$$

Using this PMF, the *average* feedback load (AFL) $\bar{N}_e \triangleq \mu_{N_e}$ per time-slot is equal to⁵

$$\mu_{N_e} = \frac{1 - p^K}{1 - p}. \quad (\text{E.22})$$

The variance can be written as

$$\sigma_{N_e}^2 = \frac{p - (2K - 1)p^K + (2K - 1)p^{K+1} - p^{2K}}{(1 - p)^2}. \quad (\text{E.23})$$

Trade-off between ASE performance and AFL

In the following, γ_T is defined (for fixed K and $\bar{\gamma}$) as the switching threshold that maximizes the ASE subject to a possible AFL constraint. With no constraint, γ_T is identified within the set $\mathcal{X} = \{\gamma \in \mathbb{R} : \gamma_1 \leq \gamma \leq \gamma_N\}$ (see (E.8)). The set \mathcal{X} is upper bounded by γ_N , since this represents the lowest SNR threshold needed to select the highest rate of the rate-adaptive scheme. There is no point of increasing γ_T beyond γ_N , since this will only increase the AFL with no additional gain in ASE.

⁵For the SWT scheme, the result in (E.21) differs from [4, Eq. (31)], where $\mu_{N_e} = 1/(1 - p)$. In [4, Eq. (31)], the result is based on finding the average number per channel access within a time-frame longer than a single time-slot, whereas the result in (E.21) is valid per time-slot. For the SET scheme, the result in (E.21) also differs from [4, Eq. (36)], where $\mu_{N_e} = (1 - p^{K-1})/(1 - p)$. The difference is based on whether the last probed user is counted or not. In this paper, it is assumed that for all the proposed switched access schemes, the last user is examined if all the previous $K - 1$ have failed to exceed γ_T . However, the result in [4, Eq. (36)] is based on the traditional SEC combining scheme [7], where it is assumed that the last antenna is selected without comparing it to the threshold γ_T . If the last user is not examined but selected automatically, it will not contribute to increase the feedback load. Hence, both expressions are indeed correct.

When an AFL constraint is introduced, γ_T must be identified within a new set $\mathcal{X}_{\text{AFL}} = \{\gamma \in \mathbb{R} : \gamma_1 \leq \gamma \leq \gamma^*\}$, where $\gamma^* \leq \gamma_N$. The (possible) size reduction of the cardinality $|\mathcal{X}_{\text{AFL}}| \leq |\mathcal{X}|$ will be a function of the strongness of the imposed AFL constraint. The ASE performance will become suboptimal when γ_T obtained with unconstrained optimization no longer is available in \mathcal{X}_{AFL} . Hence, there is a trade-off between ASE performance and AFL.

As an example, the constraint $\mu_{N_c} \leq \alpha K$ ($0 < \alpha \leq 1$) is introduced in this paper. This constraint will ensure that the AFL do not exceed a certain percentage of the number of users connected to the BS. Since the condition $(1 - p^K)/(1 - p) \leq \alpha K$ cannot be solved in closed-form, the following condition must be satisfied: $p^K - \alpha K p + \alpha K - 1 \geq 0$. To minimize the AFL, and since the function $p^K - \alpha K p + \alpha K - 1$ is converging to zero for large γ_T (p converging to 1), the upper bound γ^* is selected as the minimum SNR which makes $p^K - \alpha K p + \alpha K - 1 = 0$. Hence, $\mathcal{X}_{\text{AFL}} = \{\gamma \in \mathbb{R} : (\gamma_1 \leq \gamma \leq \gamma^*) \cap (\gamma \leq \gamma_N)\}$, where $\gamma^* = \arg \min_{\gamma_1 \leq \gamma_T < \infty} (p^K - \alpha K p + \alpha K - 1 = 0)$.

6 Average waiting time

A specific feature of the SWT scheme is that no information is transmitted if none of the K users are above γ_T . Thus, it is of interest to know some statistics of the number of coherence times N_c the BS has to wait before an acceptable user is found. The number N_c will be a discrete RV, with PMF:

$$P[N_c = t] = p^{Kt}(1 - p^K), \quad (\text{E.24})$$

for $t = 0, 1, \dots$. Using this PMF, the average waiting time (AWT) $\bar{N}_c \triangleq \mu_{N_c}$ and variance of N_c are equal to $\mu_{N_c} = p^K/(1 - p^K)$ and $\sigma_{N_c}^2 = p^K/(1 - p^K)^2$, respectively.

7 Numerical results

In Figure E.1, ASE for all the presented access schemes are depicted for different average SNR levels. The results are based on selecting the optimal thresholds in a maximum ASE sense, subject to no restrictions on the AFL (unconstrained optimization). In the following, results are limited to the case when $\bar{\gamma} = 15$ dB due to space limitations and for the sake of clarity.⁶

⁶Average BER results are also omitted due to space limitations and since the actual shape of the curves are not important as long as they meet the target $\text{BER}_0 = 10^{-4}$. Perfect channel state information and error-free feedback from the users are assumed in this

More results will be available in [10]. As depicted in Figure E.2, when maximizing the ASE subject to no AFL constraints, the optimal thresholds of the SETps scheme will be high. This will contribute to increase the probability that all the users are examined, which enables the post-selection procedure. As a consequence, the AFL of the SETps scheme will be deterministic and equal to K for low and medium average SNR levels. At high SNR ($\bar{\gamma}$ approaching γ_T), the AFL will be less than K , since it is very likely that an acceptable user is found before all the users are examined. For the SET and SWT schemes, the optimal thresholds maximizing the ASE are in general lower than for the SETps scheme, basically to avoid that all users are examined (reducing the risk of an outage). Due to lower optimal thresholds, an acceptable user is identified more quickly, which effectively reduces the AFL. In Figure E.3, the AFL corresponding to the ASE results at $\bar{\gamma} = 15$ dB in Figure E.1 is depicted. From the results presented in Figure E.1 and E.3, it can be deduced that the reduced AFL of the SET and SWT schemes do not translate into a big performance loss in ASE compared to the SCT scheme. Hence, the additional gain offered by the SCT scheme by always identifying the best user is limited.

In Figure E.3, the (unmarked) solid line illustrates the upper bound of the AFL constraint $\mu_{N_e} \leq 0.3K$. The result of imposing this constraint is depicted in Figure E.4. The constraint will immediately limit the AFL for the SETps scheme (for all K). The SET and SWT schemes however are largely unaffected, since the optimal AFL curves of the two schemes obtained with unconstrained optimization are not in conflict with the constraint, except when $K \leq 20$ and $K > 47$ (SET scheme).

In Figure E.5, E.6, and E.7, it is depicted how the ASE curves in Figure E.1 ($\bar{\gamma} = 15$ dB) are affected when the AFL constraint $\mu_{N_e} \leq \alpha K$ is imposed on the SETps, SET, and SWT schemes, respectively.⁷

In Figure E.8, the AWT of the SWT scheme is depicted. It can be seen that the AWT is very low, even for unconstrained optimization (AWT = 0 for simplicity when the imposed AFL constraints cannot be met). Basically, this means that the SWT scheme hardly waits when $\bar{\gamma} = 15$ dB.

8 Conclusion

Several switched multiuser access schemes have been proposed for systems operating in a TDM mode. The new access schemes are aimed to reduce the

paper, and in this type of scenario, all the presented schemes will achieve the target BER_0 whenever data are transmitted.

⁷The ASE equals zero (for simplicity) when the imposed constraints cannot be met.

AFL in multiuser systems relying on feedback to maximize the ASE. Numerical results quantifying the trade-off between ASE and AFL have been presented, showing that the AFL can be reduced significantly compared to the optimal SCT scheme without experiencing a big performance loss in ASE. The proposed access schemes are quite attractive also from a fairness perspective.

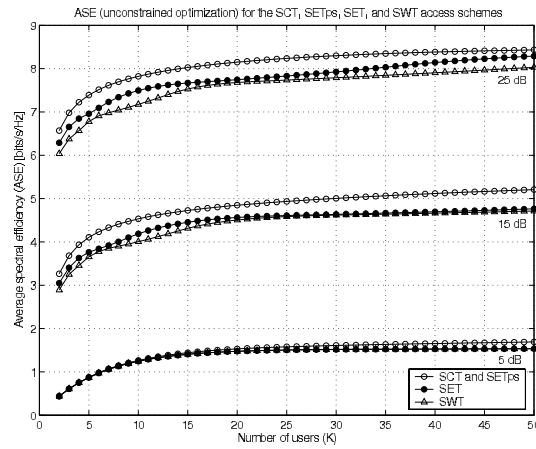


FIGURE E.1: ASE (unconstrained optimization) for the SCT, SETps, SET, and SWT access schemes when the multiuser system is assumed to be operating on i.i.d. Rayleigh fading channels with $\bar{\gamma} = [5, 15, 25]$ dB.

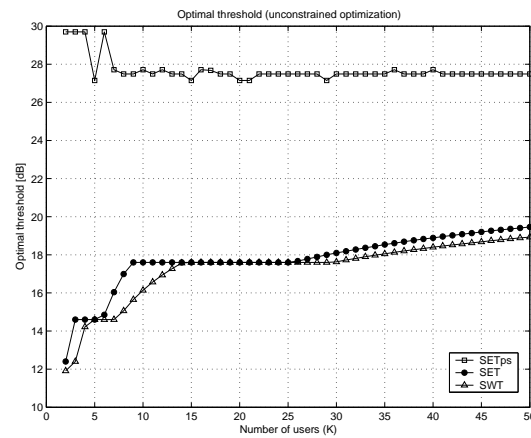


FIGURE E.2: Optimal thresholds γ_T maximizing the ASE subject to no AFL constraints (unconstrained optimization). The multiuser system is assumed to be operating on i.i.d. Rayleigh fading channels with $\bar{\gamma} = 15$ dB.

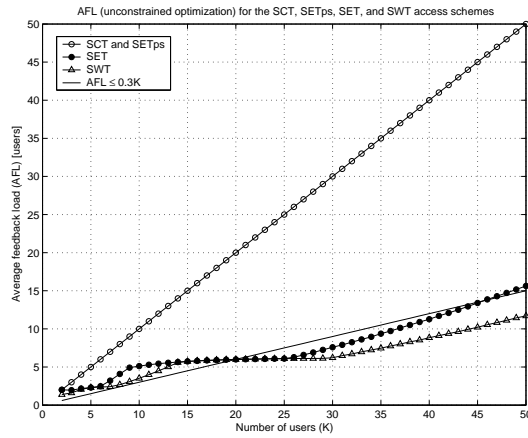


FIGURE E.3: AFL (unconstrained optimization) for the SCT, SETps, SET, and SWT access schemes. For reference purposes, the solid line visualizes the (linear) upper bound for the constraint $AFL \leq 0.3K$. The multiuser system is assumed to be operating on i.i.d. Rayleigh fading channels with $\bar{\gamma} = 15$ dB.

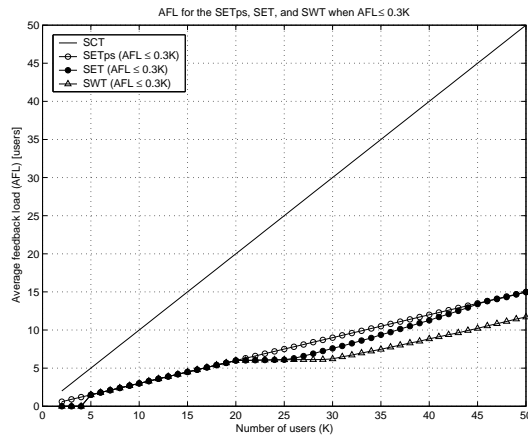


FIGURE E.4: AFL for the SCT, SETps, SET, and SWT access schemes when $AFL \leq 0.3K$. When the constraint cannot be met, $AFL = 0$ for simplicity. The multiuser system is assumed to be operating on i.i.d. Rayleigh fading channels with $\bar{\gamma} = 15$ dB.

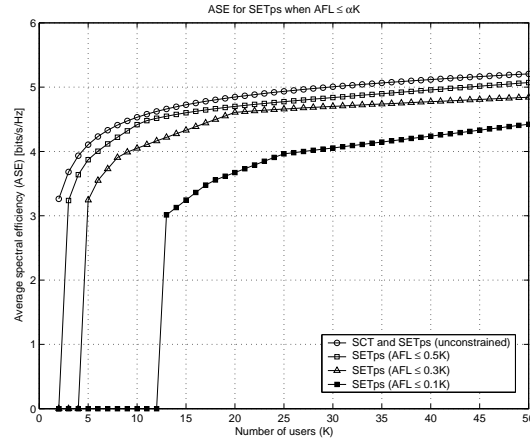


FIGURE E.5: ASE realized by the SETps access scheme when the AFL is upper bounded by $AFL \leq \alpha K$. When the constraint cannot be met, $ASE = 0$ for simplicity. The multiuser system is assumed to be operating on i.i.d. Rayleigh fading channels with $\bar{\gamma} = 15$ dB.

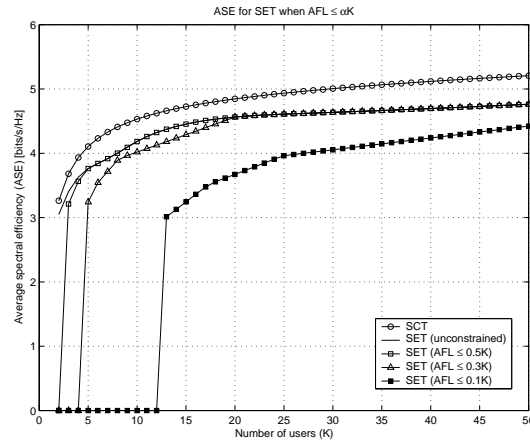


FIGURE E.6: ASE realized by the SET access scheme when the AFL is upper bounded by $AFL \leq \alpha K$. When the constraint cannot be met, $ASE = 0$ for simplicity. The multiuser system is assumed to be operating on i.i.d. Rayleigh fading channels with $\bar{\gamma} = 15$ dB.

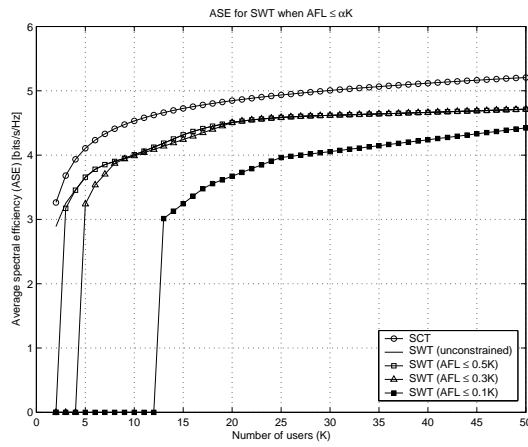


FIGURE E.7: ASE realized by the SWT access scheme when the AFL is upper bounded by $AFL \leq \alpha K$. When the constraint cannot be met, $ASE = 0$ for simplicity. The multiuser system is assumed to be operating on i.i.d. Rayleigh fading channels with $\bar{\gamma} = 15$ dB.

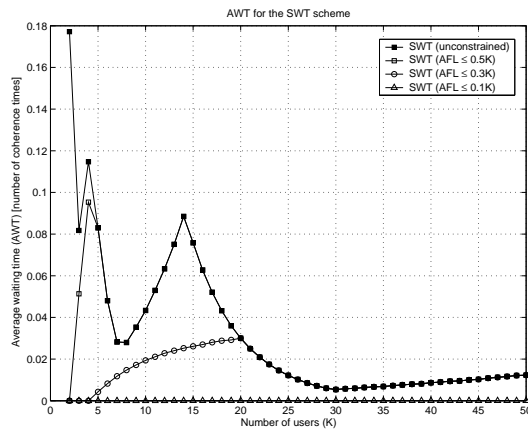


FIGURE E.8: Average waiting time (AWT) for the SWT access scheme. When the constraint cannot be met, $AWT = 0$ for simplicity (when $AFL \leq 0.1K$, $AWT = 0$ for $K \leq 12$). The multiuser system is assumed to be operating on i.i.d. Rayleigh fading channels with $\bar{\gamma} = 15$ dB.

References

- [1] R. Knopp and P. A. Humblet, "Information capacity and power control in single cell multiuser communications," in *Proc. International Conference on Communications*, pp. 331–335, June 1995.
- [2] P. Viswanath, D. N. Tse, and R. Laroia, "Opportunistic beamforming using dumb antennas," *IEEE Transactions on Information Theory*, vol. 48, no. 6, pp. 1277–1294, June 2002.
- [3] M. K. Simon and M. -S. Alouini, *Digital Communication over Fading Channels: A Unified Approach to Performance Analysis*. John Wiley & Sons, Inc., 2000.
- [4] M. -S. Alouini, M. K. Simon, and H. -C. Yang, "Scan and wait combining (SWC): A switch and examine strategy with a performance-delay tradeoff," in *Proc. IEEE First International Symposium on Control, Communications, and Signal Processing*, pp. 153–157, March 2004.
- [5] K. J. Hole, H. Holm, and G. E. Øien, "Adaptive multidimensional coded modulation on flat fading channels," *IEEE Journal on Selected Areas in Communications*, vol. 18, no. 7, pp. 1153–1158, July 2000.
- [6] M. -S. Alouini and A. Goldsmith, "Adaptive modulation over Nakagami fading channels," *Wireless Personal Communications*, vol. 13, pp. 119–143, May 2000.
- [7] H. -C. Yang and M. -S. Alouini, "Performance analysis of multibranch switched diversity systems," *IEEE Transactions on Communications*, vol. 51, no. 5, pp. 782–794, May 2003.
- [8] —, "Improving the performance of switched diversity with post-examining selection," *IEEE Transactions on Wireless Communications*, submitted August 2003.

- [9] G. L. Stüber, *Principles of Mobile Communications*. Norwell, MA, Kluwer, 1996.
- [10] B. Holter, M. -S. Alouini, G. E. Øien, and H. -C. Yang, "Multiuser switched diversity transmission," *IEEE Transactions on Wireless Communications*, to be submitted.

Part III

Appendices

Appendix 1

The generalized Marcum Q-function

The generalized Marcum Q-function as defined by Nuttall is equal to [1]

$$Q_m(a, b) = \frac{1}{a^{m-1}} \int_b^\infty x^m e^{-\frac{(x^2+a^2)}{2}} I_{m-1}(ax) dx, \quad (1.1)$$

where a and b are nonnegative real numbers, and m is a nonnegative integer. The function $I_{m-1}(\cdot)$ is the modified Bessel function of the first kind of order $m - 1$ [2]. In [3, Ch. 11.4], Temme uses a slightly different definition, written as

$$\tilde{Q}_m(\alpha, \beta) = \int_\beta^\infty \left(\frac{x}{\alpha}\right)^{\frac{1}{2}(m-1)} e^{-x-\alpha} I_{m-1}(2\sqrt{\alpha x}) dx. \quad (1.2)$$

The conversion between these two definitions is defined

$$Q_m(a, b) = \tilde{Q}_m\left(\frac{a^2}{2}, \frac{b^2}{2}\right). \quad (1.3)$$

Proof: By substituting $z = x^2/2$ and $c = a^2/2$ in (1.1), and defining $d = b^2/2$, the following chain of equalities are obtained

$$\begin{aligned} Q_m(a, b) &= \frac{1}{(\sqrt{2c})^{m-1}} \int_{b^2/2}^\infty (\sqrt{2z})^m e^{-z-c} I_{m-1}(2\sqrt{cz}) \frac{1}{\sqrt{2z}} dz \\ &= \int_d^\infty \left(\frac{z}{c}\right)^{\frac{1}{2}(m-1)} e^{-z-c} I_{m-1}(2\sqrt{cz}) dz = \tilde{Q}_m(c, d) = \tilde{Q}_m\left(\frac{a^2}{2}, \frac{b^2}{2}\right). \end{aligned}$$

References

- [1] A. H. Nuttall, "Some integrals involving the Q_M function," *IEEE Transactions on Information Theory*, vol. IT-21, no. 1, pp. 95–96, January 1975.
- [2] I. S. Gradshteyn and I. M. Ryzhik, *Table of Integrals, Series, and Products*. 5th ed., San Diego, CA: Academic Press, 1994.
- [3] N. M. Temme, *Special Functions: An Introduction to Classical Functions of Mathematical Physics*. New York: Wiley, 1996.

Appendix 2

Useful integration rules

$$\int_0^y e^{-au} Q_1(\alpha\sqrt{u}, \beta) du = \frac{1}{a} \left[e^{-\frac{a\beta^2}{2a+\alpha^2}} Q_1\left(\sqrt{y}\sqrt{2a+\alpha^2}, \frac{\alpha\beta}{\sqrt{2a+\alpha^2}}\right) - e^{-ay} Q_1(\alpha\sqrt{y}, \beta) \right] \quad (2.1)$$

Proof: Substitute $x^2 = u$ in [1, Eq. (B.19)] and the proof follows easily. \square

$$\begin{aligned} \int_x^y e^{-au} Q_1(\alpha\sqrt{u}, \beta) du &= \frac{1}{a} (e^{-ax} Q_1(\alpha\sqrt{x}, \beta) - e^{-ay} Q_1(\alpha\sqrt{y}, \beta)) \\ &+ \frac{1}{a} e^{-\frac{a\beta^2}{2a+\alpha^2}} \left[Q_1\left(\sqrt{y}\sqrt{2a+\alpha^2}, \frac{\alpha\beta}{\sqrt{2a+\alpha^2}}\right) - Q_1\left(\sqrt{x}\sqrt{2a+\alpha^2}, \frac{\alpha\beta}{\sqrt{2a+\alpha^2}}\right) \right] \end{aligned} \quad (2.2)$$

Proof: Define the finite range integral as the difference between two integrals defined in (2.1) and the proof follows easily. \square

$$\begin{aligned} \int_0^\infty u^{\frac{m-1}{2}} e^{-\beta u} I_{m-1}(c\sqrt{u}) Q_m(a\sqrt{u}, b) du &= \\ \frac{2}{c} \left(\frac{c}{2\beta}\right)^m e^{\frac{c^2}{4\beta}} Q_m\left(\frac{ac}{\sqrt{2\beta}\sqrt{2\beta+a^2}}, \frac{b\sqrt{2\beta}}{\sqrt{2\beta+a^2}}\right) \end{aligned} \quad (2.3)$$

Proof: Substitute $x^2 = u$ in [2, Eq. (15)] and the proof follows easily. \square

$$\begin{aligned} \int_x^y u^{m-1} e^{-cu} Q_m(a\sqrt{u}, b) du &= \sum_{i=0}^{\infty} \frac{a^{2i}}{2^i i!} \frac{\Gamma(m+i, b^2/2)}{(c+a^2/2)^{m+i}} \\ &\times [\bar{\Gamma}(m+i, (c+a^2/2)x) \\ &- \bar{\Gamma}(m+i, (c+a^2/2)y)] \end{aligned} \quad (2.4)$$

Proof: Employ (1.3) in Appendix 1 to the generalized Marcum-Q function and then use the infinite series representation of the Marcum-Q function as defined by Temme [3, Eq. (11.61)] and solve the new integral by employing [4, Eq. (C.1)]. \square

For integer α and $\beta u \geq 0$:

$$\begin{aligned} \int_x^y u^{m-1} e^{-au} \bar{\Gamma}(\alpha, \beta u) du &= \\ \sum_{n=0}^{\alpha-1} \frac{\beta^n}{n!} &\left[\frac{\Gamma(m+n, x(a+\beta)) - \Gamma(m+n, y(a+\beta))}{(a+\beta)^{m+n}} \right] \end{aligned} \quad (2.5)$$

Proof: Substitute $\bar{\Gamma}(\alpha, \beta u) = e^{-\beta u} \sum_{n=0}^{\alpha-1} \frac{(\beta u)^n}{n!}$ [3, Eq. (11.6)] and the proof follows easily. \square

References

- [1] M. K. Simon, *Probability distributions involving gaussian random variables*. Kluwer Academic Publishers, 2002.
- [2] A. H. Nuttall, "Some integrals involving the Q_M function," *IEEE Transactions on Information Theory*, vol. IT-21, no. 1, pp. 95–96, January 1975.
- [3] N. M. Temme, *Special Functions: An Introduction to Classical Functions of Mathematical Physics*. New York: Wiley, 1996.
- [4] H. Holm, "Adaptive coded modulation and channel estimation tools for flat fading channels," Ph.D. dissertation, The Norwegian University of Science and Technology, April 2002 (available at: <http://www.tele.ntnu.no/projects/beats/theses.htm>).

Appendix 3

Detailed derivation of the expression in (B.35)

Following the steps outlined in [1, Appendix B] for the term $\mathcal{E}\{\hat{\alpha}_h^2 \alpha_i^2\}$:

$$\begin{aligned}\mathcal{E}\{\hat{\alpha}_h^2 \alpha_i^2\} &= \mathcal{E}\left[|\mathbf{f}_j^H \mathbf{z}_h|^2 \cdot |z_i(n+j)|^2\right] \\ &= \mathbf{f}_j^H \mathcal{E}\left[(\mathbf{z}_h + (1/a_p)\mathbf{n})(\mathbf{z}_h^H + (1/a_p)\mathbf{n}^H)\right. \\ &\quad \times \left.|z_i(n+j)|^2\right] \mathbf{f}_j.\end{aligned}\quad (3.1)$$

Since noise and fading are statistically independent and both zero-mean,

$$\begin{aligned}\mathcal{E}\{\hat{\alpha}_h^2 \alpha_i^2\} &= \mathbf{f}_j^H \mathcal{E}\left[\mathbf{z}_h \mathbf{z}_h^H \cdot |z_i(n+j)|^2 + (1/a_p^2) \mathbf{n} \mathbf{n}^H \cdot |z_i(n+j)|^2\right] \mathbf{f}_j \\ &= \mathbf{f}_j^H \mathcal{E}\left[\mathbf{z}_h \mathbf{z}_h^H \cdot |z_i(n+j)|^2\right] \mathbf{f}_j + \Omega \frac{N_0 B}{a_p^2} \|\mathbf{f}_j\|^2.\end{aligned}\quad (3.2)$$

Introducing $\mathbf{z}_{r,h} = \Re(\mathbf{z})_h$ and $\mathbf{z}_{i,h} = \Im(\mathbf{z})_h$ (and similarly for the complex scalar $z_i(n+j)$), where $\Re(\cdot)$ and $\Im(\cdot)$ denotes the real and imaginary parts of a complex symbol, respectively:

$$\begin{aligned}\mathcal{E}\{\hat{\alpha}_h^2 \alpha_i^2\} &= \mathbf{f}_j^H \mathcal{E}\left[(\mathbf{z}_{r,h} \mathbf{z}_{r,h}^T + \mathbf{J} \mathbf{z}_{i,h} \mathbf{z}_{i,h}^T) \cdot (z_{r,i}^2(n+j) + z_{i,i}^2(n+j))\right] \mathbf{f}_j \\ &\quad + \frac{\Omega^2}{\gamma_i} \|\mathbf{f}_j\|^2,\end{aligned}\quad (3.3)$$

which is identical to

$$\begin{aligned}
 \mathcal{E}\{\hat{\alpha}_h^2 \alpha_i^2\} &= \mathbf{f}_j^H \mathcal{E} \left[z_{r,i}(n+j) z_{r,i}(n+j) \mathbf{z}_{r,h} \mathbf{z}_{r,h}^T \right] \mathbf{f}_j \\
 &+ \mathbf{f}_j^H \mathcal{E} \left[z_{i,i}(n+j) z_{i,i}(n+j) \mathbf{z}_{r,h} \mathbf{z}_{r,h}^T \right] \mathbf{f}_j \\
 &+ \mathbf{f}_j^H \mathcal{E} \left[z_{r,i}(n+j) z_{r,i}(n+j) \mathbf{z}_{i,h} \mathbf{z}_{i,h}^T \right] \mathbf{f}_j \\
 &+ \mathbf{f}_j^H \mathcal{E} \left[z_{i,i}(n+j) z_{i,i}(n+j) \mathbf{z}_{i,h} \mathbf{z}_{i,h}^T \right] \mathbf{f}_j \\
 &+ \frac{\Omega^2}{\gamma_i} \|\mathbf{f}_j\|^2.
 \end{aligned} \tag{3.4}$$

Using [1, Lemma 1] for the fourth order moment of a Gaussian process, the previous result can be written as

$$\begin{aligned}
 \mathcal{E}\{\hat{\alpha}_h^2 \alpha_i^2\} &= \mathbf{f}_j^H \left(\mathcal{E}[z_{r,i}(n+j) z_{r,i}(n+j)] \mathcal{E}[\mathbf{z}_{r,h} \mathbf{z}_{r,h}^T] \right. \\
 &+ \mathcal{E}[z_{r,i}(n+j) \mathbf{z}_{r,h}] \mathcal{E}[z_{r,i}(n+j) \mathbf{z}_{r,h}^T] \\
 &+ \left. \mathcal{E}[z_{r,i}(n+j) \mathbf{z}_{r,h}^T] \mathcal{E}[z_{r,i}(n+j) \mathbf{z}_{r,h}] \right) \mathbf{f}_j \\
 &+ \mathbf{f}_j^H \left(\mathcal{E}[z_{i,i}(n+j) z_{i,i}(n+j)] \mathcal{E}[\mathbf{z}_{r,h} \mathbf{z}_{r,h}^T] \right. \\
 &+ \mathcal{E}[z_{i,i}(n+j) \mathbf{z}_{r,h}] \mathcal{E}[z_{i,i}(n+j) \mathbf{z}_{r,h}^T] \\
 &+ \left. \mathcal{E}[z_{i,i}(n+j) \mathbf{z}_{r,h}^T] \mathcal{E}[z_{i,i}(n+j) \mathbf{z}_{r,h}] \right) \mathbf{f}_j \\
 &+ \mathbf{f}_j^H \left(\mathcal{E}[z_{r,i}(n+j) z_{r,i}(n+j)] \mathcal{E}[\mathbf{z}_{i,h} \mathbf{z}_{i,h}^T] \right. \\
 &+ \mathcal{E}[z_{r,i}(n+j) \mathbf{z}_{i,h}] \mathcal{E}[z_{r,i}(n+j) \mathbf{z}_{i,h}^T] \\
 &+ \left. \mathcal{E}[z_{r,i}(n+j) \mathbf{z}_{i,h}^T] \mathcal{E}[z_{r,i}(n+j) \mathbf{z}_{i,h}] \right) \mathbf{f}_j \\
 &+ \mathbf{f}_j^H \left(\mathcal{E}[z_{i,i}(n+j) z_{i,i}(n+j)] \mathcal{E}[\mathbf{z}_{i,h} \mathbf{z}_{i,h}^T] \right. \\
 &+ \mathcal{E}[z_{i,i}(n+j) \mathbf{z}_{i,h}] \mathcal{E}[z_{i,i}(n+j) \mathbf{z}_{i,h}^T] \\
 &+ \left. \mathcal{E}[z_{i,i}(n+j) \mathbf{z}_{i,h}^T] \mathcal{E}[z_{i,i}(n+j) \mathbf{z}_{i,h}] \right) \mathbf{f}_j \\
 &+ \frac{\Omega^2}{\gamma_i} \|\mathbf{f}_j\|^2.
 \end{aligned} \tag{3.5}$$

Introducing the notation $z_i(n) = x_1 + jy_1$ and $z_h(n) = x_2 + jy_2$, the following assumption is used:

$$\begin{aligned}\rho_{z,st} &= \frac{\mathcal{E}[z_i(n+\tau)z_h^*(n)]}{\Omega} \\ &\triangleq \frac{\mathcal{E}[z_i(n)z_h^*(n)]}{\Omega} \cdot \frac{\mathcal{E}[z_i(n+\tau)z_i^*(n)]}{\Omega} \\ &= \rho_{z,s} \cdot \rho_{z,t},\end{aligned}\quad (3.6)$$

where $\rho_{z,s}$ and $\rho_{z,t}$ are the normalized correlation coefficients between complex Gaussians in space and time, respectively. This implies that

$$\mathcal{E}[z_i(n+\tau)z_h^*(n)] = \rho_{z,s} \cdot \mathcal{E}[z_i(n+\tau)z_i^*(n)].\quad (3.7)$$

Using the Jakes model, $\rho_{z,t}$ is real and $\mathcal{E}[z_i(n+\tau)z_i^*(n)] = \Omega \cdot J_0(2\pi f_D \tau)$ [2]. In terms of its real and imaginary parts, $\rho_{z,st}$ may then also be written as [3, Appendix A]

$$\begin{aligned}\rho_{z,st} &= \frac{\mathcal{E}[z_i(n+\tau)z_h^*(n)]}{\Omega} \\ &= \frac{\mathcal{E}[(x_1 + jy_1)(x_2 - jy_2)]}{\Omega} \\ &= \frac{\mathcal{E}[x_1x_2] + \mathcal{E}[y_1y_2] + j(\mathcal{E}[x_2y_1] - \mathcal{E}[x_1y_2])}{\Omega} \\ &= \frac{2\mathcal{E}[x_1x_2] - j2\mathcal{E}[x_1y_2]}{\Omega} \\ &= \rho_{z,s} \cdot \rho_{z,t} = (c - jd) \cdot \rho_{z,t},\end{aligned}\quad (3.8)$$

where c and d are the normalized real and imaginary parts of $\rho_{z,s}$, respectively. Hence,

$$\mathcal{E}[x_1x_2] = \mathcal{E}[y_1y_2] = c \cdot \frac{\Omega}{2} J_0(2\pi f_D \tau)\quad (3.9)$$

$$\mathcal{E}[x_1y_2] = -\mathcal{E}[x_2y_1] = d \cdot \frac{\Omega}{2} J_0(2\pi f_D \tau).\quad (3.10)$$

Now, expressions included in (3.5) may be written

$$\mathcal{E}[z_{r,i}(n+j)z_{r,h}] = \mathcal{E}[z_{i,i}(n+j)z_{i,h}] = c \cdot \frac{\Omega}{2} \mathbf{r}_j\quad (3.11)$$

$$\mathcal{E}[z_{r,i}(n+j)z_{i,h}] = -\mathcal{E}[z_{i,i}(n+j)z_{r,h}] = d \cdot \frac{\Omega}{2} \mathbf{r}_j\quad (3.12)$$

where $\mathbf{r}_j = \frac{1}{\Omega} \mathcal{E}[\mathbf{z}_h \mathbf{z}_h^*(n+j)]$. An element $[\mathbf{r}_j]_k$ of \mathbf{r}_j will be function of the lag τ between the relevant pilot symbol time instant $n - kL$ and of the time $n + j$ of the CSNR to be predicted only. Finally, the following result is obtained:

$$\begin{aligned}
 \mathcal{E}\{\hat{\alpha}_h^2 \alpha_i^2\} &= \mathbf{f}_j^H \left(\frac{\Omega^2}{4} \mathbf{R} + 2c^2 \frac{\Omega^2}{4} \mathbf{r}_j \mathbf{r}_j^T \right) \mathbf{f}_j + \mathbf{f}_j^H \left(\frac{\Omega^2}{4} \mathbf{R} + 2d^2 \frac{\Omega^2}{4} \mathbf{r}_j \mathbf{r}_j^T \right) \mathbf{f}_j \\
 &+ \mathbf{f}_j^H \left(\frac{\Omega^2}{4} \mathbf{R} + 2d^2 \frac{\Omega^2}{4} \mathbf{r}_j \mathbf{r}_j^T \right) \mathbf{f}_j + \mathbf{f}_j^H \left(\frac{\Omega^2}{4} \mathbf{R} + 2c^2 \frac{\Omega^2}{4} \mathbf{r}_j \mathbf{r}_j^T \right) \mathbf{f}_j \\
 &+ \frac{\Omega^2}{\gamma_i} \|\mathbf{f}_j\|^2 \\
 &= \Omega^2 \mathbf{f}_j^H \mathbf{R} \mathbf{f}_j + \frac{\Omega^2}{\gamma_i} \|\mathbf{f}_j\|^2 + (c^2 + d^2) \Omega^2 \mathbf{f}_j^H \mathbf{r}_j \mathbf{r}_j^T \mathbf{f}_j \\
 &= \Omega^2 r + \rho_s \Omega^2 |\mathbf{f}_j^H \mathbf{r}_j|^2,
 \end{aligned} \tag{3.13}$$

where $r = \mathbf{f}_j^H \mathbf{R} \mathbf{f}_j + \frac{1}{\gamma_i} \|\mathbf{f}_j\|^2$ [4, Appendix], $\mathbf{R} = \frac{1}{\Omega} \text{Cov}(\mathbf{z}_h, \mathbf{z}_h) = \frac{1}{\Omega} \mathcal{E}[\mathbf{z}_h \mathbf{z}_h^H]$, and $c^2 + d^2 = |\rho_{z,s}|^2 = \rho_s$ is the spatial power correlation coefficient [3].

References

- [1] H. Holm, "Adaptive coded modulation and channel estimation tools for flat fading channels," Ph.D. dissertation, The Norwegian University of Science and Technology, April 2002 (available at: <http://www.tele.ntnu.no/projects/beats/theses.htm>).
- [2] G. L. Stüber, *Principles of Mobile Communications*. Second edition, Kluwer Academic Publishers, 2001.
- [3] M. O. Hasna, M. -S. Alouini, and M. K. Simon, "Effect of fading correlation on the outage probability of cellular mobile radio systems," in *Proc. IEEE Vehicular Technology Conference*, vol. 3, pp. 1794–1798, October 2001.
- [4] G. E. Øien, H. Holm, and K. J. Hole, "Impact of channel prediction on adaptive coded modulation performance in Rayleigh fading," *IEEE Transactions on Vehicular Technology*, vol. 53, no. 3, pp. 758–769, May 2004.

Appendix 4

ASE and average BER under idealized assumptions

In this Appendix, expressions for the ASE and the average BER are derived under idealized assumptions, i.e., perfect channel knowledge and zero delay on the feedback channel. In this case, the predicted CSNR $\hat{\gamma} = \gamma$, and $\rho = 1$. The bivariate gamma distribution in (B.10) may then be exchanged for the exact/approximate PDF of γ . This is done in order to validate the accuracy of the approximate PDF. Note that in the following, the results are in general derived for identically distributed and spatially correlated Nakagami- m fading channels. The results for Rayleigh fading channels are obtained by letting $m = 1$.

Exact PDF

Let $\{\gamma_h\}_{h=1}^H$ be a set of H correlated and identically distributed gamma variates $\gamma_h \sim \mathcal{G}(m, \bar{\gamma}_h/m)$. The exact PDF of the combined CSNR at the output of an MRC receiver is then equal to [1, Eq. (5)]

$$f_\gamma(\gamma) = \prod_{h=1}^H \left(\frac{\lambda_1}{\lambda_h} \right)^m \sum_{k=0}^{\infty} \delta_k \cdot \frac{\gamma^{Hm+k-1} e^{-\gamma/\lambda_1}}{\lambda_1^{Hm+k} \Gamma(Hm+k)}, \quad (4.1)$$

where $\lambda_1 = \min_h \{\lambda_h\}$. The set $\{\lambda_h\}_{h=1}^H$ contains the eigenvalues of the matrix $\mathbf{A} = \mathbf{D}\mathbf{C}$, where \mathbf{D} is a $H \times H$ diagonal matrix with entries $\{\bar{\gamma}_h/m\}_{h=1}^H$, and \mathbf{C} is a $H \times H$ positive definite matrix defined by

$$\mathbf{C} = \begin{bmatrix} 1 & \sqrt{\rho_{12}} & \cdots & \sqrt{\rho_{1H}} \\ \sqrt{\rho_{21}} & 1 & \cdots & \sqrt{\rho_{2H}} \\ \vdots & \vdots & \ddots & \vdots \\ \sqrt{\rho_{H1}} & \cdots & \cdots & 1 \end{bmatrix}. \quad (4.2)$$

The coefficients δ_k can be obtained recursively by the formula [1, Eq. (7)]

$$\delta_{k+1} = \frac{m}{k+1} \sum_{i=1}^{k+1} \left[\sum_{h=1}^H \left(1 - \frac{\lambda_1}{\lambda_h}\right)^i \right] \cdot \delta_{k+1-i}, \quad (4.3)$$

for $k = 0, 1, 2, \dots$, and $\delta_0 = 1$. For a constant correlation model, $\lambda_1 = \lambda_2 = \dots = \lambda_{H-1}$, and when inserting for the eigenvalues [1, Eq. (12)], the inner sum of (4.3) may be simplified to

$$\sum_{h=1}^H \left(1 - \frac{\lambda_1}{\lambda_h}\right)^i = \left(\frac{\sqrt{\rho_s} H}{1 + \sqrt{\rho_s}(H-1)} \right)^i. \quad (4.4)$$

With the aid of [2, Eq. (C.1)], the average BER when code n is applied, $\overline{\text{BER}}_n$, is equal to

$$\overline{\text{BER}}_n = a_n \prod_{h=1}^H \left(\frac{\lambda_1}{\lambda_h} \right)^m \sum_{k=0}^{\infty} \frac{\delta_k}{(\lambda_1 \mu_n)^\alpha} [\bar{\Gamma}(\alpha, \gamma_n \mu_n) - \bar{\Gamma}(\alpha, \gamma_{n+1} \mu_n)], \quad (4.5)$$

where $\alpha = Hm + k$, and $\mu_n = \frac{b_n \lambda_1 + M_n}{M_n \lambda_1}$. The probability of selecting code n , P_n , is given by the expression

$$P_n = \prod_{h=1}^H \left(\frac{\lambda_1}{\lambda_h} \right)^m \sum_{k=0}^{\infty} \delta_k [\bar{\Gamma}(\alpha, \gamma_n / \lambda_1) - \bar{\Gamma}(\alpha, \gamma_{n+1} / \lambda_1)]. \quad (4.6)$$

The ASE and average BER may then be derived from (B.41) and (B.44) respectively, where $R_n = \log_2(M_n) - 1/2$ is the information rate of code n . For numerical evaluation, the infinite sums are truncated to S terms. Denoting the truncated version of the PDF in (4.1) as $f_\gamma(\gamma, S)$, the error of the area under the PDF due to truncation can be obtained as [3]

$$I_e(S) = 1 - \int_0^{\infty} f_\gamma(\gamma, S) d\gamma = 1 - c \sum_{k=0}^S \delta_k, \quad (4.7)$$

where $c = \prod_{h=1}^H \left(\frac{\lambda_1}{\lambda_h} \right)^m$. In this paper, the infinite sums are terminated at $S = 260$ terms. For the number of antennas and correlation values used in the numerical examples, $I_e(S)$ is then less than 10^{-3} in all cases.

Approximate PDF

When the rate-adaptive system is operating on correlated Nakagami- m fading channels, an approximate PDF of the combined CSNR at the output of the MRC receiver may be written as [4]

$$p_\gamma(\gamma) = \frac{\gamma^{m_d-1} e^{-\gamma/\theta}}{\theta^{m_d} \Gamma(m_d)}. \quad (4.8)$$

Using this PDF, the average BER when code n is applied, $\overline{\text{BER}}_n$, is equal to

$$\overline{\text{BER}}_n = \frac{a_n}{(\theta v_n)^{m_d}} [\bar{\Gamma}(m_d, \gamma_n v_n) - \bar{\Gamma}(m_d, \gamma_{n+1} v_n)], \quad (4.9)$$

where $v_n = \frac{b_n \theta + M_n}{M_n \theta}$. The probability of selecting code n , P_n , is given by

$$P_n = \bar{\Gamma}(m_d, \gamma_n / \theta) - \bar{\Gamma}(m_d, \gamma_{n+1} / \theta). \quad (4.10)$$

The ASE and average BER may then be derived from (B.41) and (B.44) respectively, where $R_n = \log_2(M_n) - 1/2$ is the information rate of code n .

References

- [1] M. -S. Alouini, A. Abdi, and M. Kaveh, "Sum of gamma variates and performance of wireless communication systems over Nakagami-fading channels," *IEEE Transactions on Vehicular Technology*, vol. 50, no. 6, pp. 1471–1479, November 2001.
- [2] H. Holm, "Adaptive coded modulation and channel estimation tools for flat fading channels," Ph.D. dissertation, The Norwegian University of Science and Technology, April 2002 (available at: <http://www.tele.ntnu.no/projects/beats/theses.htm>).
- [3] T. A. Tran and A. B. Sesay, "Distribution of the sum of arbitrarily correlated gamma variates and performance of MRC over Nakagami- m fading channels," *submitted to IEEE Transactions on Vehicular Technology*.
- [4] C. Mun, C. -H. Kang, and H. -K. Park, "Approximation of SNR statistics for MRC diversity systems in arbitrarily correlated Nakagami fading channels," *IEE Electronics Letters*, vol. 35, no. 4, pp. 266–267, February 1999.

Appendix 5

Comments on the results in [1]

In [1, Fig. 1], the curves for the exact distribution are correct, but they do not correspond to the analytical result in [1, Eq. (8)]. In order to reproduce the same set of curves as depicted in [1, Fig. 1], ρ^2 in [1, Eq. (8)] must be replaced by ρ . Then, [1, Eq. (8)] is in accordance with related results reported in the literature [2, Eq. (D.14)], [3, Eq. (5)], [4, Eq. (18)].

In addition, we believe that the covariance matrix in [1, Eq. (9)] should be redefined, so that the entries outside the main diagonal become complex correlation coefficients, since \mathbf{R} originally is defined as the normalized covariance matrix between complex fading amplitudes. This change leads to a new set of curves for the approximate distribution in [1, Fig. 1]. In [5], closed-form expressions for m_d based on complex covariance matrices are derived (reproduced as ψ in Table B.1), from which the corrected approximate PDF curves can be computed from [1, Eq. (7)] and [1, Eq. (3)]. In Figure 5.1, a new set of curves for the approximate PDF (denoted corrected) are compared to the original ones in [1, Fig. 1].

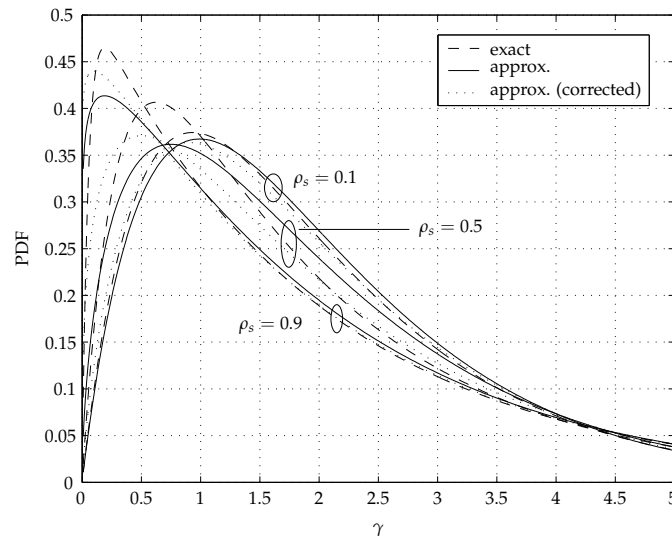


FIGURE 5.1: Comparison of the exact and approximate PDFs in [1, Fig. 1], including corrected results based on a complex representation of the covariance matrix in [1, Eq. (9)]. The curves are obtained for $\bar{\gamma} = 1$ and $m = 1$.

References

- [1] C. Mun, C. -H. Kang, and H. -K. Park, "Approximation of SNR statistics for MRC diversity systems in arbitrarily correlated Nakagami fading channels," *IEE Electronics Letters*, vol. 35, no. 4, pp. 266–267, February 1999.
- [2] H. Holm, "Adaptive coded modulation and channel estimation tools for flat fading channels," Ph.D. dissertation, The Norwegian University of Science and Technology, April 2002 (available at: <http://www.tele.ntnu.no/projects/beats/theses.htm>).
- [3] M. -S. Alouini, A. Abdi, and M. Kaveh, "Sum of gamma variates and performance of wireless communication systems over Nakagami-fading channels," *IEEE Transactions on Vehicular Technology*, vol. 50, no. 6, pp. 1471–1479, November 2001.
- [4] V. A. Aalo, "Performance of maximal-ratio diversity systems in a correlated Nakagami-fading environment," *IEEE Transactions on Communications*, vol. 43, no. 8, pp. 2360–2369, August 1995.
- [5] B. Holter and G. E. Øien, "On the amount of fading for MIMO diversity systems," *accepted for publication in IEEE Transactions on Wireless Communications*.

Appendix 6

Proof of the Amount of Fading expression in (D.11)

Using a mathematical model assuming that the transmit and receive correlation properties are decoupled in a MIMO diversity system operating on identically distributed spatially correlated Nakagami- m channels, the amount of fading may be expressed as

$$\text{AF} = \frac{\sum_{j=1}^{n_T} \|\mathbf{t}_j\|^2 \sum_{i=1}^{n_R} \|\mathbf{r}_i\|^2}{N^2 m}, \quad (6.1)$$

where $\|\cdot\|^2$ denotes the squared Euclidean vector norm, m is the common fading parameter of all the channels, n_T denotes the number of transmit antennas, n_R denotes the number of receive antennas, and $N = n_T \cdot n_R$. The vectors \mathbf{t}_j and \mathbf{r}_i denote rows j and i of the transmit and receive correlation matrices, respectively.

Proof: Let Λ represent the diagonal eigenvalue matrix of the complex correlation matrix \mathbf{R}_H . Assuming decoupled correlation properties at the receiver and transmitter, the correlation matrix \mathbf{R}_H may be written as $\mathbf{R}_H = \mathbf{R}_{T_x} \otimes \mathbf{R}_{R_x}$, where the symbol \otimes denotes the Kronecker product, and the matrices \mathbf{R}_{T_x} and \mathbf{R}_{R_x} denote the decoupled transmit and receive correlation matrices, respectively. Due to multiplicative properties of the eigenvalues of matrices in a Kronecker product, the nominator in (D.10) may be decomposed into the product $\text{tr}(\Lambda_{T_x}^2) \text{tr}(\Lambda_{R_x}^2)$, where Λ_{T_x} and Λ_{R_x} are the diagonal eigenvalue matrices of \mathbf{R}_{T_x} and \mathbf{R}_{R_x} , respectively. The following chain of equalities can then be obtained for the transmitter part:

$$\text{tr}(\Lambda_{T_x}^2) = \text{tr}(\mathbf{R}_{T_x}^2) = \sum_{j=1}^{n_T} (\mathbf{R}_{T_x} \mathbf{R}_{T_x})_{jj} = \sum_{j=1}^{n_T} \sum_{k=1}^{n_T} t_{jk} \cdot t_{kj} \stackrel{(i)}{=} \sum_{j=1}^{n_T} \sum_{k=1}^{n_T} t_{jk} \cdot t_{jk}^* = \sum_{j=1}^{n_T} \|\mathbf{t}_j\|^2, \quad (6.2)$$

where t_{jk} denotes a single entry at the j th row and k th column of \mathbf{R}_{T_x} , and \mathbf{t}_j denotes the j th row of \mathbf{R}_{T_x} . The equality (i) is true since a correlation matrix is Her-

mitian symmetric. A similar chain of equalities can be obtained for the receiver part, resulting in

$$\text{tr}(\Lambda_{R_x}^2) = \text{tr}(\mathbf{R}_{R_x}^2) = \sum_{i=1}^{n_R} \|\mathbf{r}_i\|^2, \quad (6.3)$$

where \mathbf{r}_i denotes the i th row of \mathbf{R}_{R_x} . □

Appendix 7

An alternative expression for the determinant of a constant correlation matrix

A constant correlation matrix \mathbf{R} of size $L \times L$ is called a L th order intraclass correlation matrix if it has the following structure [1]

$$\mathbf{R} = \begin{bmatrix} a & b & b & \cdots & b \\ b & a & b & \cdots & b \\ b & b & a & \cdots & b \\ \vdots & \vdots & \vdots & \ddots & \vdots \\ b & b & b & \cdots & a \end{bmatrix}, \quad (7.1)$$

with $b \geq -a/(L-1)$. By normalizing this matrix, 1s are obtained on the main diagonal and the factor b/a off the main diagonal. Denoting $x = b/a$ and assuming that $x \in [0, 1]$, a closed-form expression for the determinant of \mathbf{R} may be written as [2]

$$\det(\mathbf{R}) = (1-x)^{L-1}(1+x(L-1)). \quad (7.2)$$

Due to the normalized main diagonal and the fact that the variable x is confined to the finite interval range $x \in [0, 1]$, we have observed (depicted in Figure D.1) that the cumulative distribution function (CDF) of a beta distributed RV can be used in an alternative expression for the determinant given in (7.2). The alternative expression may be derived as follows.

The probability distribution function (PDF) of a beta distributed RV with free parameters $\alpha > 0$ and $\beta > 0$ is given by [3]

$$betapdf(x) = \frac{\Gamma(\alpha + \beta)}{\Gamma(\alpha)\Gamma(\beta)}(1-x)^{\beta-1}x^{\alpha-1}. \quad (7.3)$$

The CDF can then be expressed as

$$betacdf(x; \alpha, \beta) = \int_0^x \frac{\Gamma(\alpha + \beta)}{\Gamma(\alpha)\Gamma(\beta)} (1-u)^{\beta-1} u^{\alpha-1} du. \quad (7.4)$$

Evaluating the function $f(x, \alpha, \beta) = 1 - betacdf(x; \alpha, \beta)$ when $\alpha = 2$, the following result is obtained:

$$\begin{aligned} f(x, 2, \beta) &= 1 - betacdf(x; 2, \beta) = 1 - \int_0^x \frac{\Gamma(\beta + 2)}{\Gamma(\beta)} (1-u)^{\beta-1} u du \\ &= 1 - \frac{\Gamma(\beta + 2)}{\Gamma(\beta)} \left[\frac{1 - (1-x)^\beta (1 + \beta x)}{\beta(\beta + 1)} \right] \\ &= (1-x)^\beta (1 + \beta x). \end{aligned} \quad (7.5)$$

By comparison, (7.5) and (7.2) represent identical expressions by selecting $\beta = L - 1$. Hence, the determinant of a constant correlation matrix \mathbf{R} can be written as

$$\det(\mathbf{R}) = 1 - betacdf(x; 2, L - 1). \quad (7.6)$$

Since the parameter β must be larger than zero, this expression is valid only when $L \geq 2$. The CDF of a beta distributed RV is equal to the regularized beta function $I(\cdot; \cdot, \cdot)$ [4], and the determinant can also be written as

$$\det(\mathbf{R}) = 1 - betacdf(x; 2, L - 1) = 1 - I(x; 2, L - 1) = I(1 - x; L - 1, 2), \quad (7.7)$$

where $I(x; \alpha, \beta) = 1 - I(1 - x; \beta, \alpha)$ [5]. Hence,

$$\det(\mathbf{R}) = betacdf(1 - x; L - 1, 2). \quad (7.8)$$

References

- [1] M. K. Simon and M. -S. Alouini, *Digital Communication over Fading Channels: A Unified Approach to Performance Analysis*. John Wiley & Sons, Inc., 2000.
- [2] S. J. Press, *Applied Multivariate Analysis: Using Bayesian and frequentist methods of inference*. Holt, Rinehart, Winston, 2nd edition, 1972.
- [3] M. H. DeGroot and M. J. Schervish, *Probability and Statistics*. Addison-Wesley, 2002.
- [4] <http://mathworld.wolfram.com>.
- [5] <http://functions.wolfram.com>.

Appendix 8

Proofs of statistical results presented in Paper E

Feedback load

Given the mode of operation of the SET, SETps and SWT multiuser access schemes, the number of probed users per time-slot before channel access N_e when operating on i.i.d. channels is a discrete RV whose PMF is given by

$$P[N_e = k] = \begin{cases} p^{k-1} \cdot (1-p) & k = 1, 2, \dots, K-1 \\ p^{K-1} & k = K \\ 0 & \text{otherwise} \end{cases} \quad (8.1)$$

Using this PMF, the mean of N_e is equal to

$$\mu_{N_e} = \frac{1-p^K}{1-p}. \quad (8.2)$$

Proof: The mean of N_e may in general be written as

$$\mu_{N_e} = (1-p) \sum_{k=1}^{K-1} kp^{k-1} + Kp^{K-1}. \quad (8.3)$$

An expression for the finite sum in (8.3) can be obtained by taking the derivative of an existing sum identify in [1, Appendix A], leading to the following relation:

$$\sum_{k=1}^{K-1} kp^{k-1} = \frac{1-p^K - Kp^{K-1}(1-p)}{(1-p)^2}, \quad (8.4)$$

for $p \neq 1$. Hence,

$$\mu_{N_e} = (1-p) \cdot \frac{1-p^K - Kp^{K-1}(1-p)}{(1-p)^2} + Kp^{K-1} = \frac{1-p^K}{1-p}.$$

□

Using the PMF in (8.1), the variance of N_e is equal to

$$\sigma_{N_e}^2 = \frac{p - (2K-1)p^K + (2K-1)p^{K+1} - p^{2K}}{(1-p)^2}. \quad (8.5)$$

Proof: The variance of N_e is expressed as

$$\begin{aligned} \sigma_{N_e}^2 &= \mathcal{E}\{N_e^2\} - \mu_{N_e}^2 \\ &= (1-p) \sum_{k=1}^{K-1} k^2 p^{k-1} + K^2 p^{K-1} - \mu_{N_e}^2. \end{aligned} \quad (8.6)$$

An expression for the finite sum in (8.6) can be obtained by taking the derivative of an existing sum identify in [1, Appendix A], leading to the following relation:

$$\sum_{k=1}^{K-1} k^2 p^{k-1} = \frac{1+p - K^2 p^{K-1} + (2K^2 - 2K - 1)p^K - (K^2 - 2K + 1)p^{K+1}}{(1-p)^3}, \quad (8.7)$$

for $p \neq 1$. Hence,

$$\begin{aligned} \sigma_{N_e}^2 &= (1-p) \cdot \frac{1+p - K^2 p^{K-1} + (2K^2 - 2K - 1)p^K - (K^2 - 2K + 1)p^{K+1}}{(1-p)^3} \\ &\quad + K^2 p^{K-1} - \mu_{N_e}^2 \\ &= \frac{p - (2K-1)p^K + (2K-1)p^{K+1} - p^{2K}}{(1-p)^2}. \end{aligned}$$

□

Waiting time

Given the mode of operation of the SWT multiuser access scheme, the number of coherence times N_c the BS has to wait before an acceptable user is found when operating on i.i.d. channels will be a discrete RV, with PMF:

$$P[N_c = t] = p^{Kt}(1-p^K), \quad (8.8)$$

for $t = 0, 1, \dots$ Using this PMF, the mean of N_c is equal to

$$\mu_{N_c} = \frac{p^K}{1-p^K}. \quad (8.9)$$

Proof:

$$\mu_{N_c} = (1 - p^K) \sum_{t=0}^{\infty} t p^{Kt} = (1 - x) \sum_{t=0}^{\infty} t x^t = \frac{x}{1 - x},$$

for $x = p^K < 1$ [2, Eq. (0.231)]. \square

Using the PMF in (8.8), the variance of N_c is equal to

$$\sigma_{N_c}^2 = \frac{p^K}{(1 - p^K)^2}. \quad (8.10)$$

Proof:

$$\begin{aligned} \sigma_{N_c}^2 &= \mathcal{E}\{N_c^2\} - \mu_{N_c}^2 \\ &= (1 - p^K) \sum_{t=0}^{\infty} t^2 p^{Kt} - \mu_{N_c}^2 \\ &= (1 - x) \sum_{t=0}^{\infty} t^2 x^t - \mu_{N_c}^2 \\ &= \frac{x(1+x)}{(1-x)^2} - \frac{x^2}{(1-x)^2} \\ &= \frac{x}{(1-x)^2}, \end{aligned}$$

for $x = p^K < 1$ [1, Appendix A]. \square

References

- [1] A. Ambardar, *Analog and Digital Signal Processing*. PWS Publishing Company, 1995.
- [2] I. S. Gradshteyn and I. M. Ryzhik, *Table of Integrals, Series, and Products*. 5th ed., San Diego, CA: Academic Press, 1994.

Appendix 9

The optimal weights of an MRC receiver by means of an eigenfilter approach

Maximum ratio combining (MRC) is an efficient spatial diversity strategy to reduce signal fluctuations caused by multipath propagation in wireless communications. Among several different spatial diversity techniques, MRC represents the optimal (in a maximum signal-to-noise ratio (SNR) sense) diversity scheme in the absence of interference.¹ However, it also represents the diversity scheme with the highest complexity, since it requires knowledge of all channel fading parameters. Despite its complexity, the MRC receiver is frequently utilized for analysis purposes as a benchmark receiver with which to compare other (less complex) spatial diversity schemes.

A narrowband, flat-fading, single-input multiple-output (SIMO) system with n_R receive antennas is considered. Using a complex baseband representation, the received signal s_i at antenna $i \in \{1, 2, \dots, n_R\}$ may be expressed as

$$s_i = h_i x + n_i, \quad (9.1)$$

where x , h_i and n_i are all random variables denoting the transmitted signal, the channel observed at receive antenna i , and additive white Gaussian noise (AWGN) received at antenna i , respectively. In the following, we shall have a reason to make a distinction between the random variable h_i

¹When interference is introduced, the optimal combining scheme is denoted an *optimum combiner*, maximizing the instantaneous received signal-to-interference plus noise ratio (SINR) [1], [2, Ch. 10].

and the realizations (outcomes) of h_i at certain instants in time, in order to later be able to explicitly refer to the instantaneous received SNR for the current observed channel. For that purpose, a discrete time index k will be introduced into the expression in (9.1). Denoting the transmitted signal at time index $k \in \{0, 1, \dots\}$ by $x^{(k)}$, the received signal $s_i^{(k)}$ may then be written as

$$s_i^{(k)} = h_i^{(k)} x^{(k)} + n_i^{(k)}. \quad (9.2)$$

Note that $h_i^{(k)}$ represents a specific realization (outcome) of the random variable h_i and by assumption, $h_i^{(k)}$ is perfectly known by the receiver by the time it is observed. Using vector notation, the received array response vector at time instant k may be compactly written as

$$\mathbf{s}_k = \mathbf{h}_k x^{(k)} + \mathbf{n}_k, \quad (9.3)$$

where² $\mathbf{s}_k = [s_1^{(k)}, \dots, s_{n_R}^{(k)}]^T$, $\mathbf{h}_k = [h_1^{(k)}, \dots, h_{n_R}^{(k)}]^T$, and $\mathbf{n}_k = [n_1^{(k)}, \dots, n_{n_R}^{(k)}]^T$. The vector channel \mathbf{h}_k may be looked upon as a single realization of a random channel vector \mathbf{h} (multivariate random variable) with possibly correlated entries. Depending on the radio propagation environment, various multipath fading models may be used to characterize the statistical behavior of the fading envelopes in \mathbf{h} . However, in this letter, a specific choice of fading model for each of the fading envelopes in the set $\{|h_i|\}_{i=1}^{n_R}$ is not needed, since the results are not influenced by such a selection. In the following, the optimal weights of an MRC receiver are obtained by means of an eigenfilter approach.

An MRC receiver represents a linear combiner, and the output y may in general be expressed as

$$y = \mathbf{w}^H \mathbf{s} \quad (9.4)$$

$$= \mathbf{w}^H \mathbf{h} x + \mathbf{w}^H \mathbf{n}, \quad (9.5)$$

where $\mathbf{w} \in \mathbb{C}^{n_R}$ are the (as yet unknown) weights of the linear combiner.³ With an average power constraint $P_T = \mathcal{E}\{|x|^2\}$ at the transmitter, the instantaneous received signal power S at the output of the MRC receiver at time instant k can be expressed as

$$S = P_T \cdot \mathbf{w}^H \mathbf{h}_k \mathbf{h}_k^H \mathbf{w}. \quad (9.6)$$

²The superscript $(\cdot)^T$ denotes matrix transpose.

³The superscript $(\cdot)^H$ denotes Hermitian transpose and \mathbb{C} denotes the set of complex numbers. The notation \mathbb{C}^n denotes the set of complex-valued vectors of length n .

Recall that \mathbf{h}_k represents a specific realization (outcome) of the random variable \mathbf{h} observed at time instant k and that by assumption, \mathbf{h}_k is perfectly known by the receiver by the time it is observed. The output noise power N may be expressed as

$$N = \mathcal{E}\{|\mathbf{w}^H \mathbf{n}|^2\} = \mathbf{w}^H \mathbf{R}_n \mathbf{w}, \quad (9.7)$$

where $\mathbf{R}_n = \mathcal{E}\{\mathbf{nn}^H\}$ denotes the noise covariance matrix.⁴ Using (9.6) and (9.7), the instantaneous SNR at the output of the MRC receiver at time instant k , $\gamma_{mrc}^{(k)}$, can be expressed as

$$\gamma_{mrc}^{(k)} = \frac{S}{N} = \frac{P_T \cdot \mathbf{w}^H \hat{\mathbf{R}}_k \mathbf{w}}{\mathbf{w}^H \mathbf{R}_n \mathbf{w}}, \quad (9.8)$$

where $\hat{\mathbf{R}}_k = \mathbf{h}_k \mathbf{h}_k^H$ denotes an estimate of the channel covariance matrix at time instant k . The optimization problem is now to determine the coefficient vector \mathbf{w} so as to maximize (9.8) for the current observed channel vector \mathbf{h}_k .

Equal noise power

In the following, we assume equal noise power at each of the branches, and also that the noise is uncorrelated between the branches. This means that the noise correlation matrix introduced in the previous section can be represented as $\mathbf{R}_n = \sigma^2 \mathbf{I}$, where σ^2 represents the noise power common to all branches and \mathbf{I} represents the identity matrix. Taking the *conjugate derivative* $\partial/\partial \mathbf{w}^*$ [3] of (9.8) with respect to the weight vector \mathbf{w} , we obtain the following set of implications:

$$\begin{aligned} \frac{\partial \gamma_{mrc}^{(k)}}{\partial \mathbf{w}^*} &= 0 \\ &\Downarrow \\ P_T \cdot \hat{\mathbf{R}}_k \mathbf{w} (\sigma^2 \mathbf{w}^H \mathbf{w}) &= \sigma^2 \mathbf{w} (P_T \cdot \mathbf{w}^H \hat{\mathbf{R}}_k \mathbf{w}) \\ &\Downarrow \\ \hat{\mathbf{R}}_k \mathbf{w} &= \left(\frac{\mathbf{w}^H \hat{\mathbf{R}}_k \mathbf{w}}{\mathbf{w}^H \mathbf{w}} \right) \mathbf{w}. \end{aligned} \quad (9.9)$$

Introducing $\lambda = \frac{\mathbf{w}^H \hat{\mathbf{R}}_k \mathbf{w}}{\mathbf{w}^H \mathbf{w}}$ and using the result of (9.9) in (9.8), we obtain

$$\gamma_{mrc}^{(k)} = \frac{P_T \cdot \mathbf{w}^H \hat{\mathbf{R}}_k \mathbf{w}}{\sigma^2 \mathbf{w}^H \mathbf{w}} = \frac{P_T \cdot \mathbf{w}^H \lambda \mathbf{w}}{\sigma^2 \mathbf{w}^H \mathbf{w}} = \frac{P_T \cdot \lambda}{\sigma^2}. \quad (9.10)$$

⁴ $\mathcal{E}\{\cdot\}$ denotes the statistical average.

It can be seen that the maximum value of the output SNR is given as $\frac{P_T \cdot \lambda_{max}}{\sigma^2}$, where λ_{max} is the largest eigenvalue of the matrix $\hat{\mathbf{R}}_k$. The optimal weight vector that yields the maximum output SNR is thus given by the eigenvector associated with λ_{max} . To obtain a non-trivial solution of (9.9), \mathbf{w} must reside within the column space (range) of $\hat{\mathbf{R}}_k$, denoted $\mathcal{R}(\hat{\mathbf{R}}_k)$. Since all the columns in $\hat{\mathbf{R}}_k$ are linear combinations of the single vector \mathbf{h}_k , it is a rank one matrix and $\mathcal{R}(\hat{\mathbf{R}}_k) = \{\mathbf{h}_k\}$. Since $\mathcal{R}(\hat{\mathbf{R}}_k)$ consists of just a single vector, the only way of obtaining a non-trivial solution is to select $\mathbf{w}_{opt} = c \cdot \mathbf{h}_k$ for an arbitrary $c \neq 0$. Inserting this result into the left side of (9.9), we obtain

$$\|\mathbf{h}_k\|^2 c \cdot \mathbf{h}_k = \lambda_{max} \mathbf{w}_{opt}. \quad (9.11)$$

The maximum eigenvalue is thus identified as $\lambda_{max} = \|\mathbf{h}_k\|^2$. Using this result in (9.10), the maximum output SNR is given by

$$\gamma_{mrc}^{(k)} = \frac{P_T \cdot \|\mathbf{h}_k\|^2}{\sigma^2} = \sum_{i=1}^{n_R} \frac{P_T \cdot |h_i^{(k)}|^2}{\sigma^2} = \sum_{i=1}^{n_R} \gamma_i^{(k)}, \quad (9.12)$$

where $|h_i^{(k)}|$ and $\gamma_i^{(k)} = \frac{P_T \cdot |h_i^{(k)}|^2}{\sigma^2}$ denote the fading envelope and the instantaneous SNR at the i th branch at time index k , respectively. This result confirms that the output SNR may be expressed as a sum of the SNR values from the individual branches, which is a specific feature of the MRC receiver [4].

Unequal noise power

With unequal noise power in the diversity branches, the SNR expressed in (9.8) can not be simplified. Taking the conjugate derivative of (9.8) with respect to the weight vector \mathbf{w} , we obtain the following set of implications:

$$\begin{aligned} \frac{\partial \gamma_{mrc}^{(k)}}{\partial \mathbf{w}^*} &= 0 \\ &\Downarrow \\ P_T \cdot \hat{\mathbf{R}}_k \mathbf{w} (\mathbf{w}^H \mathbf{R}_n \mathbf{w}) &= (P_T \cdot \mathbf{w}^H \hat{\mathbf{R}}_k \mathbf{w}) \mathbf{R}_n \mathbf{w} \\ &\Downarrow \\ \hat{\mathbf{R}}_k \mathbf{w} &= \left(\frac{\mathbf{w}^H \hat{\mathbf{R}}_k \mathbf{w}}{\mathbf{w}^H \mathbf{R}_n \mathbf{w}} \right) \mathbf{R}_n \mathbf{w}. \end{aligned} \quad (9.13)$$

Introducing $\lambda = \frac{\mathbf{w}^H \hat{\mathbf{R}}_k \mathbf{w}}{\mathbf{w}^H \mathbf{R}_n \mathbf{w}}$ and exploiting the fact that \mathbf{R}_n is nonsingular (diagonal matrix with all entries $\sigma_i^2 > 0$), (9.13) may be expressed as

$$\mathbf{R}_n^{-1} \hat{\mathbf{R}}_k \mathbf{w} = \lambda \mathbf{w}. \quad (9.14)$$

The optimal weight vector is now the eigenvector of the matrix $\mathbf{R}_n^{-1}\hat{\mathbf{R}}_k = \mathbf{R}_n^{-1}\mathbf{h}_k\mathbf{h}_k^H$ corresponding to the largest eigenvalue of the same matrix. By letting $\mathbf{h}'_k = \mathbf{R}_n^{-1}\mathbf{h}_k$, the current eigenvalue problem may be expressed as

$$\hat{\mathbf{R}}'_k \mathbf{w} = \lambda \mathbf{w}, \quad (9.15)$$

where $\hat{\mathbf{R}}'_k = \mathbf{h}'_k\mathbf{h}'_k{}^H$. A non-trivial solution of this equation is obtained if \mathbf{w} resides within the column space of $\hat{\mathbf{R}}'_k$, denoted $\mathcal{R}(\hat{\mathbf{R}}'_k)$. Every matrix of the simple form $\mathbf{h}'_k\mathbf{h}'_k{}^H$ has rank one [5] and the column space $\mathcal{R}(\hat{\mathbf{R}}'_k) = \{\mathbf{h}'_k\}$. As in the previous section, the only choice to obtain a non-trivial solution is to select $\mathbf{w}_{opt} = c \cdot \mathbf{h}'_k$ for an arbitrary $c \neq 0$. Inserting this result into the left side of (9.15), we obtain

$$\mathbf{h}_k^H \mathbf{R}_n^{-1} \mathbf{h}_k c \cdot \mathbf{h}'_k = \lambda_{max} \mathbf{w}_{opt}, \quad (9.16)$$

and the maximum eigenvalue can be identified as $\lambda_{max} = \mathbf{h}_k^H \mathbf{R}_n^{-1} \mathbf{h}_k$. Inserting the optimal weight vector $\mathbf{w}_{opt} = c \cdot \mathbf{h}'_k = c \cdot \mathbf{R}_n^{-1} \mathbf{h}_k$ into (9.8), we obtain

$$\gamma_{mrc}^{(k)} = P_T \cdot \mathbf{h}_k^H \mathbf{R}_n^{-1} \mathbf{h}_k = \sum_{i=1}^{n_R} \frac{P_T \cdot |h_i^{(k)}|^2}{\sigma_i^2} = \sum_{i=1}^{n_R} \gamma_i^{(k)}, \quad (9.17)$$

where $\gamma_i^{(k)} = \frac{P_T \cdot |h_i^{(k)}|^2}{\sigma_i^2}$. As in the previous subsection, the output SNR may be expressed as the sum of the SNR values from the individual branches.

To summarize, we have obtained the following optimal weights:

$$\mathbf{w}_{opt} \propto \begin{cases} \mathbf{h}_k & \text{Equal noise power} \\ \mathbf{R}_n^{-1} \mathbf{h}_k & \text{Unequal noise power} \end{cases} \quad (9.18)$$

Using these optimal weights, the output SNR from a MRC receiver may be expressed as

$$\gamma_{mrc}^{(k)} = \begin{cases} \frac{P_T \cdot \|\mathbf{h}_k\|^2}{\sigma^2} & \text{Equal noise power} \\ P_T \cdot \mathbf{h}_k^H \mathbf{R}_n^{-1} \mathbf{h}_k & \text{Unequal noise power} \end{cases} \quad (9.19)$$

Looking at the inner product in (9.4), the actual weights used in the inner product are the complex conjugate of the weights presented in (9.18). The optimal weights are then in agreement with the result presented in [4]. Since the solutions in this section is linked to an eigenvalue problem, the optimal (spatial) filter obtained using this method is commonly called an eigenfilter. As noted in [3], the optimum filter characterized in this way may be viewed as the stochastic counterpart of a matched filter.

References

- [1] J. H. Winters, "Optimum combining in digital mobile radio with co-channel interference," *IEEE Transactions on Vehicular Technology*, vol. VT-33, no. 3, pp. 144–154, August 1984.
- [2] M. K. Simon and M.-S. Alouini, *Digital Communication over Fading Channels: A Unified Approach to Performance Analysis*. John Wiley & Sons, Inc., 2000.
- [3] S. Haykin, *Adaptive filter theory*. Prentice Hall, Inc., 2001.
- [4] D. G. Brennan, "Linear diversity combining techniques," in *Proc. IRE*, vol. 47, pp. 1075–1102, 1959.
- [5] G. Strang, *Linear algebra and its applications*. Harcourt Brace Jovanovich, Inc., 1988.

